2014

KEY ROLES OF SUB-CELLULAR MEMBRANES AND CO-CHAPERONE IN TOMBUSVIRUS REPLICATION

Kai Xu
University of Kentucky, xukai05@gmail.com

STUDENT AGREEMENT:

I represent that my thesis or dissertation and abstract are my original work. Proper attribution has been given to all outside sources. I understand that I am solely responsible for obtaining any needed copyright permissions. I have obtained needed written permission statement(s) from the owner(s) of each third-party copyrighted matter to be included in my work, allowing electronic distribution (if such use is not permitted by the fair use doctrine) which will be submitted to UKnowledge as Additional File.

I hereby grant to The University of Kentucky and its agents the irrevocable, non-exclusive, and royalty-free license to archive and make accessible my work in whole or in part in all forms of media, now or hereafter known. I agree that the document mentioned above may be made available immediately for worldwide access unless an embargo applies.

I retain all other ownership rights to the copyright of my work. I also retain the right to use in future works (such as articles or books) all or part of my work. I understand that I am free to register the copyright to my work.

REVIEW, APPROVAL AND ACCEPTANCE

The document mentioned above has been reviewed and accepted by the student's advisor, on behalf of the advisory committee, and by the Director of Graduate Studies (DGS), on behalf of the program; we verify that this is the final, approved version of the student's thesis including all changes required by the advisory committee. The undersigned agree to abide by the statements above.

Kai Xu, Student

Dr. Peter D. Nagy, Major Professor

Dr. Lisa J. Vaillancourt, Director of Graduate Studies

KEY ROLES OF SUB-CELLULAR MEMBRANES AND CO-CHAPERONE IN TOMBUSVIRUS REPLICATION

DISSERTATION

A dissertation submitted in partial fulfillment of the
requirements for the degree of Doctor of Philosophy in the
College of Agriculture, Food and Environment
at the University of Kentucky

By

Kai Xu

Lexington, Kentucky

Director: Peter D. Nagy, Ph.D., Professor of Plant Pathology

Lexington, Kentucky

2014

ABSTRACT OF DISSERTATION

KEY ROLES OF SUB-CELLULAR MEMBRANES AND CO-CHAPERONE IN TOMBUSVIRUS REPLICATION

Positive strand RNA viruses, inculding tombusviruses, are known to utilize cellular membranes to assemble their replicase complexes (VRCs). Two tombusviruses , Tomato bushy stunt virus (TBSV) and Carnation Italian ringspot virus (CIRV), replicate on different organellar membranes, peroxisomes or endoplasmic reticulum (ER) for TBSV and mitochodria outer membranes in case of CIRV. I showed that both TBSV and CIRV replicase proteins could assemble VRCs and replicate viral RNA on purified microsomes (ER) and mitochondria. Different efficiencies of assembly was shown determined by multiple domains on TBSV or CIRV replication proteins.

To study why VRC assembly could occur on an alternative organellar membranes, I focused on the phospholipids, key lipid components in ER or mitochondria membranes. Phospholipids directly interact with viral replicases, however, their specific roles during (+)RNA virus replication are far less understood. I used TBSV as a model (+) RNA virus, and established a cell-free TBSV replication system using artificial membranes prepared from different phospholipids. I showed that phosphatidylethanolamine (PE) is required for full cycle replication of the viral RNA.Moreover, PE is enriched at the sites of TBSV replication in plant and yeast cells, and was up-regulated during TBSV replication. Furthermore, up-regulation of total cellular PE content in yeast due to deletion of CHO2 leads to dramatically stimulated TBSV replication. Overall, I identified PE as the key lipid component of membranes required for TBSV replication, and my data highlighted that PE, an abundant phospholipid in all eukaryotic cells, not only serves as a structural component of membrane bilayers, its interaction with the viral replication proteins also stimulates (+)RNA virus replication. Further experiments indicated both early secretory pathway and endocytic pathway are involved in PE re-distribution to site of replication.

In addition to lipids and subcellular membranes, certain host proteins are also involved in (+) RNA virus replication and VRC assembly. I identified Hop-like stress-inducible protein 1 (Sti1p), which interacts with heat shock protein 70, is required for the

inhibition of CIRV replication. My findings indicate that Hop/Sti1 co-chaperone could act as a virus restriction factor in case of mitochondrial CIRV, but not against peroxisomal tombusvirus.

KEY WORDS: Positive strand RNA virus, phospholipids, phosphatidylethanolamine, subcellular membrane, Sti1p

Kai Xu

May 1, 2014

KEY ROLES OF SUB-CELLULAR MEMBRANES AND CO-CHAPERONE IN TOMBUSVIRUS REPLICATION

By

Kai Xu

Peter D. Nagy, Ph.D.
Director of Dissertation

Lisa J. Vaillancourt, Ph.D.
Director of Graduate Studies

ACKNOWLEDGEMENT

I thank my committee chair and mentor Dr. Peter Nagy who accepted me as a student into his lab in Department of Plant Pathology, University of Kentucky, at 2007, and continually supported my research. He not only gave me suggestions on specific experiments, he also encouraged me of free thinking and independently designing and conducting experiments. I enjoyed much of my research work with fun. Without his encouragement, I would not find so much enjoyment during my Ph.D. studies and would not accomplish this dissertation. I also would like to thank my graduate study committee members: Dr. Brian Rymond, Dr. Michael Goodin, Dr. Mark Farman. I have learned how to do research in scientific field from their guidance.

I express my sincere gratitude to all the Nagy lab members who gave me support and helped me since the first day of my arrival at Lexington. I would also like to thank Department Chair Dr. Christopher L. Schardl, Director of Graduate Studies Lisa J. Vaillancourt and former Department Chair Dr. David A. Smith for supporting and helping me, and other department members for helping me during days and nights in this 7 years of study.

TABLE OF CONTENTS

ACKNOWLEDGEMENT iii
TABLE OF CONTENTS iv
TABLE OF FIGURES vi

Chapter 1 INTRODUCTION 1
Chapter 2 AUTHENTIC IN VITRO REPLICATION OF TWO TOMBUSVIRUSES IN ISOLATED MITOCHONDRIAL AND ENDOPLASMIC RETICULUM MEMBRANES 8
2.1 Introduction 8
2.2 Materials And Methods 11
2.3 Results 21
2.4 Discussion 33
Chapter 3 THE HOP-LIKE STRESS INDUCED PROTEIN 1 CO-CHAPERONE IS A NOVEL RESTRICTION FACTOR FOR MITOCHONDRIAL TOMBUSVIRUS REPLICATION 56
3.1 Introduction 56
3.2 Materials And Methods 60
3.3 Results 68
3.4 Discussion 75
Chapter 4 RNA VIRUS REPLICATION DEPENDS ON ENRICHMENT OF PHOSPHATIDYLETHANOLAMINE AT REPLICATION SITES IN SUBCELLULAR MEMBRANES 104
4.1 Introduction 104
4.2 Materials and Methods 105
4.3 Results 111
4.4 Discussion 118
Chapter 5 VACUOLE TARGETING PATHWAY IS REQUIRED FOR EFFICIENT TBSV REPLICATION AND MAYBE RELATED TO PE ENRICHMENT IN THE PEROXISOMAL MEMBRANES 146
5.1 Introduction 146
5.2 Materials and Methods 151
5.3 Results 153
5.4 Discussion 161

Chapter 6 CLASS III PHOSPHOINOSITIDE 3-KINASE VPS34 IS A KEY HOST FACTOR IN TOMBUSVIRUS REPLICATION 181
6.1 Introduction 181
6.2 Materials and Methods 183
6.3 Results 185
6.4 Discussion 190
Chapter 7 CONCLUSION AND PERSPECTIVE 207
7.1 Conclusion 207
7.2 Perspective 211
REFERENCES 219
VITA 241

LIST OF FIGURES

Fig. 2.1 *In vitro* reconstitution of the CIRV replicase in yeast cell extract. 38
Fig. 2.2 The heterologous combinations of TBSV and CIRV replication proteins are functional in *N. benthamiana*..... 40
Fig. 2.3 *In vitro* reconstitution of the TBSV and CIRV replicases in yeast microsome and mitochondrial preparations. 42
Fig. 2.4 *In vitro* reconstitution of the TBSV and CIRV replicases in yeast membrane fractions..... 44
Fig. 2.5 The *in vitro*-assembled TBSV or CIRV replicases form an RNase-resistant structure in microsomal or mitochondrial preparations. 46
Fig. 2.6 *In vitro* reconstitution of heterologous combinations of tombusvirus replicases in yeast microsome and mitochondrial preparations..... 48
Fig. 2.7 *In vitro* reconstitution of chimeric tombusvirus replicases in yeast microsome and mitochondrial preparations..... 50
Fig. 2.8 *In vitro* reconstitution of additional chimeric tombusvirus replicases in yeast microsome and mitochondrial preparations. 52
Fig. 2.9 Distribution of TBSV and CIRV replication proteins when expressed in heterologous combinations. 54
Fig 3.1 Increased CIRV replication in *sti1*Δ yeast..... 82
Fig 3.2 Over-expression of Sti1p inhibits CIRV accumulation in yeast..... 84
Fig 3.3 Interaction between Sti1p and CIRV p36 replication protein in yeast and in vitro. 86
Fig 3.4 Defining the sequence within the tombusvirus replication proteins needed for binding to Sti1p in vitro. 88
Fig 3.5 Relocalization of yeast Sti1p co-chaperone when co-expressed with CIRV p36 replication protein in yeast. 90
Fig 3.6 Functional TPR1 domain of Sti1p is required for inhibition of CIRV replication in yeast. 92
Fig 3.7 Functional TPR1 domain of Sti1p blocks CIRV replication in vitro. 94
Fig 3.8 Comparison of the inhibitory effects of TPR-containing cellular proteins on CIRV replication in isolated mitochondria *in vitro*. 96
Fig 3.9 Inhibition of CIRV replication by expression of the orthologous AtHop-1 in yeast. 98
Fig 3.10 Knockdown of Hop gene by VIGS increases CIRV accumulation in whole plants. 100
Fig 3.11 Models on the inhibitory role of Sti1p co-chaperone in CIRV replication. 102
Fig. 4.1 *In vitro* reconstitution of the TBSV replicase in artificial PE vesicles..... 122
Fig. 4.2 *In vitro* reconstitution of the TBSV replicase in artificial phospholipid vesicles. 124
Fig. 4.3 Effects of various phospholipids on the TBSV replicase activity in artificial PE vesicles. 126
Fig. 4.4 Binding of TBSV p33 to artificial vesicles containing different phospholipids. 128

Fig. 4.5 TBSV p33/p92-mediated binding of TBSV RNA to artificial vesicles containing different phospholipids. 130
Fig. 4.6 Enrichment of PE at TBSV replication sites in yeast and plant cells. 132
Fig. 4.7 Increased level of PE in yeast and plant cells replicating TBSV. 134
Fig. 4.8 Lipidomics analyses of phospholipids in yeast and plant cells replicating TBSV. 136
Fig. 4.9 Deletion of the *CHO2* PEMT gene enhances TBSV repRNA accumulation in yeast. 138
Fig. 4.10 Increased PE level facilitates TBSV RNA replication in the ER in *pex3*Δ*cho2*Δ yeast. 140
Fig. 4.11 Increased PE level facilitates CNV RNA accumulation in *cho2*Δ yeast. 142
Fig. 4.12 Increased PE level facilitates CIRV and NoV RNA accumulation in *cho2*Δ yeast. 144
Fig. 5.1 Reduced TBSV replication in PE synthesis pathways deletion yeast strains... 167
Fig. 5.2 p33 co-localization to peroxisomes and TGN. 169
Fig. 5.3 PE is enriched in both peroxisome and TGN where TBSV GFP-p33 is localized. 171
Fig. 5.4 TGN tSNARE Tlg2 is required for efficient TBSV replication in yeast, affecting PE enrichment to sites of replication. 173
Fig. 5.5 Targeting of TBSV p33/p92 to vacuole through vesicle transport pathway. ... 175
Fig. 5.6 SAR1 dominant mutant SAR1-H77L inhibits vacuole targeting of GFP-p33/p92 as well as TBSV replication. 177
Fig. 5.7 COP-I dependent retrograde transport from TGN to ER is not required for TBSV replication in yeast. 179
Fig. 6.1 VPS34 is required for efficient TBSV replication in yeast and is involved in PE enrichment at the site of replication. 195
Fig. 6.2 PI3K inhibitor AS604850 inhibits positive strand RNA viruses replication.... 197
Fig. 6.3 Dissecting the function of different Vps34p complexes in tombusvirus replication. 199
Fig. 6.4 Confocal laser microscope analysis of Vps34p localization during TBSV replication in yeast. 201
Fig. 6.5 Split-ubiquitin based Y2H assay to test viral protein interaction with Vps34p. 203
Fig. 6.6 GFP-p33/p92 and a peroxisomal matrix protein Pot1p were analyzed for accumulation during TBSV repRNA replication in wild type and *vps34*Δ yeast strains. 205
Fig. 7.1 Alternative replication sites found for different (+)RNA viruses..... 217
Fig. 7.2 Working Model for sub-cellular transport of TBSV replicase proteins. 218

Chapter 1

INTRODUCTION

1.1 Tombusviruses

The group of tombusvirus belongs to positive strand RNA virus that replicate their genomes in a wild range of plant hosts (1). *Tomato bushy stunt virus* (TBSV) is the prototypical species in the Tombusvirus genus and tombusviridae family. TBSV has a single-stranded positive-sense RNA genome of ~4800 nucleotides long(1). Its RNA genome is highly structured with 5' non-capped end, 3' non-polyadenylated end, as well as many internal RNA elements which functions in viral protein translation enhancement, viral replicase complex assembly and replication (1-4).

TBSV encodes five viral proteins (1), the replication proteins p33 and p92; a capside protein p42, movement protein p22 and a suppressor of gene silencing p19. p33 and p92 are both required for viral replication (1). The sequence of p33 overlaps with N-terminal part of p92, and functions as auxiliary replication cofactor (5, 6), which is involved in template RNA recruitment(3) and replicase complex assembly (4) with RNA chaperone function (7). The p92 protein is a read-through product of p33, and has RNA dependent RNA polymerase (RdRp) activity. Both p33 and p92 have two trans-membrane domains(8, 9), which are predicted to be inserted into sub-cellular membranes and expose the N-terminal and C-terminal, including RdRp, regions of replication proteins to the cytosolic side of membranes. Besides association with the membrane, p33 and p92 could interact with each other through S1 and S2 p33:p33/p92 interaction

domains. This interaction leads to multimerization of replication proteins which is important for TBSV replication (10, 11).

Tombusviruses have been developed as model viruses for studies of (+)RNA virus replication in yeast (5, 12, 13). The tombusvirus system is based on trans-replication of a defective interfering (DI) RNAs in the presence of replication proteins p33/p92. DI RNAs are defective viral RNAs containing noncontiguous regions of the viral RNA genome due to recombination events (5, 14-17). In the yeast system, p33 and p92 are expressed from plasmids and support the replication of DI-72, the model replicon (13).

Carnation italian ringspot virus (CIRV) is another tombusvirus in the same genus and shows high sequence similarity with TBSV (14). Unlike TBSV, which use peroxisome membrane for replicase assembly(18), CIRV assembles its replicase complex on mitochondrial outer membrane (9, 19). Studies revealed that short motifs in TBSV and CIRV replication proteins p33/p92 (TBSV) or p36/p95 (CIRV) are required for replicase targeting to peroxisome (18) or mitochondria (19).

1.2 Subcellular locations of positive strand RNA virus replication

Positive strand RNA viruses are the largest group among the seven virus genetic classes (20). They cause many diseases in human history. Egyptian tombstone as early as 1500 BC recorded a priest having typical poliovirus infection syndrome of poliomyelitis (21). Recent epidemic of hepatitis C virus (22-25), dengue virus (26), West Nile virus (27, 28), severe acute respiratory syndrome (SARS) virus (29, 30) and many economically

important animal and plant viruses highlight the importance of understanding the positive strand RNA virus life cycle, and urgency of the discovery of novel medicines for curing viral diseases.

Positive strand RNA viruses share some common features: i) single-stranded RNA genome harboring ORFs on the sense-polarity (20, 31); ii) RNA genome replication occurs within specific sub-cellular membrane compartments of their eukaryotic host cells (15, 18, 20, 31-33); iii) Virion assembly often couples with genome replication (34-36). iv) Use of (-)RNA only as a template for asymmetrical replication. (37)

Despite the common feature of membrane association of (+)RNA viruses, subcellular locations of (+)RNA virus replication vary drastically throughout the whole endomembrane systems, including endoplasmic reticulum (ER) or ER derived replication organelles for bromovirus (38), potyvirus (38), flavivirus (34, 39, 40), arterivirus (41) and coronavirus (35); ER-Golgi intermediate compartment (ERGIC) for enterovirus (33); endosome for alphavirus (42); vacuole for Alfamovirus (43, 44) and tobamovirus (45); peroxisome for tombusvirus (18); mitochondria for nodavirus (46), carmovirus (47) and tombusvirus (48).

Questions were raised for these many replication sites. Why do (+)RNA viruses need to explore so many different locations for replication? Are selection of these sites random events during evolution, or some specific protein or lipid factors are determinants of subcellular membrane selectivity of different (+)RNA viruses? Is there any common pathway connecting different replication sites of (+)RNA viruses?

Tombusviruses are used as model viruses to address these questions. As two closely related viruses in genus of tombusvirus, TBSV and CIRV replicate in distinct subcellular locations (peroxisome and ER for TBSV, mitochondria for CIRV) (9).

In a host cell, due to post-translational targeting of viral replication proteins, TBSV replicase may already evolved to be peroxisome targeting and does not have a chance to meet other sub-cellular membrane, like mitochondria. However, in cell-free environment, viral protein and membrane may have a chance to interact, simply by diffusion of molecules. Could TBSV replicate on mitochondrial membranes in a cell-free environment? Or could CIRV replicate on ER or peroxisome membrane? To address these questions, an cell-free system was established for TBSV replication using yeast extract (49), which contains cytosolic proteins as well as total cellular membranes, including peroxisome, ER or mitochondria membranes.

In Chapter 2, a further modification of yeast cell-free extract will be used to explore sub-cellular membrane requirements of TBSV and CIRV replication. This study leads to a deeper understanding of (+)RNA virus replication sites. The method developed in chapter 2 was also used for identification and characterization of an inhibitory host factor, stress induced protein 1 (Sti1) co-chaperone, of CIRV replication. Results with Sti1 in tombusvirus replication will be discussed in Chapter 3.

1.3 Requirements of specific lipids for positive strand RNA virus replication

Although (+)RNA viruses adapted different subcellular locations for their replication, membranes of these organelles have one common feature: mainly composed of

phospholipids, among which glycerophospholipids are most abundant (50-53), while sphingolipids mostly occur in Golgi and the endosomal membranes count about 10% of total phospholipid content (51). Major glycerolphospholipids in eukaryotic cells include: phosphatidylcholine (PC), phosphatidylethanolamine (PE), phosphatidylserine (PS), phosphatidylinositol (PI) and phosphatidylglycerol (PG). PC is the most abundant phospholipids in eukaryotic cells (54), and it has an almost cylindrical shape which favors the organization of stable planar bilayer (51, 55). While PE is usually the second most abundant phospholipid species (54), it possesses a conical molecular structure (51, 55), which could introduce negative curvature when incorporated into stable bilayer and promotes membrane fusion (55-57). Other than PC and PE, which are neutral phosholipids, negatively charged phospholipids, such as PS, PG, PI or phosphorylated forms of PI, namely PIPs, bring negative charge to where they are enriched and could attract protein effectors specifically or non-specifically (58), like Rho GTPase (59), protein kinase C (60), SNARE protein vam7p (61) , which are involved in different cellular pathways. Since different phospholipids involve in regulating different cellular processes, they may regulate (+)RNA virus replication through their interactions with viral replication proteins.

Elevation of overall fatty acid synthesis was shown to facilitate many (+)RNA virus replication, including members of enterovirus, poliovirus (62) and coxsackievirus B3 (CVB3) (63), and members flavivirus, Dengue virus (64) and West Nile virus (65). Lipidomics analysis conducted with cells infected with Dengue virus and Hepatitis C virus (66, 67) suggest that viruses induce new lipids biosynthesis, and virus infection changes the global lipid profile of the host cell. These changes add a new level of

complexity of virus-host interaction. However, the question remains if specific lipid species or total lipids are more important to viruses?

In the past decade, virologists made different approaches to reveal interactions between specific phospholipid species and (+)RNA viruses. Enterovirus is among the most intensively studied viruses in this area. Phosphatidylinositol-4-phosphate (PI4P) was shown to be enriched with CVB3 (enterovirus, picornaviridae) replication proteins. RNA polymerase $3D^{pol}$ of poliovirus (PV, enterovirus, picornaviridae) selectively binds to PI4P (33), suggesting a PI4P-rich micro-environment is the site for enterovirus replication. Down-regulation of PI4P by Phosphatidylinositol-4-phosphate kinase (PI4K) inhibitor or knock-down of PI4K by PI4K specific siRNA reduced the cellular PI4P content as well as inhibited enterovirus replication. It was proposed that interaction of PI4P with enterovirus replication proteins is required for enterovirus replication. Recent findings (68, 69) showed that a mutant CVB3 with mutation in viral protein 3A could bypass the requirement of PI4P or PI4Ks without lost fitness and virulence (68), suggesting that PI4P is not required for the mutant CVB3 replication. It is interesting to note that RNA polymerase $3D^{pol}$ was not mutated in the mutant CVB3 and still kept the ability to interact specifically with PI4P, but the mutant virus did not require PI4P for replication, suggesting other lipids, if any, may be responsible for enterovirus replication. Nchoutmboube, J. et al. pulse-labeled PV infected HeLa cells with fluorescent fatty acid (bodipy-FA) and found that bodipy-FA was mostly converted to newly synthesized lipids which co-localized with PV replication proteins. Among the newly synthesized lipids, PC was the most abundant, suggesting that bodipy-FA labeled PC enriched at the site of PV

replication (62). Whether PC was enriched due to its abundant nature in the cell or because PV replication specifically requires PC is current not clear.

Hepatitis C Virus, hepacivirus genus, a member of Flaviviridae family, has been shown to require PI4P-enriched micro-environment for efficient replication (33, 70). While West Nile virus (WNV), flavivirus genus, a member of Flaviviridae family, does not require PI4P for its replication (65).

Besides phospholipids which form lipid bilayers needed for viral replicase assembly, sterols could also be important. Sterols affect lipid bilayer fluidity and are enriched within West Nile virus (71) and enterovirus (72) replication organelles and are required for efficient Dengue virus and enterovirus replication. Are phospholipids species less important for the virus than sterols? We don't know yet, but at least sterols cannot stably exist without being inserted into lipid bilayers.

In Chapter 4, a novel method of cell-free TBSV replication assay using artificial vesicles made from phospholipids will be shown to study phospholipids and TBSV-specific interaction. Then the findings of my research will be added to the discussion of previously raised questions, and shed new lights on this unexplored virology area. In Chapter 5 and 6, cellular pathways and mechanism of viral utilization of phosphatidylethanolamine will be discussed.

Chapter 2

AUTHENTIC *IN VITRO* REPLICATION OF TWO TOMBUSVIRUSES IN ISOLATED MITOCHONDRIAL AND ENDOPLASMIC RETICULUM MEMBRANES

(This chapter was published on Journal of Virology, December 2012 vol. 86 no. 23 12779-12794.,

2.1 Introduction

Replication of plus-stranded (+)RNA viruses takes place in membrane-bound viral replicase complexes (VRCs) in the cytoplasm of infected cells (13, 39, 73-79). Various (+)RNA viruses usurp different intracellular membranes, including ER, mitochondria, peroxisomes or endosomal membranes to aid the replication process. Other viruses induce the formation of “viral replication organelles” or “membranous web” made from various intracellular membranes (33, 39, 77, 79, 80). The recruited membranes are thought to facilitate virus replication by (i) providing surfaces to assemble the VRCs; (ii) sequestering and concentrating viral and host components; (iii) protecting the viral RNA and proteins from nucleases and proteases (81); and (iv) facilitating regulated RNA synthesis by harboring the (-)RNA template for production of abundant (+)RNA progeny.

The emerging picture with several (+)RNA viruses is that their replication proteins bind to different lipids and recruit a number of host proteins, which are involved in lipid synthesis, or modification, to the site of replication (33, 79, 82, 83). In addition, (+)RNA

virus replication is also dependent on bending intracellular membranes that form characteristic viral structures, such as spherules (vesicles with narrow openings) or vesicles (76). Therefore, (+)RNA viruses likely recruit host proteins affecting membrane curvature, as shown for ESCRT, reticulon and amphiphysin proteins in case of tombusviruses, *Brome mosaic virus* and *Semliki Forest virus* (81, 84-86). Lipids also affect membrane curvature and fluidity. Indeed, replication of several viruses has been shown to be affected by sterols, fatty acids and phospholipids (31, 71, 87-90).

Tomato bushy stunt virus (TBSV) is a small (+)RNA virus that has emerged as a model virus to study virus replication, recombination, and virus - host interactions due to the development of yeast (*Saccharomyces cerevisiae*) as a model host (1, 5, 79, 91, 92). Over 400 host genes/proteins that affected either TBSV replication or recombination have been identified via genome-wide screens of yeast genes or global proteomics approaches (12, 93-96). The highly purified tombusvirus replicase complex (VRC) is known to contain the two viral replication proteins (i.e., p33 and $p92^{pol}$) and 6-10 host proteins (97-99). These host proteins have different functions during TBSV replication. For example, heat shock protein 70 (Hsp70), eukaryotic elongation factor 1A (eEF1A) and the ESCRT (endosomal sorting complexes required for transport) family of host proteins are involved in the assembly of the VRC (75, 81, 86, 100-103). In addition, eEF1A and eEF1Bγ facilitate (-)strand synthesis (103, 104); glyceraldehyde-3-phosphate dehydrogenase (GAPDH) and Ded1 DEAD-box helicase have been shown to promote viral (+)RNA synthesis (37, 105, 106); while Pex19 shuttle protein is involved in targeting of the replication proteins to peroxisomes, the sites of replication (107).

The auxiliary p33 replication protein, which has RNA chaperone function, is an abundant protein and is essential for replication of TBSV in both yeast and plants (3, 7, 10, 32). The tombusvirus p33 is an integral membrane protein that has been shown to recruit the TBSV (+)RNA into replication. The current picture is that the p33 replication protein is the master regulator of TBSV replication by interacting with the viral RNA, $p92^{pol}$ and numerous host proteins and host membranes. The host also targets p33 or the viral RNA via nucleolin, cyclophilins or WW-domain proteins to limit tombusvirus infections (108-112). On the other hand, the viral $p92^{pol}$, which is a translational readthrough product containing the p33 sequence at its N-terminus and a unique RdRp domain at the C-terminus, is present in a lesser amount (1). Interaction between $p92^{pol}$ and p33 replication proteins is required for assembling the functional VRC (2, 10, 49, 92). Interestingly, the activation of the RdRp function of $p92^{pol}$ protein requires not only p33, *cis*-acting sequences present in the viral (+)RNA and host factors, but also host membranes (2-4, 92). This complex VRC assembly process and the many factors needed for the RdRp activation opens the exciting questions whether tombusviruses could utilize different cellular membranes or if various heterologous combinations of tombusvirus replication proteins are functional.

Most tombusviruses, including TBSV, Cucumber necrosis virus (CNV), and Cymbidium ringspot virus (CymRSV), show preference for peroxisomal membranes (10, 18, 113). Interestingly, these viruses can also replicate efficiently on the ER membrane in the absence of peroxisomes, suggesting flexibility in intracellular membrane utilization (15, 32, 107). Another tombusvirus, Carnation Italian ringspot virus (CIRV), however, prefers to use mitochondrial membrane for replication (19, 48). Artificial retargeting of

the CIRV replication proteins to the peroxisomes or CymRSV to the mitochondria via chimeric constructs also supported CIRV and CymRSV replication (114), suggesting that these viruses could utilize more than one intracellular environment for their replication. To analyze if tombusviruses are indeed capable of utilizing various intracellular membranes for their replication, we used in vitro approaches with recombinant viral proteins and isolated intracellular organelles/membranes. Interestingly, we found that TBSV, which originally uses the peroxisomal membrane, could also utilize ER and mitochondrial membranes for replication *in vitro*. On the other hand, CIRV, which originally utilizes the mitochondrial membranes, replicated on the isolated mitochondrial membranes, while it could use the ER membrane less efficiently in vitro. Using heterologous combinations of replication proteins and chimeric constructs, we identified that multiple domains in the replication proteins are determinants of membrane preference for tombusvirus replication. Altogether, the current paper promotes the idea that TBSV is less restricted, while CIRV is more restricted in utilizing various intracellular membranes for replication.

2.2 Materials And Methods

Yeast strains and expression plasmids. Saccharomyces cerevisiae strain Saccharomyces cerevisiae strain BY4741 (MATa his3Δ1 leu2Δ0 met15Δ0 ura3Δ0) and single-gene deletion strains pex3 were obtained from Open Biosystems. Constructs pMAL-p33 and pMAL-p92, to express TBSV p33 (renamed here as T33) and p92 (re-

named as T92) as fusion proteins to the C-terminus of MBP were described previously (102).

To generate the E. coli expression constructs pMAL-p36, pMAL-p95, pMAL-C36-T92, pMAL-T33-C95, pMAL-T33c, pMAL-T92c, pMAL-T33tc, and pMAL-T92tc, we used the following approaches: The CIRV p36 sequence was amplified from CIRV full-length cDNA (obtained from A. White, York University, Canada) with primers #642 (5'-GTATTTGACACCGAGGG-3') and #3230 (CCGCTCGAGCTATTTGACACCGAGGGATT). The CIRV p95 sequence was obtained by blunt-end ligation of PCR product of C36 amplified by primer #642 and #643 (GGAGGCCTAGTGCGTCTAC) from CIRV cDNA and the C95 C-terminal sequence was amplified by PCR using primers # 644 (GGAGCTCGAGCTATTTGACACCCAGGGAC) and #970 (CCTAGGGAAAAACTGTCGGTA) and CIRV cDNA. C36-T92 chimeric sequence was obtained by blunt-end ligation of PCR product of C36 sequence PCR-amplified with primers #642 and #643 using CIRV full-length cDNA, and T92 C-terminal sequence was amplified by PCR with primers #6 (GGAGGCCTAGTACGTCTAC) and #826 (GATTACATTGTCCCTCTATCT) using TBSV full-length cDNA. T33-C95 chimeric sequence was obtained by blunt-end ligation of PCR products of T33 [generated by PCR with primers #473 (GAGGAATTCGAGACCATCAAGAGAATG) and #3960 (GTATTTGACACCCAGGGAC)] and C-terminal sequence of C95 (generated by PCR with primers #644 and #970). The T33c sequence was obtained by blunt-end ligation of PCR product using primers #642 and #4102 amplified from CIRV cDNA and PCR product using primers #4099 and #810 amplified from TBSV cDNA. The T92c sequence

was obtained by blunt-end ligation of T33c (generated by PCR with primers #642 and #3960) and T92 C-terminal sequence. The T33tc sequence was obtained by blunt-end ligation of PCR product using primers #642 and #4090 (ACGAGCCACACCCCGTTTAGC) and CIRV cDNA and the PCR-product generated by using primer #4087 (GATTACATTGTCCCTCTATCT) and #810 (CCCGCTCGAGTCAAGCTACGGCGGAGTCGAGGA) and TBSV cDNA. The T92tc sequence was obtained by blunt-end ligation of T33tc (generated by PCR using primers #642 and #3960) and the PCR-amplified C-terminal sequence of T92. All the above PCR products were digested by EcoRI and XhoI restriction enzymes and inserted into pMAL-c2X (New England BioLabs).

To generate N-terminal GST-His6 fusion proteins, the C-terminal sequence of TBSV p33 was PCR-amplified using primers #633 (GGAGGAATTCATGGAGGGTTTGAAGGC) and #1593 (CGGCTCGAGCTATTTGACACCCAGGGACTCCTGT) and TBSV cDNA. The C-terminal sequence of CIRV p36 was PCR-amplified using primers #633 (GGAGGAATTCATGGAGGGTTTGAAGGC) and #3230 (CCGCTCGAGCTATTTGACACCGAGGGATT) and CIRV cDNA. The PCR products were digested with BamHI and XhoI and cloned into BamHI/XhoI digested pGEX-His (111).

To generate pGD-L-T33, pGD-L-T92, pGD-L-C36, pGD-L-95 constructs for agro-infiltration in plants, the PCR product of TBSV p33 sequence [using primers: #788 (GGAGCTCGAGTCAAGCTACGGCGGAGTC)/ #810 (CCCGCTCGAGTCAAGCTACGGCGGAGTCGAGGA)] was digested with BamHI

and XhoI; the TBSV p92 sequence [obtained using primers: #4000 (CCAGAGATCTATGGAGACCATCAAGAGAATG) / #826 (GATTACATTGTCCCTCTATCT)] was digested with BglII and XhoI, the PCR product of CIRV p36 sequence [obtained using primers: #900 (ACGAGCCACACCCCGTTTAGC) / #3230 (CCGCTCGAGCTATTTGACACCGAGGGATT)] was digested with BamHI and XhoI, while the PRC product of CIRV p95 sequence [obtained using primers: #900 (ACGAGCCACACCCCGTTTAGC) / #970 (CCTAGGGAAAAACTGTCGGTA)] was digested with BamHI and XhoI. Then, the above PCR products were separately inserted into pGD-L (81), which was digested with BamHI and XhoI, generating transient expression vectors for agro-infiltration.

For the imaging experiments, we have constructed the following plasmids: pESC-T33/DI72, pESC-C36/DI72, pYES-T92 and pYES-C95. For this, sequences of full-length TBSV p33 (primers: #788/#810), CIRV p36 (primers: #900/#3230) and p95 (primers: #900/#970) were PCR-amplified and digested with BamHI and XhoI, while the PCR-amplified sequence of TBSV p92 (primers: #4000/#826) were digested with BglII and XhoI. Digested PCR products were then inserted into pESC-HisCNVp33-DI72, or pYES-CNVp92 digested with BamHI/XhoI.

To track viral protein localization in yeast cells, we cloned rsGFP (red-shifted) sequence upstream of the N-terminus of TBSV p33/p92, and CIRV p36/p95. The rsGFP sequence was PCR-amplified with primers #1262 (CGGCGGATCCGGTAAAGGAGAAGAACTTTTCACT) and #1263 (CGGCGGATCCGAGTCCGGACTTGTATAGTTCA) using pGDG vector as a template

[provided by Dr. M. Goodin (115)], followed by digestion with BamHI and inserted into pESC-C36/DI72 or pYES-C95 digested with BamHI, generating pESC-rsGFP-C36/DI72 and pYES-rsGFP/C95. The cDNA sequence of TBSV p33 was PCR-amplified using primers #4000/#810, while the cDNA sequence of TBSV p92 was PCR-amplified with primers #4000/#826. The obtained PRC products were digested with BglII, followed by ligation with the PCR-amplified rsGFP sequence digested with BamHI, generating the cDNAs of rsGFP-T33 and rsGFP-T92. Then, the cDNAs of rsGFP-T33 and rsGFP-T92 were digested with BamHI and XhoI, and inserted into pESC-C36/DI72 or pYES-C95 digested with BamHI/XhoI, resulting in pESC-rsGFP-T33/DI72 and pYES-rsGFP-T92 expression plasmids.

Agroinfiltration and RNA extraction. *N. benthamiana* leaves were agroinfiltrated with *A. tumefaciens* cultures containing combinations of pGD-L-T33, pGD-L-T92, pGD-L-C36 or pGD-L-C95 as well as pGD-DI72sat and pGD-p19 as described (81). After 3.5 days post infiltration, agro-infiltrated leaves were collected, total RNA was extracted and subjected for Northern blot analysis as described (81).

Preparation of CFE and soluble fraction (S100). The yeast CFE from BY4741yeast strain was prepared as described (49). For production of S100 soluble fraction, yeast CFE was further centrifuged at 100,000 g for 1 hour, and the supernatant (S100) was carefully collected without disturbing the pellet, and then stored at –80°C.

Purification of yeast microsomal membranes. Yeast microsomes were prepared as

previously described (116), except that yeast microsomes were washed in 30 mM HEPES-KOH, pH 7.4, 150 mM potassium acetate, 2 mM magnesium acetate, containing complete mini Protease Inhibitor Cocktail (Roche applied science). The protein concentration of obtained yeast microsomal membranes was 4 mg/ml.

Purification of intact yeast mitochondria. Yeast intact mitochondria were purified according to REF.: (117). Briefly, yeast cells were made into spheroplasts by incubating with 5 mg/g (wet weight) Zymolyase-20T (Seikagaku, America), and then the spheroplasts were homogenized and lysed with glass Dounce homogenizer in ice-cold homogenization buffer (0.6 M sorbitol, 10 mM Tris-HCl, pH 7.4, 1 mM PMSF, 0.2% (w/v) BSA). Then, the homogenized spheroplasts were centrifuged at 3,000 g for 5 min at 4°C and the supernatant was subjected to additional centrifugation at 12,000 g for 15 min to obtain the crude mitochondria preparation. To further remove contaminating membranes, the crude mitochondrial preparation was subjected to two sequential centrifugations at 134,000 g on a sucrose gradient (0.7 ml 60%, 1.5 ml 32%, 0.7 ml 23% and 0.7 ml 15% (w/v) sucrose with 1mM EDTA and 10 mM MOPS-KOH). The purified mitochondrial preparation was recovered between the 60% / 32% sucrose gradient interface and stored in SEM buffer [250 mM sucrose, 1 mM EDTA, 10 mM MOPS-KOH, pH 7.2, containing complete mini Protease Inhibitor Cocktail (Roche applied science)] at -80°C. The protein concentration was about 3 mg/ml.

Isolation of oleate-induced peroxisomes using sucrose gradients. The isolation of peroxisomes was according to REF.: (118). Yeast was grown in peroxisome induction

medium containing 0.12% (w/v) oleic acid, 0.2% Tween 40, 0.5% Bacto peptone and 0.3% yeast extract till 1.0 OD_{600}. Cell wall was digested with Zymolyase to generate spheroplasts in MES buffer (5 mM MES pH5.5, 1 mM EDTA, 1 mM KCl) with 1.2 M sorbitol, and homogenized by gradually adding MES buffer until sorbitol concentration reached to 0.65 M. Unlysed cells and cell debris were removed by centrifuging at 2,000 g, and crude peroxisome preparations were collected via centrifugation at 20,000 g. The crude peroxisome preparations were applied to a linear sucrose gradient (10%-80%) using Beckman VTi 50 rotor at 34,500 g for 2.5 hours. Fractions were collected and stored at -80°C. Before in vitro replicase assembly assay, each membrane fraction (100 µl) was thawed on ice and diluted 5x with 30% sucrose/MES buffer, followed by centrifugation at 20,000 g for 30 min. Then, the pellets of each fraction were carefully suspended into 10 µl of 30% sucrose/MES buffer. The protein density in peroxisome fractions #11 to #16 was about 1 mg/ml.

In vitro replication assay. The yeast CFE-based replication assay was modified from Ref: (54) to study TBSV and CIRV replication using the isolated organelle preparations. The yeast cell extract (2 µl) or purified membrane fractions (1 µl) together with S100 soluble fraction (1 µl) was incubated at 25°C water bath for 1 hour in 8 µl cell-free replication buffer A containing 30 mM HEPES-KOH, pH 7.4, 150 mM potassium acetate, 5 mM magnesium acetate, 0.6 M sorbitol, as well as 15 mM creatine phosphate; 1 mM ATP, CTP, GTP and 0.025 mM UTP; 0.1 µl of [32P]UTP, 0.1 mg/ml creatine kinase, 0.1 µl of RNase inhibitor, 10 mM dithiothreitol, 0.5 µg DI-72 RNA transcript and 0.5 µg recombinant MBP-fused viral proteins. Then the volume of reaction was adjusted by

adding 16 □l cell-free replication buffer B containing 30 mM HEPES-KOH, pH 7.4, 150 mM potassium acetate, 5 mM magnesium acetate, together with 15 mM creatine phosphate; 1 mM ATP, CTP, GTP and 0.025 mM UTP; 0.2 µl of [32P]UTP, 0.1 mg/ml creatine kinase, 0.2 µl of RNase inhibitor, 10 mM dithiothreitol, 0.05 mg/ml actinomycin D. The reaction mixture was incubated at 25°C for 3 h. The reaction was terminated by adding 110 µl stop buffer (1% sodium dodecyl sulfate [SDS] and 0.05 M EDTA, pH 8.0), followed by phenol-chloroform extraction, isopropanol-ammonium acetate precipitation, and a washing step with 70% ethanol. RNA samples were electrophoresed in denaturing gel (5% PAGE containing 8 M urea) and analyzed by phosphorimager(Typhoon; GE). To test the effect of sorbitol on in vitro tombusvirus replication, the purified membrane preparations (1 µl) together with S100 fraction (1 µl) was incubated at 25 °C water bath for 4 hour in 24 □l of modified cell-free replication buffer A containing 0, 0.2 and 0.6 M sorbitol.

Micrococcal nuclease treatment of the in vitro replication assay mixture. The The replication assay was conducted as described above, except that at different time points of the reaction, each sample was treated with 0.25 U/µl micrococcal nuclease and 1 mM $CaCl_2$ at different time point after staring of the incubation in the replication buffer A as described previously (54). 2.5 mM EGTA was added to each sample after 15 min incubation of micrococcal nuclease to stop the nuclease digestion.

Replication assay to determine viral (+)RNA/(−)RNA ratio. This assay was done as described in a previous publication (95). Briefly, 2 µg of *in vitro* transcripts of minus-

strand and plus-strand DI-72 RNAs were separately dot blotted onto a Hybond XL membrane (Amersham) followed by UV cross-linking. *In vitro* replication products were hybridized to the blots in ULTRAhyb solution (Ambion) at 68°C and quantified after washing.

Western blotting. Western blotting of yeast membrane proteins was done according to REF.: (100). The following antibodies were used: anti-porin, anti-ALP, anti-PGK and anti-dpm1 (purchased from Invitrogen, CA, USA). Sec61p antibody was provided by Dr. Tom Rapoport from Harvard Medical School. Fox3p antibody was provided by Dr. Daniel J. Klionsky from University of Michigan.

In vitro membrane association assay. [35S]methionine-labeled TBSV p33 and CIRV p36 were obtained in nuclease-treated rabbit reticulocyte lysates (Promega) in the presence of 400 μCi/ml [35S]methionine. 1 □l of translation mixture was incubated at 25°C for 1 hour with 2 □l purified yeast microsomes or purified yeast mitochondrial preparations and 2 □l S100 fraction in 40 □l reaction containing cell-free replication buffer A (30 mM HEPES-KOH, pH 7.4, 150 mM potassium acetate, 5 mM magnesium acetate, 0.6 M sorbitol) as well as 15 mM creatine phosphate; 1 mM rNTP; 0.1 mg/ml creatine kinase, 0.1 μl of RNase inhibitor, 10 mM dithiothreitol, 0.5 μg DI-72 RNA transcript. Each reaction mixture was diluted 3 times with the cell-free reaction buffer A, followed by incubation on ice for 30 min. The samples were centrifuged at 100,000 g for 2 hours. Pellet was dissolved in SDS-PAGE sample buffer. Proteins from the supernatant fractions were precipitated in 10% trichloroacetic acid (TCA) and dissolved in SDS-

PAGE sample buffer. Samples were separated by SDS-PAGE.

In vitro MBP pulldown assay. MBP-tagged TBSV T33 (p33), T92 (p92), CIRV C36, C95 and GST- His_6-tagged TBSV p33C and CIRV p36C were expressed in *E. coli*, transformed with one of the following plasmids: pMAL-T33, pMAL-T92, pMAL-C36, pMAL-C95, pGEX-his-T33C, pGEX-his-C36C. *E. coli* cultures were lysed by sonication, followed by affinity-purification via amylose columns and washed with cold column buffer with high salt (10 mM Tris-Cl, pH 7.4; 1 mM EDTA, 200 mM NaCl, 10 mM 2-mercaptoethanol) as described (119). The GST-His_6-tagged p33C, GST-His_6-p36C or GST-His_6 (negative control) were incubated with the MBP-tagged proteins for 1 hour at 4 °C and washed by column buffer with high salt. The bound proteins were eluted with column buffer with high salt supplemented with 10 mM maltose (119). The presence of GST-tagged proteins was analyzed by SDS-PAGE and Western blotting using an anti-GST antibody.

Confocal laser microscopy. Visualization of Pho86-CFP ER marker protein and various combination of tagged viral proteins in live yeast cells were as described previously (32, 107). To visualize yeast mitochondrial distribution of various viral proteins, we transformed yeast with combinations of plasmids: pESC-GFP-T33/DI72, pESC-GFP-C36/DI72, pYES-GFP-T92 or pYES-GFP-C95 with pESC-T33/DI72, pESC-C36/DI72, pYES-T92 and pYES-C95 as described in the legend to Fig. 2.9. Transformed yeast were grown at 23°C in minimal media supplemented with 2% galactose, and then we used Rhodamine B (hexyl ester-perchlorate, a mitochondria-specific dye used in yeast, Catalog

R-648MP, Invitrogen, CA, USA) to visualize yeast mitochondria (120-122) with an Olympus FV1000 microscope (Olympus America Inc., Melville, New York).

2.3 Results

CIRV replication proteins support RNA replication in yeast cell-free preparations in vitro. We have previously shown that TBSV can efficiently replicate in cell-free extracts (CFE) prepared from yeast (4, 49, 102). The CFE-based TBSV replication assay contained purified recombinant TBSV p33 and $p92^{pol}$ replication proteins and T7 polymerase-made DI-72 (+)-stranded replicon (rep)RNA transcripts. The CFE supported one single cycle of replication, starting with (-)RNA synthesis on the added (+)repRNA transcripts, followed by robust synthesis of (+)repRNA progeny (4, 49, 102). The CFE-based assay recapitulated the known features of TBSV replication, including the requirement of *cis*-acting viral RNA elements, dependence on viral and host factors and the need for both membranous and soluble fractions of CFE. Other features of the assay included asymmetrical replication, leading to 10-to-40-fold more (+) than (-)RNA; association of the VRCs with membranes that led to protection against ribonucleases and proteases after the assembly of VRCs; the release of (+)repRNA progeny to the soluble fraction during the reaction, while retaining the (-)repRNA in the VRCs (4, 49, 102).

To test if CIRV replication proteins, which are originally associated with mitochondrial membranes (19, 48), could support repRNA replication in the CFE-based assay, we added purified recombinant p36 and $p95^{pol}$ (called C36 and C95 in this paper to discriminate them form the homologous TBSV p33 and $p92^{pol}$, named T33 and T92) in combination with the TBSV-derived DI-72(+) repRNA to yeast CFE. Interestingly, we

observed the replication of repRNA in samples containing both C36 and C95 (Fig. 2.1A, lane 7), which reached about 10% of that supported by T33/T92 (lane 1). No replication was observed when C95 protein was omitted from the CFE-based assay (Fig. 2.1A, lane 8), confirming that both CIRV replication proteins are required for repRNA replication. The supernatant or membrane fractions of CFE alone or the Triton X100-treated CFE could not support repRNA replication in the presence of C36 and C95 (Fig. 2.1A, lanes 10-12), similar to that observed with T33/T92 (lanes 4-6). Thus, these experiments showed that the CIRV C36/C95 replication proteins could support repRNA replication in CFE, albeit with reduced efficiency when compared with the TBSV T33/T92 replication proteins.

To further test the CIRV replication process in the yeast CFE, we estimated the ratio of newly made (+)-strand versus (-)-strand repRNA levels in the replication assay (Fig. 2.1C). This showed that, similar to the TBSV replication proteins, the CIRV replication proteins also performed asymmetrical viral RNA synthesis by producing ~10 times more new (+)-strands than (-)-strands in the yeast CFE (Fig. 2.1C).

Since the repRNA was the TBSV-derived DI-72 in the above assays, it is possible that the reduced replication was due to the less efficient utilization of the heterologous repRNA by the CIRV replication proteins in comparison with repRNA replication supported by the homologous TBSV replication proteins. To test this possibility, we also used the CIRV-derived DI-1 repRNA (14) in the CFE-based assay. These experiments revealed that both repRNAs were used more efficiently by T33/T92 than C36/C95 in vitro (Fig. 2.1B, and D, lanes 1-2 versus 3-4). Thus, the viral replication proteins determine the efficiency of repRNA replication in this assay.

Heterologous combinations of replication proteins supports RNA replication in yeast cell-free preparations in vitro and in planta. To test if the heterologous combinations of tombusvirus replication proteins could support repRNA replication, we used the CFE-based assay with the purified recombinant proteins. The CFE-based assay revealed that the heterologous combinations of replication proteins did support repRNA replication (Fig. 2.1B and D, lanes 5-8), albeit less efficiently than T33/T92 (Fig. 2.1B and D, lanes 1-2). Moreover, we observed that the viral RdRp protein was the major factor controlling the efficiency of repRNA replication. Accordingly, the homologous combination of T33/T92 (Fig 2.1B and D, lanes 1-2) or the heterologous combination of C36/T92 (lanes 5-6) supported more efficient replication than C36/C95 (lanes 3-4) or T33/C95 (lanes 7-8). Thus, it seems that T92 RdRp protein is ~6-20-fold more active in the CFE-based assay than C95 RdRp. However, the small replication protein also affected the efficiency of replication since the combinations of replication proteins that included T33 supported up to ~3-fold more replication than C36 in a complex with the RdRp protein (compare T33/T92 versus C36/T92; Fig. 2.1B and D, lanes 1-2 versus 5-6).

To test if the tombusvirus replication proteins behave similarly in plant cells, we used an agro-infiltration-based approach to express the TBSV and CIRV replication proteins and DI-72 repRNA in *Nicotiana benthamiana*. These experiments also revealed that T33/T92 combination supported repRNA replication more efficiently (Fig. 2.2, lanes 1-4) than C36/C95 (lanes 5-8). However, the use of heterologous combination of tombusvirus replication proteins revealed that T33 replication protein and not the T92 replication protein is responsible for the enhanced level of replication in plants (Fig. 2.2).

This difference between *in vitro* and *in planta* data could be due to the ability of T33 or C36 to induce membrane proliferation in plant cells that promote more efficient replication (these features cannot manifest in the CFE). Nevertheless, the *in planta* experiments demonstrated that the heterologous combinations of tombusvirus replication proteins are functional in supporting repRNA replication.

Tombusvirus replication depends on the interaction between the S1/S2 subdomains common in the T33/C36 RNA chaperone and T92/C95 RdRp proteins, which is needed for the assembly of the functional VRC (11). The above observations that the heterologous combinations of tombusvirus replication proteins support tombusvirus RNA replication in the CFE assay and *in planta* suggest that the heterologous replication proteins likely interact with one another. To test the heterologous interactions, we performed pull-down assay with immobilized MBP-tagged viral replication proteins and the GST-tagged T33C (the C-terminal half, p33C) or GST-C36C (the C-terminal half, p36C). This assay confirmed interaction between the heterologous replication proteins that were comparable with the interaction between the homologous replication proteins (Fig. 2.2B).

Tombusviruses can replicate in microsomal and mitochondrial preparations in vitro. To better understand the role of different subcellular membranes in tombusvirus replication and to test what subcellular membranes can be used for repRNA replication by TBSV and CIRV replication proteins *in vitro*, we isolated microsomal (representing the ER membrane), peroxisomal and mitochondrial fractions from yeast, followed by in vitro replication assay with purified recombinant tombusvirus replication proteins (Fig.

2.3A). Interestingly, we found that the microsomal preps, which lacked detectable peroxisomal and mitochondrial marker proteins (Fig. 2.3B, bottom panels), supported repRNA replication ~16-fold more efficiently in the presence of T33/T92 than C36/C95 and the S100 fraction of CFE (the membrane-free supernatant that provides essential soluble host proteins) (Fig. 2.3B, lane 1 versus 2). These data suggest that the isolated ER membrane can support the assembly of both TBSV and CIRV VRCs, although the CIRV replication proteins show poor activity in this environment.

To test if viral RNA synthesis includes the full cycle of replication in the microsomal preparations, we estimated the ratio of newly made (+)-strand versus (-)-strand repRNA levels in the *in vitro* replication assay (Fig. 2.3C). Interestingly, both TBSV and CIRV replication proteins supported asymmetrical viral RNA synthesis by producing ~11-14 times more new (+)-strands than (-)-strands in the microsomal preparations (Fig. 2.3C). Thus, even CIRV replication proteins are capable of supporting full replication, albeit less efficiently than the TBSV replication proteins, in the microsomal preparations.

Similar experiments with purified mitochondrial preparations revealed that both TBSV and CIRV replication proteins supported repRNA replication *in vitro* (Fig. 2.3D). Thus, unlike with the microsomal preparations, the CIRV replication proteins are fully active on the mitochondrial membrane, which is also used by CIRV in yeast and plants (19, 48). Both TBSV and CIRV replication proteins supported asymmetrical viral RNA synthesis by producing ~9-10 times more new (+)-strands than (-)-strands in the mitochondrial preparations (Fig. 2.3E). Thus, these data indicate that the mitochondrial membrane can support full TBSV and CIRV replication *in vitro*.

Unfortunately, the isolated oleate-induced peroxisomal preparations did not support repRNA replication with TBSV and CIRV replication proteins (not shown). Therefore, we decided to test tombusvirus RNA replication using sucrose-gradient fractionated crude mitochondrial and peroxisomal preparations (Fig. 2.4). We found that fractions 12 to 16 of the crude peroxisomal preparation (obtained from yeast after induction with oleic acid), which had the highest concentration of Fox3 peroxisomal marker (Fig. 2.4A, lanes 12-16), while contained Sec61 ER marker or porin mitochondrial marker proteins in small amounts, did not support repRNA replication by C36/C95 and T33/T92. The only repRNA replication with C36/C95 and T33/T92 was seen with fractions 3-to-11, which contained the highest amount of contaminating ER and mitochondrial membranes (based on the presence of Sec61 ER and porin mitochondrial marker proteins in these fractions) (Fig. 2.4A, lanes 3-11). Based on these data, we conclude that the peroxisomal preparations obtained from yeast induced by oleic acid cannot support tombusvirus replication *in vitro*. This could be due to the fragile nature of the peroxisomes during the isolation procedure or other unknown factors.

In contrast, fractions 17 and 18 of the crude mitochondrial preparation (after high speed centrifugation in sucrose-gradient) supported repRNA replication by C36/C95 and T33/T92 at the highest efficiency (Fig. 2.4B, lanes 17-20). These fractions were enriched for mitochondria since they had the porin mitochondrial marker protein in the highest concentration, but contained Sec61 ER marker or peroxisomal, vauolar and cytosolic markers at low levels These data confirmed that the enriched mitochondrial membrane could provide suitable environment for tombusvirus VRC assembly and repRNA replication *in vitro*.

Since the ER membrane has been shown to support efficient TBSV replication in yeast (32, 107), we decided to use both the purified microsomal and mitochondrial preparations for the follow up experiments. Accordingly, to further test if the microsomal and mitochondrial preparations could assemble authentic tombusvirus VRCs, we performed time-course experiments with micrococcal nuclease, which digests the unprotected viral RNA (Fig. 2.5A) (49, 102). Interestingly, similar to CFE (49, 102), both microsomal and mitochondrial preparations with C36/C95 and T33/T92 replication proteins protected ~15-24% of the newly made ^{32}P-labeled repRNA (representing the minus- and plus-stranded replication products) if added 60 min after the start of the assay (Fig. 2.5B-C, lanes 5 and 15). The addition of micrococcal nuclease during the first 15 min of the assay eliminated repRNA synthesis (Fig. 2.5B-C, lanes 2 and 12), likely due to the lack (or incomplete) of VRC assembly, which takes 30-60 min *in vitro* (49, 102). Altogether, we observed that the recruited repRNA becomes nuclease-protected after 30-45 min in the microsome preparation in the presence of the viral replication proteins (Fig. 2.5B, lanes 3 and 13), while it takes 45-60 min in the mitochondrial preparation to assemble VRC and protect the recruited repRNA from micrococcal nuclease (Fig. 2.5C, lanes 4-5 and 14-15). These data suggest that both microsomal and mitochondrial preparations with C36/C95 and T33/T92 replication proteins could assemble authentic VRCs that protect the VRC-bound viral RNA from nucleases. In addition, it seems that the VRC assembly with C36/C95 and T33/T92 replication proteins is faster in the microsomal than in the mitochondrial preparations.

Osmotic pressure is important during the isolation of pure and intact mitochondria (117). To test if the osmotic pressure is important during tombusvirus replication *in vitro*

in microsomal or mitochondrial membranes, we compared the effect of different concentrations of sorbitol in the assay buffer. We found that in the absence of sorbitol in the assay buffer, neither TBSV nor CIRV could replicate in microsomal or mitochondrial preparations (Fig. 2.5D, lanes 3 and 7). These data suggest that intact microsomal or mitochondrial membranes should be maintained to support viral VRC assembly or replication. On the other hand, the purified tombusvirus replicase does not require sorbitol for RNA synthesis *in vitro* (2, 92), excluding that the replicase depends on sorbitol for function. We propose that the sorbitol is needed in the assay buffer to keep the organellar membranes intact and functional during the assay.

Multiple domains within the replication proteins are responsible for different level of tombusvirus replication in ER or mitochondrial membranes. To test what domain of the tombusvirus replication proteins is responsible for the observed differences between the TBSV and CIRV in utilizing microsomal and mitochondrial membranes, first we used heterologous combinations of CIRV and TBSV replication proteins to support RNA replication *in vitro* based on microsomal and mitochondrial preparations. Interestingly, the heterologous combination of C36/T92 supported repRNA replication almost as efficiently as the homologous combination of T33/T92 (Fig. 2.6A, lanes 5-6 versus 1-2) in the microsomal preparation, while combinations of C36/C95 and T33/C95 replication proteins supported repRNA replication only at ~10-15% level of T33/T92 (Fig. 2.6A, lanes 3-4, and 7-8 versus 1-2). Thus, we conclude that the T92 RdRp protein is far more active than the C95 RdRp protein and T92 is the major determinant of the efficient use of the ER membrane for *in vitro* repRNA replication. In addition, we note that T33

replication cofactor has a better stimulatory effect on the activity of the tombusvirus replicase than C36 replication cofactor in case of the ER membrane.

The picture was different with the mitochondrial preparation because of the improved stimulatory effect of the C36 replication cofactor on the activity of the tombusvirus replicase (Fig. 2.6B). Accordingly, high replication level was supported by C36/T92 and C36/C95 combinations (Fig. 2.6B). While the homologous combination of T33/T92 supported high level replication (Fig. 2.6B, lanes 1-2), the heterologous combination of T33 and C95 supported the lowest level of repRNA replication (Fig. 2.6B, lanes 7-8), suggesting that the T33 protein is less efficient than C36 in the mitochondrial membrane. The observed differences between T33 and C36 is unlikely due to differences in membrane associations, since we found that both T33 and C36 replication proteins associated with microsomal and mitochondrial membranes efficiently *in vitro* (Fig. 2.6C-D).

Since the tombusvirus RdRp proteins have two major domains (Fig. 2.7A), we have made chimeric constructs between the TBSV T92 and CIRV C95 proteins as shown in Fig. 2.7B. The N-terminal domain of the TBSV T92 and CIRV C95 RdRp proteins is identical with the T33 or C36 co-factor proteins (Fig. 2.7A), while the C-terminal domain harbors the highly conserved RdRp functional motifs. Testing the chimeric RdRp proteins in microsomal preparations revealed that C36-T92 (in combination with C36 co-factor), carrying the RdRp domain of the TBSV T92 and the N-terminal C36 domain, supported repRNA replication up to 40% level of combination of T33 co-factor and T92 RdRp (Fig. 2.7C, lanes 7-8 versus 1-2). In contrast, the chimeric T33-C95 RdRp protein (in combination with T33 co-factor) supported repRNA replication poorly in microsomal

preparations (lanes 5-6). Thus, these experiments indicate that the C-terminal RdRp domain in T92 is responsible for the efficient utilization of the ER membrane, while the homologous RdRp domain of C95 is less efficient in this environment. The data also support that T33 over-lapping domain within the RdRp protein is more active in the ER than the C36 over-lapping domain.

Similar experiments with mitochondrial preparations revealed that the RdRp domain of the TBSV T92 is still ~3-fold more active than the corresponding domain of the CIRV C95 (compare the chimeric C36-T92 RdRp with C95 RdRp in combination with C36 co-factor, lanes 7-8 versus 3-4, Fig. 2.7D). However, we also observed a ~2-fold stimulatory effect of C36 over-lapping domain when present in the RdRp protein (compare the chimeric C36-T92 RdRp with T92 RdRp, lanes 7-8 versus 1-2, Fig. 2.7D). In addition, T33 co-factor and T33-C95 RdRp combination supported low level of repRNA replication, demonstrating that the T33 over-lapping domain is poorly adapted to the mitochondrial membrane, as noted above with the heterologous combination of replication proteins (Fig. 2.6B, lanes 7-8).

Since it seems that the T33 protein and the T33 over-lapping domain when present in the RdRp protein is not well suited to support RNA replication in the mitochondrial membrane when compared with C36 cofactor, we made chimeras between T33 and C36 and their corresponding domains in the RdRp proteins as shown in Fig. 2.8A, D. We have divided T33 and C36 sequences into three subdomains: the N-terminal subdomain known to be involved in intracellular localization of T33 and C36 cofactors (10, 18, 48); the central subdomain that includes the two trans-membrane sequences (TMD); and the C-terminal subdomain involved in protein-RNA and protein-protein

interactions (11, 119, 123).

Testing the chimeric constructs in the mitochondrial preps revealed that replacing the N and TMD subdomains of T33 with those of C36 in T33 cofactor and T92 RdRp resulted in a highly active chimera (T33c and T92c), which replicated the most efficiently (Fig. 2.8C, lanes 5-6 versus 1-2). This chimera, however, replicated the repRNA more efficiently even in the microsome preparations (Fig. 2.8B, lanes 5-6 versus 1-2), suggesting that chimeric tombusviruses might have increased potential to replicate in various intracellular membranes. These observations could be relevant for the evolution of tombusviruses (see Discussion).

Combinations of heterologous replication proteins show both ER and mitochondrial localization in yeast. The *in vitro* data show that TBSV can efficiently replicate in both ER and mitochondrial membranes, while the CIRV replication proteins favor the mitochondrial membrane over the ER membrane to support viral repRNA replication. To test if the tombusvirus replication proteins can indeed utilize these membranes in cells, we performed localization studies with GFP-, YFP- and CFP-tagged proteins in yeast using homologous and heterologous combinations of the tombusvirus replication proteins.

As expected, the homologous combination of T33/T92 localized mostly in the ER membrane in yeast (in *pex3Δ* yeast to mimic the *in vitro* situation with isolated microsomal preparations by using yeast lacking peroxisomes) based on the Pho86 ER protein, while only a small fraction of C36 and C95 localized to the ER membrane, albeit these proteins were frequently located in the vicinity of the ER (Fig. 2.9A). On the contrary, the homologous combination of C36 and C95 localized mostly in the

mitochondrial membranes in yeast based on Rhodamine B-staining (a mitochondrial dye used in yeast) (120-122), while only a small fraction of T33 and T92 localized in the mitochondrial membranes (Fig. 2.9B). Indeed, most of T33 and T92 proteins did not co-localize with MTS-CFP mitochondrial marker protein or with Rhodamine B mitochondrial dye (Fig. 2.9B). Altogether, these experiments established that the homologous combination of T33/T92 is mostly localized in the ER (in *pex3Δ* yeast) and a fraction in the mitochondria, while C36/C95 is located in the mitochondrial membrane as shown previously (32, 48, 107).

To test the membrane preference of the heterologous combinations of the tombusvirus replication proteins in *pex3Δ* yeast, first we performed co-localization studies. We found that the heterologous combinations of either T33/C95 or C36/T92 are co-localized in yeast cells (Fig. 2.9C). Second, we performed subcellular localization of YFP-C95 in *pex3Δ* yeast co-expressing T33, which showed partial co-localization with the CFP-Pho86 ER marker protein (Fig. 2.9D) and the mitochondrial dye (Fig. 2.9E). Similarly, YFP-T33 showed partial co-localization with the CFP-Pho86 ER marker protein (Fig. 2.9D) and the mitochondrial dye (Fig. 2.9E) in yeast co-expressing the heterologous C95. Thus, it seems that T33 and C95, albeit they are co-localized, they are present in both ER and mitochondria, with fractions of the T33 and C95 molecules divided between the two organelles.

Intriguingly, we observed similar split/divided distribution of C36 and T92 between the ER and mitochondrial membranes (Fig. 2.9F-G) in heterologous co-expression studies in *pex3Δ* yeast. Therefore, we suggest that the tombusviruses replication proteins can be localized to both ER and mitochondrial membranes in yeast

co-expressing the heterologous combinations (T33/C95 or C36/T92) of replication proteins. This distribution could be interesting during tombusvirus evolution by allowing less restricted use of subcellular membranes by putative interviral tombusvirus recombinants (see discussion).

2.4 Discussion

All known (+)RNA viruses of plants and animals depend on various subcellular membranes for their replication. Yet, we do not know why different (+)RNA viruses select different subcellular membranes/compartments for replication. Tombusviruses could be valuable for understanding the roles of various subcellular membranes in viral replication since they show different preferences. For example, TBSV, CNV and CymRSV preferably utilize the peroxisomal membranes, or in the absence of peroxisomes, the ER membranes (10, 18, 32, 107, 113). On the other hand, CIRV replicates in the mitochondrial membranes (19, 48). At a late stage of tombusvirus replication in plants, however, large multivesicular bodies form that frequently contain ER membranes and mitochondria as well (124). These observations suggest complex interactions between subcellular membranes and tombusvirus replication proteins.

In this paper, we have developed *in vitro* tombusvirus replication assays with isolated organelles (Fig. 2.3) or enriched organellar preparations (Fig. 2.4) to directly address the roles of the various subcellular membranes in tombusvirus replication. We have shown that (i) both (+) and (-)-strand RNA synthesis occurring in these assays; (ii) the process is asymmetrical leading to excess amount of (+) over (-)-strands; (iii) membrane-bound replicase complex forms; (iv) there is requirement of cellular factors;

(v) there is requirement of both p33 and p92 replication proteins for replication; (vi) the newly made (+) RNAs are released to the solution; (vii) while the (-) RNA is kept protected in the replicase bound to the membrane. All these pieces of evidence support that the tombusvirus replication in the isolated organelles is a complete cycle of authentic replication process, similar to that developed using the whole CFE (49, 102).

Interestingly, we find that TBSV replication proteins utilized the isolated ER membrane efficiently for repRNA replication, while the CIRV replication proteins did not (Fig. 2.3-2.4). These data are in agreement with the *in vivo* observations that TBSV uses the ER membranes (in the absence of the peroxisomes), while CIRV favors the mitochondria for replication in yeast and plant cells (10, 19, 32, 48, 107, 113). Surprisingly, however, TBSV was also able to utilize the isolated mitochondria for replication (Fig. 2.3-2.4), suggesting that this tombusvirus could be less restricted in its ability to utilize subcellular membranes. Indeed, we did see some co-localization of TBSV T33 and T92 replication proteins with mitochondrial markers (based on both MTS-CFP and a mitochondrial dye, Fig. 2.9B) in *pex3Δ* yeast, suggesting that mitochondria is likely used for TBSV replication at some extent, possibly at the late stage of replication when peroxisomal or ER membranes had already been fully exploited. Similarly, we observed some co-localization of CIRV C36 and C95 replication proteins with the ER marker protein (Fig. 2.9A), supporting that ER membranes might be targeted for CIRV replication. However, the activity of the CIRV replicases in the ER membranes is likely less robust than in the mitochondrial membranes, based on the *in vitro* experiments with the isolated microsomes (Fig. 2.3). Altogether, the *in vitro* and *in vivo* experiments suggest that TBSV show rather high flexibility in membrane utilization for

replication, while CIRV is somewhat more restricted, at least in vitro.

Unfortunately, we failed to obtain peroxisomal preparations supporting either TBSV or CIRV replication from yeast cultured in oleic acid media to induce peroxisome formation (Fig. 2.4). It is possible that peroxisomes are too fragile and damaged during the isolation procedure. It is also possible that the oleic-acid induced peroxisomes are not suitable to support TBSV replication. Indeed, addition of oleic acid to the culture media did not increase TBSV replication in yeast (Panavas and Nagy, unpublished). Therefore, it is highly likely that the CFEs obtained from yeast support TBSV replication occurring mainly in the ER-derived membranes (Fig. 2.1). Because ER is as suitable to support TBSV replication as the peroxisomes in yeast (32, 107), the obtained *in vitro* data are likely valuable in dissecting TBSV replication *in vitro*. We also propose that the CFE likely supports weak CIRV replication (when compared with TBSV) due to the limiting amount of mitochondria present in the CFE prepared from yeast cultured under the standard conditions. Indeed, comparison of CFE (Fig. 2.1) and microsomal and mitochondrial preps (Figs. 2.3-2.4) revealed similarity between CFE and microsomal preparations, suggesting that most of the *in vitro* repRNA replication in the CFE is likely supported by the ER membrane. This could be due to the growth conditions for yeast, which favors the presence of low number of mitochondria and peroxisomes, but abundant ER membranes (125). The isolated mitochondrial preparation, however, supported CIRV-based repRNA replication efficiently, making this approach suitable for future mechanistic studies.

Combinations of heterologous replication proteins reveal remarkable flexibility of membrane usage by tombusviruses. One of the surprising discoveries from the *in vitro*

tombusvirus replication assays with the combinations of heterologous replication proteins is the extended ability of tombusviruses to utilize subcellular membranes more efficiently than some homologous combinations. For example, CIRV C36 and C95 co-localized more efficiently with the ER membranes when present in heterologous than in homologous combinations (Fig. 2.9). Moreover, the CIRV C36 protein became part of a more efficient replicase in the ER membranes when associated with T92 RdRp protein than in homologous combination with C95 (Fig. 2.6A) without becoming less efficient in the mitochondrial membrane (Fig. 2.6B). Also, the TBSV T92 RdRp showed increased activity in the mitochondrial membrane when combined with C36 cofactor than in combination with TBSV T33 (Fig. 2.6B). This suggests that tombusviruses might be able to utilize various subcellular membranes more efficiently during some co-infections with other tombusviruses when compared with single infections.

Even more interesting is the possibility of generation of chimeric tombusviruses due to RNA recombination between tombusviruses. RNA recombination is well documented for tombusviruses *in vitro*, in yeast, and *in planta* (16, 17, 93, 94, 126-130). The formation of chimeric tombusviruses could expand the efficiency of using various subcellular compartments by the tombusvirus replicase, based on the chimeric constructs tested in Figs. 2.7-2.8. Indeed, particular chimeric constructs replicated efficiently in both ER and mitochondrial preps (e.g., T33c/T92c, Fig. 2.8). We propose that the extra flexibility in membrane-usage by these chimeric tombusviruses could be useful for tombusviruses when infecting some plant species, thus expanding the wide range of plants supporting tombusvirus replication. Accordingly, recombinant CIRV strains were recently isolated that had similar N-terminal sequences to the TBSV p33 replication

protein and targeted the peroxisome for replication (131, 132). Thus, recombination involving the p33/p36 ORF can occur in nature creating new variants or strains.

Adaptation to subcellular membranes for robust tombusvirus replication depends on multiple domains within the replication proteins. The heterologous combinations of tombusvirus replication proteins revealed that T92 and C95 are major determinants of repRNA replication in particular subcellular membranes. For example, the C95 RdRp was mostly functional in the mitochondrial preps, while the T92 RdRp was active in both microsomal and mitochondrial preps (Fig. 2.6C-D). Furthermore, the results with chimeric proteins suggest that the RdRp domain in T92 is very active in both microsomal and mitochondrial preps (Fig. 2.7C-D), while the origin of the N-terminal, overlapping domain in the tombusvirus RdRp was also important for the activity of VRC during replication. Therefore, we suggest that multiple domains within the replication proteins affect the ability and efficiency of the tombusvirus VRCs to support repRNA replication in particular subcellular membranes. It is also possible that C36 forms a single 'domain' that favors mitochondrial targeting as a whole, and swapping its C-terminal and/or trans-membrane regions with corresponding regions of T33 disrupts the structure necessary for specific targeting to mitochondria.

Altogether, the developed *in vitro* tombusvirus replication assays based on CFE, isolated microsomes and mitochondrial preparations will be powerful to gain mechanistic insights into the roles of membranes in (+)RNA virus replication, virus-host interactions and possibly viral evolution.

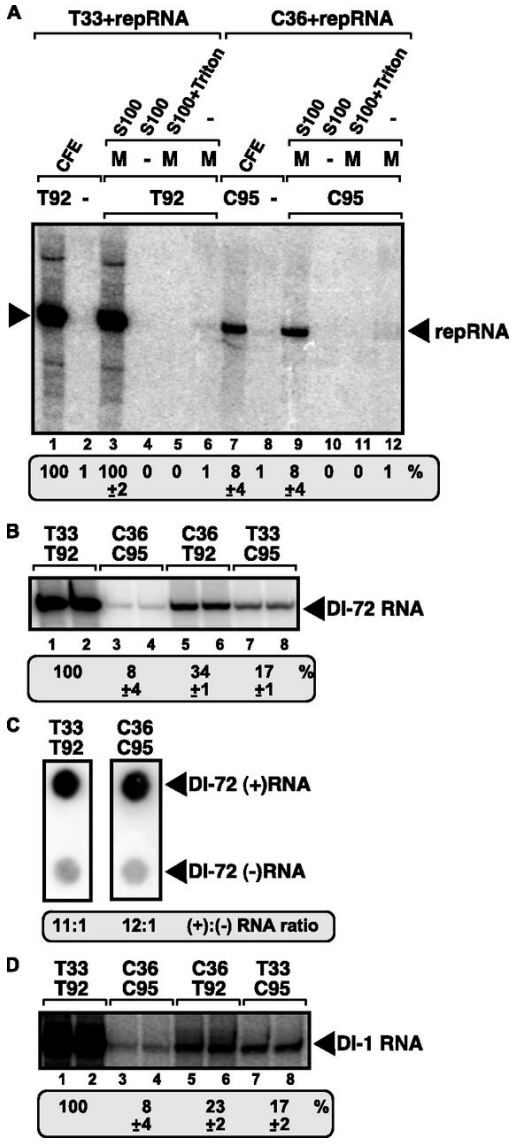
A
T33+repRNA
C36+repRNA
CFE
S100
S100
S100+Triton
-
M - M M
T92 -
T92
C95 -
C95
repRNA
1 2 3 4 5 6 7 8 9 10 11 12
100 1 100 ±2 0 0 1 8 ±4 1 8 ±4 0 0 1 %
B
T33 T92
C36 C95
C36 T92
T33 C95
DI-72 RNA
1 2 3 4 5 6 7 8
100 8 ±4 34 ±1 17 ±1 %
C
T33 T92
C36 C95
DI-72 (+)RNA
DI-72 (-)RNA
11:1 12:1 (+):(-) RNA ratio
D
T33 T92
C36 C95
C36 T92
T33 C95
DI-1 RNA
1 2 3 4 5 6 7 8
100 8 ±4 23 ±2 17 ±2 %

Fig. 2.1

Fig. 2.1 In vitro reconstitution of the CIRV replicase in yeast cell extract.

(A) Purified recombinant p33 (named T33) and p92pol (named T92) replication proteins of TBSV or purified recombinant p36 (named C36) and p95pol (named C95) replication proteins of CIRV in combination with the TBSV-derived DI-72 (+)repRNA were added to the cell extract (lanes 1 and 7), to the membrane plus soluble fractions (lanes 3 and 9), to the soluble fraction (lanes 4 and 10), to the 1% Triton-treated membrane plus soluble fractions (lanes 5 and 11), and to the membrane fraction (lanes 6 and 12) of the yeast cell extract. The CFE-based replication assay mixture lacked T92 (lane 2) or C95 (lane 8) as a negative control. Denaturing PAGE analysis of the 32P-labeled repRNA products obtained is shown. The full-length repRNA is indicated by an arrowhead. The result of the CFE-based replication assay with T33 and T92 was chosen as 100% (lane 1). (B) The heterologous combinations of TBSV and CIRV replication proteins are functional in the CFE-based replication assay. The activity of the reconstituted tombusvirus replicases is estimated as for panel A. Denaturing PAGE analysis of the replicase products is as shown in panel A. (C) Detection of plus- and minus-stranded RNA products produced by the reconstituted TBSV and CIRV replicases in the CFE-based replication assay. The blot contains the same amounts of cold plus- and minus-strand DI-72 RNA, while the 32P-labeled repRNA probes were generated in the CFE-based replication assay. Note that we used 5 times more CIRV replication products than TBSV to increase the signal. The ratio of plus- and minus-strand RNA products was estimated. (D) The heterologous combinations of TBSV and CIRV replication proteins with the CIRV-derived DI-1 repRNA are functional in the CFE-based replication assay. See further details described for panel B. Each experiment was repeated.

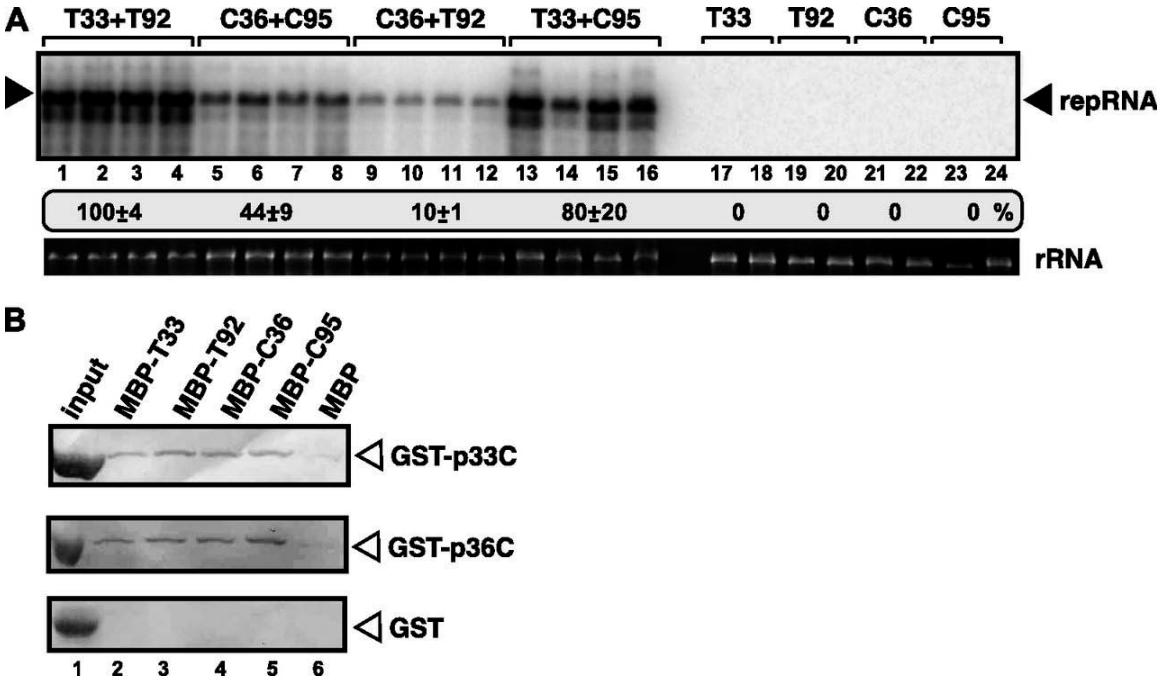
A
T33+T92
C36+C95
C36+T92
T33+C95
T33
T92
C36
C95
repRNA
1 2 3 4 5 6 7 8 9 10 11 12 13 14 15 16 17 18 19 20 21 22 23 24
100±4
44±9
10±1
80±20
0
0
0
0 %
rRNA
B
input
MBP-T33
MBP-T92
MBP-C36
MBP-C95
MBP
GST-p33C
GST-p36C
GST
1 2 3 4 5 6

Fig. 2.2

Fig. 2.2 The heterologous combinations of TBSV and CIRV replication proteins are functional in N. benthamiana.

The accumulation of DI-72 repRNA was measured by Northern blotting in N. benthamiana leaves. The expression of TBSV and CIRV replication proteins and the repRNA was launched from the 35S promoter in an Agrobacterium plasmid (introduced into the leaves via agroinfiltration). Samples were taken from the infiltrated leaves at 3.5 days after infiltration. Note that coagroinfiltration of single protein-expressing constructs with the repRNA-expressing construct did not result in repRNA accumulation (lanes 17 to 24). Each experiment was repeated. (B) Affinity binding (pulldown) assay to detect interaction between GST-His6-p33C (representing the C-terminal half of T33, involved in protein interaction) or GST-His6-p36C (representing the C-terminal half of C36) and the MBP-tagged TBSV and CIRV replication proteins. The MBP-tagged TBSV and CIRV replication proteins and the MBP produced in E. coli were immobilized on amylose-affinity columns. GST-His6-tagged p33C or GST-His6-p36C expressed in E. coli was then passed through the amylose affinity columns with immobilized MBP-tagged proteins. The affinity-bound proteins were specifically eluted with maltose from the columns. The eluted proteins were analyzed by Western blotting with anti-6×His or anti-GST antibody to detect the amount of GST-His6, GST-His6-p33C, or GST-His6-p36C specifically bound to MBP-tagged viral proteins. A similarly produced GST-His6 protein preparation was used as a negative control.

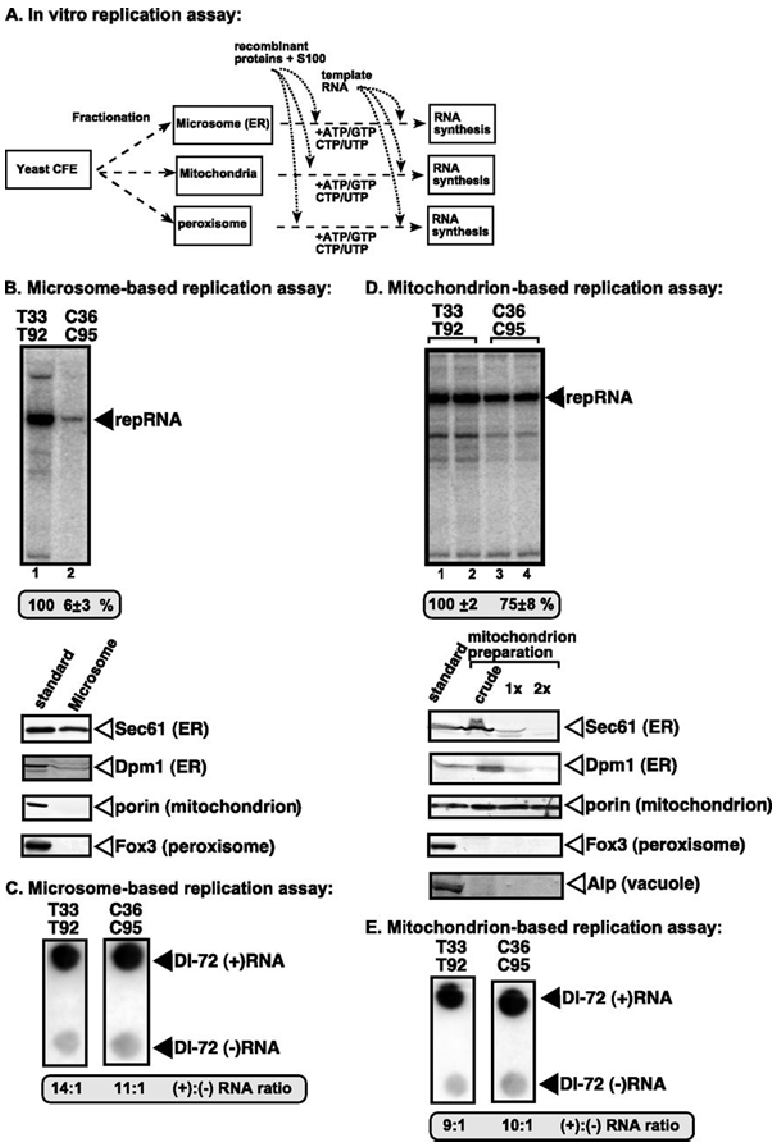
A. In vitro replication assay:
recombinant proteins + S100
template RNA
Fractionation
Yeast CFE
Microsome (ER)
Mitochondria
peroxisome
+ATP/GTP CTP/UTP
RNA synthesis
B. Microsome-based replication assay:
T33 C36
T92 C95
repRNA
1 2
100 6±3 %
standard
Microsome
Sec61 (ER)
Dpm1 (ER)
porin (mitochondrion)
Fox3 (peroxisome)
C. Microsome-based replication assay:
DI-72 (+)RNA
DI-72 (-)RNA
14:1 11:1 (+):(-) RNA ratio
D. Mitochondrion-based replication assay:
1 2 3 4
100 ±2 75±8 %
mitochondrion preparation
crude
1x 2x
Alp (vacuole)
E. Mitochondrion-based replication assay:
9:1 10:1 (+):(-) RNA ratio

Fig. 2.3

Fig. 2.3 In vitro reconstitution of the TBSV and CIRV replicases in yeast microsome and mitochondrial preparations.

(A) Scheme of the replication assays. The purified recombinant T33 and T92 as well as C36 and C95 replication proteins and the TBSV-derived (+)repRNA were used as described for Fig. 2.1. (B) Top panel, denaturing PAGE analysis of the 32P-labeled repRNA products obtained in the replication assays with the isolated yeast microsome preparation. The synthesized full-length repRNA is indicated by an arrowhead. The result from the replication assay with T33 and T92 was chosen as 100% (lane 1). Each experiment was repeated. Bottom panels, Western blot analysis of various marker proteins in the microsome preparation with the help of specific antibodies. The left lane represents the standard yeast proteins present in CFE as positive controls. (C) Detection of plus- and minus-strand RNA products produced by the reconstituted TBSV and CIRV replicases in the microsome-based replication assay. See further details described for Fig. 2.1C. (D) The TBSV and CIRV replication proteins are functional in the mitochondrion-based replication assay. Top panel, the activity of the reconstituted tombusvirus replicases is estimated as for panel B. Denaturing PAGE analysis of the replicase products is as shown for panel B. Note that we used the 2× purified mitochondria preparations for this assay. Bottom panels, Western blot analysis of various marker proteins in the microsome preparations with the help of specific antibodies. The left lane represents the standard yeast proteins from yeast induced with oleic acid as positive controls. The crude mitochondrial sample was prepared without sucrose density gradient centrifugation, while 1× and 2× indicate single and double sucrose density gradient-purified mitochondrial preparations, respectively. (E) Detection of plus- and minus-strand RNA products produced by the reconstituted TBSV and CIRV replicases in the mitochondrion-based replication assay. See further details described for Fig. 2.1C.

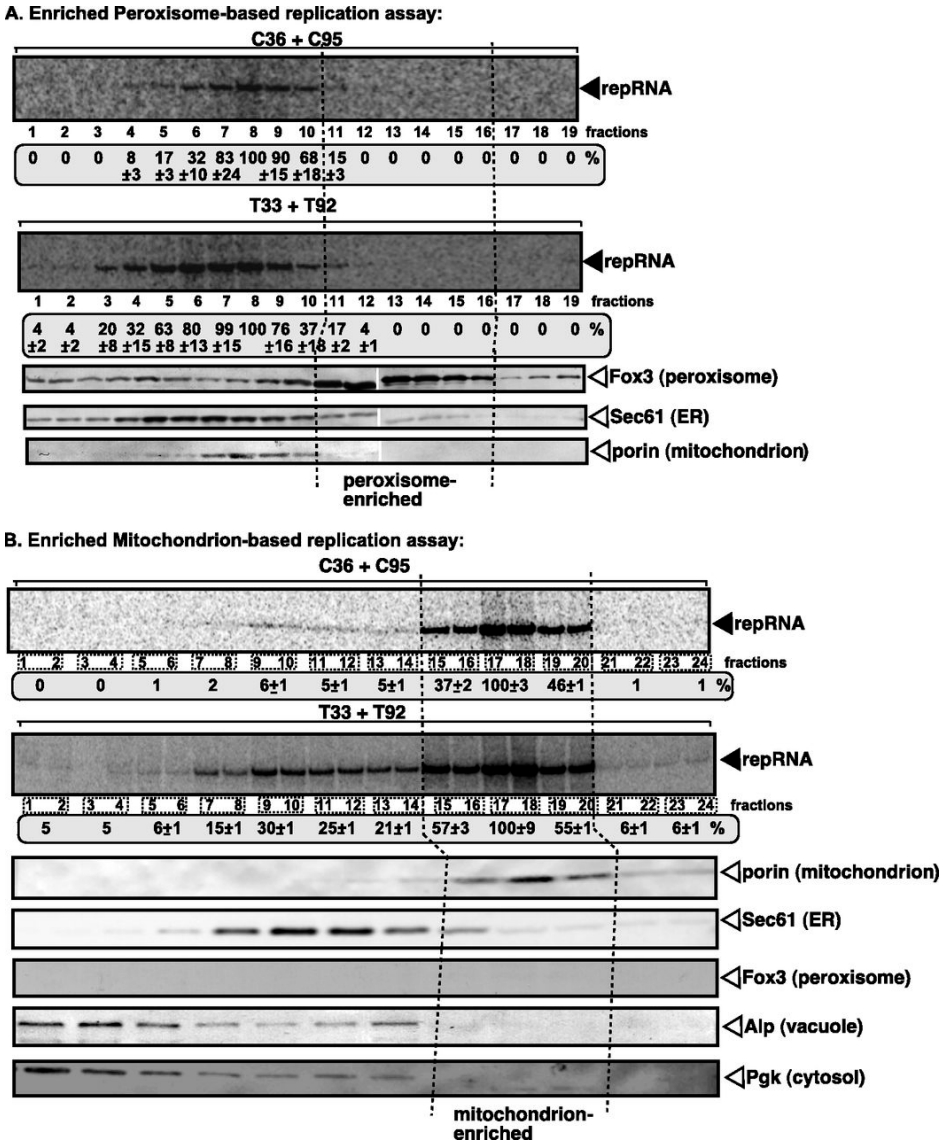
A. Enriched Peroxisome-based replication assay:
C36 + C95
repRNA
1 2 3 4 5 6 7 8 9 10 11 12 13 14 15 16 17 18 19 fractions
0 0 0 8 ±3 17 ±3 32 ±10 83 ±24 100 ±15 90 ±18 68 ±3 15 0 0 0 0 0 0 0 0 %
T33 + T92
repRNA
1 2 3 4 5 6 7 8 9 10 11 12 13 14 15 16 17 18 19 fractions
4 ±2 4 ±2 20 ±8 32 ±15 63 ±8 80 ±13 99 ±15 100 ±16 76 ±18 37 ±2 17 ±1 4 0 0 0 0 0 0 0 %
Fox3 (peroxisome)
Sec61 (ER)
porin (mitochondrion)
peroxisome-enriched
B. Enriched Mitochondrion-based replication assay:
C36 + C95
repRNA
1 2 3 4 5 6 7 8 9 10 11 12 13 14 15 16 17 18 19 20 21 22 23 24 fractions
0 0 1 2 6±1 5±1 5±1 37±2 100±3 46±1 1 1 %
T33 + T92
repRNA
1 2 3 4 5 6 7 8 9 10 11 12 13 14 15 16 17 18 19 20 21 22 23 24 fractions
5 5 6±1 15±1 30±1 25±1 21±1 57±3 100±9 55±1 6±1 6±1 %
porin (mitochondrion)
Sec61 (ER)
Fox3 (peroxisome)
Alp (vacuole)
Pgk (cytosol)
mitochondrion-enriched

Fig. 2.4

Fig. 2.4 In vitro reconstitution of the TBSV and CIRV replicases in yeast membrane fractions.

(A) Yeast was grown on oleate-rich medium to increase peroxisome numbers prior to isolation. The crude peroxisome sample was subjected to 10 to 70% sucrose density gradient centrifugation, and the fractions of the sucrose gradient were tested for the ability to support RNA replication by the CIRV or TBSV replicases assembled in vitro. The purified recombinant T33 and T92 as well as C36 and C95 replication proteins and the TBSV-derived (+)repRNA were used as described for Fig. 2.1. Top two panels, denaturing PAGE analysis of the 32P-labeled repRNA products obtained in the replication assays with various membrane fractions. The synthesized full-length repRNA is indicated by an arrow. The most active fraction in the replication assay was chosen as 100%. The fractions most enriched for peroxisome are boxed with dotted lines. The samples on the left represent the top of the gradient (10%), while the samples on the right are from the bottom of the gradient (70%). Bottom panels, Western blot analysis of various marker proteins in the membrane fractions with the help of specific antibodies. (B) The crude mitochondrial sample was subjected to 10 to 70% sucrose density gradient centrifugation, and the fractions of the sucrose gradient were tested for the ability to support RNA replication by the CIRV or TBSV replicases assembled in vitro. The most active fraction in the replication assay was chosen as 100%. The fractions most enriched for mitochondria are boxed with dotted lines. See further details described for panel A.

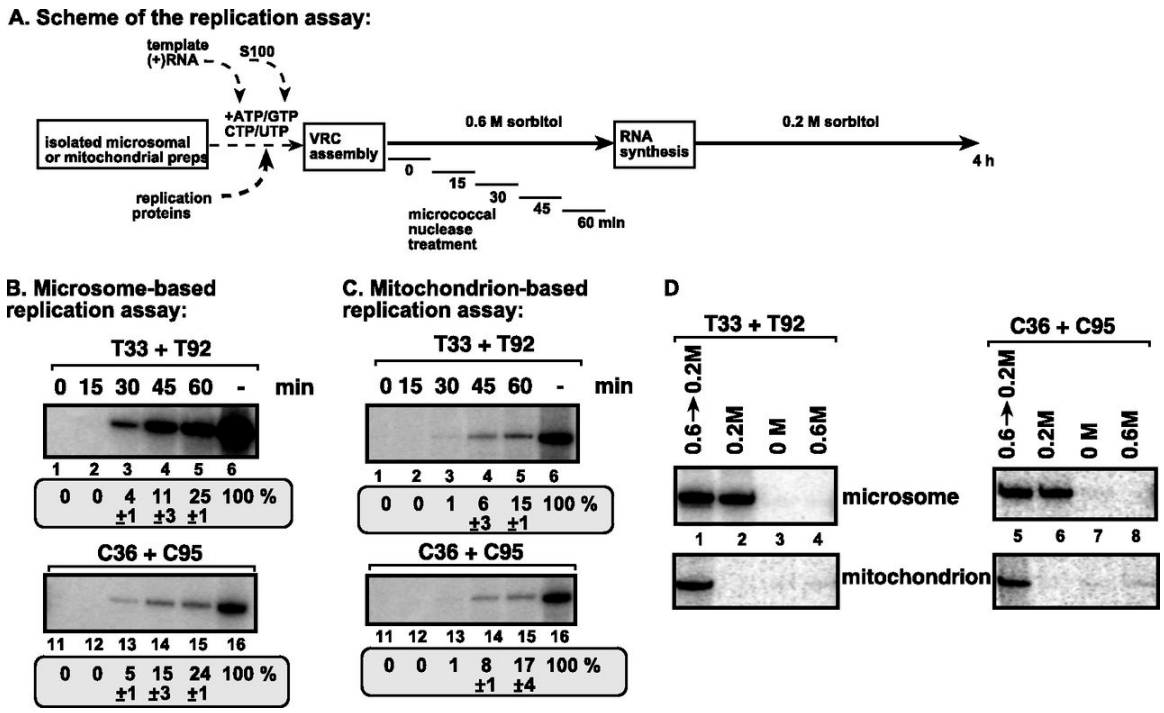
A. Scheme of the replication assay:
template (+)RNA
S100
+ATP/GTP CTP/UTP
isolated microsomal or mitochondrial preps
VRC assembly
0.6 M sorbitol
RNA synthesis
0.2 M sorbitol
4 h
0
15
30
45
60 min
micrococcal nuclease treatment
replication proteins
B. Microsome-based replication assay:
T33 + T92
0 15 30 45 60 - min
1 2 3 4 5 6
0 0 4 ±1 11 ±3 25 ±1 100 %
C36 + C95
11 12 13 14 15 16
0 0 5 ±1 15 ±3 24 ±1 100 %
C. Mitochondrion-based replication assay:
T33 + T92
0 15 30 45 60 - min
1 2 3 4 5 6
0 0 1 ±3 6 ±1 15 100 %
C36 + C95
11 12 13 14 15 16
0 0 1 ±1 8 ±4 17 100 %
D
T33 + T92
C36 + C95
0.6→0.2M
0.2M
0 M
0.6M
microsome
mitochondrion
1 2 3 4
5 6 7 8

Fig. 2.5

Fig. 2.5 The in vitro-assembled TBSV or CIRV replicases form an RNase-resistant structure in microsomal or mitochondrial preparations.

(A) Scheme of the in vitro assay. The in vitro reconstitution of the TBSV or CIRV replicases is started by the addition of purified recombinant T33 and T92 as well as C36 and C95 replication proteins and the TBSV-derived (+)repRNA (zero time point) as described for Fig. 2.1. Note that we applied a 15-min treatment with micrococcal nuclease (which was inactivated by addition of EGTA at the end of the treatment) at various time points, followed by RNA synthesis up to 4 h (total length of incubation). (B and C) Denaturing PAGE analysis of the 32P-labeled repRNA products obtained. Note that only the VRC-bound (membrane-associated) repRNA is resistant to nuclease treatment and not the (+)repRNA released to the buffer from the VRCs. (B) Results with microsomal preparations; (C) results with mitochondrial preparations. (D) Intact organellar membranes are required for tombusvirus replication in vitro. Various amounts of sorbitol in the assay buffer were used to test TBSV and CIRV replication.

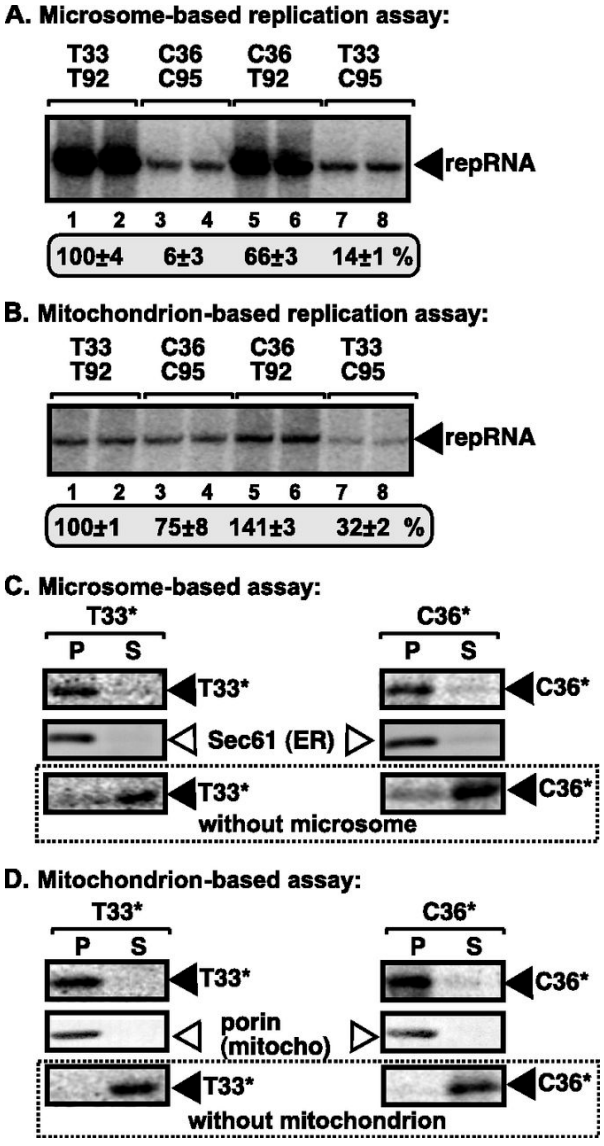
A. Microsome-based replication assay:
T33 T92
C36 C95
C36 T92
T33 C95
repRNA
1 2 3 4 5 6 7 8
100±4 6±3 66±3 14±1 %
B. Mitochondrion-based replication assay:
T33 T92
C36 C95
C36 T92
T33 C95
repRNA
1 2 3 4 5 6 7 8
100±1 75±8 141±3 32±2 %
C. Microsome-based assay:
T33*
C36*
P S
P S
T33*
C36*
Sec61 (ER)
T33*
C36*
without microsome
D. Mitochondrion-based assay:
T33*
C36*
P S
P S
T33*
C36*
porin (mitocho)
T33*
C36*
without mitochondrion

Fig. 2.6

Fig. 2.6 In vitro reconstitution of heterologous combinations of tombusvirus replicases in yeast microsome and mitochondrial preparations.

(A) Denaturing PAGE analysis of the 32P-labeled repRNA products obtained in replication assays with the isolated yeast microsome preparation. The synthesized full-length repRNA is indicated by an arrow. The result from the replication assay with T33 and T92 was chosen as 100% (lanes 1 and 2). (B) Denaturing PAGE analysis of the 32P-labeled repRNA products obtained in the replication assays with the isolated yeast mitochondrial preparation. (C) SDS-PAGE analysis of microsome membrane association assay using [35S]methionine-labeled recombinant T33 or C36 and a microsome preparation in the presence of the soluble extract from yeast. The bottom panel (encircled) represents samples incubated in the absence of the microsome preparation. (D) Mitochondrial membrane association assay. [35S]methionine-labeled recombinant T33 or C36 was used with the mitochondrial preparation in the presence of the soluble extract from yeast. Asterisks represent 35S-labeled proteins. See further details described for panel C.

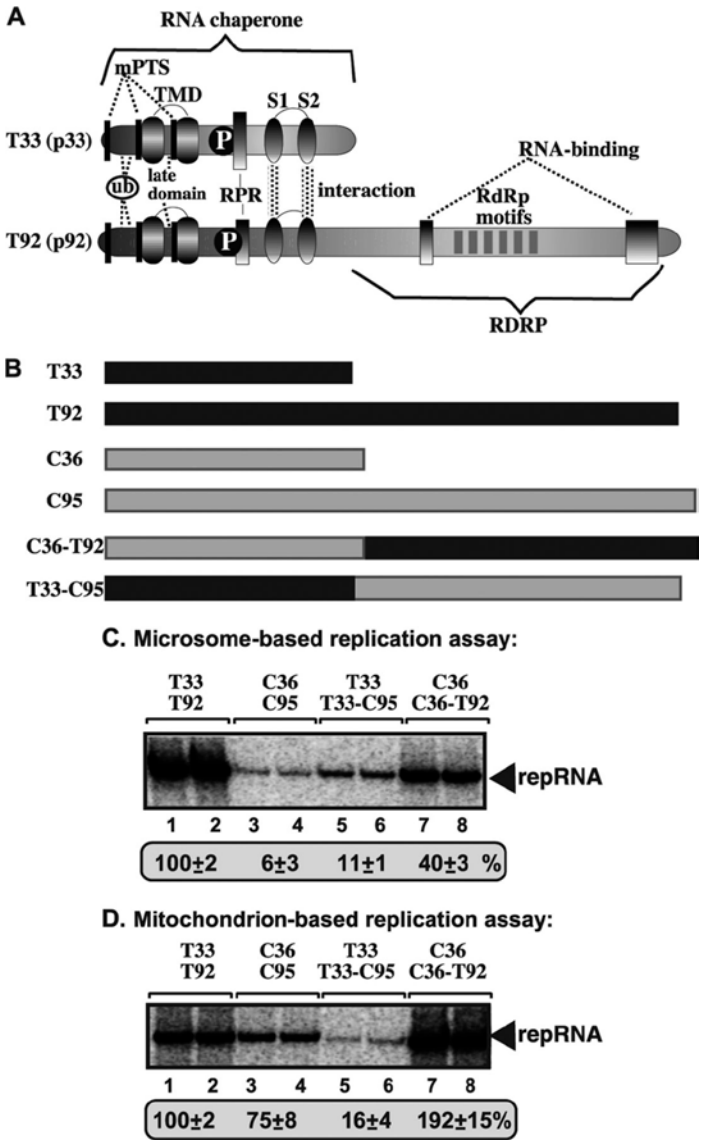
A
RNA chaperone
mPTS
TMD
S1 S2
T33 (p33)
P
ub
late domain
RPR
interaction
RNA-binding
RdRp motifs
T92 (p92)
P
RDRP
B
T33
T92
C36
C95
C36-T92
T33-C95
C. Microsome-based replication assay:
T33 T92
C36 C95
T33 T33-C95
C36 C36-T92
repRNA
1 2 3 4 5 6 7 8
100±2 6±3 11±1 40±3 %
D. Mitochondrion-based replication assay:
T33 T92
C36 C95
T33 T33-C95
C36 C36-T92
repRNA
1 2 3 4 5 6 7 8
100±2 75±8 16±4 192±15%

Fig. 2.7

Fig. 2.7 In vitro reconstitution of chimeric tombusvirus replicases in yeast microsome and mitochondrial preparations.

(A) The known functional domains in the TBSV p33 RNA chaperone and the p92pol RdRp protein. The N-terminal segment in p92pol contains the same sequence as in p33 due to the strategy for overlapping expression of the TBSV genome, while the C-terminal region of p92pol carries the RdRp domain. mPTS, peroxisomal membrane targeting sequences; ub, monoubiquitinated region; TMD, transmembrane domains; late domain, sequence recognized by the ESCRT factors; P, phosphorylation sites; RPR, arginine-proline-rich RNA binding domain; S1 and S2, subdomains of the p33:p33/p92 interaction domain. (B) Schematic representation of the chimeric RdRp proteins made between the corresponding TBSV and CIRV replication proteins as shown. (C) Denaturing PAGE analysis of the 32P-labeled repRNA products obtained in replication assays using the chimeric RdRp proteins based on the isolated yeast microsome preparation. The synthesized full-length repRNA is indicated by an arrow. The result from the replication assay with T33 and T92 was chosen as 100% (lanes 1 and 2). (D) Denaturing PAGE analysis of the 32P-labeled repRNA products obtained in the replication assays with the chimeric RdRp proteins using the isolated yeast mitochondrial preparation. See further details described for panel C.

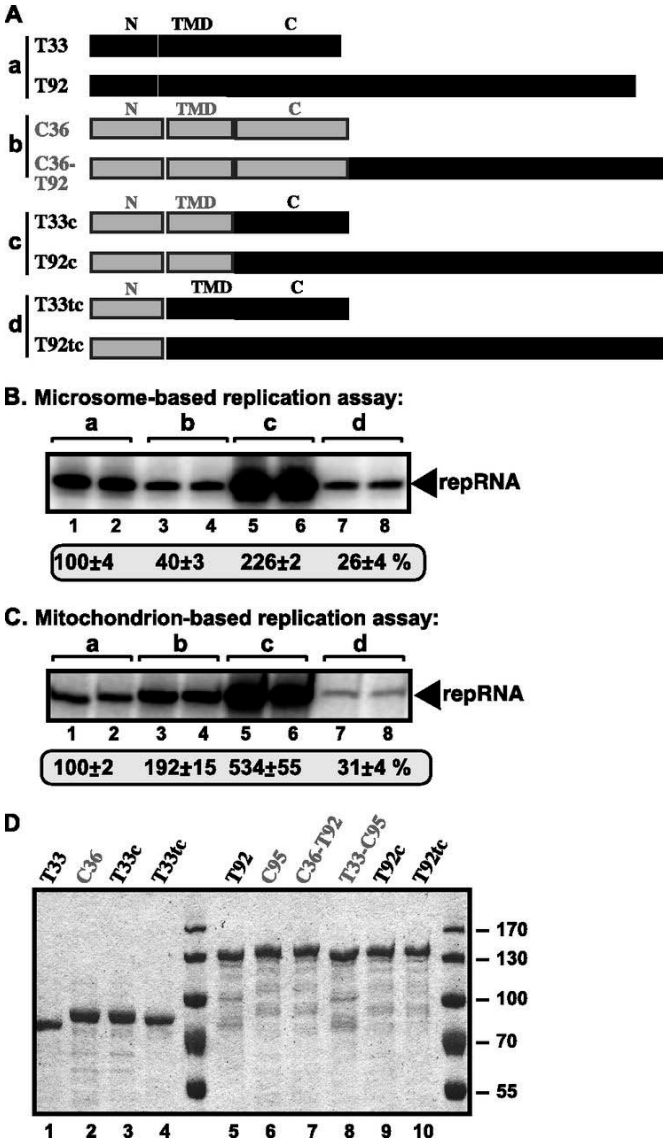
A
N
TMD
C
a
T33
T92
b
C36
C36-T92
c
T33c
T92c
d
T33tc
T92tc
B. Microsome-based replication assay:
a
b
c
d
repRNA
1 2 3 4 5 6 7 8
100±4 40±3 226±2 26±4 %
C. Mitochondrion-based replication assay:
a
b
c
d
repRNA
1 2 3 4 5 6 7 8
100±2 192±15 534±55 31±4 %
D
T33
C36
T33c
T33tc
T92
C95
C36-T92
T33-C95
T92c
T92tc
170
130
100
70
55
1 2 3 4 5 6 7 8 9 10

Fig. 2.8

Fig. 2.8 In vitro reconstitution of additional chimeric tombusvirus replicases in yeast microsome and mitochondrial preparations.

(A) Schematic representation of the chimeric replication proteins made between the corresponding TBSV and CIRV replication proteins as shown. The T33 and C36 sequences were divided into three segments based on the known functions/roles (see Fig. 2.7A). (B) Denaturing PAGE analysis of the 32P-labeled repRNA products obtained in replication assays using the chimeric tombusvirus replication proteins based on the isolated yeast microsome preparation. The synthesized full-length repRNA is indicated by an arrow. The result from the replication assay with T33 and T92 was chosen as 100% (lanes 1 and 2). (C) Denaturing PAGE analysis of the 32P-labeled repRNA products obtained in the replication assays with the chimeric tombusvirus replication proteins using the isolated yeast mitochondrial preparation. See further details described for panel B. (D) Coomassie blue-stained SDS-PAGE of the affinity-purified replication proteins expressed in E. coli as MBP fusion proteins.

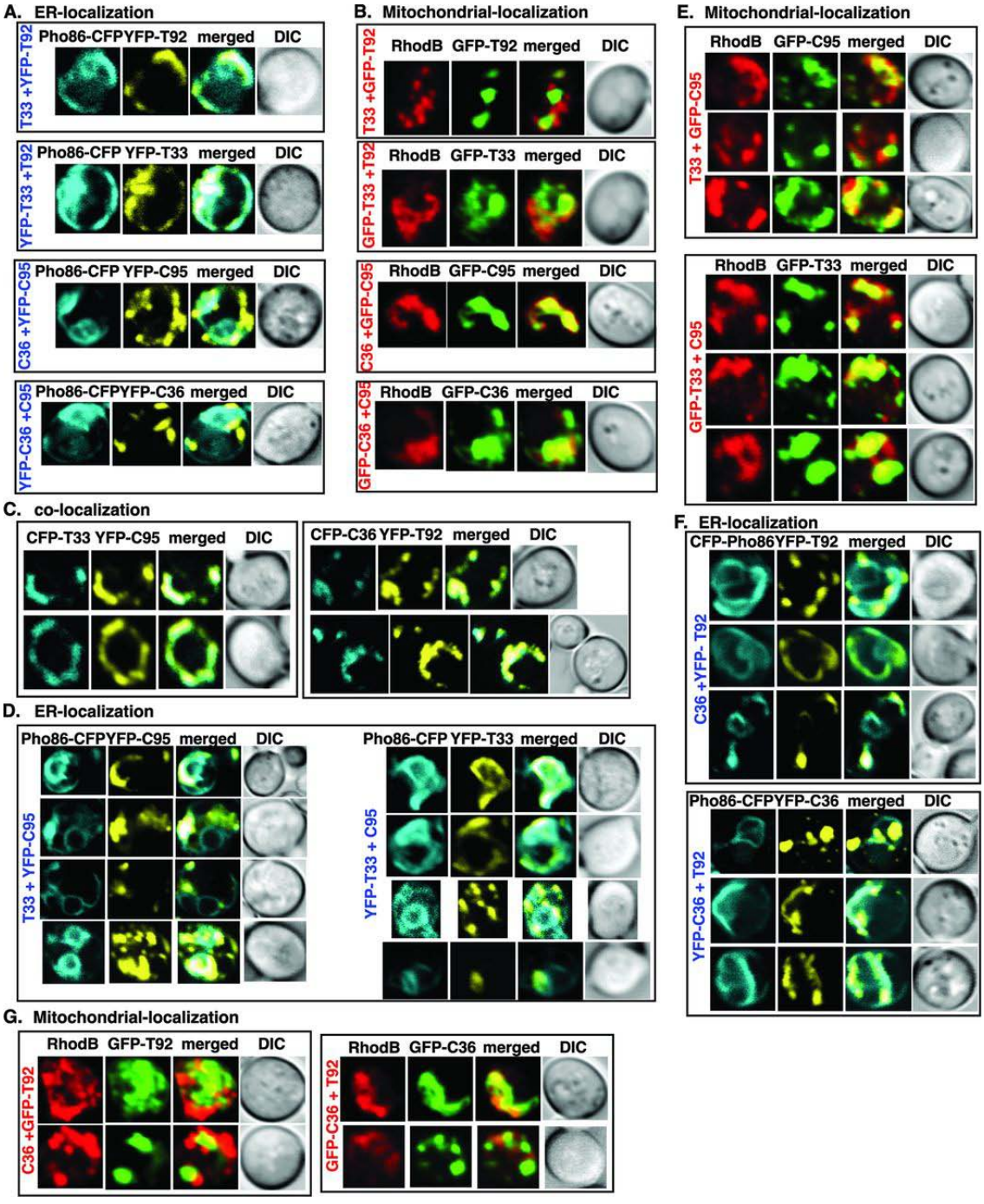
A. ER-localization
Pho86-CFPYFP-T92 merged DIC
T33 +YFP-T92
Pho86-CFP YFP-T33 merged DIC
YFP-T33 +T92
Pho86-CFP YFP-C95 merged DIC
C36 +YFP-C95
Pho86-CFPYFP-C36 merged DIC
YFP-C36 +C95
B. Mitochondrial-localization
RhodB GFP-T92 merged DIC
T33 +GFP-T92
RhodB GFP-T33 merged DIC
GFP-T33 +T92
RhodB GFP-C95 merged DIC
C36 +GFP-C95
RhodB GFP-C36 merged DIC
GFP-C36 +C95
E. Mitochondrial-localization
RhodB GFP-C95 merged DIC
T33 + GFP-C95
RhodB GFP-T33 merged DIC
GFP-T33 + C95
C. co-localization
CFP-T33 YFP-C95 merged DIC
CFP-C36 YFP-T92 merged DIC
F. ER-localization
CFP-Pho86YFP-T92 merged DIC
C36 +YFP- T92
Pho86-CFPYFP-C36 merged DIC
YFP-C36 + T92
D. ER-localization
Pho86-CFPYFP-C95 merged DIC
T33 + YFP-C95
Pho86-CFP YFP-T33 merged DIC
YFP-T33 + C95
G. Mitochondrial-localization
RhodB GFP-T92 merged DIC
C36 +GFP-T92
RhodB GFP-C36 merged DIC
GFP-C36 + T92

Fig. 2.9

Fig. 2.9 Distribution of TBSV and CIRV replication proteins when expressed in heterologous combinations.

(A) Confocal laser microscopy images show the colocalization of Pho86p-CFP (ER marker protein) with YFP-T92, YFP-T33, YFP-C95, or YFP-C36 expressed from the GAL1 promoter in a pex3Δ yeast strain. The description on the left shows the combination of replication proteins expressed in yeast. The merged images show the colocalization of Pho86p-CFP with YFP-tagged replication proteins. Differential interference contrast (DIC) images are shown on the right. (B) Localization of YFP-T92 or GFP-T92, YFP-T33 or GTP-T33, GFP-C95, or GFP-C36 expressed from the GAL1 promoter to the mitochondria in a pex3Δ yeast strain. We used rhodamine B (RhodB, red) fluorescent dye to visualize the mitochondria. See further details described for panel A. (C) Colocalization of YFP- or CFP-tagged TBSV and CIRV replication proteins in a pex3Δ yeast strain. See further details described for panel A. (D) ER localization of YFP-C95 or YFP-T33 in a pex3Δ yeast strain expressing heterologous combinations of tombusvirus replication proteins. See further details described for panel A. (E) Mitochondrial localization of GFP-C95 or GFP-T33 in a pex3Δ yeast strain expressing heterologous combinations of tombusvirus replication proteins. See further details described for panel A. (F) ER localization of YFP-T92 or YFP-C36 in a pex3Δ yeast strain expressing heterologous combinations of tombusvirus replication proteins. See further details described for panel A. (G) Mitochondrial localization of GFP-T92 or GFP-C36 in a pex3Δ yeast strain expressing heterologous combinations of tombusvirus replication proteins. See further details described for panel A. Yeast was grown under similar conditions and images were taken as described for panel A. Each experiment was repeated.

Chapter 3

THE HOP-LIKE STRESS INDUCED PROTEIN 1 CO-CHAPERONE IS A NOVEL RESTRICTION FACTOR FOR MITOCHONDRIAL TOMBUSVIRUS REPLICATION

(This chapter was published on Journal of Virology ahead of print at 11 June 2014, doi:10.1128/JVI.00561-14, Copyright © American Society for Microbiology)

3.1 Introduction

Cells produce a yet unknown number of host restriction factors that limit replication of plus-stranded (+)RNA viruses. The cellular restriction factors could be virus-specific or components of the cell-intrinsic innate systems of the host through targeting diverse pathogens (133-139). Cellular factors are also recruited by (+)RNA viruses to aid viral replication, which takes place in membrane-bound viral replicase complexes (VRCs) in the cytoplasm of infected cells (13, 39, 40, 73-76, 78, 79). The diverse, often opposite roles of host factors, is reflected by the identification of stimulatory as well as inhibitory host proteins in genome-wide screens with various hosts and viruses, such as tomato bushy stunt virus (TBSV), West Nile virus, brome mosaic virus (BMV), hepatitis C virus (HCV), dengue virus and Drosophila virus C (12, 95, 140-146). However, the detailed functions of the majority of the identified host proteins in (+)RNA virus replication have not been fully revealed.

TBSV is a plant-infecting (+)RNA virus used extensively to study virus replication, recombination, and virus - host interactions based on yeast (*Saccharomyces*

cerevisiae) model (1, 5, 91, 92). We have performed several genome-wide screens of yeast genes and different global proteomics approaches that have led to the identification of over 500 host genes/proteins putatively involved in TBSV replication or recombination (12, 93-99, 110, 126, 147-149). The above systematic screens have also identified host stimulatory and restriction factors of TBSV replication. For example, the Cyp40-like Cpr7p cyclophilin and the Ttc4 oncogene-like Cns1p co-chaperone are strong inhibitors of TBSV replication in yeast and *in vitro* (109, 150). Additional cellular cyclophilins, such as the CypA, and the related Ess1p parvulin also decrease TBSV RNA accumulation in yeast and plants (109, 110, 151). Moreover, the cellular nucleolin, an RNA binding protein, inhibits TBSV replication by blocking the recruitment of the viral RNA into replication (112). Another group of cellular restriction factors is the WW-motif containing host proteins, such as Rsp5p Nedd4-like E3 ubiquitin ligase, which regulate the degradation of tombusviral $p92^{pol}$ in yeast cells and inhibit the activity of VRC *in vitro* (108, 111). Cellular kinases, such as Pkc1p, could also restrict TBSV replication in yeast (96). Altogether, studies on cellular restriction factors could help unraveling the full arsenal of the native cell-intrinsic innate immune system in the host cell.

Similar to other (+)RNA viruses, tombusviruses, such as TBSV, uses intracellular membranes for replication. Interestingly, TBSV utilizes the peroxisomal membrane, while the closely related *Carnation Italian ringspot virus* (CIRV) takes advantage of the outer mitochondrial membranes to build VRCs in infected plants and yeast (18, 19, 48). The two viral replication proteins (i.e., p33 and $p92^{pol}$ for TBSV and p36 and $p95^{pol}$ in case of CIRV) co-opt 8-10 host proteins to assemble the tombusvirus VRC (97-99, 152). The highly homologous p33 of TBSV and p36 of CIRV replication proteins are master

regulators of replication, playing multifunctional role in recruitment of the tombusviral (+)RNA to the site of replication, the assembly of the VRC and viral RNA synthesis by acting as RNA chaperones (3, 7, 9, 10, 32, 152). The RdRp protein $p92^{pol}$ of TBSV and $p95^{pol}$ of CIRV are also components of the functional VRCs (2, 9, 10, 49, 92). The subverted host proteins have been shown to bind to the viral RNA and the viral replication proteins (13, 37, 98). Detailed studies showed that heat shock protein 70 (Hsp70), eukaryotic elongation factor 1A (eEF1A) and several members of the ESCRT (endosomal sorting complexes required for transport) family of host proteins are required for the assembly of VRCs (81, 100, 101, 103). Additional subverted host proteins include the DDX3-like Ded1p and the human p68-like Dbp2 DEAD-box RNA helicases, glyceraldehyde-3-phosphate dehydrogenase (GAPDH), eEF1Bγ and eEF1A, all of which have been shown to affect viral RNA synthesis (37, 103, 104, 106, 153, 154).

Previous works with TBSV revealed the unexpected inhibitory function for several TPR domain (tetratricopeptide repeats)-containing proteins, such as the Cyp40-like Cpr7p cyclophilin and Ttc4-like Cns1p co-chaperone in yeast and *in vitro* (109, 150). Mechanistic studies showed that the inhibitory effect of Cpr7p was due to its interaction with the RNA-binding domain of the tombusviral p33 replication protein that leads to inhibition of $p33/p92^{pol}$ -based recruitment of the TBSV (+)RNA for replication and decrease of the efficiency of the VRC assembly. Importantly, the key element in Cpr7p was not the cyclophilin domain, but its TPR domain consisting of three TPR modules in Cpr7p (109). Similarly, via its TPR-domain, Cns1p bound to the tombusviral p33 and $p92^{pol}$ replication proteins and inhibited VRC assembly and reduced TBSV replication in yeast and *in vitro* based on a yeast cell-free (CFE) assay (150). However, in case of

Cns1p, the interaction targeted the p33:p33/p92 interaction domain, suggesting that TPR-containing cellular proteins might restrict TBSV replication via different mechanisms.

The TPR domains consists of repeats of 34 amino acid sequence adopting a right-handed helical helix-loop-helix structure with an amphipathic channel, which are involved in many protein-protein interactions (155, 156). Although the TPR-domains are highly variable, which likely affect substrate specificity, the canonical TPR-domain contains a pattern of small and large hydrophobic amino acids. The TPR-domain proteins are abundant in all kingdoms of life, including 200 proteins in mammals, 80 in *C. elegans* and 29 in yeast (157). TPR-domain proteins function in protein trafficking, protein import to organelles, transposon silencing, apoptosis and synaptic vesicle fusion (158, 159). Various TPR-domain proteins are involved in numerous human diseases, such as cancer, amyloidosis, cystic fibrosis, prion protein propagation, and bacterial pathogenesis (160-165). Several TPR-domain proteins have been shown to affect infections by viruses, such as Chikungunya virus, West Nile virus, Vesicular stomatitis virus, herpes simplex virus, poxvirus, and baculovirus (166-171). TPR-domain proteins are also important in interferon-induced antiviral responses, including the IFIT protein family (137, 171-174).

Our previous discoveries invited our attention to TPR-like sequences, including the well-studied stress-induced protein 1 (Sti1p in yeast, Hop protein in mammals and plants) co-chaperone. Sti1p, which is a conserved highly abundant protein lacking chaperone activity on its own, is a co-chaperone of Hsp70 and Hsp90 chaperones (175, 176). Sti1p contains three TPR domains, which are involved in binding to Hsp90s and Hsp70s. Sti1p plays a role in client protein transfer from the Hsp70 complex to the Hsp90 complex. Interestingly, Sti1p can simultaneously bind to Hsp70 and Hsp90 and by

inhibiting the ATPase activity of Hsp90, Sti1p stabilizes the ternary Hsp70 : Hsp90 : client protein intermediate complex (177, 178).

In this paper, we show that the yeast Sti1p co-chaperone has a strong inhibitory function during the mitochondrial CIRV replication but not in the peroxisomal tombusvirus replication. Detailed analysis of Sti1p revealed that it interacted with the RNA-binding domain of CIRV p36 replication protein and ultimately restricted VRC assembly *in vitro* and CIRV RNA accumulation in yeast and the orthologous Hop inhibited CIRV accumulation in plants. Thus, TPR-containing cellular co-chaperone proteins emerge as new cell-intrinsic restriction factors of a mitochondrial (+)RNA virus.

3.2 Materials And Methods

Yeast strains and expression plasmids. Yeast strains BY4741 (MAT a *his3Δ1 leu2Δ0 met15Δ0 ura3Δ0*) and *sti1Δ* (single-gene deletion strain) were obtained from Open Biosystems (Huntsville, AL, USA). For tombusviral replication in yeast, pESC-HisCNVp33-DI72, pYES-CNVp92, pESC-C36/DI72, pYES-C95 were described previously (9). To generate pESC-C36/DI1, CIRV DI-1 (14) (constructed by D. Barajas and Nagy, unpublished) was PCR-amplified using primers #4124 (CCGGAATTCAGAAATATCTCAGGATTTGACCGTCC)/#1069(CCGGTCGAGCTC TACCAGGTAATATACCACAACGTGTGT) and digested with *Eco*RI/*Sac*I, then inserted into *Eco*RI/*Sac*I-digested pESC-HisCNVp33-DI72, generating pESC-HisCNVp33-DI1. Then, CNV p33 sequence was removed by *BamH*I/*Xho*I digestion, and replaced with *BamH*I/*Xho*I-digested CIRV p36 sequence, which was PCR-amplified from

pESC-C36/DI72 using primers #900 (CGACGGATCCGAGGGTTTGAAGGCTGAGTCTACCA)/#3230 (CCGCTCGAGCTATTT-GACACCGAGGGATT), generating pESC-C36/DI1. To generate Twin-Strep-tagged CIRV and CNV replication proteins, the following primer pairs: #5351 (CATCCACAATTCGAAAAATCTGCTGGTGGAGGTGG-ATCCATGGATACCATCAAGAGGATG)/#952 (CCCGCTCGAGTCATGCTACGG-CGGAGTCAAGGA), #5350 (GTGGTTCTGGTGGTGGTTCTGGTGGTTCTGCTTGG-TCTCATCCACAATTCGAAAAATCTG)/#952, #5349 (GGAAGATCTAAAAA-TGTCTGCTTGGTCTCATCCACAATTCGAAAAAGGTGGTGGTTCTGGTGGTGGT TCTGGTGG)/#952, were sequentially used for PCR using template pYES-CNVp92 to introduce Twin-Strep tag on CNV p92, generating Twin-Strep-tagged CNVp92 sequence. The DNA was then digested with *Bgl*II/*Xho*I and inserted into pESC-DI72, generating pESC-StrepCNVp92/DI72. CIRV p36 sequence was PCR-amplified using primers #900/#3230 and digested with *BamH*I/*Xho*I, and then inserted into *BamH*I/*Xho*I-digested pESC-StrepCNVp92/DI72, generating pESC-StrepC36/DI72. To generate pYES-StrepC95, pYES2-NTA (Invitrogen) was digested with *Hind*III/*Kpn*I and then treated with T4 DNA polymerase, and subsequently self-ligated to remove 6xHis tag. The modified pYES2-NTA vector without 6xHis tag was digested with *BamH*I/*Xho*I and used with *Bgl*II/*Xho*I-digested PCR product of Twin-strep-tagged CNVp92 for ligation, generating pYES-StrepC92. CIRV p95 sequence was PCR-amplified using primers #900/#970 (CCCGCTCGAGTCAAGCTACGGCGGAGTCGAGGA) from pYES-C95 and digested with *BamH*I/*Xho*I, and then inserted into *BamH*I/*Xho*I-digested pYES-

StrepC92, generating pYES-StrepC95. To generate yeast vector expressing *STI1* gene, p*TEF1* promoter and *tCYC1* terminator was PCR-amplified from yeast genomic DNA and pESC-C36/DI72 (9), respectively, using primer pair #2764 (CCGCGAGCTCATAGCTTCAAAATGTTTCTAC)/#3726 (CCGCGCGGCCGCGTAATTAAAACTTAGATTAGATTGC), or #3728 (CCGCGTCGACGAGGGCCGCATCATGTAA) /#3730 (CCGCGGGCCCAGCTTGCAAATTAAAGCCTTC), and digested with *Sac*I/*Not*I or *Apa*I/*Sal*I. Digested *pTEF1* and *tCYC1* were sequentially inserted into *Sac*I/*Not*I or *Apa*I/*Sal*I-digested pRS315 vector, generating pRS315-pTEF1 (Zhenghe Li and PD Nagy, unpublished data). pRS315-pTEF1 was digested with *Not*I/*Sal*I and ligated with annealed primers of #5157 GGCCGAAAATGAGATCTGGCACTAGTGACTACAAGGACGACGATGACAAGG GTGGCGGTC /#5158 CTAGGACCGCCACCCTTGTCATCGTCGTCCTTGTAGTCACTAGTGCCAGATCT CATTTTC to introduce Flag-tag, generating pRS315-NFlag.

Plasmids expressing wt Sti1p or derivatives ($C_{49}Y$, $G_{325}D$; ΔTPR2; or ΔTPR1) were generated by using available *STI1* mutants (179, 180) in PCR-amplifications using primer pairs #2863 CGCGGGATCCATGTCATTGACAGCCGATG /#2864 CGCGCTCGAGTTAGCGGCCAGTCCGGATG or #5156 CGCGGGATCCAACCCAAAAACTAGCGAAATGATG /#2864, and the obtained PCR products were treated with *BamH*I/*Sal*I and then were inserted into *BamH*I/*Sal*I-digested pRS315-NFlag. To visualize Sti1p in yeast, mRFP1 was PCR-amplified from pGAD-PEX13-RFP (81) using primers #2630

CGCGGGATCCATGGCCTCCTCCGAGGACGTC /#5159 GGACTAGTGGCGCC-GGTGGAGTGG, and the PCR product was digested with *BamH*I/*Pst*I, and inserted into *Bgl*II/*Pst*I-digested pRS315-Sti1 to generate pRS315-mRFP1-Sti1.

E. coli-based expression plasmids, pGEX-2T-Sti1 and mutated derivatives (C_{49}Y, G_{325}D, ΔTPR1, ΔTPR2) were generated by PCR using primers #2863 (CGCGGGATCCATGTCATTGACAGCCGATG) and #4860 (CGCCGAATTCTTAGCGGCCAGTCCGGATGAT), followed by digestion with *BamH*I/*EcoR*I and then ligation into *BamH*I/*EcoR*I-digested pGEX-2T.

Arabidopsis thaliana STI1 ortholog *AtHOP-1* (181) and the TPR1 deletion version (AtHOP1ΔTPR1) were PCR-amplified from *Arabidopsis* cDNA using primers #5659 CGCTGATCAATGGCGGAAGAAGCAAAATCCAAAGG /#5661 CCGCTCGAGTTACCGGACCT-GAACAATTCCGGCACTAACC and #5660 CGCTGATCAATGGATCCGGGGACTAGGGTTTATTTGGAG /#5661, respectively, followed by digestion with *Bcl*I/*Xho*I, and the PCR products were inserted into *BamH*I/*Sal*I digested pRS315-NFlag, generating pRS315-AtHOP1 and pRS315-AtHOP1ΔTPR1, respectively.

Analysis of CIRV repRNA replication in yeast. For measuring CIRV repRNA accumulation, yeast strains BY4741 and *sti1Δ* were transformed with plasmids pESC-C36/DI72 and pYES-C95. For complementation and overexpression studies, we transformed yeast strains BY4741 and *sti1Δ* with pRS315-Sti1 (FLAG-Sti1 plasmid). Tombusvirus repRNA replication was induced by culturing in sc-ULH$^-$ with 2% galactose medium after overnight culture and then yeast was cultivated for 2 days at

23°C. Total RNA was isolated from yeast and used for detection of repRNA levels by Northern blot analysis as described previously (182). Replication was calculated by measuring the accumulation of CIRV DI1 repRNA or the TBSV DI-72(+) repRNA relative to the accumulation of 18S ribosomal RNA. The tombusvirus replication protein analysis was performed as described previously using an anti-His_6 antibody as the primary antibody for the detection of His_6-p36 and His_6-p95. Detection of Flag-Sti1p and Sti1p was carried out using primary anti-Flag and anti-Sti1 antibody, respectively. The secondary antibody for both primary was alkaline phosphatase-conjugated anti-mouse immunoglobulin G (Sigma) (109).

Analysis of protein-protein interaction by split-ubiquitin assay. The bait constructs, pGAD-BT2-N-His36 and pGAD-BT2-N-His33, expressing CIRV replication protein p36 and p33 tombusvirus replication protein have been published before (99, 110). The PCR products of *STI1* and its various truncation versions were digested with *BamH*I/*Xho*I and ligated into the pPRN-N-RE vector digested with *BamH*I/*Sal*I enzymes. Yeast strain *sti1*Δ/NMY51 was co-transformed with pGAD-BT2-N-His36 or pGAD-BT2-N-His33 and pPR-N-RE (NubG) or one of the prey-constructs carrying *STI1* and plated onto Trp-/Leu- (TL^-) synthetic minimal medium plates for plasmid selection (99, 110). Yeast colonies were re-suspended in 50 µl water and spotted onto Trp-/Leu-/His-/Ade- ($TLHA^-$) plates for 2-4 days to detect bait–prey interactions. Plasmid containing the yeast *SSA1* Hsp70 gene served as the positive control and empty vector (pPR-N-RE) as negative control in this assay (99, 110).

Protein purification from E. coli. pMAL-p33 (TBSV p33), pMAL-p92 (TBSV p92), pMAL-p36 (CIRV p36), and pMAL-p95 (CIRV p35) (149) were transformed separately into *E. coli* strain BL21DE3CodonPlus. Protein expression was induced using isopropyl β-D-thiogalactopyranoside (IPTG) for 8 h at 16°C, and the cells were harvested by centrifugation at 5,000 rpm at 4°C for 5 min to remove the medium prior to -80°C storage. Affinity columns containing amylose resin (NEB) were used to purify MBP-tagged recombinant proteins. The frozen pellets were suspended and sonicated in MBP column buffer containing 20 mM Tris-Cl pH 8.0, 150 mM NaCl, 1 mM EDTA, 10 mM β-mercaptoethanol and 1 mM phenylmethylsulfonyl fluoride (PMSF). The sonicated extract was centrifuged at 15,000 rpm for 5 min, and the supernatant was added to the pre-equilibrated amylose resin for 1 h rotating incubation at 4°C. After washing the resin 3 times with column buffer and once with a low salt column buffer (25 mM NaCl), the proteins were eluted with a low salt column buffer containing 0.18% (V/W) maltose and stored at -80°C in 6% (V/V) glycerol. Protein fractions used for the replication assays were 95% pure, as determined by 12% SDS-PAGE and staining with Coomassie-Blue.

Expression of GST-tagged proteins Cpr7p, Cpr7-TPRp, Cns1p, Sti1p and its mutated versions ($C_{49}Y$, $G_{325}D$, ΔTPR1, and ΔTPR2) were induced using isopropyl β-D-thiogalactopyranoside (IPTG) for 6 h at 23°C, and the cells were harvested by centrifugation at 5,000 rpm at 4°C for 5 min to remove the medium and stored at -80°C. Purification of GST-tagged proteins was carried out using glutathione resin and eluted with 10 mM glutathione, 10 mM ß-mercaptoethanol in the column buffer following the same protocol as MBP-proteins.

In vitro tombusvirus replication assay using yeast mitochondrial preparations. Yeast intact mitochondria were purified as described previously (149). The purified mitochondrial fraction (1 µl) and different dilutions of GST, Sti1p, Cpr7p, or Cns1p proteins (8, 16, 32 µM each) were incubated at 25°C for 1 hr in 8 µl buffer A (containing 30 mM HEPES-KOH [pH 7.4], 150 mM potassium acetate, 5 mM magnesium acetate, and 0.6 M sorbitol) with 15 mM creatine phosphate, 1 mM ATP, and GTP, 0.1 mg/ml creatine kinase, 0.1 µl of RNase inhibitor, 10 mM dithiothreitol, 0.5 µg DI-72 RNA transcript, and affinity-purified 0.5 µg MBP-36 (CIRV p36) and MBP-p95 (CIRV p95). The volume of the reaction mixture was then adjusted by adding 16 µl buffer B (containing 30 mM HEPES-KOH [pH 7.4], 150 mM potassium acetate, and 5 mM magnesium acetate) with 15 mM creatine phosphate, 1 mM ATP, CTP, and GTP, 0.025 mM UTP, 0.2 µl of [^{32}P]UTP, 0.1 mg/ml creatine kinase, 0.2 µl of RNase inhibitor, 10 mM dithiothreitol, and 0.05 mg/ml actinomycin D. The reaction mixture was incubated at 25°C for 3 h and terminated by adding 100 µl stop buffer (1% sodium dodecyl sulfate and 0.05 M EDTA, pH 8.0) followed by 100 µl phenol-chloroform extraction, isopropanol-ammonium acetate precipitation overnight at -20°C and washing by 70% ethanol. The newly synthesized ^{32}P-labeled RNA products were incubated at 85°C for 5 min and separated by electrophoresis in a 5% polyacrylamide gel containing 0.5× Tris-borate-EDTA buffer with 8 M urea. Signals were detected using a Typhoon 9400 imaging scanner (GE/Amersham) and quantified by imageQuant software.

Co-purification of host proteins with Twin-Strep-tagged CIRV replication proteins from yeast. To purify the protein of interest, 200 mg BY4741 yeast cells transformed

with plasmids pESC-StrepC36/DI72 pYES-StrepC95 and pFLAG-Sti. Cultured yeasts were re-suspended and homogenized in Buffer B (50 mM Tris-HCl, pH 7.5; 15 mM $MgCl_2$, 10 mM KCl, 10 mM β-mercaptoethanol, 1% [V/V] yeast protease inhibitor cocktail) by glass beads [modified from (92)]. Membrane fractions from cell homogenates were collected and solubilized with column buffer (50 mM Tris-HCl pH 7.5, 15 mM $MgCl_2$, 500 mM KCl, 1% Triton X-100, 5% SB3–10 [caprylyl sulfobetaine] (Sigma), 10 mM β-mercaptoethanol, 1% [V/V] yeast protease inhibitor cocktail), and incubated with 40 μl StrepTactin Superflow hi-capacity 50% resin (IBA Life Sciences) for 1 hour at 4°C in a column. StrepTactin resin was then washed two times with column buffer, two times with wash buffer (50m M Tris-HCl pH 7.5, 15 mM $MgCl_2$, 10 mM KCl, 0.1% Triton X-100, 10 mM β-mercaptoethanol, 1% [V/V] yeast protease inhibitor cocktail), and eluted with SDS-PAGE loading buffer, then subjected to SDS-PAGE and Western blotting analysis with Strep-Tactin AP Conjugate (IBA Life Sciences), anti-Flag and anti-Hsp70 antibodies (Abcam).

Confocal laser microscopy. Wild type BY4741 or *sti1*Δ yeast strains were transformed with the following expression plasmids: pESC-GFP-C36/DI72, pYES-C95, or pESC-GFP-C33/DI72, pYES-C92 (9), as well as pRS315-RFP-Sti1p. The yeast cultures were incubated in galactose medium overnight, sampled and imaged with Olympus FV1000 confocal laser scanning microscope (Olympus America Inc., Melville, NY). The microscope settings were the following: excitation and emission for GFP and RFP were 488nm laser/500-530nm filter and 543nm laser/560-660nm filter, respectively.

Virus induced gene silencing of Sti1/HOP ortholog gene. Virus induced gene silencing (VIGS) in *Nicotiana benthamiana* was performed as described in (183). The C-terminal fragment of *N. benthamiana HOP* gene (yeast *STI1* ortholog, based on *Arabidopsis AtHOP-1* gene) was PCR-amplified from total *N. benthamiana* cDNA using primers #5786 (CGCGGATCCAGGGCATACAGCAACAGGGC) /#5787 (CCGCTCGAGTTATTTGACTTGAATAATTCCTGCACTAACCAAC). The obtained PCR product was digested with *BamH*I/*Xho*I and inserted into pTRV2 digested with *BamH*I/*Xho*I, generating pTRV2-NbHop. As a control for the VIGS experiments, the C-terminal-half of GFP sequence was PCR-amplified by primers #5353 CGCGGATCCGAAGGTGATACCCTTGTTAATAGAATCGAG /#3712 CGGCCTCGAGTTACGCATAGTCAGGAACATCGTATGGGTAGAGTCCGGACTT GTATAGTT from pESC-GFP-C36/DI72, digested with *BamH*I/*Xho*I and inserted into pTRV2 generating pTRV2-1/2GFP. VIGS-treated *N. benthamiana* plants were sap inoculated with CIRV or CNV inocula on the 14th day post silencing. Samples from the inoculated leaves were harvested and subjected to total RNA extraction and Northern blot analysis for viral RNA (81, 183). Efficiency of *NbHOP* silencing was evaluated by semi-quantitative reverse transcription PCR using *NbHOP* and *Actin* gene-specific primer pairs: #5785 (CGCGGATCCAGAGCAGCAAGAGTATTTCGATCCAC) /#5787 and #3993 (GGAAGTAGCATAAGATGGCAGATGGAGAGG) /#3994 (CCAGATCTTCTCCATATCATCCCAGTTGCTGAC), respectively.

3.3 Results

Yeast-based studies reveal that Sti1p co-chaperone selectively inhibits mitochondrial CIRV replication, but not the peroxisomal TBSV replication. Based on our previous findings that two abundant cytosolic TPR-containing cellular proteins, namely Cpr7p cyclophilin and Cns1p co-chaperone, showed robust restriction activity against TBSV (109, 150), we also tested the abundant TPR-containing protein Sti1p co-chaperone for possible effect on the accumulation of TBSV and CIRV replicon (rep)RNAs in *sti1Δ* yeast versus wt yeast cells. Interestingly, *sti1Δ* yeast supported CIRV repRNA accumulation at a ~3-fold higher level than in wt yeast (Fig. 3.1A, lanes 5-6 versus 1-2). However, replication of the TBSV repRNA was comparable in *sti1Δ* and wt yeast (Fig. 3.1B, lanes 4-6 versus 1-3), suggesting that Sti1p has a CIRV-specific inhibitory effect. To test if Sti1p-based inhibition targets the CIRV RNA, we also tested TBSV repRNA accumulation in the presence of CIRV p36 and $p95^{pol}$ replication proteins, which are capable of supporting the replication of the heterologous TBSV repRNA (9), in *sti1Δ* yeast versus wt yeast cells. The obtained data showed ~2-fold increased level of TBSV repRNA accumulation (Fig. 3.1C, lanes 4-6 versus 1-3), demonstrating that the inhibitory effect of Sti1p is targeted against the CIRV p36 and $p95^{pol}$ and not the viral RNA. Comparison of the accumulation of CIRV p36 and $p95^{pol}$ in *sti1Δ* yeast versus wt yeast cells revealed similar replication protein levels (Fig. 3.1C), arguing that Sti1p is unlikely to affect translation or stability of CIRV p36 and $p95^{pol}$ in yeast cells.

To further test if Sti1p can inhibit CIRV replication *in vivo*, we over-expressed N-terminally FLAG-tagged Sti1p in yeast supporting CIRV or TBSV accumulation. We found that over-expression of Sti1p reduced CIRV accumulation by ~3-fold in wt yeast (Fig. 3.2A, lanes 4-6 versus 1-3) and by ~5-fold in *sti1Δ* yeast (Fig. 3.2A, lanes 10-12

versus 7-9). The level of CIRV p36 and $p95^{pol}$ replication proteins was comparable in *sti1Δ* or wt yeasts over-expressing FLAG-Sti1p (Fig. 3.2A), suggesting that Sti1p is unlikely to affect the stability of these viral proteins in yeast. In contrast, replication of the TBSV repRNA was not affected by the over-expression of Sti1p in wt (Fig. 3.2B, lanes 13-16) or in *sti1Δ* or wt yeasts (lanes 17-24). Altogether, these data support that Sti1p is a strong inhibitor of the CIRV p36 and $p95^{pol}$ replication proteins, while Sti1p seems to be ineffective against the tombusviral p33 and $p92^{pol}$ replication proteins in yeast.

The binding of Sti1p involves different regions in CIRV p36 and the TBSV p33 replication proteins. Sti1p contains three TPR domains (Fig. 3.3A) that are predicted to interact with the tombusviral replication proteins. To test if Sti1p can interact with the CIRV p36 versus the TBSV p33 replication proteins, we first used the split-ubiquitin based two-hybrid assay in *sti1Δ* yeast (184, 185). We observed strong interaction between Sti1p and p36 (Fig. 3.3B) and Sti1p and p33 (Fig. 3.3C). We confirmed the interaction between Sti1p and p36 replication protein in *sti1Δ* yeast (Fig. 3.3D, lane 2) using a co-purification assay with recombinant Sti1p. The reciprocal co-purification assay with Strep-tagged p36 also resulted in co-purification of Flag-Sti1p from *sti1Δ* yeast (Fig. 3.3E, lane 1).

To test what region(s) of Sti1p interacts with p36, we used well-characterized Sti1p mutants lacking particular functional domains (179, 180) as shown in Fig. 3.3A. The split-ubiquitin assay showed that the interaction with p36 was not eliminated by deletion (ΔTPR1) or mutation ($C_{49}Y$, and $K_{73}E$) in the TPR1 region (Fig. 3.3B), which

binds to Hsp70 (175, 186). Similarly, deletion (ΔTPR2) or mutations ($G_{325}D$ or $T_{526}I$) in the TPR2 region (Fig. 3.3B), which binds to Hsp90, did not debilitate interaction with p36 replication protein. These findings were confirmed in the reciprocal co-purification experiments (Fig. 3.3D-E), demonstrating that Sti1p could use both the TPR1 and TPR2 sequences to bind to the p36 replication protein. Interestingly, binding of Sti1p to the TBSV p33 replication protein showed similar features with p36 binding (Fig. 3.3C versus Fig. 3.3B). Thus, the binding characteristics of Sti1p to CIRV p36 versus TBSV p33 do not explain why Stip1 can selectively inhibit CIRV replication, but not TBSV replication in yeast cells.

To map the Sti1p binding site in CIRV p36 replication protein, we have used pull-down experiments with immobilized MBP-p36 truncation derivatives (Fig. 3.4A) and Sti1p present in either *E. coli* lysate (Fig. 3.4B) or yeast extract containing Flag-Sti1p (Fig. 3.4C). These experiments revealed that Sti1p binds to a region that includes the RPR motif of p36, which is involved in RNA binding (Fig. 3.4B-C, lane 6, construct p36C4 in Fig. 3.4A). The RPR-motif in replication proteins is required for specific viral (+)RNA recruitment and replicase assembly, and it also binds to Cpr7p Cyp40-like cyclophilin (4, 102, 109, 187). Interestingly, the same RPR-containing region in p36 replication protein could bind to both the TPR1 and TPR2 sequences in Sti1p (Fig. 3.4D-E, lane 6).

To map the Sti1p binding site in the TBSV p33 replication protein, we have used similar pull-down experiments with immobilized MBP-p33 truncation derivatives (Fig. 3.4F) in combination with yeast extract containing Flag-Sti1p or its truncation derivatives (Fig. 3.4G). We found that Sti1p binds to the C-terminal region of TBSV p33 containing

the p33:p33/p92 interaction sequences (Fig. 3.4F). Deletion of the RPR motif, involved in RNA binding, did not inhibit p33 binding to Sti1p (Fig. 3.4G, lane 13). Thus, there is a major difference in Sti1p binding to CIRV (the RPR-containing sequence) and TBSV replication proteins (the C-terminal region in TBSV p33), suggesting that the mechanism of inhibition of CIRV replication by Sti1p could be based on blocking the RNA-binding function of CIRV p36 replication protein.

Sti1p is co-localized with CIRV p36 in yeast cells. To study if the mostly cytosolic Sti1p is recruited to the mitochondrial membranes, where CIRV replication takes place (9, 48), by the CIRV p36 in yeast cells, we co-expressed GFP-p36 with RFP-Sti1p in wt or *sti1Δ* yeast cells. Confocal laser microscopy revealed the robust recruitment of RFP-Sti1p by CIRV p36 to punctate structures, likely representing the mitochondrial membranes as shown before (9, 18, 48) in both wt and *sti1Δ* yeast cells (Fig. 3.5A). In contrast, the GFP-tagged p33 did not efficiently recruit RFP-Sti1p to p33-containing punctate structures (Fig. 3.5B), which likely represent peroxisomal membranes (10, 107). RFP-Sti1p showed diffused, mostly cytosolic distribution in yeast expressing p33 replication protein. Based on these data, we suggest that unlike p33, the CIRV p36 replication protein efficiently recruits Sti1p to the site of replication, leading to robust inhibition of CIRV replication.

The TPR1 domain in Sti1p is required to inhibit CIRV replication in isolated mitochondria-based assay and in yeast cells. To test what domain of Sti1p is required to block CIRV replication, we expressed mutated versions of Sti1p in wt yeast. We

observed ~2-fold inhibition of CIRV repRNA accumulation by ΔTPR2 and $G_{325}D$ mutants, comparable to that obtained with the full-length Sti1p (Fig. 3.6A), while expression of ΔTPR1 or $C_{49}Y$ mutants had no detectable and lesser inhibitory effects, respectively (lanes 9-12 and 21-24 in Fig. 3.6A). All these mutated versions of Sti1p were expressed at comparable levels in wt yeast without substantially affecting CIRV p36 or p95 levels (Fig. 3.6B-C). Altogether, based on these data, we suggest that the TPR1 domain of Sti1p is required to inhibit CIRV replication in yeast.

To further test the roles of the TPR sequences of Sti1p in CIRV replication, we applied an isolated mitochondria-based replication assay, which take advantage of purified recombinant CIRV p36, $p95^{pol}$ replication proteins and repRNA transcripts to support full CIRV replication *in vitro* (Fig. 3.7A) (9, 49, 102). Addition of the affinity-purified full-length recombinant GST-Sti1p (Fig. 3.7B) decreased the production of repRNA by up to 3-fold (Fig. 3.7C, lanes 5-7 versus 2-4), confirming that Sti1p has an inhibitory effect on CIRV replication *in vitro*. Pre-incubation of Sti1p either with Ssa1p Hsp70 chaperone or p36 replication protein to facilitate protein complex formation did not alter the inhibitory effect of Sti1p (Fig. 3.7D), suggesting that Sti1p has robust effect on CIRV replication *in vitro*. The presence of recombinant Sti1p lacking functional TPR2 domain (e.g., ΔTPR2 or mutant $G_{325}D$) was also inhibitory, reducing CIRV replication by up to ~5-fold in the isolated mitochondria-based assay (Fig. 3.7C, lanes 11-16 and 7D, lanes 15-22). In contrast, inactivation of TPR1 (ΔTPR1 or mutant $C_{49}Y$) resulted in the loss of the inhibitory function of Sti1p (Fig. 3.7C, lanes 8-10, 17-19 and 7D, lanes 11-14) in the isolated mitochondria-based replication assay, thus emphasizing the critical role of the TPR1 sequence in Sti1p.

Comparison of the inhibitory effects of host proteins carrying TPR domains on CIRV replication in isolated mitochondria-based replication assay. Two other cellular proteins with TPR domains, namely Cpr7p cyclophilin and Cns1p co-chaperone, have been shown to inhibit TBSV replication (109, 150). Test if these host proteins have comparable activities to Sti1p in inhibition of CIRV replication, we used the isolated mitochondria-based *in vitro* replication assay and purified recombinant cellular proteins and CIRV replication proteins (Fig. 3.8A-B). Interestingly, all these TPR-containing proteins inhibited CIRV replication *in vitro* with Sti1p and the TPR region of Cpr7p showing up to ~10-fold reduction in repRNA production in the isolated mitochondria-based replication assay (Fig. 3.8A, lanes 6-8 and 12-14 versus 3-5). Cns1p was the least effective in this assay (Fig. 3.8A, lanes 15-17), but this could be due to the lower amount of recombinant GST-Cns1p obtained from *E. coli* (Fig. 3.8B). However, the purified recombinant GST-Cns1p was the most effective inhibitor of TBSV replication by reducing TBSV replication by up to ~20-fold in total cell-free extract (CFE)-based replication assay (Fig. 3.8C) (150). Altogether, the TPR-containing Cpr7p seems to have strong inhibitory effect against both TBSV and CIRV replication, while Sti1p efficiently inhibits CIRV, but its effect is only moderate on TBSV replication *in vitro*.

The plant Hop ortholog of the yeast Sti1p inhibits CIRV replication in yeast and plants. *Arabidopsis thaliana* has three orthologs of Sti1p co-chaperone, namely AtHop1-3, that carry TPR1 and TPR2 domains (181, 188). To test if AtHop-1 could inhibit CIRV replication, we expressed it in yeast. Similar to the yeast Sti1p, AtHop-1 inhibited CIRV

accumulation by ~5-fold in yeast (Fig. 3.9, lanes 4-6). Deletion of the TPR1 sequence made AtHop-1 less effective inhibitor of CIRV replication (Fig. 3.9, lanes 7-9), suggesting that the TPR1 sequence is important for the inhibitory function of AtHop-1.

To test the relevance of the plant Hop protein in tombusvirus replication, we tested the accumulation level of Hop mRNA in *Nicotiana benthamiana* host. The semi-quantitative RT-PCR analysis revealed the induction of NbHop mRNA upon infection with CIRV (Fig. 3.10A). In addition, knockdown of NbHop level via VIGS in *N. benthamiana* led to ~3-fold increased CIRV genomic RNA accumulation (Fig. 3.10B). As expected, due to the high level CIRV accumulation, the Hop-knockdown in *N. benthamiana* plants died even more rapidly than control plants when infected with CIRV (Fig. 3.10C). In contrast, the accumulation of the genomic RNA of the related CNV (a peroxisomal replicating tombusvirus, closely related to TBSV) was not significantly affected by Hop-knockdown *N. benthamiana* plants (Fig. 3.10D). Also, the symptom severity of CNV-infected knockdown or control plants was comparable (Fig. 3.10E). Based on these *in planta* experiments, we suggest that the plant Hop ortholog plays a potent inhibitory role, similar to the yeast Sti1p, in the mitochondrial CIRV replication, but not in the peroxisomal CNV replication.

3.4 Discussion

Identification of the Hop-like Sti1p co-chaperone as a novel cell-intrinsic restriction factor against CIRV replication in mitochondria. Cellular protein chaperones are important for virus replication and during other steps of the infectious process (74, 189-

195). For example, Hsp70 has been shown to affect the intracellular localization and membrane insertion of TBSV replication proteins and the assembly of the tombusviral VRCs (100-102). Although Hsp70 interacts directly with the tombusviral replication proteins, it is possible that other cellular factors could affect the subversion of Hsp70s by TBSV. Since co-chaperones facilitate selection and delivery of client proteins to the major Hsp70 and Hsp90 chaperones (196-198), some co-chaperones might also be involved in viral infections as demonstrated in this paper and earlier (74, 189-195).

Our finding that the conserved cellular Hop-like Sti1p co-chaperone is a restriction factor for CIRV replication in the mitochondria contributes to the emerging complex roles of cellular chaperones in virus replication (74). While deletion of Sti1p led to a 2-to-4-fold increase in CIRV replication in yeast model host or knockdown of the orthologous Hop in *N. benthamiana* increased CIRV accumulation by ~3-fold, over-expression of Sti1p or AtHop-1 in yeast was inhibitory. *In vitro* CIRV replication experiments based on isolated mitochondria also confirmed the robust inhibitory effect of Sti1p on CIRV. Moreover, the expression of the Sti1 ortholog Hop is increased during CIRV replication in plant leaves. Thus, Sti1p is a new member of the growing family of cell-intrinsic restriction factors.

However, Sti1p did not have robust effect on replication of the closely related TBSV in yeast or on the replication of CNV in plants, both of which utilize the peroxisomal membranes for replication (10, 107). This contrasting finding with Sti1/Hop for different tombusviruses exploiting different subcellular locations could be due to the difference in accessibility of Sti1/Hop to replication proteins of tombusviruses in their respective cellular environments. For example, it has been shown in plants that Hop/Sti1 is involved

in transportation of freshly synthesized mitochondrial and chloroplast proteins from the cytosol into these organelles (199). Moreover, the delivery/import of mitochondrial preproteins from the cytosol to the mitochondria often depends on Hsp70/Hsp90 chaperones and includes Hop/Sti1 and the TPR domain in Tom70 mitochondrial receptor (200, 201). Also, the CIRV p36 replication protein was shown to interact with various Tom receptor proteins, which might have roles in mitochondrial membrane insertion of p36 (19). Based on these studies, we propose that Sti1/Hop might be easily accessible and bind efficiently to the mitochondria-targeted CIRV replication proteins in cells, while the cellular Sti1/Hop co-chaperone has a lesser chance to bind to the peroxisome-targeted TBSV and CNV replication proteins. Accordingly, live cell imaging showed the re-localization of Sti1p to the mitochondria in the presence of CIRV p36, while Sti1p showed mostly cytosolic localization in yeast cells expressing the CNV p33 replication protein (Fig. 3.5). Thus, the difference in accessibility of Sti1/Hop could be the major mechanism restricting CIRV but not TBSV or CNV replication.

Mechanisms of Sti1p co-chaperone-driven restriction of CIRV replication. Recruitment of the tombusvirus (+)RNA into replication requires selective binding by the tombusvirus replication proteins via recognition of a RNA recruitment element (named p33RE) within the polymerase gene sequence (3, 202). The same p33RE element is also required for the VRC assembly and activation of the polymerase function of the replication protein (4, 203). The specific recognition of p33RE is performed by arginines within the RPR motif in p33/p92^{pol} (123, 204). Therefore, binding of cellular factors to the RPR motif containing region could block the ability of p33/p92^{pol} to bind the viral

(+)RNA, thus inhibiting the essential viral processes of (+)RNA recruitment, VRC assembly and replicase activation (203, 205). Indeed, the TPR domain of Cpr7p binds to the RPR region in the tombusvirus replication proteins and blocks the above viral processes, thus acting as a restriction factor (109). We find that Sti1p also binds to the RPR region in the CIRV p36/p95^{pol} replication proteins (Fig. 3.4) and this could explain the strong *in vitro* inhibitory effect of recombinant Sti1p on CIRV replication based on mitochondrial preparations (Fig. 3.7). The CIRV p36 interaction with Sti1p also leads to the recruitment of Sti1p to punctate structures (mitochondrial membranes) in yeast cells, suggesting robust p36:Sti1p interaction in cells. Thus, direct interaction between the Sti1p and CIRV p36 might block viral RNA recruitment (see Model 1, Fig. 3.11).

However, the picture on the mechanism of CIRV inhibition is likely more complex. This is because both the TPR1 and TPR2 regions of Sti1p bind to the RPR domain of CIRV p36, yet the expression of TPR1 is inhibitory, while TPR2 is less effective in reducing CIRV accumulation in yeast or CIRV replication *in vitro* with mitochondrial preparations (Figs. 3.6-3.7). Thus, the binding to the RPR domain in p36 is unlikely enough for Sti1p to effectively inhibit p36 functions.

Interestingly, Sti1p does not bind to the RPR region of the TBSV p33 replication protein. The binding between p33 and Sti1p involves the C-terminal region of p33 containing the p33:p33/p92 interaction sequence (Fig. 3.4F-G). It is possible that this interaction is not robust/stable enough to interfere with p33 functions in cells. It is likely that p33 could readily interact with additional p33 molecules, while binding to Sti1p molecules by p33 might be less favored in cells. Indeed, Sti1p is not efficiently relocalized to punctate structures containing the p33 molecules in yeast cells (Fig. 3.5B).

A similar situation was observed with Cpr6p Cyp40-like cyclophilin, which also binds to p33 within the C-terminal domain and does not inhibit p33 functions (109). Yet, this rule is not general, since Cns1p co-chaperone binds to the p33:p33/p92 interaction sequence in TBSV p33 replication protein and effectively inhibits TBSV replication in yeast (150) and *in vitro* (Fig. 3.8C). It seems that the intracellular accessibility of these TPR-containing host proteins might be a major factor in their ability to inhibit replication of different tombusviruses.

Although direct interaction between the RPR region of CIRV p36 and the TPR1 sequence in Sti1p might explain the inhibitory effect on CIRV replication (Fig. 3.11, model 1), it is also possible that Sti1p limits the functions of subverted cellular factors, such as Hsp70, for its ontiviral activity. Cytosolic Hsp70s are co-opted by tombusviruses and they are permanent residents in the tombusviral VRCs (98). This model is supported by the observation that, in spite of the binding of both TPR1 and TPR2 sequences to the RPR region of CIRV p36 (Fig. 3.3), only the expression of the Hsp70-interacting TPR1 region (175, 177) was able to robustly inhibit CIRV replication in yeast and *in vitro* (Figs. 3.6-3.7). Moreover, mutation within the TPR1 sequence (i.e., mutant $C_{49}Y$) that debilitates the interaction with Hsp70, but not with p36 (Fig. 3.3) had lesser inhibitory effects on CIRV replication when expressed in yeast (Fig. 3.6). In contrast, a mutation (i.e., mutant $G_{325}D$) that affects interaction with Hsp90 did not interfere with the inhibitory function of Sti1p *in vivo* or *in vitro*. Based on these findings, we propose that the recruited Sti1p co-chaperone inhibits the proviral function of the co-opted cellular Hsp70 molecules during CIRV replication. For example, the predicted Sti1p:Hsp70 interaction during the formation of VRC or within the assembled VRC might inhibit the

Hsp70-driven activation of the polymerase function of p95 or other steps/functions (Fig. 3.11, model 2).

The major role of Sti1p co-chaperone in eukaryotic cells is to bring Hsp70:client protein complex together with Hsp90 chaperone to facilitate robust refolding/activation of client proteins by the powerful Hsp90 system (177, 206, 207). This is facilitated by the ability of Sti1p to bind simultaneously to Hsp70 (via the TPR1 sequence) and Hsp90 (via the TPR2A region). However, based on our data, it is unlikely that this function of Sti1p is critical to inhibit CIRV replication. This is because deletion of the entire TPR2 domain from Sti1p did not eliminate the inhibitory function of Sti1p *in vitro* or in yeast (Fig. 3.6-3.7). Also, blocking the function of Hsp90 by applying geldanamycin inhibitor in yeast had no effect on tombusvirus replication (data not shown), arguing against the functional role of Hsp90 in tombusvirus replication. Therefore, the direct effect of Sti1p on CIRV p36/p95 and the co-opted Hsp70 is the best suited to explain the current experimental data (Fig. 3.11).

Sti1/Hop is the first cellular restriction factor specifically affecting one tombusvirus (i.e., the mitochondria replicating CIRV), but not other tombusviruses (TBSV and CNV, both replicating in peroxisomal membranes). The previously identified TPR domain-containing cellular proteins, namely Cpr7p and Cns1p, could inhibit the replication of all these tombusviruses [this work and (109, 150)]. Interestingly, all three cellular factors are part of the Hsp70/Hsp90 chaperone system, suggesting that they, at least in part, inhibit tombusvirus replication via regulating chaperone functions. Because the Hsp70/Hsp90 chaperone system is known to affect many viruses [reviewed in (74, 208)], it is possible

that the identified restriction factor activities of these TPR-containing cellular proteins might be functional against other viruses and pathogens.

Another use of Hop/Sti1 in host innate defense against pathogens is its role in maturation and transport of rice chitin receptor OsCERK1, which is a pattern recognition receptor (PRRs), against rice blast fungus (209). This function of Hop/Sti1 might link the functions of PRRs, small Rho-type GTPases and resistance against pathogens. Sti1p is also known to affect prion propagation in yeast (210) and its expression is increased in SV40-transformed MRC-5 fibroblasts and some tumor tissues (165, 211). Thus, Hop/Sti1 is emerging as a possibly key component in propagations of several infectious agents and innate defense responses of host cells.

Summary: The current and recent works (109) with tombusviruses indicate that some members of the large family of TPR-containing proteins might act as cell-intrinsic restriction factors of tombusviruses. The list includes the Hop-like Sti1p and Ttc4 oncogene-like Cns1p co-chaperones and Cyp40-like Cpr7p cyclophilin. Yet, based on the yeast Cyp40-like Cpr6p cyclophilin (109), we already know that not all TPR-containing proteins are viral restriction factors in spite of their abilities to interact with tombusvirus replication proteins. Since many TPR-containing proteins are expressed in all eukaryotes, it will be important to identify all the members of these cellular protein family that act as restriction factors during tombusvirus and other (+)RNA virus replication.

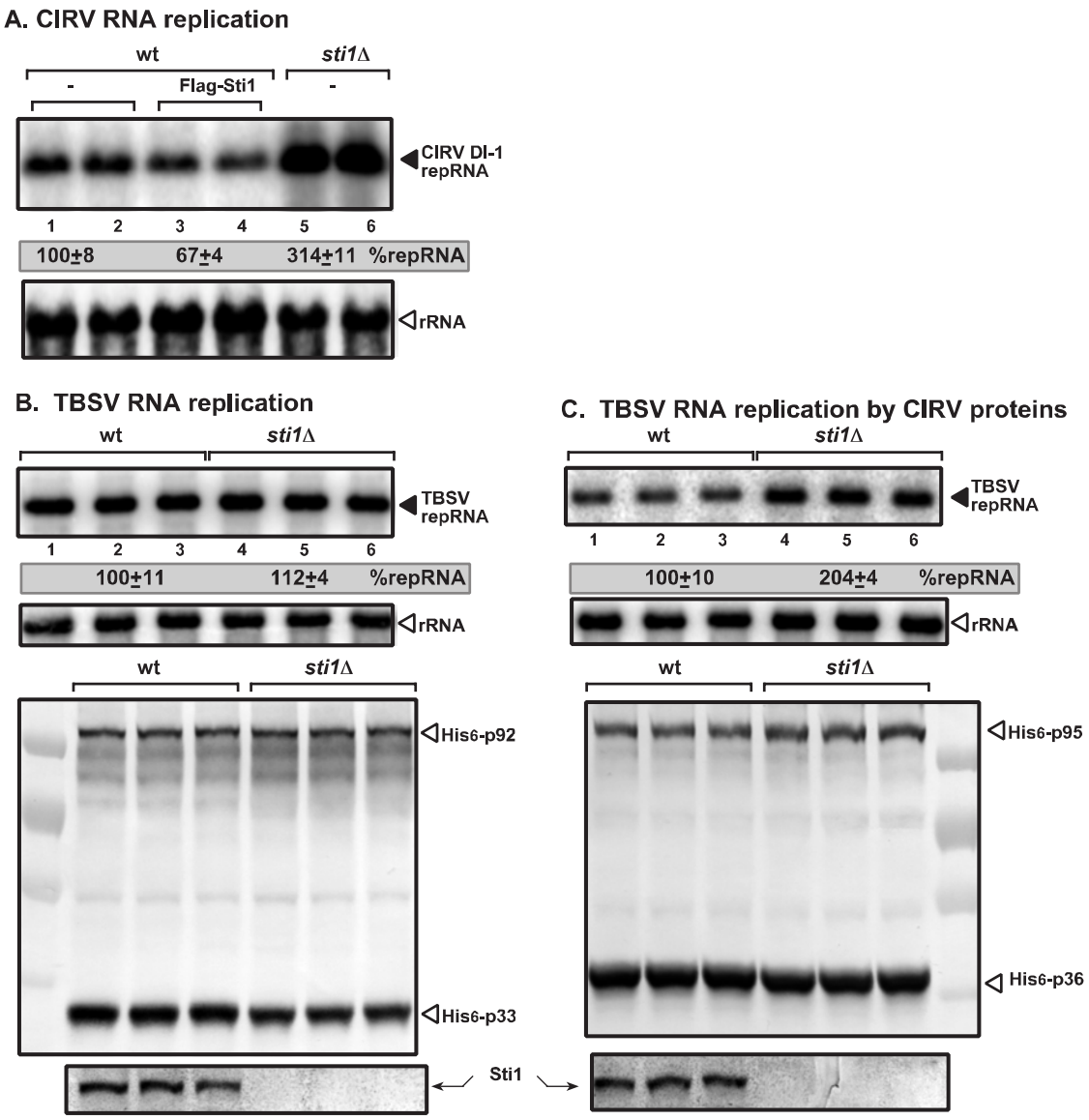
A. CIRV RNA replication
wt
sti1Δ
-
Flag-Sti1
-
CIRV DI-1 repRNA
1 2 3 4 5 6
100±8 67±4 314±11 %repRNA
rRNA
B. TBSV RNA replication
wt
sti1Δ
TBSV repRNA
1 2 3 4 5 6
100±11 112±4 %repRNA
rRNA
wt
sti1Δ
His6-p92
His6-p33
Sti1
C. TBSV RNA replication by CIRV proteins
wt
sti1Δ
TBSV repRNA
1 2 3 4 5 6
100±10 204±4 %repRNA
rRNA
wt
sti1Δ
His6-p95
His6-p36

Fig 3.1

Fig. 3.1 Increased CIRV replication in sti1Δ yeast.

(A) Northern blot analysis of accumulation of CIRV DI-1 repRNA in *sti1Δ* or wt yeast strains at 23ºC. We launched CIRV repRNA replication by expressing CIRV His_6-p36 and His_6-p95 from the galactose-inducible *GAL1* promoter and DI-1 (+)repRNA from the galactose-inducible *GAL10* promoter in *sti1Δ* and the parental (wt, BY4741) yeast strains. Note that the data were normalized based on 18S rRNA. Each experiment was repeated three times. (B) Northern blot analysis of accumulation of TBSV DI-72 repRNA in *sti1Δ* or wt yeast strains. TBSV repRNA replication was launched by expressing CNV His_6-p33 and CNV His_6-p92 from the *GAL1* promoter and DI-72 (+)repRNA from the *GAL10* promoter in *sti1Δ* and the parental (wt BY4741) yeast strains. See further details in panel A. Bottom images: Western blot analysis of CNV His_6-p33, CNV His_6-p92 accumulation by anti-His antibody and Sti1p accumulation by anti-Sti1 antibody. (C) Top images: Northern blot analysis of the CIRV p36/p95-driven TBSV DI-72 RNA accumulation in *sti1Δ* or wt yeast strains. Same as panel A except DI-72 was used as a repRNA with CIRV His_6-p36 and His_6-p95, which support viral RNA replication on mitochondrial membrane surfaces. Bottom images: Western blot analysis of CIRV His_6-p36, CIRV His_6-p95 accumulation by anti-His antibody and Sti1p accumulation by anti-Sti1 antibody.

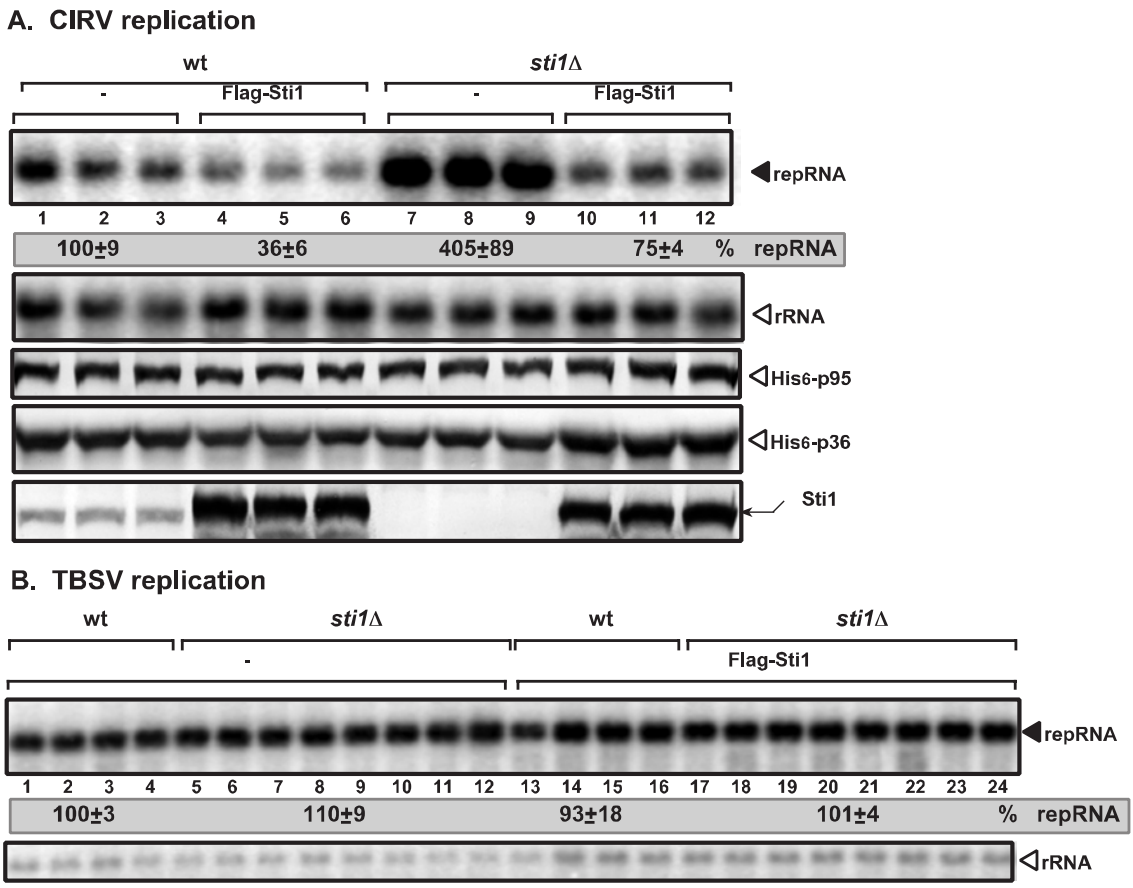
A. CIRV replication
wt
sti1Δ
-
Flag-Sti1
-
Flag-Sti1
repRNA
1 2 3 4 5 6 7 8 9 10 11 12
100±9 36±6 405±89 75±4 % repRNA
rRNA
His6-p95
His6-p36
Sti1
B. TBSV replication
wt
sti1Δ
wt
sti1Δ
-
Flag-Sti1
repRNA
1 2 3 4 5 6 7 8 9 10 11 12 13 14 15 16 17 18 19 20 21 22 23 24
100±3 110±9 93±18 101±4 % repRNA
rRNA

Fig 3.2

Fig. 3.2 Over-expression of Sti1p inhibits CIRV accumulation in yeast.

(A) Top panel: Northern blot analysis of CIRV RNA accumulation in wt or *sti1Δ* yeasts overproducing the FLAG-tagged Sti1p. Second panel: Northern blot analysis to demonstrate the comparable level of ribosomal RNA loading in the yeast samples. Bottom panels: Western blot analysis of CIRV His_6-p95 and CIRV His_6-p36 accumulation by anti-His antibody and Sti1p accumulation by anti-Sti1 antibody. (B) Northern blot analysis of TBSV DI-72 repRNA accumulation in wt or *sti1Δ* yeasts overproducing the FLAG-tagged Sti1p in the presence of peroxisomal CNV p33/p92 replication proteins. See further details in panel A

.

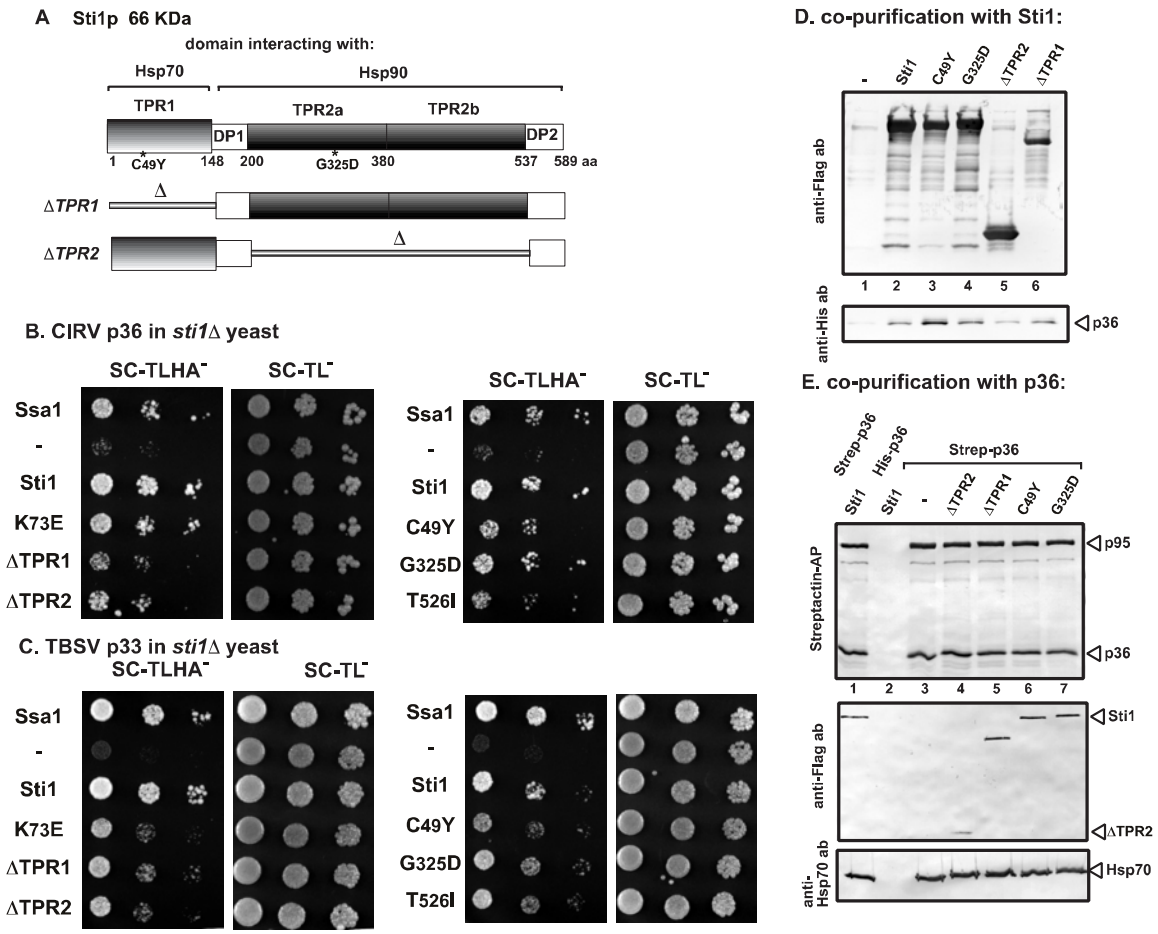
A Sti1p 66 KDa
domain interacting with:
Hsp70
Hsp90
TPR1
TPR2a
TPR2b
DP1
DP2
1 C49Y 148 200 G325D 380 537 589 aa
ΔTPR1
ΔTPR2
B. CIRV p36 in sti1Δ yeast
SC-TLHA-
SC-TL-
Ssa1
-
Sti1
K73E
ΔTPR1
ΔTPR2
C49Y
G325D
T526I
C. TBSV p33 in sti1Δ yeast
D. co-purification with Sti1:
anti-Flag ab
anti-His ab
p36
E. co-purification with p36:
Strep-p36
His-p36
Streptactin-AP
p95
p36
anti-Hsp70 ab
Hsp70

Fig 3.3

Fig. 3.3 Interaction between Sti1p and CIRV p36 replication protein in yeast and in vitro.

(A) Domain structure of the yeast Sti1p. TPR1 (tetratricopeptide repeat) sequence interacts with Hsp70, while DP1 (dipeptide repeat of aspartic acid and proline) might stabilize the bound client protein. TPR2A and TPR2B bind to Hsp90 and together inhibit the ATPase activity of Hsp90. TPR2B also binds to Hsp70, but only in concert with Hsp90 binding to TPR2A. The debilitating mutations are marked with an asterisk and deletion constructs are shown schematically at the bottom of the panel. (B) Split ubiquitin MYTH assay was used to test intracellular interaction between CIRV p36 and the wt or mutated yeast Sti1p. The bait p36 was co-expressed with the prey Sti1p protein in *sti1Δ* yeast. *SSA1* (HSP70 chaperone), and the empty prey vector (NubG) were used as positive and negative controls, respectively. (C) The same split ubiquitin MYTH assay as in panel B, except TBSV p33 was used as a bait protein. (D) Co-purification of CIRV p36 replication protein with the yeast Sti1p from yeast cells. The membrane fraction of yeast co-expressing the wt or mutated FLAG-Sti1p and His_6-p36 was solubilized and the Sti1p variants were purified using a FLAG-column. The eluted proteins were tested using Western blotting with anti-FLAG antibody (top image) and anti-His_6 antibody (bottom image). (E) Reciprocal co-purification of the yeast Sti1p with CIRV p36 and p95 replication proteins from yeast cells. The same as in panel D, except yeast co-expressed the twin-strep-tagged CIRV p36 and p95 and Flag-Sti1p. The purification was based on streptactin columns. The eluted proteins were tested using Western blotting with anti-Strep-Tactin-AP conjugate (top image), anti-Flag antibody (middle image) and anti-Hsp70 antibody (bottom image).

Note: Experiments in Fig. 3.3B, C&D were in collaboration with Dr. Jing-Yi Lin.

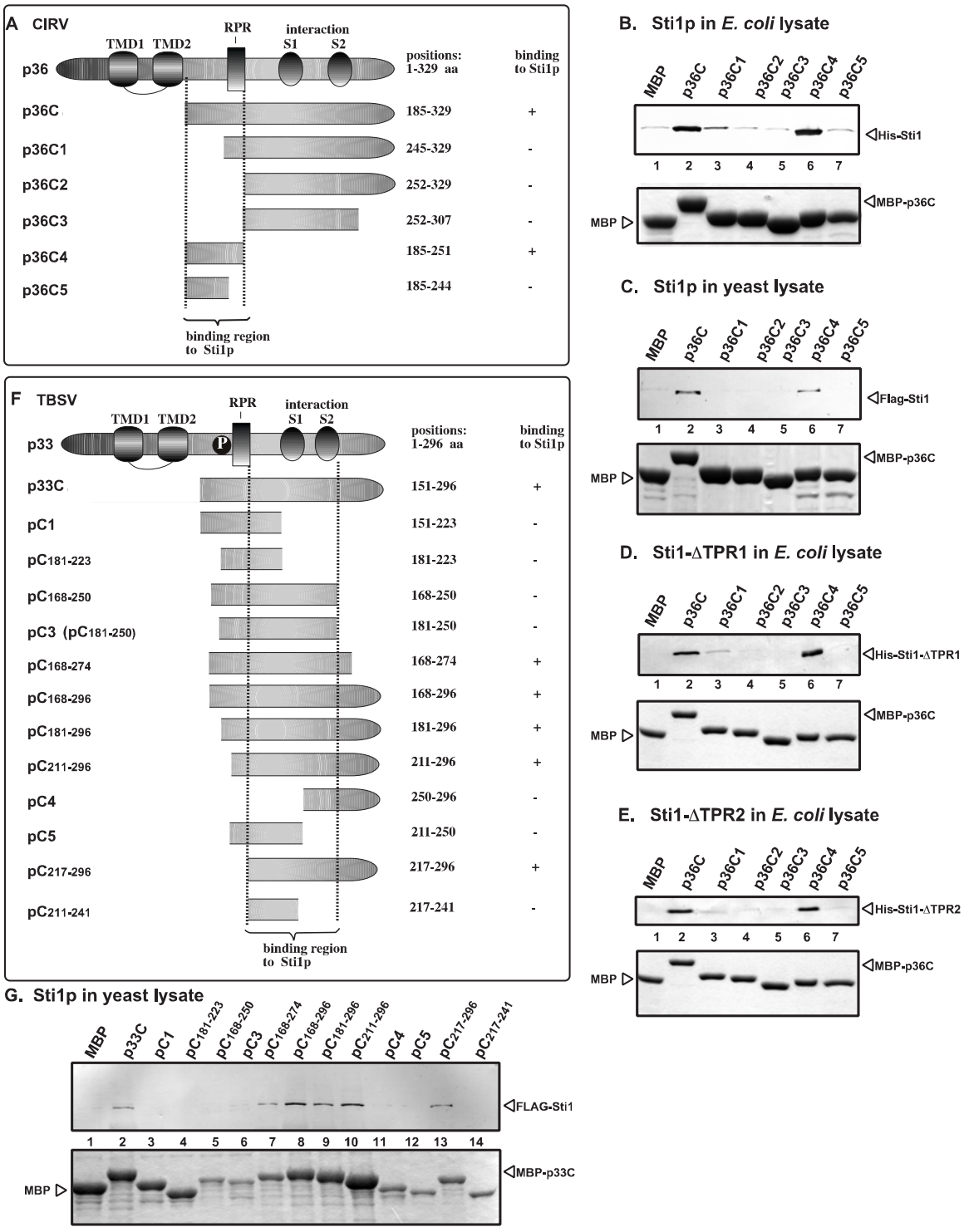
A CIRV
TMD1 TMD2
RPR
interaction S1 S2
positions: 1-329 aa
binding to Sti1p
p36
p36C 185-329 +
p36C1 245-329 -
p36C2 252-329 -
p36C3 252-307 -
p36C4 185-251 +
p36C5 185-244 -
binding region to Sti1p
F TBSV
TMD1 TMD2
RPR
interaction S1 S2
positions: 1-296 aa
binding to Sti1p
p33
P
p33C 151-296 +
pC1 151-223 -
pC181-223 181-223 -
pC168-250 168-250 -
pC3 (pC181-250) 181-250 -
pC168-274 168-274 +
pC168-296 168-296 +
pC181-296 181-296 +
pC211-296 211-296 +
pC4 250-296 -
pC5 211-250 -
pC217-296 217-296 +
pC211-241 217-241 -
binding region to Sti1p
G. Sti1p in yeast lysate
MBP p33C pC1 pC181-223 pC168-250 pC3 pC168-274 pC168-296 pC181-296 pC211-296 pC4 pC5 pC217-296 pC217-241
FLAG-Sti1
1 2 3 4 5 6 7 8 9 10 11 12 13 14
MBP
MBP-p33C
B. Sti1p in E. coli lysate
MBP p36C p36C1 p36C2 p36C3 p36C4 p36C5
His-Sti1
1 2 3 4 5 6 7
MBP
MBP-p36C
C. Sti1p in yeast lysate
MBP p36C p36C1 p36C2 p36C3 p36C4 p36C5
Flag-Sti1
1 2 3 4 5 6 7
MBP
MBP-p36C
D. Sti1-ΔTPR1 in E. coli lysate
MBP p36C p36C1 p36C2 p36C3 p36C4 p36C5
His-Sti1-ΔTPR1
1 2 3 4 5 6 7
MBP
MBP-p36C
E. Sti1-ΔTPR2 in E. coli lysate
MBP p36C p36C1 p36C2 p36C3 p36C4 p36C5
His-Sti1-ΔTPR2
1 2 3 4 5 6 7
MBP
MBP-p36C

Fig 3.4

Fig. 3.4 Defining the sequence within the tombusvirus replication proteins needed for binding to Sti1p in vitro.

(A) Schematic representation of the CIRV p36 and its truncated derivatives used in the binding assay. The various domains include: TMD, transmembrane domain; RPR, arginine-proline-rich RNA binding domain; P; phosphorylated serine and threonine; S1 and S2 subdomains involved in p36:p36/p95 interaction. (B-E) Affinity binding (pull-down) assay to detect interaction between Flag- or His_6-Sti1p, ΔTPR1, ΔTPR2 and the MBP-tagged CIRV p36 protein derivatives. The MBP-tagged viral proteins produced in *E. coli* were immobilized on amylose-affinity columns. Then, the recombinant Sti1p and derivatives expressed in *E. coli* (panels B, D, E) or in yeast (panel C) was passed through the amylose-affinity columns with immobilized MBP-tagged p36 protein (its truncated versions). The affinity-bound proteins were eluted with maltose from the columns (shown in the bottom image). Top images in each panel: The eluted proteins were analyzed by Western blotting with anti-Flag or anti-His antibodies to detect the amount of Flag- or His_6-Sti1p specifically bound to MBP-tagged viral proteins. Bottom image: SDS-PAGE analysis of the viral protein and its truncated derivatives after elution from the amylose-affinity columns. Note that the MBP has a C-terminal extra tail sequence (not present in the fusion protein constructs) due to the sequence in the original cloning vector. (F) Schematic representation of the TBSV p33 and its truncated derivatives used in the binding assay. (G) Affinity binding (pull-down) assay to detect interaction between FLAG-Sti1p and the MBP-tagged viral p33 protein (the soluble C-terminal portion). The MBP-tagged viral protein or MBP control produced in *E. coli* was immobilized on amylose-affinity columns. See further details in panel B above. The eluted proteins were analyzed by Western blotting with anti-FLAG antibody to detect the amount of FLAG-Sti1p specifically bound to MBP-tagged viral protein.

Note: Experiments in Fig. 3.4G were in collaboration with Dr. Jing-Yi Lin.

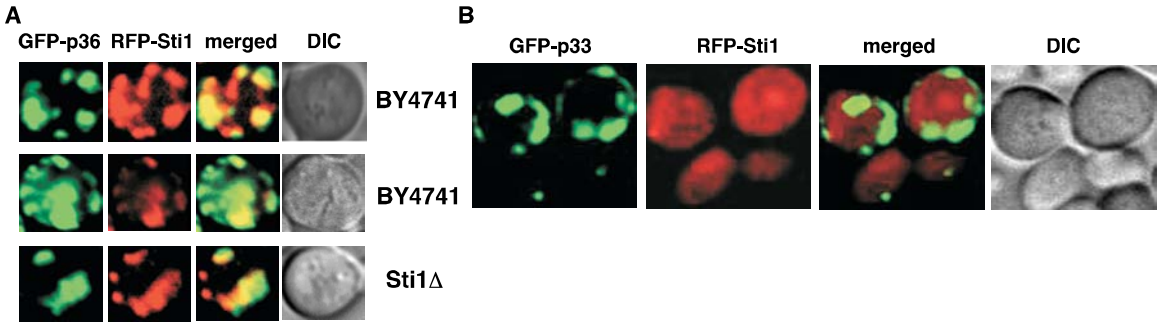
A
GFP-p36
RFP-Sti1
merged
DIC
BY4741
BY4741
Sti1Δ
B
GFP-p33
RFP-Sti1
merged
DIC

Fig 3.5

Fig. 3.5 Relocalization of yeast Sti1p co-chaperone when co-expressed with CIRV p36 replication protein in yeast.

(A) Confocal laser microscopy images show the partial co-localization of RFP-Sti1 with CIRV GFP-p36 in wt (top images), or in *sti1Δ* yeast strains. The merged images show the co-localization within punctate structures, likely representing mitochondria, which are the sites of CIRV replication. DIC (differential interference contrast) images are shown on the right. (B) Absence of co-localization of RFP-Sti1 and GFP-p33 in yeast. Note the cytosolic distribution of RFP-Sti1, while GFP-p33 is present in punctate structures representing the peroxisomes. Each experiment was repeated.

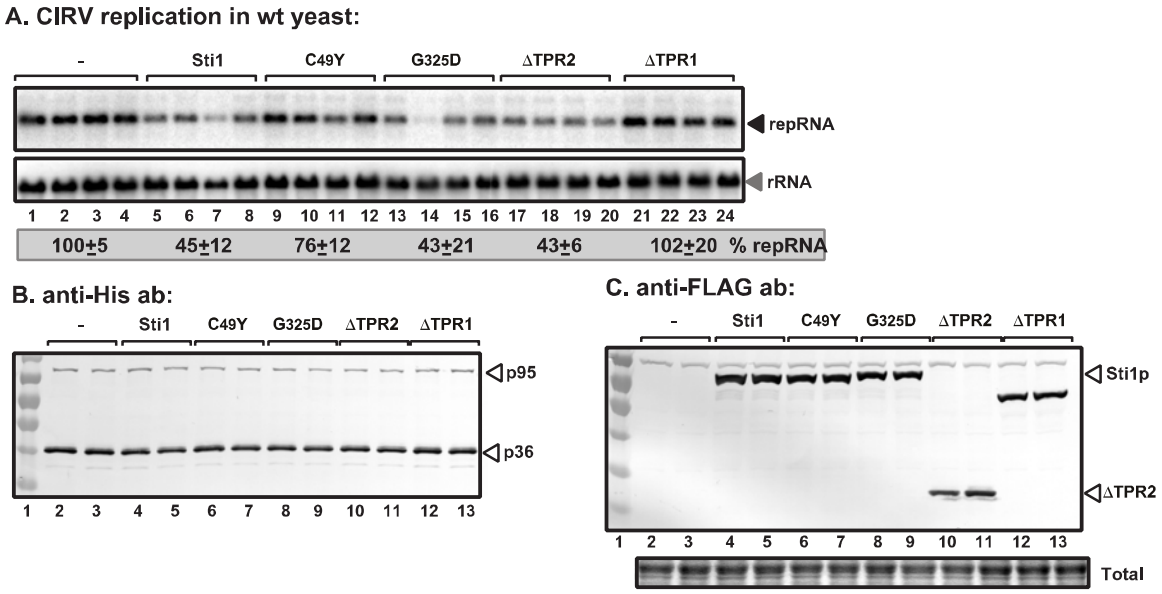
A. CIRV replication in wt yeast:
-
Sti1
C49Y
G325D
ΔTPR2
ΔTPR1
repRNA
rRNA
1 2 3 4 5 6 7 8 9 10 11 12 13 14 15 16 17 18 19 20 21 22 23 24
100±5
45±12
76±12
43±21
43±6
102±20 % repRNA
B. anti-His ab:
-
Sti1
C49Y
G325D
ΔTPR2
ΔTPR1
p95
p36
1 2 3 4 5 6 7 8 9 10 11 12 13
C. anti-FLAG ab:
-
Sti1
C49Y
G325D
ΔTPR2
ΔTPR1
Sti1p
ΔTPR2
1 2 3 4 5 6 7 8 9 10 11 12 13
Total

Fig 3.6

Fig. 3.6 Functional TPR1 domain of Sti1p is required for inhibition of CIRV replication in yeast.

(A) Northern blot analysis of CIRV accumulation in wt yeast overproducing the FLAG-tagged Sti1p or derivatives. Bottom panel: Northern blot analysis to demonstrate the comparable level of ribosomal RNA loading in the yeast samples. (B) Western blot analysis of CIRV His_6-p36, and CIRV His_6-p95 accumulation by anti-His antibody from yeast overproducing Sti1p or derivatives. (C) Detection of the overproduced FLAG-Sti1p or its derivatives in yeast by Western blot analysis using anti-FLAG antibody.

Note: Experiments in Fig. 3.6 were in collaboration with Dr. Jing-Yi Lin.

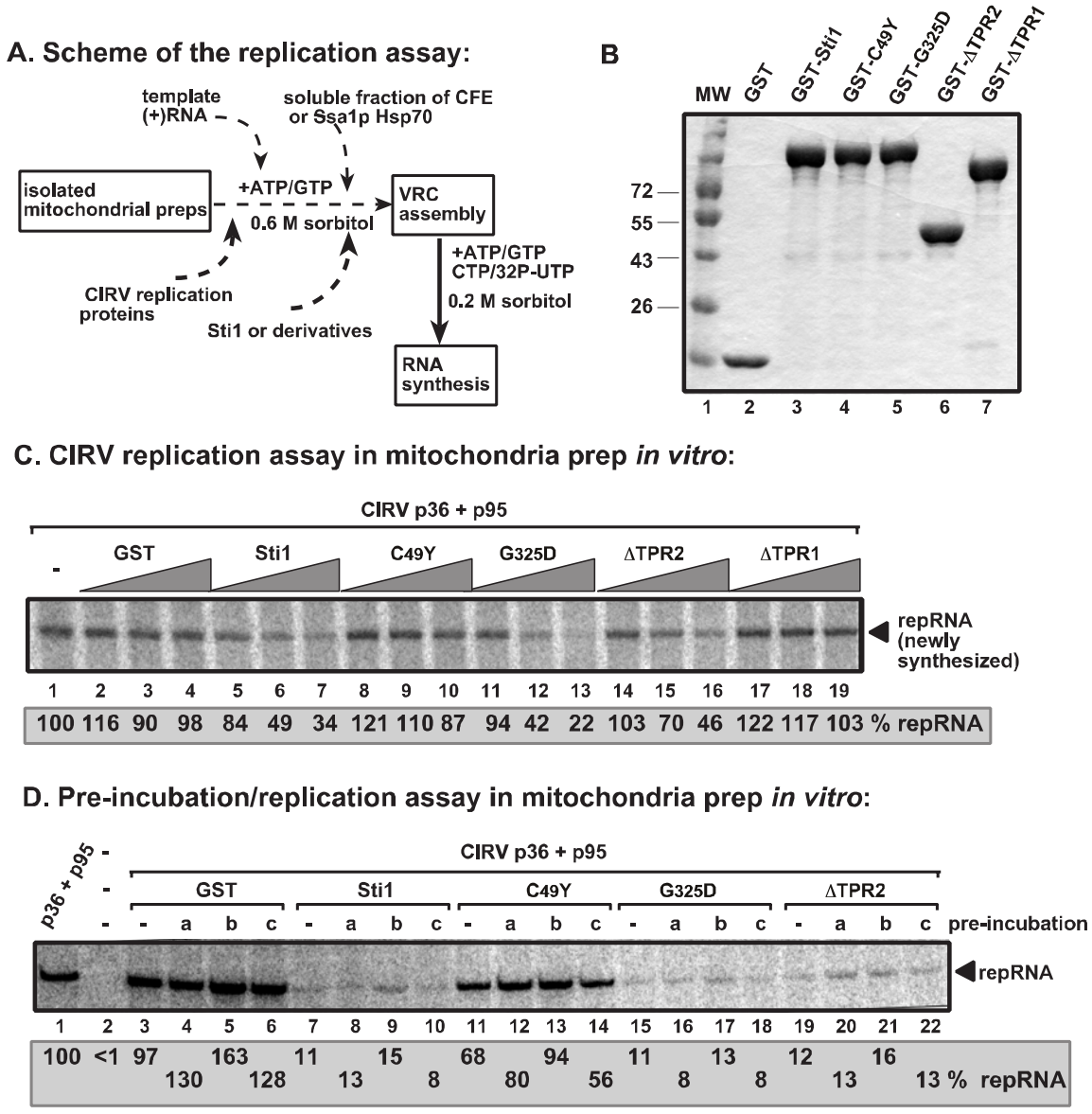
A. Scheme of the replication assay:
template (+)RNA
soluble fraction of CFE or Ssa1p Hsp70
isolated mitochondrial preps
+ATP/GTP
0.6 M sorbitol
VRC assembly
+ATP/GTP CTP/32P-UTP
0.2 M sorbitol
RNA synthesis
CIRV replication proteins
Sti1 or derivatives
B
MW
GST
GST-Sti1
GST-C49Y
GST-G325D
GST-ΔTPR2
GST-ΔTPR1
72
55
43
26
1 2 3 4 5 6 7
C. CIRV replication assay in mitochondria prep in vitro:
CIRV p36 + p95
-
GST
Sti1
C49Y
G325D
ΔTPR2
ΔTPR1
repRNA (newly synthesized)
1 2 3 4 5 6 7 8 9 10 11 12 13 14 15 16 17 18 19
100 116 90 98 84 49 34 121 110 87 94 42 22 103 70 46 122 117 103 % repRNA
D. Pre-incubation/replication assay in mitochondria prep in vitro:
p36 + p95
CIRV p36 + p95
GST
Sti1
C49Y
G325D
ΔTPR2
- a b c
pre-incubation
repRNA
1 2 3 4 5 6 7 8 9 10 11 12 13 14 15 16 17 18 19 20 21 22
100 <1 97 130 163 128 11 13 15 8 68 80 94 56 11 8 13 8 12 13 16 13 % repRNA

Fig 3.7

Fig. 3.7 Functional TPR1 domain of Sti1p blocks CIRV replication in vitro.

(A) Scheme of *in vitro* reconstitution of the CIRV replicase in yeast mitochondrial preparation. The purified GST-tagged Sti1p or derivatives, the purified recombinant CIRV MBP-p36 and MBP-p95 proteins and the TBSV-derived (+)repRNA were used in isolated mitochondrial preparations. (B) Coomassie Blue stained SDS-PAGE was used for analysis of affinity-purified GST-tagged Sti1 or derivatives. (C) Denaturing PAGE analysis of the ^{32}P-labeled repRNA products obtained in the replication assays with the isolated yeast mitochondrial preparation and the soluble fraction of yeast CFE that provided soluble host factors. The synthesized full-length repRNA is pointed at by an arrow. The replication assay with CIRV p36 and p95 (without added Sti1) was chosen as 100% (lane 1). The recombinant proteins were added in 8, 16 and 32 μM amounts. Each experiment was repeated. (D) CIRV mitochondrial replication assays were performed (see panel A) to test the effect of pre-incubation of various components. Lanes "a" show samples when the purified Ssa1p Hsp70 (from *sti1Δ* yeast strain) was pre-incubated for 10 min with comparable amount of GST, GST-Sti1p or mutants (from *E. coli*), while in lanes "b", the MBP-p36/MBP-p95 of CIRV (from *E. coli*) was pre-incubated with Ssa1p. In lanes "c", the MBP-p36/MBP-p95 of CIRV was pre-incubated with GST, GST-Sti1p or mutants, while in lanes "-" no pre-incubation was performed. In each experiment, we used comparable amounts of each component for pre-incubation that lasted for 10 min in the reaction buffer. After the pre-incubation step, we added the missing components and performed the CIRV replication assay (see panel A). Each experiment was repeated at least twice.

Note: Experiments in Fig. 3.7 were in collaboration with Dr. Jing-Yi Lin.

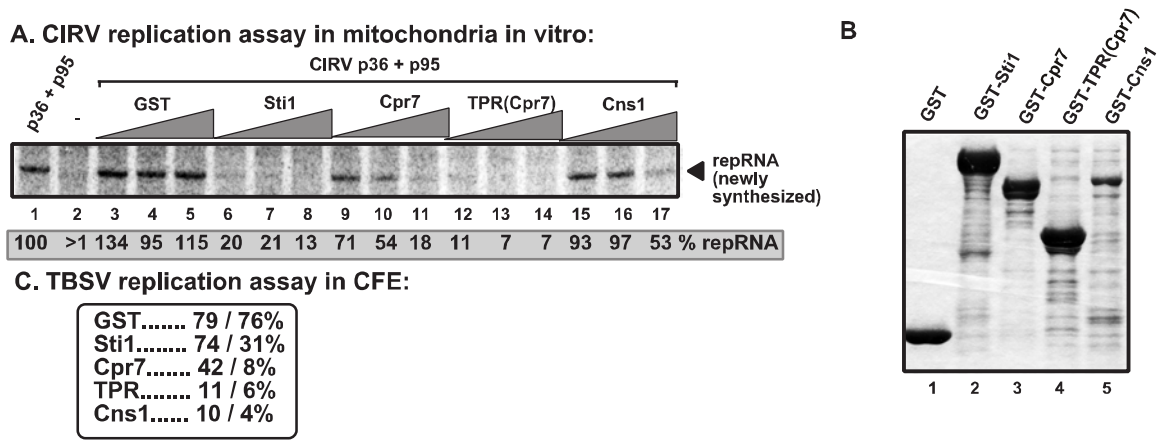
A. CIRV replication assay in mitochondria in vitro:
p36 + p95
-
CIRV p36 + p95
GST
Sti1
Cpr7
TPR(Cpr7)
Cns1
repRNA
(newly
synthesized)
1 2 3 4 5 6 7 8 9 10 11 12 13 14 15 16 17
100 >1 134 95 115 20 21 13 71 54 18 11 7 7 93 97 53 % repRNA
C. TBSV replication assay in CFE:
GST..... 79 / 76%
Sti1..... 74 / 31%
Cpr7..... 42 / 8%
TPR..... 11 / 6%
Cns1..... 10 / 4%
B
GST
GST-Sti1
GST-Cpr7
GST-TPR(Cpr7)
GST-Cns1
1 2 3 4 5

Fig 3.8

Fig. 3.8 Comparison of the inhibitory effects of TPR-containing cellular proteins on CIRV replication in isolated mitochondria in vitro.

(A) Denaturing PAGE analysis of the ^{32}P-labeled repRNA products obtained in the replication assays with the isolated yeast mitochondrial preparations. The purified GST-tagged Sti1p, the yeast Cpr7p Cyp40-like cyclophilin, the TPR domain of Cpr7p or Cns1p co-chaperone (8, 16 and 32 μM) was added in combination with purified recombinant CIRV MBP-p36 and MBP-p95 proteins and the TBSV-derived (+)repRNA to the isolated mitochondrial preparations to perform the *in vitro* replication assay. The synthesized full-length repRNA is marked by an arrow. See further details in Fig. 3.7. (B) Coomassie Blue stained SDS-PAGE was used for analysis of affinity-purified GST-tagged Sti1p, Cpr7p and Cns1p. (C) The level of *in vitro* TBSV repRNA replication in total yeast cell-free extracts in the presence of purified TBSV p33 and p92 replication proteins and purified GST-tagged Sti1p, Cpr7p, the TPR domain of Cpr7p or Cns1p (16 and 32 μM).

Note: Experiments in Fig. 3.8 were in collaboration with Dr. Jing-Yi Lin.

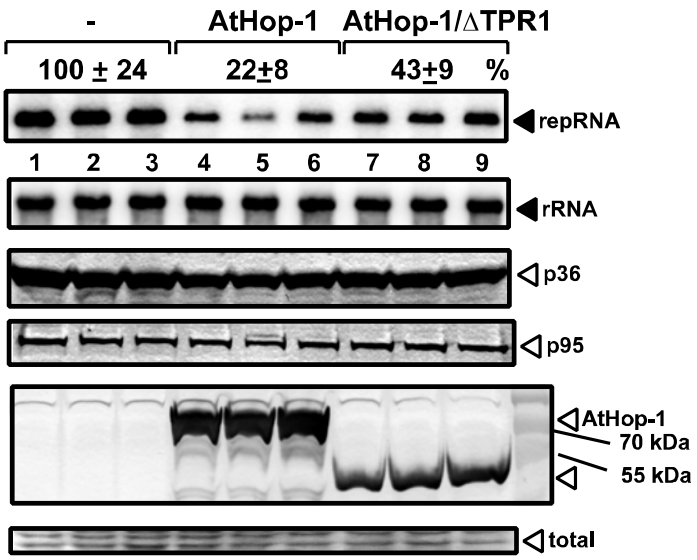
-
AtHop-1
AtHop-1/ΔTPR1
100 ± 24
22±8
43±9
%
repRNA
1 2 3 4 5 6 7 8 9
rRNA
p36
p95
AtHop-1
70 kDa
55 kDa
total

Fig 3.9

Fig. 3.9 Inhibition of CIRV replication by expression of the orthologous AtHop-1 in yeast.

(A) Northern blot analysis of CIRV RNA accumulation in wt yeast overproducing the FLAG-tagged AtHop-1 or its TPR1-deletion derivative. Second panel: Northern blot analysis to demonstrate the comparable level of ribosomal RNA loading in the yeast samples. Third and fourth panels: Western blot analysis of CIRV His_6-p36, and CIRV His_6-p95 accumulation by anti-His antibody. Bottom panels: Detection of the overproduced FLAG-AtHop-1 in yeast by Western blot analysis using anti-FLAG antibody and the Coomassie-stained SDS-PAGE as a loading control.

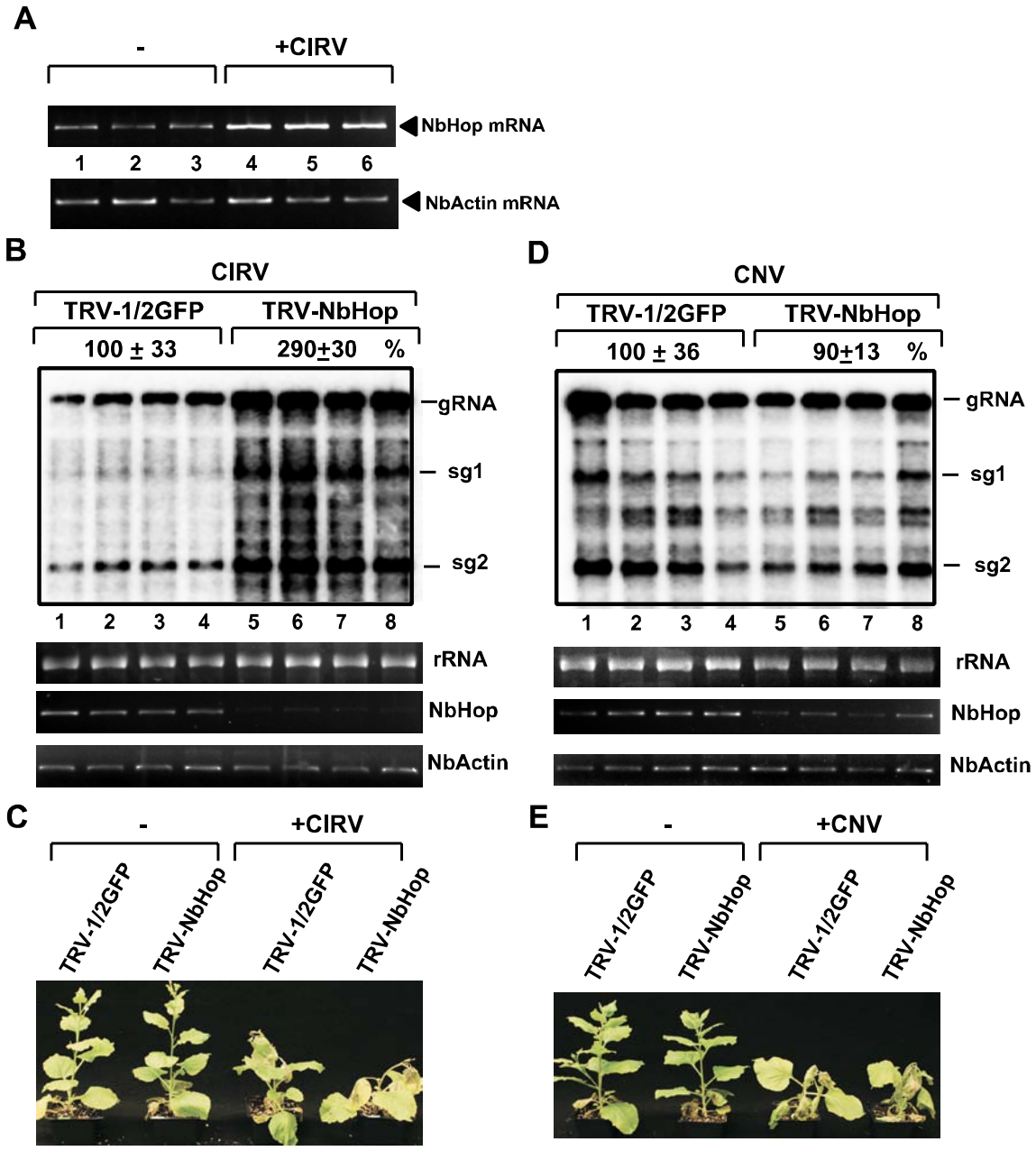
A
-
+CIRV
NbHop mRNA
1 2 3 4 5 6
NbActin mRNA
B
CIRV
TRV-1/2GFP
TRV-NbHop
100 ± 33
290±30 %
gRNA
sg1
sg2
1 2 3 4 5 6 7 8
rRNA
NbHop
NbActin
D
CNV
TRV-1/2GFP
TRV-NbHop
100 ± 36
90±13 %
gRNA
sg1
sg2
1 2 3 4 5 6 7 8
rRNA
NbHop
NbActin
C
-
+CIRV
TRV-1/2GFP
TRV-NbHop
TRV-1/2GFP
TRV-NbHop
E
-
+CNV
TRV-1/2GFP
TRV-NbHop
TRV-1/2GFP
TRV-NbHop

Fig 3.10

Fig. 3.10 Knockdown of Hop gene by VIGS increases CIRV accumulation in whole plants.

(A) Semi-quantitative RT-PCR analysis of the accumulation of *NbHOP* mRNAs in CIRV-infected *N. benthamiana* plants (3 dpi, days post-inoculation) and in the control mock-inoculated plants. Semi-quantitative RT-PCR analysis of NbActin mRNA level served as a control. (B) Top image: Accumulation of CIRV genomic and subgenomic RNAs in the inoculated leaves of *HOP* knockdown *N. benthamiana* plants 2 dpi, based on Northern blot analysis. VIGS was performed via agroinfiltration of TRV vectors carrying *NbHOP* sequence or the TRV vector carrying the C-terminal half of GFP insert (as a control). Inoculation with CIRV gRNA was done 14 days after VIGS. Second image: Ribosomal RNA level in the samples used as loading control. Bottom images: Semi-quantitative RT-PCR analysis of the accumulation of *NbHOP* mRNA in the knockdown *N. benthamiana* plants and in the control plants 2 days after inoculation with CIRV. Semi-quantitative RT-PCR analysis of the NbActin mRNA from the same samples served as a control. (C) Accelerated CIRV-induced symptom development in the *NbHOP* knockdown plant (shown on the right) at 7 dpi when compared to the control plant infiltrated with the control TRV vector. Note the minor phenotypic effect in the uninfected *NbHOP* knockdown *N. benthamiana* plants when compared to the control plants, which were agroinfiltrated with the pTRV1/2GFP vector (the plants on the left side of the images). (D) Accumulation of CNV gRNA in the inoculated leaves of *HOP* knockdown *N. benthamiana* plants 2 days post-inoculation, based on Northern blot analysis. See further details in Panel B. (E) Comparable CNV-induced symptom development in the *HOP* knockdown and control plants. See further details in Panel C.

Model 1: Sti1/Hop inhibits viral RNA binding by p36/p95

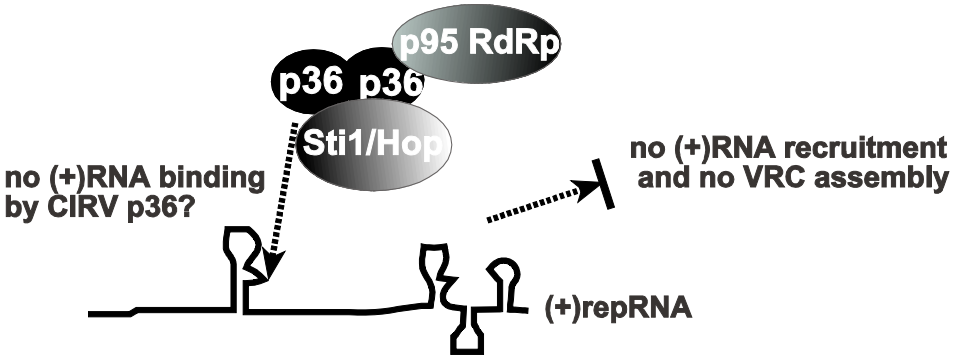

Model 2. Sti1/Hop blocks the co-opted Hsp70 in its function to facilitate the assembly of the CIRV replicase on mitochondria

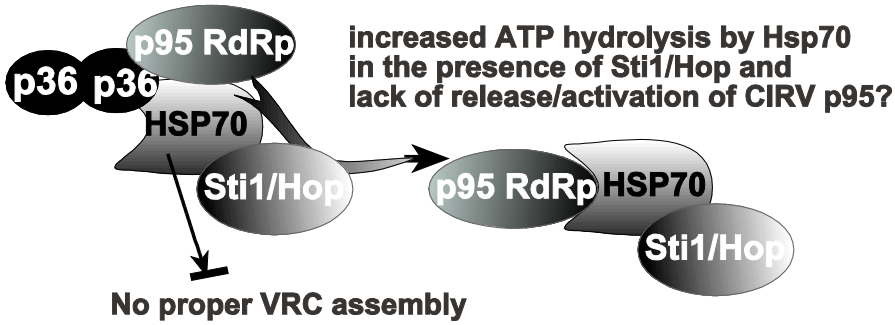

Fig 3.11

Fig. 3.11 Models on the inhibitory role of Sti1p co-chaperone in CIRV replication.

Model 1 predicts that direct interaction between Sti1p and the RPR region of CIRV p36 replication protein blocks the viral (+)RNA recruitment function of p36, and thus blocks replication of CIRV. Model 2 emphasizes the additional role of Sti1p through the co-opted Hsp70 chaperone. Binding of the TPR1 domain of Sti1p to Hsp70 within the CIRV replicase might inhibit the function of the subverted Hsp70 in VRC assembly, by possibly stabilizing the Hsp70-p95 complex. Note that both mechanisms might operate inside the cell.

Chapter 4

RNA VIRUS REPLICATION DEPENDS ON ENRICHMENT OF PHOSPHATIDYLETHANOLAMINE AT REPLICATION SITES IN SUBCELLULAR MEMBRANES

4.1 Introduction

Many steps in the infection cycles of positive-strand RNA viruses, including entry into the cell, replication, virion assembly and egress, are associated with subcellular membranes(20). Therefore, viruses have to interact with different lipids, such as phospholipids and sterols, which affect the biophysical features of membranes, including the fluidity and curvature (57, 64, 70, 144). The subverted cellular membranes could protect the viral RNA from recognition by the host nucleic acid sensors or from destruction by the cellular innate system. In addition, membranes facilitate the sequestration of viral and co-opted host proteins to increase their local concentrations and promote macromolecular assembly, including formation of the replicase complex or virion assembly. To optimize viral processes, RNA viruses frequently manipulate lipid composition of various intracellular membranes. Overall, the interaction between cellular lipids and viral components is emerging as one of the possible targets for antiviral methods against a great number of viruses.

Among the various lipids, the highly abundant phospholipids are especially targeted by RNA viruses (57). In general, phospholipids likely affect the replication of most RNA viruses, which takes place within membranous structures(31). Accordingly, lipidomics analyses of cells infected with Dengue virus and Hepatitis C virus (66, 67) revealed enhanced virus-induced lipids biosynthesis, resulting in changes in the global lipid profile of host cells. Phosphatidylinositol-4-phosphate (PI4P) was shown to be enriched at sites of enterovirus replication, and RNA polymerase of Poliovirus selectively binds to PI4P (33), suggesting that micro-environment enriched for PI4P facilitates enterovirus replication. However, our knowledge on the roles of various phospholipids in RNA virus replication is currently incomplete. By using tombusviruses, small model RNA viruses of plants that can replicate in yeast surrogate host (13), a major role for phospholipid and sterol biosynthesis has been revealed (89, 90). In this paper, development of artificial vesicle-based replication of tomato bushy stunt virus (TBSV) identified the essential role of phosphatidylethanolamine (PE) in RNA virus replication. It is also shown that TBSV could recruit and enrich PE to the sites of viral replication in yeast and plant cells. Moreover, genetic changes that increase PE levels in yeast greatly stimulated TBSV replication, confirming the key role of PE in the formation of TBSV replicase.

4.2 Materials and Methods

Yeast Strains and expression plasmids. Parental yeast strain BY4741 (MAT a *his3Δ1 leu2Δ0 met15Δ0 ura3Δ0*) and single-gene deletion yeast strains (*cho2*Δ, *pex3*Δ) were from Open Biosystems. *E. coli* protein expression plasmids for recombinant TBSV p33 and

p92, pMAL-p33 and pMAL-p92, were previously described (102). pESC-T33/DI72 and pYES-T92 used for yeast expression of viral components were described (9).

Preparation of CFE, membrane fraction (P40) and soluble fraction (S40). The yeast cell-free extracts (CFE) from train BY4741 were prepared according to (49). CFE preparations were centrifuged at 40,000 x g for 1hr to separate the membrane fraction (P40) and the soluble fraction (S40). Collected P40 and S40 were immediately stored at -80 °C until use.

Artificial phospholipid vesicles preparation. Phospholipids were obtained from Avanti Polar lipids, Inc. Phospholipids (269 nmol/preparation) were dissolved in chloroform and transferred into glass vials, mixed, and subsequently dried under a small stream of nitrogen for 1 hour under fume hood. The phospholipids were further dried in a speed-vacuum for additional 2-3 hours to completely remove chloroform. To each glass vial, 400 µl HEPES buffer (30 mM, pH 7.4) was added, followed by sonication in a bath sonicator (Avanti Polar lipids, Inc.) filled with ice for 20 minutes. The mixtures became visually homogeneous. The concentrations of the obtained phospholipid vesicle preparations were 672 µM. Phospholipids vesicles were prepared in the same day of *in vitro* replication assay.

***In vitro* TBSV replication assay using artificial phospholipid vesicles.** The procedure for *in vitro* replication assay using phospholipid vesicles was adapted from the previously published procedure using purified yeast organelles (9), except that 100,000 xg supernatant

(S100) was replaced with S40 fraction of CFE. Briefly, 2 μl of phospholipid vesicles and 1 μl of S40 fraction were incubated at 25 °C for 1 hour in 8 μl buffer containing 30 mM HEPES-KOH (pH7.4), 150 mM potassium acetate, 5 mM magnesium acetate, 0.6 M sorbitol, 15 mM creatine phosphate, 1 mM ATP, CTP and GTP and 0.025 mM UTP, 0.1 μl of [^{32}P]UTP, 0.1 mg/ml creatine kinase, 0.1 μl of RNase inhibitor (Thermo Scientific), 10 mM dithiothreitol, 0.5 μg DI-72 RNA transcript, and 0.5 μg MBP-tagged recombinant TBSV p33 and p92 replication proteins. Then, the reaction mix was incubated for 3 hours in 16 μl cell-free replication buffer B (30 mM HEPES-KOH pH7.4, 150 mM potassium acetate, 5 mM magnesium acetate) with 15 mM creatine phosphate 1 mM ATP, CTP and GTP 0.025 mM UTP, 0.2 μl of [^{32}P]UTP, 0.1 mg/ml creatine kinase, 0.2 μl of RNase inhibitor, 10 mM dithiothreitol and 0.05 mg/ml actinomycin D. After reaction, total RNA was extracted and analyzed in a denaturing gel. Determination of viral (+)RNA/(-)RNA ratio, as well as micrococcal nuclease treatment were described previously (9).

Membrane flotation assay. [^{35}S]methionine-labeled TBSV p33 (101) was incubated with different phospholipid vesicles as previously described using purified yeast organelles (9). The membrane flotation assay was performed as previous described (212) with minor modifications. Briefly, the reaction mixture (24 μl) were mixed with 126 μl 85% sucrose in HEPES buffer in a final concentration of 71.25%, then overlaid with 900 μl 65% sucrose and 150 μl 10% sucrose in HEPES buffer (30 mM, pH 7.4). The gradient was centrifuged at 134,000 x g for 16 hours at 4 °C in a swing bucket rotor (Beckman TLS-55).

TBSV RNA recruitment assay. For the viral RNA recruitment assay, phospholipids vesicles were mixed with MBP-tagged recombinant TBSV p33 and p92 replication proteins (0.5μg each) as *in vitro* replication assay, except that UTP was omitted from the reaction mixture, and 1 μg/μl yeast tRNA was added as non-specific competitor and 1 μl radioactive [^{32}P]UTP labeled DI-72 RNA transcripts were added. After incubation for 1 hour at 25 °C, the reaction mixtures were subjected to membrane flotation assay in sucrose gradients as described above. Total RNA from the top fraction of each gradient was extracted and analyzed in a denaturing RNA gel (5% polyacrylamide gel containing 8M urea).

Lipid extraction and mass-spectrometry for lipidomics analysis. For yeast phospholipid analysis, yeast carrying the TBSV expression plasmids were pre-cultured in glucose-containing media overnight, washed and diluted to 0.3 OD_{600} units/ml in galactose-containing media and cultured for approximately 24 h at 23 ºC until reaching ~2 OD_{600} units/ml. Yeast cells (0.4 g) were placed into a 15 ml glass tube, containing 1.2 ml water, 2 ml chloroform, 4 ml methanol, 0.8 g glass beads, followed by mixing and vigorous vortexing. Then, 2 ml chloroform and 2 ml water were added into the tube and centrifuged at low speed. Then, the lower organic phase was collected. 2 ml chloroform was mixed with the remaining inorganic phase; lower organic phase was withdraw. The chloroform extraction step was repeated. All the organic phases from previous steps were combined and washed with 0.5 ml 1M KCl and then with water.

To determine the phospholipids profile of TBSV-infected plants, 3 weeks old *Nicotiana benthamiana* plants were inoculated with TBSV genomic RNA transcripts or

mock-inoculated with buffer. Then, at 6 days post infection, the upper leaves showing the characteristic TBSV symptoms were harvested. Lipid extraction was as described previously (213). Briefly, about 0.15-0.2 grams of leaves from one plant were collected and incubated with 3 ml isopropanol containg 0.01% butylated hydroxytoluene (BHT) at 75 °C for 15 min. Extraction of lipids with chloroform/methanol (2:1) incubated at room temperature was performed for 1 hour, in total five times. Organic phases from each extraction were combined and washed with 0.5 ml 1 M KCl and water, respectively.

Washed organic phase was analyzed on a triple quadrupole MS/MS equipped for electrospray ionization (ESI). Di 10:0 PE/PC/PG (Avanti Polar Lipids, Inc) were mixed with yeast or plant samples before extraction as spiked lipids standards for PE/PC/anionic phospholipids during the extraction step. In addition, two internal lipid standards of each phospholipid class were mixed with each sample before ESI-MS/MS analysis for quantification of each lipid class (213). Data were obtained from 3 repeats.

Purifiation of biotinylated duramycin. Biotinylation of duramycin (Sigma Cat. #: D3168), followed by purification, was performed as described for cinnamycin (214, 215). Briefly, 500 μM duramycin in 0.1 M NaHCO3 was mixed with equal volume of 8.7 mg/ml EZ-link NHS-LC-biotin dissolved in sterile water (Thermo Scientific, Product #: 21336) for 4 hours at room temperature and quenched by adding one-fifth volume of 0.1 M lysine. Biotinylated duramycin were purified by reverse-phase high-performance liquid chromatography using Waters Nova-Pak C18 Column (Model: WAT086344). The biotinylated duramycin was eluted with a linear gradient of 10 mM sodium acetate (pH 4.2) starting from 5% to 60% for 50 min, at a flow rate of 0.5 ml/min. Biotinylated

duramycin was collected at 28 to 30 min after starting of elution. No peak was detected at the “32 min” time-point, when elution of nonbiotinylated duramycin was expected, suggesting that all duramycin molecules became biotinylated.

Imaging of PE distribution and viral protein localization in yeasts and plant protoplasts. Yeast cultures were grown in glucose containing media overnight and switched to galactose containing media with initial 0.3 OD_{600}. To prepare spheroplasts, overnight cultures were harvested and the yeast cells were fixed with 3.7% formaldehyde for 40 min at room temperature in dark, washed twice with 0.1 M potassium phosphate (pH 7.5), and then re-suspended in SPP (0.1 M potassium phosphate pH 7.5, 1.2 M sorbitol) with zymolase 20T (1 mg/ml). Cells were incubated at 30 °C for 1 hour, and then incubated with SPP with 50 mM NH_4Cl for 15 min to quench free aldehyde groups. Spheroplasts were collected after washing twice with SPP, and then applied to poly-L-lysine coated slides. Slides were immersed in methanol for 6 min and acetone for 30s, respectively, at -20 °C. Biotinylated-duramycin was added into phosphate-buffered saline (PBS, pH 7.4) containing 0.05% Nonidet P-40 and 1% BSA (15 μg/ml), and incubated overnight with the fixed cells at -4 °C. Slides were washed and incubated with Streptavidin conjugated with Alexa Fluor® 405 (Life Technologies, Cat. #: S-32351) for 1 hour before imaging.

The distribution of PE was also monitored using fatty acid-labeled NBD-PE and NBD-PC internalization. M-C_6-NBD-PE (1-myristoyl-2-(6-[(7-nitro-2-1,3-benzoxadiazol-4-yl)amino]hexanoyl)-sn-glycero-3-phosphoethanolamine) and M-C_6-NBD-PC (1-myristoyl-2-(6-[(7-nitro-2-1,3-benzoxadiazol-4-yl)amino]hexanoyl)-sn-glycero-3-

phosphocholine) (Avanti Polar lipids, Inc.) were dissolved in DMSO in 8 mM concentration (216) and stored at -20 °C. Wild type yeast transformed with pESC-mRFP-T33 and pRS315-Pex13p-BFP was pre-grown in SC medium, then cultured in SC medium containing 2% galactose with 80 μM NBD-PE or NBD-PC at 0.5 OD_{600}, and incubated at 23 °C for 16 hours. Cells were washed with $SCNaN_3$ medium (216) (SC medium with 2% sorbitol and 20 mM sodium azide) and subjected to confocal laser microscope analysis.

N. benthamiana protoplasts were prepared and eletroporated with *in vitro* transcribed TBSV full length genomic RNA as described previously (204). Protoplasts were fixed with 3.7% formaldehyde in protoplast culture medium (204), applied to poly-L-lysine coated slides, and processed using the above procedure for PE staining. For dual staining of p33 and PE, anti-p33 primary antibody (a gift from Dr. Herman B. Scholthof) was diluted (1:400) and incubated with fixed protoplasts in PBS containing 1% BSA/0.05% Nonidet P-40 overnight. After washing three times with PBS/1% BSA/0.05% Nonidet P-40, cells were incubated with anti-mouse secondary antibody conjugated to Alexa Fluor® 488 (Life Technologies, Cat. #: A-11001) for 1 hour before imaging.

Confocal images were obtained with an Olympus FV1000 microscope (Olympus America, Melvie, NY). Alexa 405, GFP/Alexa 488, and RFP were excited using 405 nm, 488 nm or 543 nm lasers, respectively. Images were obtained sequentially, and merged using Olympus FLUOVIEW 1.5 software.

4.3 Results

Efficient replication of TBSV RNA in artificial PE vesicles. To test what type of

phospholipids are required for tombusvirus replication, we developed an artificial vesicle- (liposome-) based replication assay involving purified recombinant tombusvirus p33 and $p92^{pol}$ replication proteins, TBSV (+) replicon (rep)RNA and cellular cytosolic proteins present in yeast cell-free extract (CFE, Fig. 1A). Interestingly, artificial vesicles prepared only from phosphatidylethanolamine (PE) supported TBSV repRNA replication, reaching about half of the level that takes place in the standard CFE obtained from wt yeast (Fig. 1A, lanes 3-4 versus 1-2). On the contrary, vesicles consisting of only phosphatidylcholine (PC, Fig. 1A, lanes 5-6), or lysoPE showed 5% viral RNA replication activity when compared with PE vesicles (Fig. 2A, lanes 3-4 and 13-14), while PG, PS, PI, CA, and lysoPC vesicles did not support TBSV RNA replication (Fig. 2A). These data support a model that PE is the only phospholipid required for TBSV replication *in vitro*, while the other phospholipids are not sufficient by themselves.

To examine the nature of TBSV replication in PE vesicles, we measured (-) versus (+)-strand RNA synthesis. These experiments revealed that TBSV replication led to the production of ~10-fold more (+)- than (-)-stranded RNAs, similar to the ratio seen in yeast CFE preparation containing yeast membranes (Fig. 1B) (102). Thus, the *in vitro* assembled TBSV replicase in PE vesicles can support a complete cycle of replication and asymmetrical RNA synthesis, which is hallmark of (+)-strand RNA viruses. We also tested if the PE vesicles are required for RNA synthesis by adding various concentrations of Triton X-100, which could disrupt lipid bilayer. Viral RNA synthesis was inhibited up to 90% in the presence of 0.01%, while it was completely blocked by the presence of 0.1 or 1.0% Triton X-100 (Fig. 1C), suggesting that the membranous environment is needed for TBSV replication *in vitro*. To test if TBSV replicase could form a nuclease-resistant

compartment, as the case in cells and in the yeast CFE (49, 102), we performed the *in vitro* assays in the presence of micrococcal nuclease, which can destroy the unprotected viral RNAs. These studies revealed that TBSV replicase formed in the presence of PE vesicles was much less protective of the viral RNA against the nuclease than the replicase assembled in yeast CFE (Fig. 2B). This finding suggests that not only PE, but additional phospholipids, other types of lipids or membrane proteins in the yeast CFE also contribute to the assembly of the authentic TBSV replicase.

To estimate optimal PE level for TBSV replication, we made artificial vesicles containing PE and increasing amounts of a mixture of other phospholipids (PC, PI, PS, PG, lysoPE and lysoPC, mixed as their molar ratio from TBSV infected *N. benthamiana* leaves as shown in Fig. 7) (Fig. 1D). The highest level of TBSV replication was observed with the vesicle containing 82-90% PE (Fig. 1D). On the other hand, vesicles containing less than 70% PE did not support efficient TBSV replication *in vitro*. We also tested PE and other phospholipids in pair-wise combinations. These *in vitro* assays revealed that the presence of only 10% of PC or lysoPE in PE vesicles enhanced TBSV replication by more than 50%, while these phospholipids were inhibitory when applied in higher than 20% concentrations (Fig. 3A-B). In contrast, the presence of other phospholipids (PS, PI, CA, lysoPC) were inhibitory to TBV replication, except for 10% of PG (Fig. 3B). Thus, various phospholipids (other than PE) have inhibitory effects on TBSV replication when present in higher than 20% amounts. These results indicate that TBSV replication is greatly affected by different kind of phospholipids.

To test whether phospholipids affect the membrane association of the viral replication proteins, we performed membrane flotation experiments with artificial

vesicles and ^{35}S-labeled p33 replication protein. As expected, in the absence of membranes/vesicles, p33 stays at the bottom of the sucrose gradient (Fig. 4B), while ~30% of p33 are present in the top fraction in the presence of either PE or PC vesicles (Fig. 7C-D). In addition, p33 can strongly associate with PG, PS and CA vesicles, while binding to PI vesicles is poor (Fig. 4). These data suggest that, except for PI, most of phospholipids does not inhibit p33 targeting to membrane. Similar studies with the viral (+)repRNA, which has to be recruited to the sites of replication in the membranes by replication proteins (3, 102, 202), revealed that the (+)repRNA bound to membrane associated p33/p92^{pol} replication proteins with the highest efficiency in the presence of PE, PC and lysoPE vesicles, while PG, PS, PI, CA and lysoPC vesicles does not stimulate (+)repRNA recruitment (Fig. 5). Therefore, we suggest that binding of p33/p92^{pol} replication proteins to PE, PC and lysoPE phospholipids facilitate the recruitment of the viral (+)repRNA to replicase complexes.

PE is enriched at the sites of TBSV replication. Since TBSV requires membranes with high PE content to assemble the functional VRCs *in vitro*, we wondered if PE, which is among the most abundant phospholipids in yeast, is enriched at the sites of replication. We used Alexa405-labeled duromycin, which specifically binds to PE (217), to monitor the distribution of PE during TBSV replication. Interestingly, PE was highly enriched in the subcellular locations in yeast cells containing GFP-p33 expressed alone or with p92^{pol} replicating the TBSV repRNA (Fig. 6A). These sites co-localized with both Pex13p-mRFP/GFP peroxisomal marker and GFP/RFP-p33 (Fig. 6B), indicating that PE is enriched at the sites of TBSV replication in the peroxisomal membrane. On the contrary,

the peroxisomal membrane was not enriched with PE in the absence of TBSV replication proteins and PE was dispersed in many parts of the yeast cell (Fig. 6B, -TBSV treatment). We confirmed the above findings using fatty acid fluorescently-labeled PE (NBD-PE) added to the culture media. Accordingly, NBD-PE was enriched in the subcellular location also containing RFP-p33 and Pex13p-GFP (Fig. 6C). On the contrary, NBD-PE was not enriched in the peroxisomal membranes in the absence of TBSV p33 (Fig. 6C). Unlike NBD-PE, NBD-PC was not highly enriched at the sites of TBSV replication (Fig. 6C). Based on these data, we propose that PE molecules are efficiently re-localized to and enriched at the sites of viral replication in the peroxisomal membranes. To test if similar phenomena also occur in plant cells during TBSV replication, we stained TBSV infected plant cells (*N. benthamiana* protoplasts) with Alexa405-labeled duromycin and anti-p33/p92 antibody. Importantly, confocal imaging showed high enrichment of PE in subcellular locations containing the p33/p92 replication proteins (Fig. 6D). The subcellular distribution of PE was dramatically different in uninfected plant cells. Based on all these data, the emerging picture is that PE, unlike PC, is efficiently redistributed to the peroxisomal membranes to facilitate TBSV replication.

Increased PE level in yeast and plant cells supporting TBSV replication. To test if TBSV replication alters phospholipid metabolism to facilitate its replication, we performed lipidomics of yeast cells replicating TBSV repRNA or lacking all TBSV components. These experiments revealed that the relative PE percentage within 5 major phospholipids increased from 17.6% to 29.3% (~1.7 fold increase) in yeast replicating TBSV (Fig. 7A). On the contrary, PC and PI levels, which are two of the most abundant phospholipids, are

decreased by ~6% and 8.4%, respectively, when yeast supported TBSV replication (Fig. 7A). These data suggest that TBSV selectively increases PE level in yeast. The overall phospholipid content of yeast cells after normalized by cell weight before lipid extraction increased by 38.4% (Fig. 8A), suggesting that yeast cells are induced by TBSV to produce new phospholipids. Considering overall phospholipids also increased in TBSV replicating cells, the PE content of yeast cells replicating TBSV increased by ~2.3-fold. This increased level of PE in yeast cells likely serves the virus' need to build new membrane-bound replicase complexes (see below). Lipidomics analysis revealed no significant changes in the fatty acid length or saturation status of the PE in yeast replicating TBSV versus the control yeast (Fig. 8C&D).

The PE level was also increased in TBSV-infected plant leaves from 21.2% to 28.8% within 7 major phospholipids analyzed (Fig. 7B). In contrast to yeast, the PC level also increased in plants, which could be the results of overall elevated phospholipid synthesis (Fig. 8B). Nevertheless, the lipidomics data support the increased synthesis of PE in TBSV-infected plant cells, similar to the yeast counterpart.

Increased PE level in cho2Δ yeast promotes TBSV replication. To examine if PE level can directly affect TBSV replication in cells, we deleted *CHO2*, which codes for phosphatidylethanolamine methyltransferase (PEMT), in yeast. Cho2p catalyzes the first step in the conversion of PE to PC, and in its absence, PE level is increased and PC level is decreased (218). We find that TBSV replication is increased by ~10-fold in *cho2Δ* yeast in comparison with wt yeast (Fig. 9A, lanes 5-8 versus 1-4). In addition, the amounts of p33 and $p92^{pol}$ replication proteins were also increased (Fig. 9A). Lipidomics analysis of *cho2Δ*

yeast supporting TBSV replication showed that PE becomes the most abundant within 5 major phospholipids by reaching up to ~42% level (Fig. 9B, upper panel). And within same amount of cell weight, PE increased ~2.5-fold comparing with wild type yeast replicating TBSV extraction (Fig. 9B, lower panel).

We have also performed *in vitro* TBSV replicase assembly assay in isolated membrane fractions from wt or *cho2Δ* yeasts. The viral replicase assembled with membrane fractions from *cho2Δ* yeast showed ~3-fold higher activity *in vitro* than from wt yeast (Fig. 9C). Since we used the same amount of the recombinant viral proteins in the CFE preparations, the increased TBSV replicase activity from *cho2Δ* yeast suggests that the high accumulation level of TBSV repRNA in *cho2Δ* yeast is due to enhanced replicase activity in *cho2Δ* yeast (Fig. 9A). Confocal microscopy analysis of *cho2Δ* yeast showed robust re-distribution of PE to the sites of TBSV replication, containing the viral replication proteins and peroxisome membranes (Fig. 9D).

To test if the high accumulation of PE in the peroxisome membranes is critical for TBSV replication, we deleted *PEX3* peroxisome biogenesis gene in *cho2Δ* yeast. In the absence of *PEX3* there is no peroxisome or peroxisome membrane remnants in yeast (ref) and TBSV switches to the ER for replication (32). ER can support as robust TBSV replication as the peroxisomes in yeast (32, 107). We find that TBSV replication is increased by ~13-fold in *cho2Δpex3Δ* yeast (Fig. 10), suggesting that TBSV can take advantage of increased PE level in the ER membrane in the absence of peroxisomes.

To test if the pro-viral role of PE also extends to other viruses, we analyzed replication of the closely-related cucumber necrosis tombusvirus (CNV), which also replicates on peroxisomal membranes. Similar to TBSV, CNV replication was increased in

cho2Δ yeast (Fig. 11A-B) and the CNV p33 protein induced the re-localization of PE in yeast cells (Fig. 11C). To study if viruses replicating in other subcellular compartments could take advantage of the increased PE level in *cho2Δ* yeast, we used Carnation Italian ringspot virus (CIRV, a tombusvirus), which replicates in the outer mitochondrial membranes (9, 19). CIRV accumulation is increased by ~5-fold in *cho2Δ* yeast (Fig. 12A). Moreover, the p36 replication protein of CIRV induced the efficient enrichment of PE in the same subcellular locations that harbor p36 (Fig. 12B). Replication of another mitochondrial RNA virus, the unrelated Nodamura virus (NoV) insect RNA virus, also benefitted from the increased PE level in *cho2Δ* yeast (Fig. 12C). Interestingly, protein A replication protein of NoV is also localized at highly PE-enriched subcellular locations (Fig. 12C). Therefore, we conclude that tombusviruses and NoV could take advantage of the increased PE level in various subcompartments in *cho2Δ* yeast. Similar to TBSV, the replication proteins of these viruses can induce the efficient enrichment of PE at the sites of virus replication, suggesting that different (+)RNA viruses build PE enriched environment for replication.

4.4 Discussion

It is universally accepted that plant and animal RNA viruses require cellular membranes for their propagation in infected cells (20). These viruses replicate in various subcellular compartments that contain unique composition of lipids. However, it is currently poorly understood how different lipids could affect the viral replication process. By using the highly tractable tombusviruses, we show that PE plays an essential role in

viral replication. The supporting evidence includes: (i) *in vitro* data with artificial vesicles that facilitated TBSV replication only when PE was present above 70%, (ii) the relative increase of PE in yeast and plant cells replicating tombusvirus; (iii) PE enrichment in the replication sites of tombusviruses and Nov; and (iv) cell-based results showed increased tombusviruses and Nov replication in *cho2Δ* yeast that contain high level of PE at the expense of PC level.

Essential role of PE in TBSV VRC assembly. Based on *in vitro* approaches, the major function of PE is during the assembly of the VRCs. We show that VRCs are only functional in the presence of artificial PE vesicles, while other phospholipids are insufficient to support efficient VRC assembly and they are inhibitory when present in 20% or more in comparison with PE level in artificial vesicles. In addition, membrane fractions from *cho2Δ* yeast support enhanced TBSV replication *in vitro*, suggesting more efficient VRCs assembly when PE is abundant in membranes.

Interestingly, PE does not seem to be essential at the very early steps of replication (prior to the VRC assembly), because PE is not favored to bind to the TBSV p33 replication protein when compared to other phospholipids. Also, PC is even more efficient than PE for facilitating the p33/p92-driven recruitment of the viral (+)repRNA *in vitro*. However, efficient viral replication requires high level of PE at the replication sites. It is likely that p33 induce PE enrichment at sites of replication after p33 associated with subcellular membrane at the very initial step of replication. Meanwhile, binding to PE might stabilize p33/p92, because we observed elevated levels of p33/p92 in *cho2Δ* yeast in comparison with wt yeast. We have previously shown that total phospholipids are important for p33/p92 stability in yeast (89).

Based on TBSV replication studies with artificial vesicles, TBSV requires high local concentration of PE at the sites of replication (above 70%, Fig. 1). However, PE is below that level in subcellular membranes (51), such as peroxisomes(219), mitochondria(220, 221) and ER(221). TBSV changes cell lipidome upon infection with increased PE level, as shown by lipidomics data from yeast and plant cells. Meanwhile, confocal microscopy images show the robust accumulation of PE at peroxisomal sites where TBSV p33 replication protein accumulates (to form VRCs). Interestingly, PEs (NBD-PE) provided in the yeast culture media found its way to the TBSV replication sites, suggesting that existing PE is efficiently re-distributed to the sites of TBSV replication. Overall, TBSV utilizes different pathways to increase the local concentrations of PE to serve the virus' need during VRC assembly.

The development of artificial vesicle-based TBSV replication clearly demonstrates that TBSV requires PE for VRC assembly. TBSV replicase assembled on the PE vesicles could support complete cycle of RNA replication, including (-)- and (+)-RNA synthesis in an asymmetrical manner, producing ~10-times more (+)-strands than (-)-strands. Asymmetrical replication of the RNA genome is one of the hallmarks of (+)-strand RNA viruses (222). However, optimal TBSV replication also requires additional phospholipids, because the highest TBSV RNA synthesis was observed with vesicles containing ~15% additional phospholipids and ~85% PE. PE possess a conical molecular structure and introduce negative curvature into lipid bilayer. Such negative curvature likely contribute to membrane invagination occurs upon formation of spherule structures build by TBSV at the sites of replication (81).

A wide-spread role of PE in (+)RNA virus replication? Many other (+)RNA viruses also induce membrane invagination during replication (79), including CNV (223), CIRV (114) and NoV (224). Indeed, PE enrichment at replication sites seems to be a common feature among these (+)RNA viruses. Using *cho2Δ* yeast lacking PEMT to convert PE to PC, we demonstrate that the TBSV-related CNV (peroxisomal replication) and CIRV (mitochondria) and the unrelated NoV (mitochondria) all supported enhanced replication when PE is abundant in membranes. Also "forcing" TBSV to switch to ER membranes in the absence of peroxisomes in *cho2Δ* yeast (due to *pex3Δ* background), still resulted in efficient TBSV replication, suggesting that these (+)RNA viruses could take advantage of abundant PE in various subcellular membranes. In summary, the emerging picture from our work is that various (+)RNA viruses might subvert PE in order to build VRCs and replicate efficiently in infected cells.

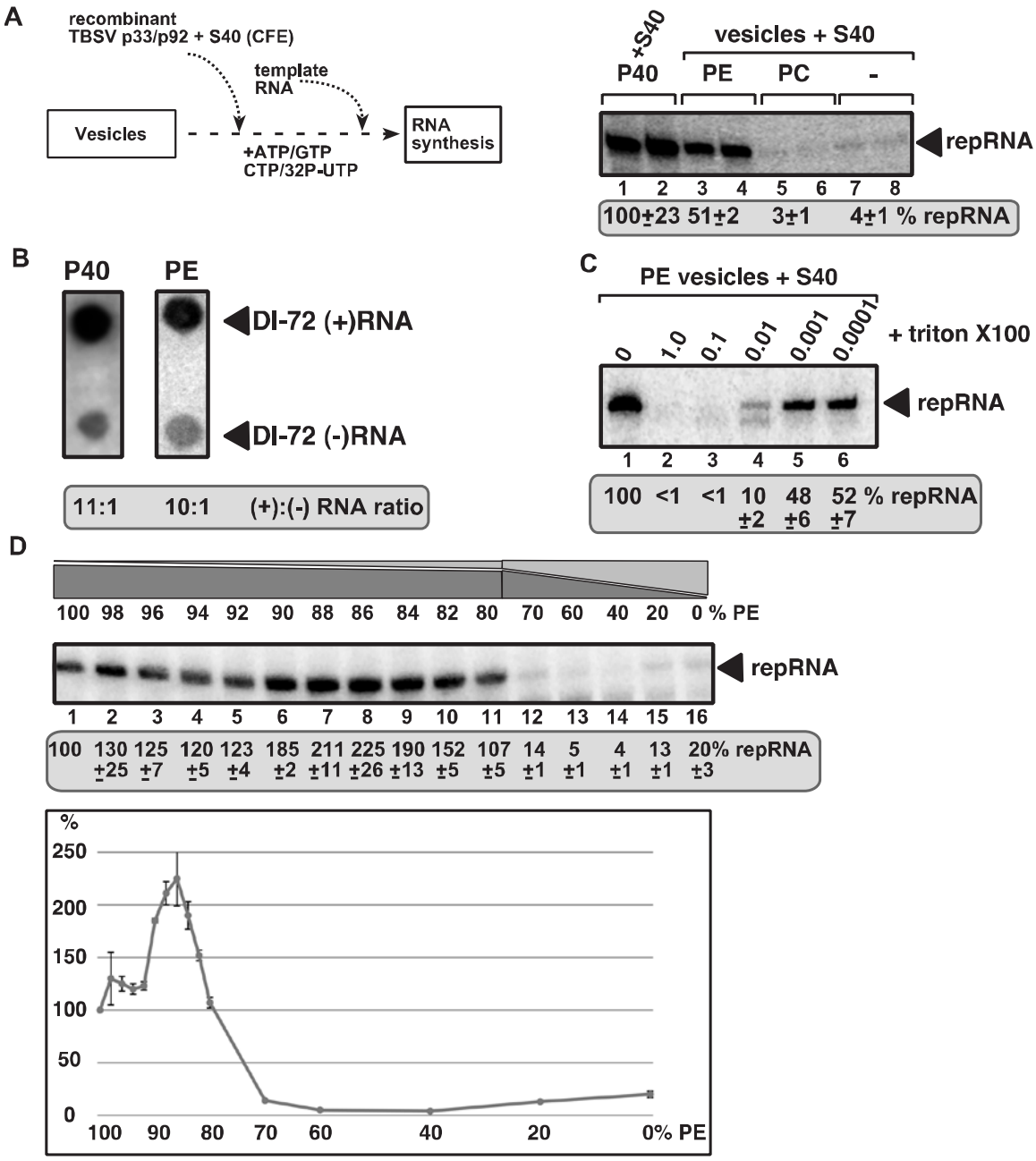
A
recombinant
TBSV p33/p92 + S40 (CFE)
template
RNA
Vesicles
RNA
synthesis
+ATP/GTP
CTP/32P-UTP
+S40
vesicles + S40
P40
PE
PC
-
repRNA
1 2 3 4 5 6 7 8
100±23 51±2 3±1 4±1 % repRNA
B
P40
PE
DI-72 (+)RNA
DI-72 (-)RNA
11:1 10:1 (+):(-) RNA ratio
C
PE vesicles + S40
0 1.0 0.1 0.01 0.001 0.0001
+ triton X100
repRNA
1 2 3 4 5 6
100 <1 <1 10 ±2 48 ±6 52 ±7 % repRNA
D
100 98 96 94 92 90 88 86 84 82 80 70 60 40 20 0 % PE
repRNA
1 2 3 4 5 6 7 8 9 10 11 12 13 14 15 16
100 130 ±25 125 ±7 120 ±5 123 ±4 185 ±2 211 ±11 225 ±26 190 ±13 152 ±5 107 ±5 14 ±1 5 ±1 4 ±1 13 ±1 20% ±3 repRNA
%
250
200
150
100
50
0
100 90 80 70 60 40 20 0% PE

Fig. 4.1

Fig. 4.1. In vitro reconstitution of the TBSV replicase in artificial PE vesicles.

(A) Scheme of the assay. Purified recombinant p33 and $p92^{pol}$ replication proteins of TBSV in combination with the TBSV-derived (+)repRNA were added to PE or PC vesicles or the P40 membrane-fraction of yeast CFE. The S40 fraction of CFE was also added to each sample to provide soluble host factors required for TBSV VRC assembly. The denaturing PAGE analysis of the ^{32}P-labeled repRNA products obtained is shown. The full-length repRNA is pointed at by an arrow. The CFE-based replication assay with CFE was chosen as 100% (lanes 1-2). (B) Asymmetrical RNA synthesis by TBSV VRCs assembled in PE vesicles. The amounts of TBSV (+) and (-)-stranded RNA products produced by the reconstituted TBSV VRCs are measured by using the ^{32}P-labeled repRNA probes generated in the *in vitro* assays. The blot contains the same amount of cold (+) and (-)-stranded DI-72 RNA. (C) TBSV RNA synthesis by the reconstituted VRCs in PE vesicles requires vesicles/membranes. The PE vesicles were disturbed by Triton-X100 treatment as shown. The denaturing PAGE analysis of the replicase products is as shown in Panel A. (D) Increased VRC activity in PE vesicles containing a fraction of other phospholipids. The PE vesicles contained the shown % of PE plus a mixture of other phospholipids (the ratio was: 54.5 of PC, 6.1 of PI, 1.2 of PS, 8.3 of PG, 0.9 of LPE, and 0.6 of LPC). The denaturing PAGE analysis of the replicase products is as shown in Panel A.

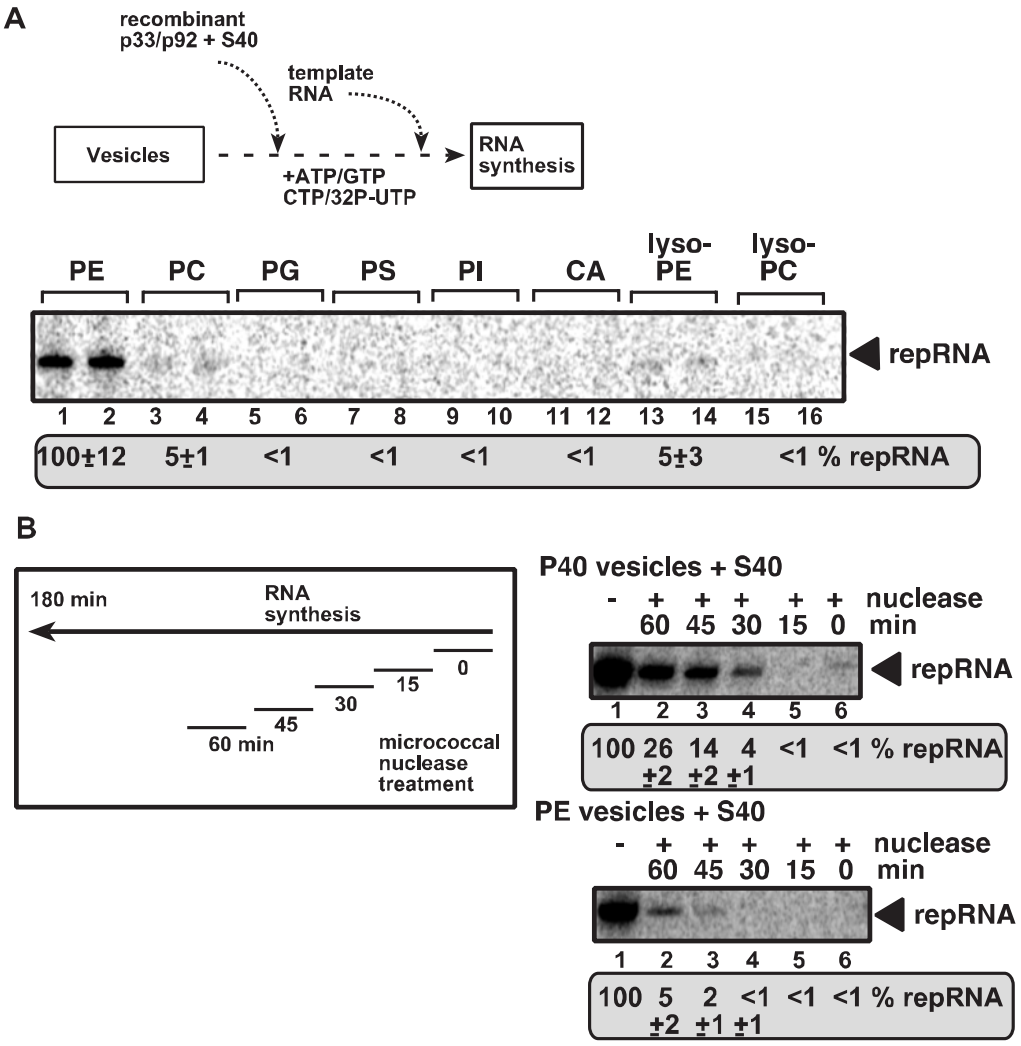
A
recombinant
p33/p92 + S40
template
RNA
Vesicles
+ATP/GTP
CTP/32P-UTP
RNA
synthesis
PE
PC
PG
PS
PI
CA
lyso-
PE
lyso-
PC
repRNA
1 2 3 4 5 6 7 8 9 10 11 12 13 14 15 16
100±12 5±1 <1 <1 <1 <1 5±3 <1 % repRNA
B
180 min
RNA
synthesis
0
15
30
45
60 min
micrococcal
nuclease
treatment
P40 vesicles + S40
- + + + + + nuclease
60 45 30 15 0 min
repRNA
1 2 3 4 5 6
100 26 14 4 <1 <1 % repRNA
±2 ±2 ±1
PE vesicles + S40
- + + + + + nuclease
60 45 30 15 0 min
repRNA
1 2 3 4 5 6
100 5 2 <1 <1 <1 % repRNA
±2 ±1 ±1

Fig. 4.2

Fig. 4.2. In vitro reconstitution of the TBSV replicase in artificial phospholipid vesicles.

(A) Artificial vesicles were prepared from the shown phospholipids, followed by *in vitro* TBSV replication assay in the presence of purified recombinant TBSV p33 and $p92^{pol}$ replication proteins, TBSV repRNA in combination with the S40 fraction of yeast CFE to provide soluble host factors required for TBSV VRC assembly. The denaturing PAGE analysis of the ^{32}P-labeled repRNA products obtained is shown. The full-length repRNA is pointed at by an arrow. The PE vesicle-based replication assay was chosen as 100% (lanes 1-2). (B) High level nuclease-sensitivity of the tombusvirus replicase assembled in artificial vesicles. Scheme of the vesicle-based TBSV replication assay shows that micrococcal nuclease was added to the assay for 15 minutes at various time points as shown (after which it was inactivated by EGTA). The total length of the *in vitro* replication assay was 3 h. Denaturing PAGE analysis of *in vitro* replicase activity in comparison with the untreated preparation (that was chosen as 100%). Note that the repRNA is protected from micrococcal nuclease degradation by the proper formation of the membrane-bound viral replicase complex.

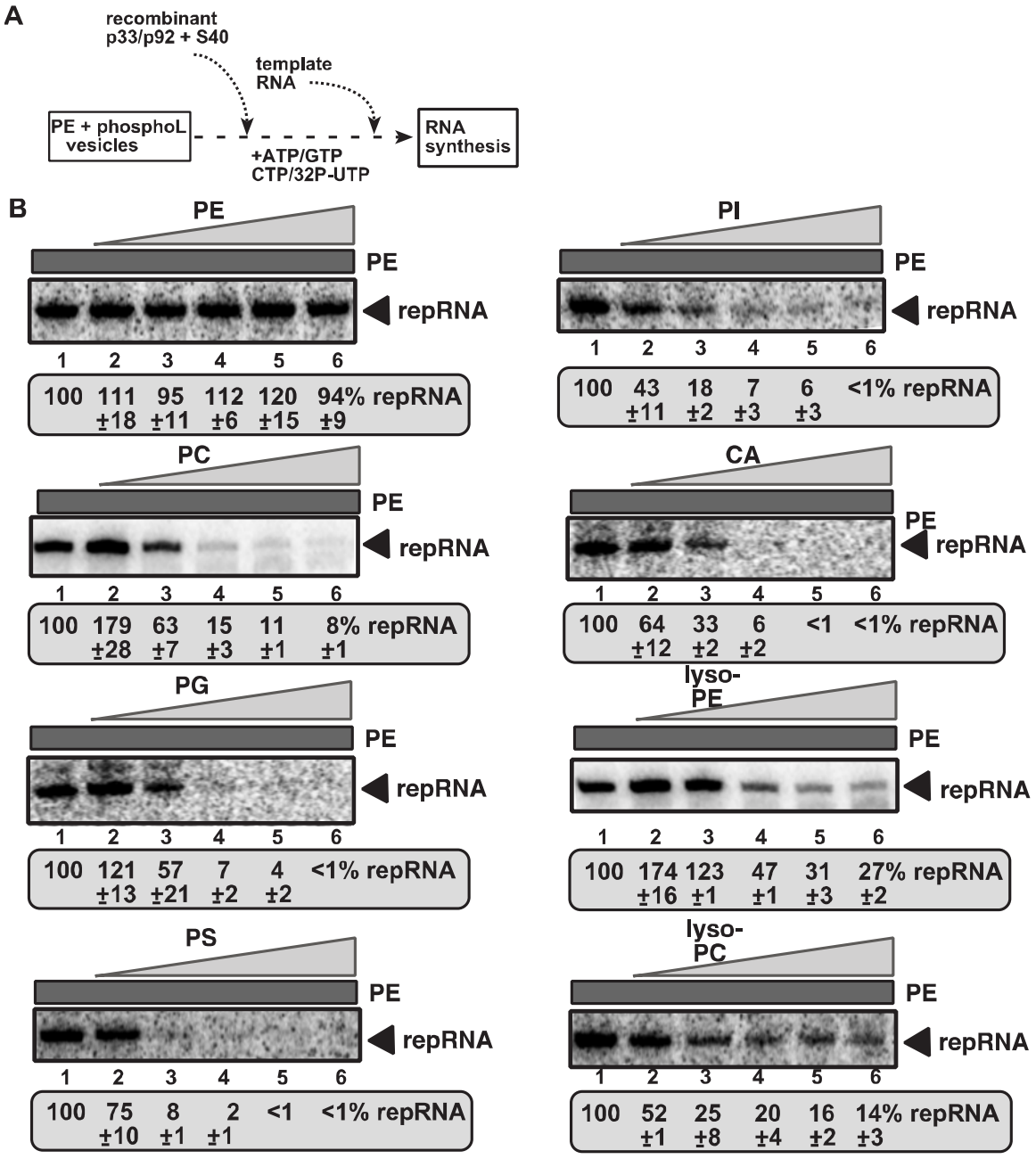
A
recombinant p33/p92 + S40
template RNA
PE + phosphoL vesicles
+ATP/GTP CTP/32P-UTP
RNA synthesis
B
PE
PE
repRNA
1 2 3 4 5 6
100 111 ±18 95 ±11 112 ±6 120 ±15 94% repRNA ±9
PI
PE
repRNA
1 2 3 4 5 6
100 43 ±11 18 ±2 7 ±3 6 ±3 <1% repRNA
PC
PE
repRNA
1 2 3 4 5 6
100 179 ±28 63 ±7 15 ±3 11 ±1 8% repRNA ±1
CA
PE
repRNA
1 2 3 4 5 6
100 64 ±12 33 ±2 6 ±2 <1 <1% repRNA
PG
PE
repRNA
1 2 3 4 5 6
100 121 ±13 57 ±21 7 ±2 4 ±2 <1% repRNA
lyso-PE
PE
repRNA
1 2 3 4 5 6
100 174 ±16 123 ±1 47 ±1 31 ±3 27% repRNA ±2
PS
PE
repRNA
1 2 3 4 5 6
100 75 ±10 8 ±1 2 ±1 <1 <1% repRNA
lyso-PC
PE
repRNA
1 2 3 4 5 6
100 52 ±1 25 ±8 20 ±4 16 ±2 14% repRNA ±3

Fig. 4.3

Fig. 4.3. Effects of various phospholipids on the TBSV replicase activity in artificial PE vesicles.

(A) Scheme of the assay. (B) Artificial vesicles were prepared from PE only (lane 1), or PE (always the same amount as in lane 1) + 10% (lane 2, ratio of PE versus other phospholipid is 10:1), 20% (lane 3, 5:1 ratio), 40% (lane 4, 5:2 ratio), 60% (lane 5, 5:3 ratio) or 80% (lane 6, 5:4 ratio) of the shown phospholipids, followed by *in vitro* TBSV replication assay in the presence of purified recombinant TBSV p33 and $p92^{pol}$ replication proteins, TBSV repRNA in combination with the S40 fraction of yeast CFE. The denaturing PAGE analysis of the ^{32}P-labeled repRNA products obtained is shown. The full-length repRNA is pointed at by an arrow. The PE vesicle-based replication assay was chosen as 100% (lane 1). Each experiment was done three times.

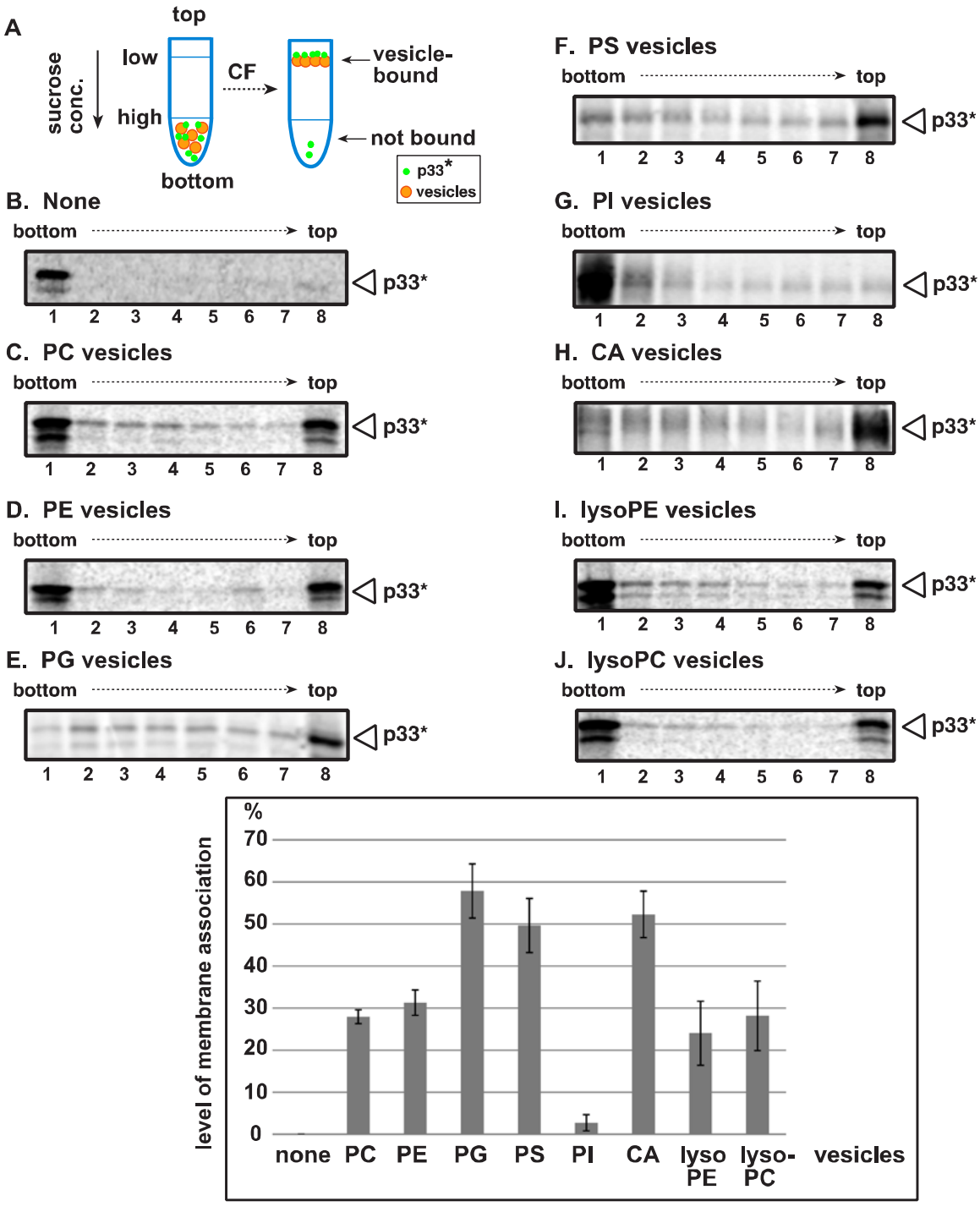
A
top
low
high
sucrose conc.
CF
vesicle-bound
not bound
bottom
p33*
vesicles
B. None
C. PC vesicles
D. PE vesicles
E. PG vesicles
F. PS vesicles
G. PI vesicles
H. CA vesicles
I. lysoPE vesicles
J. lysoPC vesicles
bottom
top
p33*
1 2 3 4 5 6 7 8
level of membrane association
%
70
60
50
40
30
20
10
0
none
PC
PE
PG
PS
PI
CA
lyso PE
lyso-PC
vesicles

Fig. 4.4

Fig. 4.4. Binding of TBSV p33 to artificial vesicles containing different phospholipids.

(A) Scheme of the *in vitro* binding assay and membrane-flotation experiments. The ^{35}S-labeled p33 was incubated with artificial vesicles (in the presence of the in vitro translation system to provide soluble cellular factors, such as heat shock protein 70), followed by centrifugation in 10-to-70% sucrose density gradient. Eight fractions of the sucrose gradient were tested for the presence of ^{35}S-p33. (B-J) SDS-PAGE analysis of the presence of ^{35}S-p33 in the eight fractions with the 1st fraction representing the bottom fraction with the free (not membrane-bound) ^{35}S-p33. The total amount of ^{35}S-p33 applied to the gradient was chosen as 100%. The graph shows the amount of ^{35}S-p33 present in the top fraction, representing the vesicle-bound ^{35}S-p33.

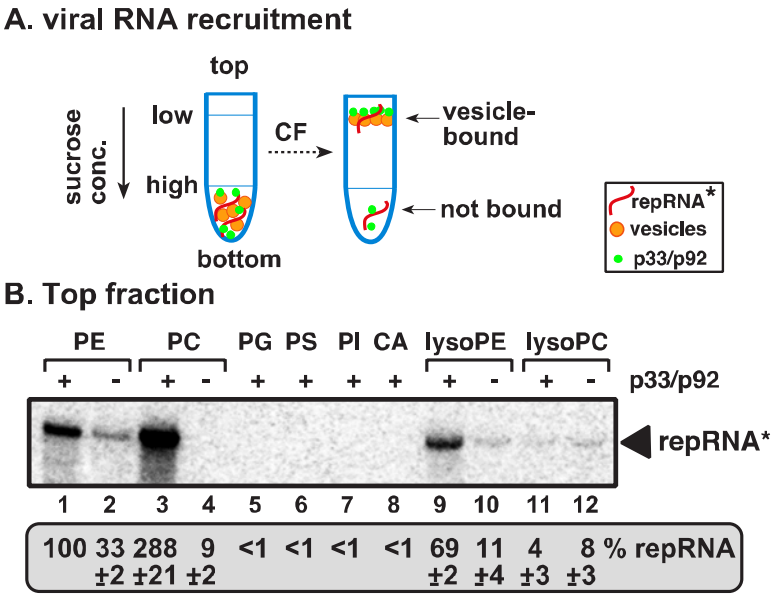
A. viral RNA recruitment
top
sucrose conc.
low
high
bottom
CF
vesicle-bound
not bound
repRNA*
vesicles
p33/p92
B. Top fraction
PE
PC
PG
PS
PI
CA
lysoPE
lysoPC
+ - + - + + + + + - + -
p33/p92
repRNA*
1 2 3 4 5 6 7 8 9 10 11 12
100 33 ±2 288 ±21 9 ±2 <1 <1 <1 <1 69 ±2 11 ±4 4 ±3 8 ±3 % repRNA

Fig. 4.5

Fig. 4.5. TBSV p33/p92-mediated binding of TBSV RNA to artificial vesicles containing different phospholipids.

(A) Scheme of the *in vitro* binding assay and membrane-flotation experiments. The ^{32}P-labeled TBSV (+)repRNA (DI-72) was incubated with artificial vesicles in the presence of purified recombinant TBSV p33 and p92 (in the presence of S40 fraction of yeast CFE to provide soluble cellular factors, such as heat shock protein 70), followed by centrifugation in 10-to-70% sucrose density gradient. The top fraction of the sucrose gradient was tested for the presence of ^{32}P-labeled TBSV (+)repRNA. (B) Denaturing RNA gel analysis of the presence of ^{32}P-labeled TBSV (+)repRNA in the top fraction. The amount of ^{32}P-labeled TBSV (+)repRNA with the PE vesicles was chosen as 100%.

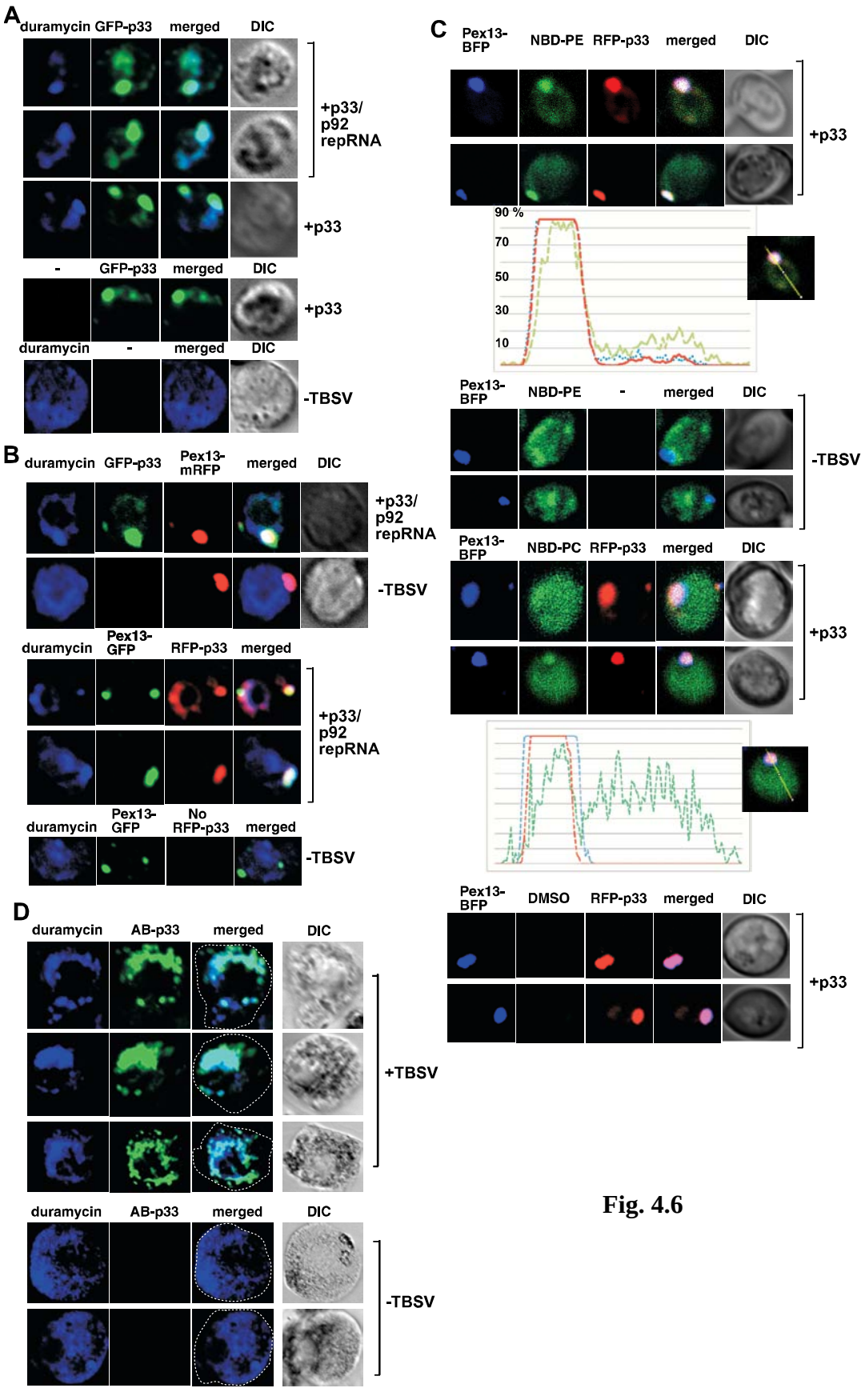
A
duramycin GFP-p33 merged DIC
+p33/ p92 repRNA
+p33
- GFP-p33 merged DIC
+p33
duramycin - merged DIC
-TBSV
B
duramycin GFP-p33 Pex13-mRFP merged DIC
+p33/ p92 repRNA
-TBSV
duramycin Pex13-GFP RFP-p33 merged
+p33/ p92 repRNA
duramycin Pex13-GFP No RFP-p33 merged
-TBSV
C
Pex13-BFP NBD-PE RFP-p33 merged DIC
+p33
90 %
70
50
30
10
Pex13-BFP NBD-PE - merged DIC
-TBSV
Pex13-BFP NBD-PC RFP-p33 merged DIC
+p33
Pex13-BFP DMSO RFP-p33 merged DIC
+p33
D
duramycin AB-p33 merged DIC
+TBSV
duramycin AB-p33 merged DIC
-TBSV

Fig. 4.6

Fig. 4.6. Enrichment of PE at TBSV replication sites in yeast and plant cells.

(A) Confocal laser microscopy images show the enrichment of PE and its co-localization with the GFP-tagged TBSV p33 expressed from *GAL1* promoter in the presence of TBSV repRNA replication (top two images) or only GFP-p33. DIC (differential interference contrast) images are shown on the right. Localization of PE is detected by using biotinylated duramycin peptide and streptavidin conjugated with Alexa Fluor 405. The bottom image shows the more even distribution of PE in the absence of viral components. (B) Peroxisomal enrichment of PE in the presence of TBSV replication proteins. Peroxisomal membranes are visualized with the help of mRFP-tagged (top images) or GFP-tagged (middle images) yeast Pex13 protein. The bottom image shows the lack of PE enrichment in peroxisomes in the absence of viral components. See further details in panel A. (C) Enrichment of exogenous PE in subcellular compartment containing the p33 replication protein. NBD-PE was added to yeast cultures (D) Enrichment of PE in *N. benthamiana* protoplasts with viral proteins replicating TBSV genomic RNA. The TBSV p33/p92 replication proteins were detected with p33/p92-specific primary antibody and secondary antibody conjugated with Alexa Fluor488. The bottom images show the more even distribution of PE in the absence of viral components. See further details in panel A.

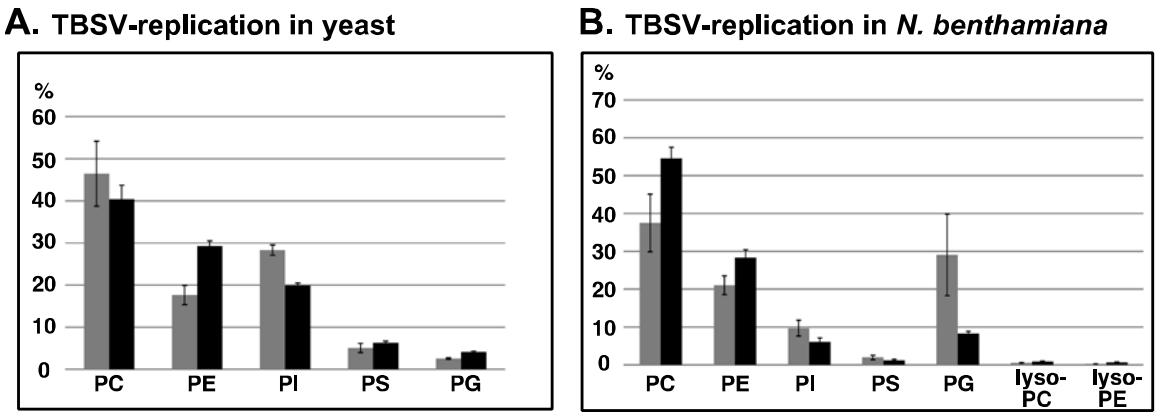
A. TBSV-replication in yeast
%
60
50
40
30
20
10
0
PC
PE
PI
PS
PG
B. TBSV-replication in N. benthamiana
%
70
60
50
40
30
20
10
0
PC
PE
PI
PS
PG
lyso-PC
lyso-PE

Fig. 4.7

Fig. 4.7. Increased level of PE in yeast and plant cells replicating TBSV.

Relative levels of phospholipids in yeast (~24 h after induction of replication, panel A) and plants (from systemic leaves showing symptoms, 6 days after infection, panel B) replicating TBSV RNA or the TBSV-free control were determined using mass-spec analysis.

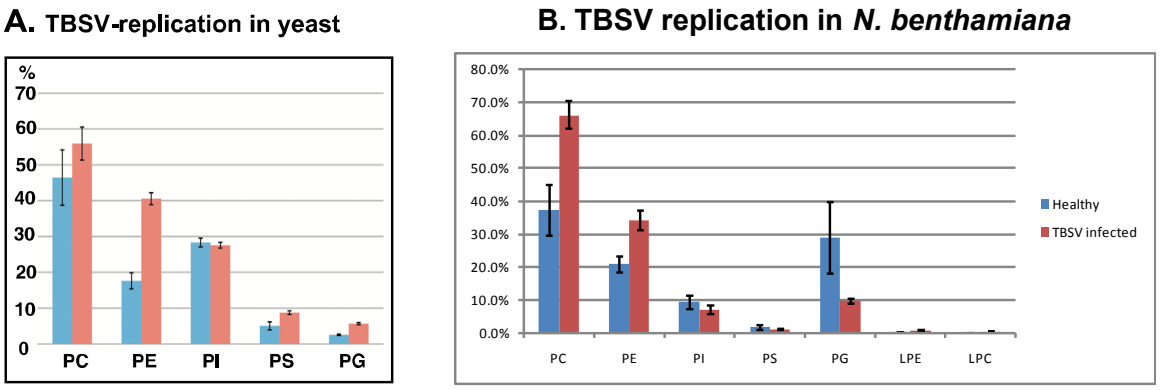
A. TBSV-replication in yeast
%
70
60
50
40
30
20
10
0
PC
PE
PI
PS
PG
B. TBSV replication in N. benthamiana
80.0%
70.0%
60.0%
50.0%
40.0%
30.0%
20.0%
10.0%
0.0%
PC
PE
PI
PS
PG
LPE
LPC
Healthy
TBSV infected

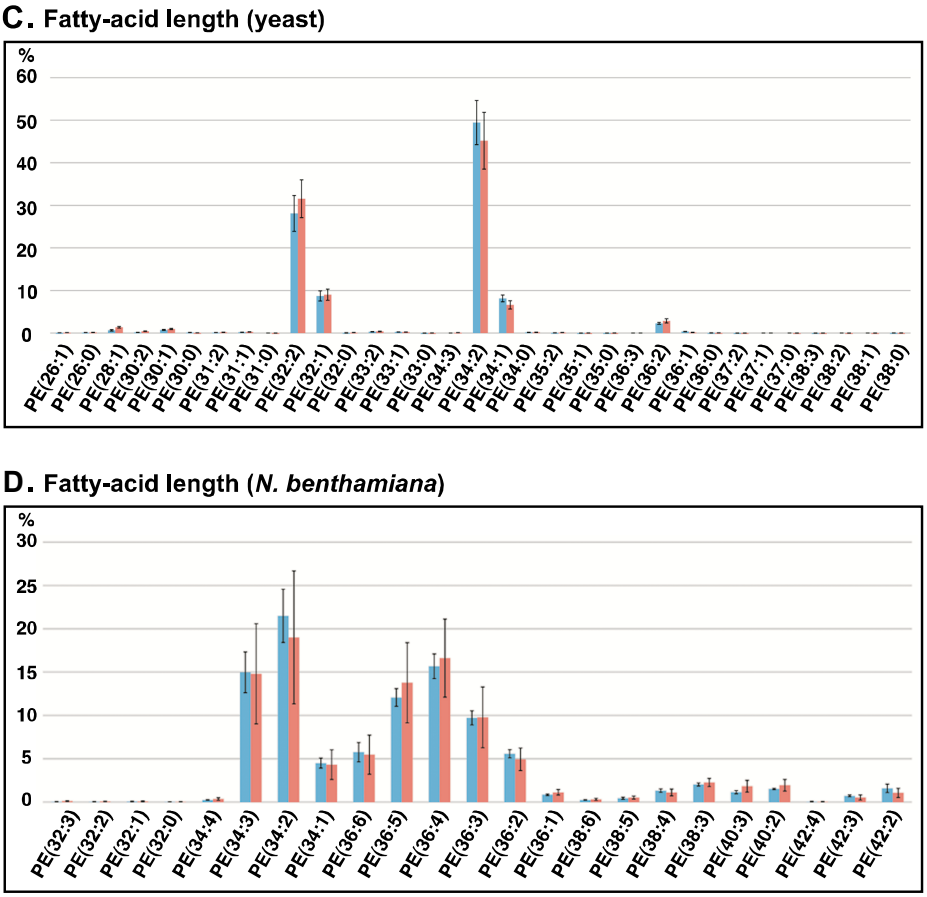
C. Fatty-acid length (yeast)
%
60
50
40
30
20
10
0
PE(26:1)
PE(26:0)
PE(28:1)
PE(30:2)
PE(30:1)
PE(30:0)
PE(31:2)
PE(31:1)
PE(31:0)
PE(32:2)
PE(32:1)
PE(32:0)
PE(33:2)
PE(33:1)
PE(33:0)
PE(34:3)
PE(34:2)
PE(34:1)
PE(34:0)
PE(35:2)
PE(35:1)
PE(35:0)
PE(36:3)
PE(36:2)
PE(36:1)
PE(36:0)
PE(37:2)
PE(37:1)
PE(37:0)
PE(38:3)
PE(38:2)
PE(38:1)
PE(38:0)

D. Fatty-acid length (N. benthamiana)
%
30
25
20
15
10
5
0
PE(32:3)
PE(32:2)
PE(32:1)
PE(32:0)
PE(34:4)
PE(34:3)
PE(34:2)
PE(34:1)
PE(36:6)
PE(36:5)
PE(36:4)
PE(36:3)
PE(36:2)
PE(36:1)
PE(38:6)
PE(38:5)
PE(38:4)
PE(38:3)
PE(40:3)
PE(40:2)
PE(42:4)
PE(42:3)
PE(42:2)

Fig. 4.8

Fig. 4.8 Lipidomics analyses of phospholipids in yeast and plant cells replicating TBSV.

(A) The amounts of phospholipids in yeast (~24 hours after induction of replication) replicating TBSV (red columns) or TBSV-free control (blue columns) were determined using mass-spec analysis. Each experiment was repeated three times. (B) The amounts of phospholipids in *N. benthamiana* systemic leaves (6 days after infection) infected with TBSV (red columns) or TBSV-free control (blue columns) were determined using mass-spec analysis. Each experiment was repeated three times. (C) Lack of changes in fatty-acid composition of PE in yeast (~24 hours after induction of replication) replicating TBSV (red columns) or TBSV-free control (blue columns) based on mass-spec analysis. (D) Comparable analysis of fatty-acid composition of PE in *N. benthamiana* leaves (6 day after inoculation) replicating TBSV (red columns) or TBSV-free control (blue columns).

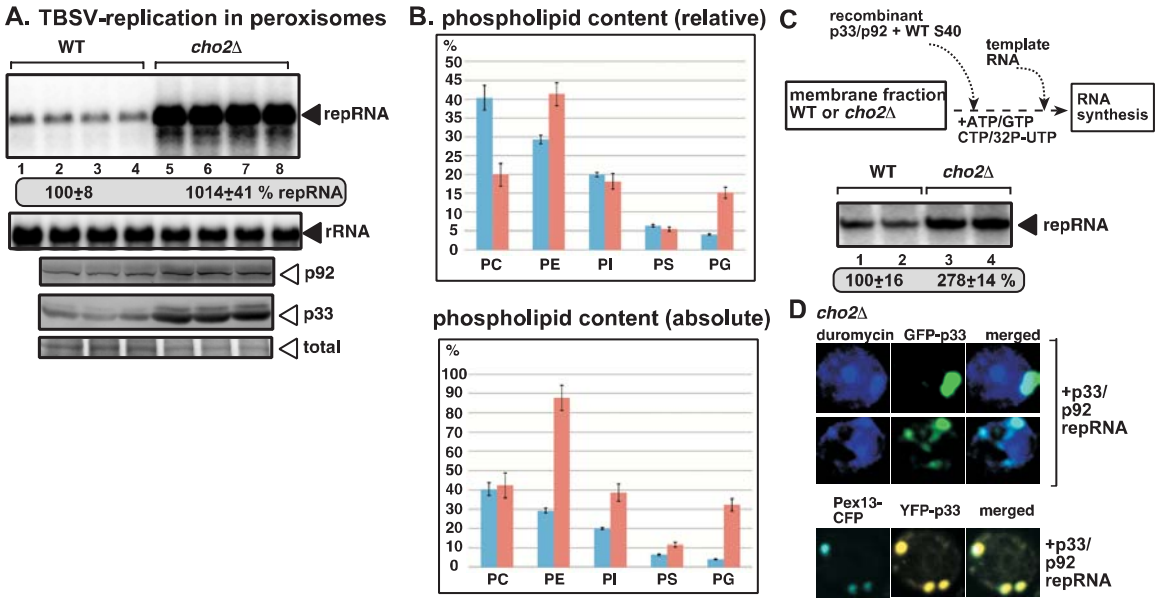
A. TBSV-replication in peroxisomes
WT
cho2Δ
repRNA
1 2 3 4 5 6 7 8
100±8
1014±41 % repRNA
rRNA
p92
p33
total
B. phospholipid content (relative)
%
50
45
40
35
30
25
20
15
10
5
0
PC PE PI PS PG
phospholipid content (absolute)
%
100
90
80
70
60
50
40
30
20
10
0
PC PE PI PS PG
C
recombinant
p33/p92 + WT S40
template
RNA
membrane fraction
WT or cho2Δ
+ATP/GTP
CTP/32P-UTP
RNA
synthesis
WT
cho2Δ
repRNA
1 2 3 4
100±16
278±14 %
D
cho2Δ
duromycin
GFP-p33
merged
+p33/
p92
repRNA
Pex13-
CFP
YFP-p33
merged
+p33/
p92
repRNA

Fig. 4.9

Fig. 4.9. Deletion of the CHO2 PEMT gene enhances TBSV repRNA accumulation in yeast.

(A) Top panel: Replication of the TBSV repRNA in wt and cho2Δ yeast was measured by Northern blotting 24 h after initiation of TBSV replication. Yeast co-expressed the TBSV p33 and p92 replication proteins. The accumulation level of repRNA was normalized based on the ribosomal (r)RNA. Each sample is obtained from different yeast colonies. Middle and bottom panels: The accumulation levels of His6-p92 and His6-p33 were tested by Western blotting. Note that in the absence of Cho2p, which catalyzes the first step in the conversion of PE to PC, the PE level is increased. Each experiment was repeated. (B) Relative and absolute levels of phospholipids in cho2Δ versus wt yeasts (~24 h after induction of replication) replicating TBSV RNA were determined using mass-spec analysis. (C) Enhanced TBSV repRNA replication in CFE prepared from cho2Δ yeast. The scheme of the CFE-based TBSV replication assay. Purified recombinant TBSV p33 (0.5 μg) and p92pol (0.5 μg) replication proteins, DI-72 (+)repRNA (0.5 μg) in combination with the soluble fraction (S40 fraction from WT yeast) were added to the membranous fraction (P40) of cho2Δ or wt CFEs. Denaturing PAGE analysis of the 32P-labeled repRNA products obtained is shown. The full-length single-stranded repRNA is pointed at by an arrow. (D) Confocal laser microscopy images show the enrichment of PE at peroxisomal sites of TBSV p33 accumulation in cho2Δ yeast. See further details in Fig. 4.6.

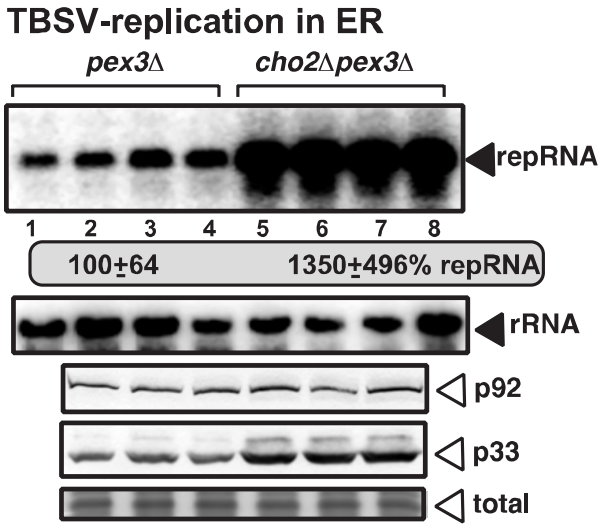
TBSV-replication in ER
pex3Δ
cho2Δpex3Δ
repRNA
1 2 3 4 5 6 7 8
100±64
1350±496% repRNA
rRNA
p92
p33
total

Fig. 4.10

Fig. 4.10. Increased PE level facilitates TBSV RNA replication in the ER in pex3Δcho2Δ yeast.

Top panel: Replication of TBSV repRNA in *pex3Δcho2Δ* versus *pex3Δ* yeast was measured by Northern blotting 24 h after initiation of TBSV replication. Yeast co-expressed the TBSV p33 and p92 replication proteins. Middle and bottom panels: The accumulation levels of His_6-p92 and His_6-p33 were tested by Western blotting. Each experiment was repeated. Note that peroxisomal membranes are absent in *pex3Δ* or *pex3cho2Δ* yeast, "forcing" TBSV to switch to the ER membranes for replication.

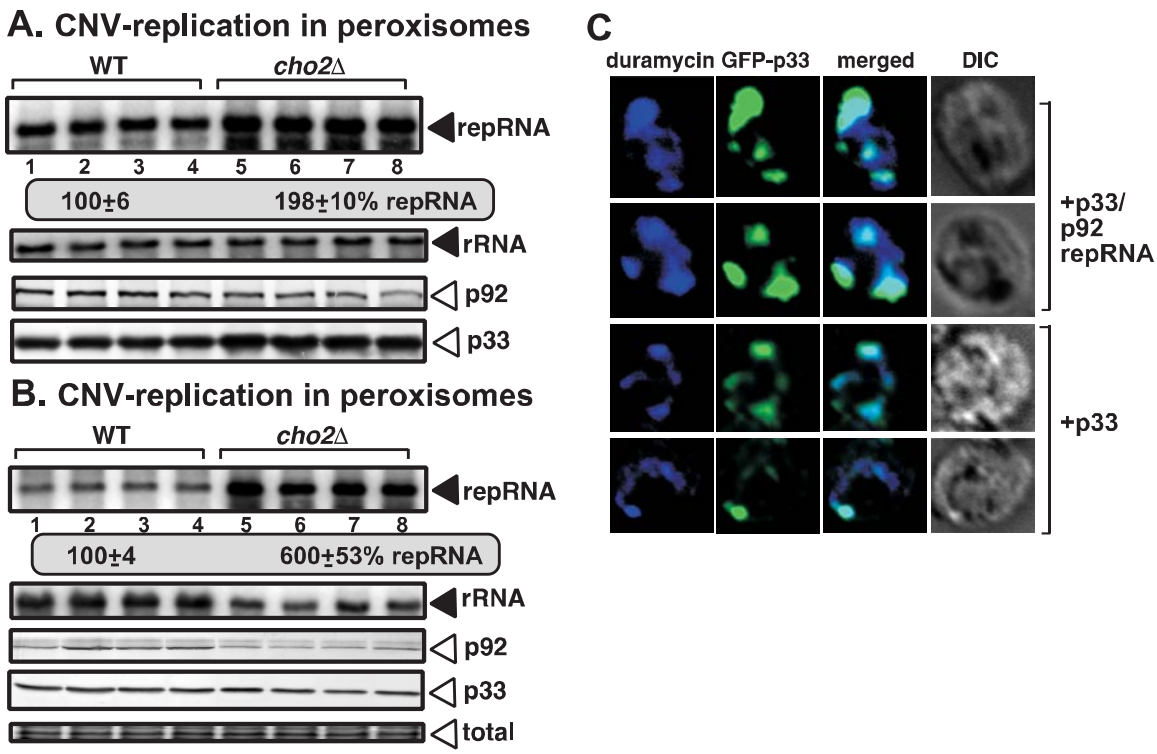
A. CNV-replication in peroxisomes
WT
cho2Δ
repRNA
1 2 3 4 5 6 7 8
100±6
198±10% repRNA
rRNA
p92
p33
B. CNV-replication in peroxisomes
WT
cho2Δ
repRNA
1 2 3 4 5 6 7 8
100±4
600±53% repRNA
rRNA
p92
p33
total
C
duramycin
GFP-p33
merged
DIC
+p33/
p92
repRNA
+p33

Fig. 4.11

Fig. 4.11. Increased PE level facilitates CNV RNA accumulation in cho2Δ yeast.

(A-B) Top panels: Replication of CNV in wt and *cho2Δ* yeast was measured by Northern blotting 24 h after initiation of CNV replication at 23 ºC (panel A) or at 29 ºC (panel B). Yeast co-expressed the CNV p33 and p92 replication proteins. Middle and bottom panels: The accumulation levels of CNV His_6-p92 and His_6-p33 were tested by Western blotting. Each experiment was repeated. (C) Confocal laser microscopy images show the enrichment of PE at peroxisomal sites of CNV p33 accumulation in *cho2Δ* yeast. See further details in Fig. 4.6.

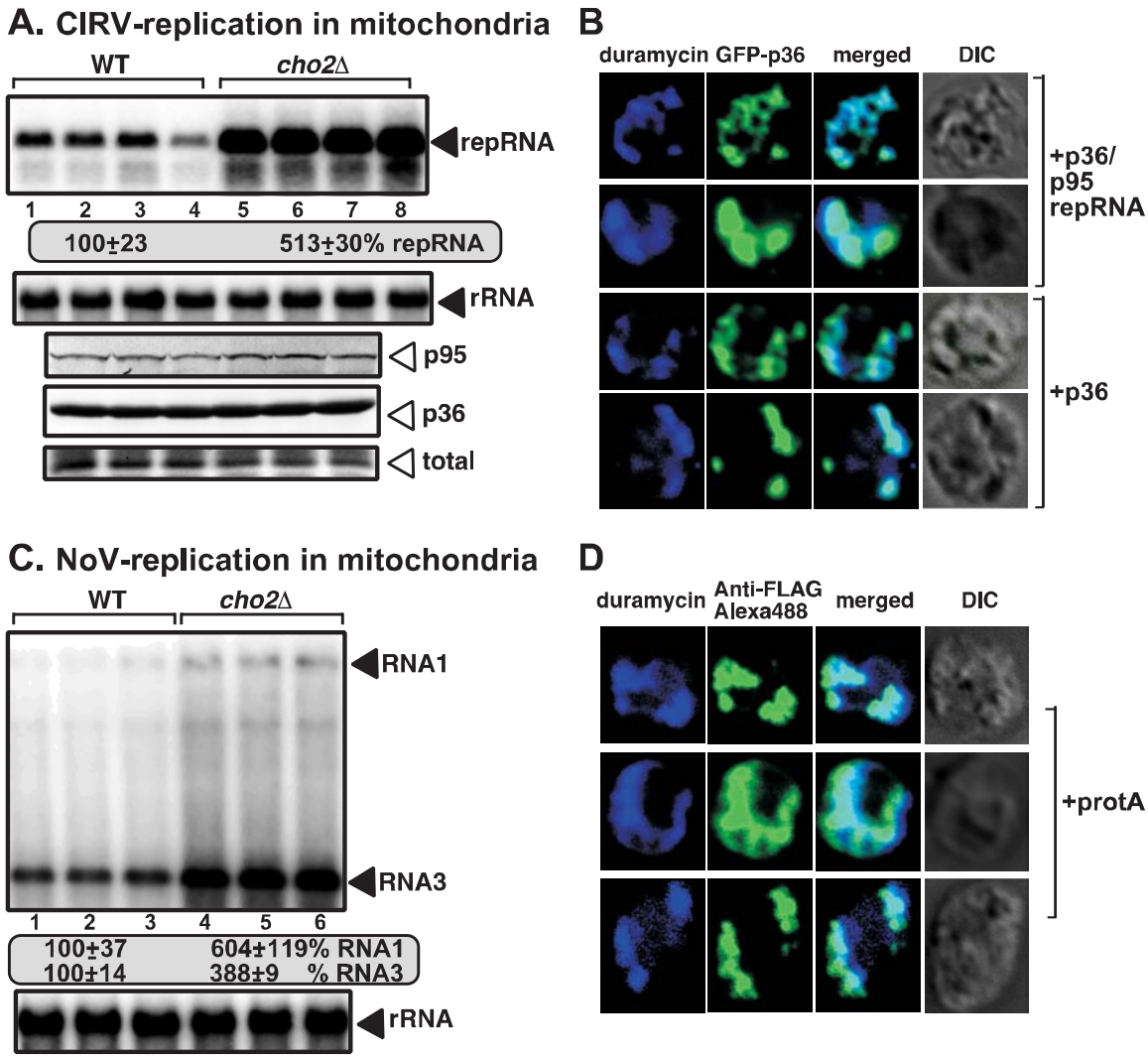
A. CIRV-replication in mitochondria
WT
cho2Δ
repRNA
1 2 3 4 5 6 7 8
100±23
513±30% repRNA
rRNA
p95
p36
total
B
duramycin
GFP-p36
merged
DIC
+p36/
p95
repRNA
+p36
C. NoV-replication in mitochondria
WT
cho2Δ
RNA1
RNA3
1 2 3 4 5 6
100±37
100±14
604±119% RNA1
388±9 % RNA3
rRNA
D
duramycin
Anti-FLAG
Alexa488
merged
DIC
+protA

Fig. 4.12

Fig. 4.12. Increased PE level facilitates CIRV and NoV RNA accumulation in cho2Δ yeast.

(A) Top panel: Replication of CIRV repRNA in wt and *cho2Δ* yeast was measured by Northern blotting 24 h after initiation of CIRV replication. Yeast co-expressed the CIRV p36 and p95 replication proteins. Middle and bottom panels: The accumulation levels of His_6-p95 and His_6-p36 were tested by Western blotting. Each experiment was repeated. (B) Confocal laser microscopy images show the enrichment of PE at mitochondrial sites of CIRV p36 accumulation in *cho2Δ* yeast. See further details in Fig. 4.6. (C) Replication of NoV RNA1 and RNA3 in wt and *cho2Δ* yeast was measured by Northern blotting 24 h after initiation of NoV replication. (D) Confocal laser microscopy images show the enrichment of PE at mitochondrial sites of NoV Flag-tagged protA replication protein accumulation in *cho2Δ* yeast. See further details in Fig. 4.6.

Chapter 5

VACUOLE TARGETING PATHWAY IS REQUIRED FOR EFFICIENT TBSV REPLICATION AND MAYBE RELATED TO PE ENRICHMENT IN THE PEROXISOMAL MEMBRANES

5.1 Introduction

Recent studies revealed an emerging picture on involvement of cellular early secretory pathway in positive strand RNA viruses replication, including those viruses infecting human (33, 225), animals (226) or plant hosts (227, 228).

Poliovirus (PV) infected cells develop special organelle-like structures specialized for virus replication (229). This viral replication organelle is derived from rearrangement of cellular early secretory membrane systems into clusters of vesicles, which harbor viral replication proteins and viral RNAs (230). Formation of Poliovirus replication organelles were identified to be associated with COPII-dependent anterograde transportation pathway between ER and Golgi (230), as well as host factors involved in retrograde transportation pathway (33, 231), like small RAS-family GTPase ADP-ribosylation factor 1 (ARF1), GBF1 [a guanine nucleotide exchange factor (GEF) for ARF1] and phosphatidylinositol 4-kinase-β (PI4KIIIβ; also known as PI4Kβ) (33). It was proposed that initial PV replication happens in Golgi-TGN compartment. This initiated by

interaction between PV viral protein 3A (232) and GBF1 which recruits Arf1 to the site of replication (33). These events then bring various of effectors, including PI4Kβ, to build ERGIC (Endoplasmic reticulum–Golgi intermediate compartment) as site for replication (33). Recently, Dorobantu CM et al. (233) found that enterovirus recruitment of PI4Kβ to ERGIC is independent of GBF1 and Arf1, suggesting GBF1/Arf1 may have other roles in enterovirus replication.

Foot-and-mouth disease virus (FMDV) belongs to *Aphthovirus* genus, *picornaviridae*, induce replication complexes on membranes that are formed from endoplasmic reticulum (ER) exit sites (ERES) (226). RNAi mediated down-regulation of Sar1 GTPase or over-expression of dominant negative Sar1a-GDP mutant inhibited FMDV replication. However over-expression of dominant active Sar1a-GTP mutant or dominant negative Arf1 mutant either have no effects or increased FMDV replication (226). Brefeldin A (BFA), a Arf GEF inhibitor, also increased FMDV replication. These data suggesting early secretory pathway is linked to FMDV replication.

A plant virus red clover necrotic mosaic virus (RCNMV), *Dianthovirus* genus, *tombusviridae*, was shown to replicate on ER membranes (234). RCNMV replication auxiliary protein p27 interacts with Arf1 directly (228). Arf1 was shown to be recruited from Golgi apparatus to ER by p27. RNAi-mediated down-regulation of Arf1 or expression of both dominant negative Arf1-GDP or dominant positive Arf1-GTP mutants inhibited RCNMV replication. Expression of dominant active Sar1-GTP mutant inhibited RCNMV replication. BFA treatment inhibited RCNMV replication and canceled ER localization of p27 replication protein. BFA treated cell expressing ER-GFP and p27-mCherry showed dispersed pattern of both proteins, however interestingly BFA did not

change localization pattern of ER-GFP when it was expressed alone. Altogether, disruption of anterograde or retrograde transportation pathway could inhibit RCNMV replication, although the importance of these events for RCNMV is currently obscure.

A major question left unanswered from those studies on different (+)RNA viruses: does early secretory pathway play a common role for (+)RNA viruses? Studies showed different involvement of anterograde or retrograde transportation in different (+)RNA viruses, however the actual functions of secretory pathway in (+)RNA viruses replication remain far from understood.

In spite of variable involvement of anterograde or retrograde transportation pathways, and different replication sites, replication proteins of many (+)RNA viruses contain transmembrane domains (TMDs) which determine membrane association of viral replication complexes. Properties of TMDs have emerged as major determinants of protein fate in secretory pathways and endocytic pathways (235, 236). Bioinformatics analyses of eukaryotic-encoded integral membrane proteins revealed that TMDs from ER is different from post-ER organelles. TMDs of ER proteins is shorter than those in post-ER organelles, and do not possess the asymmetric amino acid distribution along the membrane (236). Proteins with short TMDs are proposed to be secreted from ER to cis-Golgi via COP-II-dependent secretion, and then bound by Rer1, a transmembrane protein that cycles between the Golgi apparatus and the ER (237), at cis-Golgi (238, 239), thus cycled back to ER via COP-I mediated retrograde transportation (235). In contrast, proteins with long TMDs could interact with Erv14 (240) at ERES and be transported along the secretory pathway to TGN and beyond (241).

The physical properties of TMDs also determine localization of the given proteins within lipid micro-domains (235). Alternatively, due to different properties, TMDs were believed to attract and sort specific lipids around them (235, 236).

Since PE is an obligate phospholipid for TBSV replication (Chapter 4) and could be enriched in peroxisomal membranes by TBSV p33 replication protein alone, it could be interesting to understand which cellular pathway leads to PE enrichment at the sites of TBSV replication.

Various cellular pathways affecting PE distribution are emerging. The source of PE in autophagy has been extensively studied, and might shed lights on our understanding of PE in TBSV replication. PE is a key molecule for phagophore membrane formation in early stage of macroautophagy, where PE conjugates with Atg8p (LC3-I) to form Atg8-PE (LC3-II), which usually used as a molecular marker of macroautophagy occurrence. Different sub-cellular sources of PE has been proposed by different groups, which includes ER (242), mitochondria (243) or ER-mitochondria contact site(244). Clathrin-coated vesicles from plasma membrane also were shown to contribute to early Atg16L1-positive autophagosome precursor formation via fusion with VAMP7/SNARE complex (245, 246). In addition, trans-golgi network (247-251), early endosomes (252), vesicles from early secretory pathway (253, 254) were demonstrated to contribute to the membrane source of autophagosomes. Despite of many microscope based experiments, an cell-free LC3 lipidation assay using fractionated sub-cellular membranes from mouse embryonic fibroblast (255) showed that ERGIC is the only membrane source to trigger LC3 lipidation, which requires conjugation of LC3 with PE, suggesting ERGIC provides the initial PE source for autophagosomes formation.

In this chapter, I used varies of approaches to identify factors affecting PE enrichment at peroxisomal membranes by TBSV p33, and I will discuss possible sub-cellular route that PE was redistributed by the virus.

In yeast or plants, there are two pathways of PE synthesis, CDP-DAG pathway and de-novo synthesis pathway (Fig. 5.1A). In CDP-DAG pathway, phosphatidylserine (PS) decarboxylases directly convert PS into PE. In yeast there are two PS decarboxylase genes, PSD1 (256) and PSD2 (257). Psd1 is localized in mitochondria (256, 258), while Psd2 is localized to TGN (259, 260), endosomes(260) and vacuole membrane (259) compartments (components of post-golgi organelles). In Arabidopsis, there are three PSD genes, namely PSD1, PSD2 and PSD3 (261). AtPSD1 is localized in mitochondria, AtPSD2 localized to vacuole membrane (Tonoplast), while AtPSD3 localized to ER (261).

In de-novo synthesis pathway, ethanolamine is converted to phosphoethanolamine by ethanolamine kinase (EKI), then converted to CDP-ethanolamine by CTP:phosphoethanolamine cytidylyltransferase (ECT), and converted to PE by aminoalcoholphosphotransferase (AAPT). AAPT has substrate specificity among ethanolamine and choline. In yeast, there are two AAPTs, EPT1 and CPT1. EPT1 has major activity using ethanolamine, while minor activity using choline. While CPT1 have predominant substrate activity using choline for PC synthesis (262). In plants (263-266), AAPTs were also been identified which show both ethanolamine or choline substrate activity. TaAAPT1 and TaAAPT2 from wheat were shown to be localized to ER and Golgi apparatus (264). A human CPT1 is localized to Golgi apparatus, while human CEPT1 (major substrate activity to choline, minor to ethanolamine) localized to ER and

nuclear membrane (267). However, the localization of EPT1 is not characterized yet in yeast.

In plants, the CDP-DAG pathway is not essential since psd1/psd2/psd3 mutant arabidopsis plants are viable and display no obvious growth or morphological defects (261). The total phospholipid composition was unchanged, while PE level in isolated mitochondria from mutant plant was decresed (261). In yeast, deletion of any one of the three or two of the three PE synthesis genes, PSD1, PSD2 or EPT1, is not lethal. While deletion of all three of them is lethal in yeast (268).

5.2 Materials and Methods

Yeast strains and expression plasmids. Yeast strains BY4741 (MAT a *his3Δ1 leu2Δ0 met15Δ0 ura3Δ0*) and *pep4*Δ, *tlg2*Δ, *pep12*Δ, *vam3*Δ or *vam7*Δ (single-gene deletion strain) were obtained from Open Biosystems (Huntsville, AL, USA). For TBSV replication in yeast, pESC-T33/DI72 and pYES-T92 were described previously. Yeast double deletion strains of *tlg2*Δ*tlg1*Δ *or vam3*Δ*vam7*Δ were generated from *tlg2*Δ *or vam7*Δ using homologous recombination of a PCR fragment harboring a selection marker hygromycin B phosphotransferase amplified fragment from Euroscarf collection plasmid pFA6a-hphNT1(269) .

For yeast plasmid pRS315-CFlag, primer pairs #5100 (AGCTTGGTGGTGACTACAAGGACGACGATGACAAGGGTGGTAGATCTGGCG TCGACTAA)/#5101

(TCGATTAGTCGACGCCAGATCTACCACCCTTGTCATCGTCGTCCTTGTAGTCACCACCA) were annealed and inserted into pRS315-pTef1 (described in Chapter 3). To generate pCUP1 driven C-terminal Flag-tagged SAR1 or ARF1, pRS315-CFlag were digested with SacI/NotI and inserted with SacI/NotI digested PCR fragment of pCUP1 promoter amplified from pEsc-His/Cup-FLAG/ssa1 with primer pair #3039 (CGCGGAGCTCGACATTTGGGCGCTATACGTGCATATGT)/#5861 (GCGGCGGCCGCTACAGTTTGTTTTTCTTAATATCTATTTCGA), resulting plasmid pRS315-pCUP1p-CFlag. SAR1 and ARF1 mutants were generated via site directed mutagenesis and amplified with primer pair #5865 (CGCGGATCCATGGCTGGTTGGGATATTTTTGG)/#5866 (GCCCTGCAGAATATATTGAGATAACCATTGGAACGCCTC), or #3132 (gccggatccatgggtttgtttgcctctaagttgttc)/#5742 (GCCCTGCAGAGTTGAGTTTTTCAAACTGTTACTTAACCATTC), digested with BamHI/PstI, and inserted into pRS315-pCUP1-CFlag.

To generate N-Terminal Flag-tagged Tlg2p, TLG2 was amplified from yeast genome using primer pair #5717 (CGCGGATCCATGTTTAGAGATAGAACTAATTTATTTTTATCATACCGTAGG) and #5718 (GCGCTCGAGTCAAAGTAGGTCATCCAAAGCATCATTC), digested with BamHI/XhoI, and inserted into BamHI/SalI digested pRS315-NFlag (described in Chapter 3), generating pRS315-NFlag-Tlg2.

To generate pTef1 promoter driven no tagged COP1 expressing vector, PCR fragment of COP1 were amplified from yeast genome using primer pair #1858 (GGCGGGATCCATGAAGATGTTAACTAAATTTG)/ #1859

(GGCGCTCGAGTTATACACGTATTCTTAATCCGGA), digested with BamHI/XhoI and inserted into BamHI/SalI digested pRS315-pTef1, generating pRS315-COP1.

Confocal laser microscopy. Wild type BY4741 or sti1Δ yeast strains were transformed with the following expression plasmids: pESC-GFP-T33/DI72, pYES-T92 (9), as well as pRS315-Pex13-mRFP1 (described in Chapter 4). The yeast cultures were incubated in galactose medium overnight, sampled and imaged with Olympus FV1000 confocal laser scanning microscope (Olympus America Inc., Melville, NY). The microscope settings were the following: excitation and emission for GFP and RFP were 488nm laser/500-530nm filter and 543nm laser/560-660nm filter, respectively. PE staining with biotinylated duramycin and streptavidin conjugated with Alexa-405 was described in Chapter 4.

Free GFP detection assay. pESC-GFP-T33 (described in Chapter 4) and pYES-GFP-T92 (9) together with an empty plasmid or SAR1 mutants were transformed into wild type or mutant yeast strains. GFP-p33/p92 were induced for expression in SC media containing 2% galactose for 24 hours. Total protein was extracted and subjected to western blot analysis using an anti-GFP antibody.

5.3 Results

TBSV replication in yeast mutants defective in PE synthesis pathways. Since PE is essential for TBSV replication in vitro, we then ask: could any specific pathway of PE synthesis be hijacked by TBSV to favor virus replication? Genes of PE synthesis were

systemically deleted from wild type yeast, generating: *psd1*Δ*, psd2*Δ*, ept1*Δ*cpt1*Δ*, psd1*Δ*ept1*Δ*cpt1*Δ*, psd2*Δ*ept1*Δ*cpt1*Δ *and psd1*Δ*psd2*Δ. We tested TBSV replication in yeast grown in SD media without ethanolamine (Fig. 5.1 B) or with ethanolamine (Fig. 5.1C). Since ethanolamine is the precursor of de-novo PE synthesis pathway, *psd1*Δ*psd2*Δ of which PE synthesis is inhibited will not grow without ethanolamine. In SD media without ethanolamine, major PE synthesis come from PSD1 or PSD2 pathway. TBSV repRNA accumulation level increased ~2 fold in those mutants, *psd1*Δ *or psd1*Δ*ept1*Δ*cpt1*Δ*,* which lacked the PSD1 mediated PE synthesis pathway. In those mutants in which PSD2 pathway was deleted, TBSV repRNA accumulated to similar level as wild type (Fig. 5.1B, upper panel). While viral protein accumulated to a similar level among all the mutant strains (Fig. 5.1B lower level).

In a growth condition where ethanolamine was provided (Fig. 5.1C), all three PE synthesis pathways could contribute to the overall PE pool in the cell. In such condition, TBSV repRNA accumulation also increased by ~80% in *psd1*Δ*ept1*Δ*cpt1*Δ yeast, in which PSD2 mediated PE synthesis pathway is the only PE source. While when PSD2 and de-novo PE synthesis pathways were deleted in *psd2*Δ*ept1*Δ*cpt1*Δ yeast, TBSV repRNA accumulation decreased to ~60% (Fig. 5.1C upper panel). p33 replication protein accumulation in *psd2*Δ*ept1*Δ*cpt1*Δ yeast also decreased comparing to wild type (Fig. 5.1C lower panel). In other mutant yeasts, TBSV replication and viral protein level are comparable to those in wild type yeast (Fig. 5.1C).

TBSV p33 replication protein is partially localized within TGN. In addition to the characteristic punctuate structures, we also observed diffused pattern of GFP-p33 in

yeast, which did not co-localize with peroxisome marker protein (Fig. 5.2A). In Fig. 5.2A, GFP-p33 was co-expressed with p92 and DI72 repRNA, as well as Pex13p-mRFP as a peroxisome marker for 10 hours after induction of protein expression. We observed some GFP- p33, which did not overlap with the peroxisome marker Pex13p-mRFP. Since we know that peroxisome in yeast under microscope is visible as round punctuate structure, those diffused pattern with GFP-p33 suggested that TBSV p33 might be localized to other membrane structures during infection besides peroxisome. In chapter 4, we also observed that PE was also co-localized to these diffused structure with p33. It was interesting to identify which cellular compartment the diffused structures belong to. The answer may help us to understand PE enrichment at the site of TBSV replication.

Confocal microscopy was used to identify the localization of the diffused structure with many cellular marker proteins. Among those, TGN tSNARE protein Tlg2p (270) was identified to co-localize with the diffused structure of TBSV p33 (Fig. 5.2B).

PE is enriched at both peroxisome and TGN locations in the presence of p33. To demonstrate that PE enriched at peroxisome and TGN locations of p33, we transformed yeast with plasmids expressing GFP-p33 together with peroxisome marker Pex13p-mRFP (Fig. 5.3 A) or TGN marker mRFP-Tlg2p (Fig. 5.3 B). Viral proteins and repRNA were induced in galactose containing media for 10 hours, then the yeast cells were fixed and subsequently incubated with biotinylated duramycin, streptavidin-conjugated with Alexa Fluor 405 dye. Cells were observed under confocal microscope. In Fig. 5.3A, obvious punctuate structure was highlighted in all channels detecting PE, GFP-p33 and peroxisomes. However, PE and GFP-p33 were also co-localized and observed as diffused

pattern. To demonstrate that this diffused pattern indeed represented TGN, mRFP-Tlg2p were used to label TGN in addition to GFP-p33 and PE (Fig. 5.3B). In Fig. 5.3B, indeed, PE and GFP-p33 were co-localized and showed a diffused area outside the punctuate structure. This diffused area was labeled with TGN marker protein mRFP-Tlg2p.

Deletion of TLG2 interfered with the enrichment of PE at site of TBSV replication. Since both the genetic study of PE synthesis pathway and confocal microscope study of PE localization site suggested the relevance of Trans-Golgi network in PE enrichment to TBSV site of replication. As well as in previously yeast single gene deletion library screen (12), deletion of TLG2 was shown to affect tombusvirus replication. We focused on the role of Trans-Golgi network in TBSV replication.

First, we confirmed that deletion of TLG2 could reduce TBSV replication to about 16% , by comparing repRNA accumulation with that of wild type yeast (Fig. 5.4A). Meanwhile, overexpression of a N-terminus Flag-tagged Tlg2 could compliment TBSV replication caused by the deletion of TLG2 in the mutant strain.

Secondly, in *tlg2*Δ yeast, plasmids expressing GFP-p33, p92, repRNA and pex13p-mRFP were co-transformed. Cells were induced for viral protein expression and labeled with biotinylated duramycin to detect PE localization. Importantly, in *tlg2*Δ yeast, PE was not co-localized with GFP-p33 (Fig. 5.4B).

Deletion of genes coding for SNARE proteins in post-Golgi organelles reduces TBSV replication. Since genetic analysis showed that in mutant strains, in which only PSD2 mediated PE synthesis, TBSV repRNA accumulation was ~2x fold more than wild type,

it suggested that PSD2 pathway might be the easiest for TBSV to hijack. PSD2 were shown to be localized at TGN or compartments of endocytic pathway in yeast or in plant (259-261). Furthermore, deletion of TLG2 in yeast also lead to dramatically decreased TBSV replication possibly due to lack of PE enrichment at TBSV replication sites. Tlg2p is a tSNARE on TGN (270). It would be interesting to see if gene deletion of other tSNAREs in endocytic pathway where Psd2p is localized could affect TBSV replication.

We tested deletion strains of TGN tSNAREs: *tlg2*Δ *or tlg2*Δ*tlg1*Δ*,* late endosome tSNARE: *pep12*Δ and vacuole tSNAREs: *vam3*Δ*, vam7*Δ *or vam3*Δ*vam7*Δ*.* Surprisingly, all the SNARE protein deletions decreased TBSV repRNA accumulation to about 10% comparing to the wild type (Fig. 5.5A upper panel). Also p33 accumulation was decreased in all the mutant strain (Fig. 5.5A lower panel).

To test if p33 was targeted to the endocytic pathway, we utilized the vacuolar protease resistant feature of GFP when present as a fusion protein. TBSV p33 or p92 was tagged with GFP at the N-terminus (Fig. 5.5B). Free GFP detected by GFP-antibody would suggest presence of GFP-p33 or GFP-p92 in vacuole. We first checked GFP-p33/p92 degradation pattern in wild type yeast, by western blot using anti-GFP antibody (Fig. 5.5C). In wild type yeast expressing GFP-p33/p92, anti-GFP antibody detected free GFP with size about 30kDa (Fig. 5.5C middle and right panel). While in wild type yeast expressing His-GFP, a expected ~33kDa band was detected (Fig. 5.5C left panel).

In addition, wild type yeast and SNARE gene mutants described above as well as a yeast strain with single gene deletion of PEP4, which aborts protein degradation in vacuole (271), were transformed with plasmids containing GFP-p33/p92 and induced for gene expression for 24 hours in 23°C. Total protein were analyzed by western blot using

anti-GFP antibody (Fig. 5.5D). In every strain, GFP-p33 and GFP-p92 were detected, however free GFP were only detected in wild type, *tlg2*Δ*, vam3*Δ*, vam7*Δ *or vam3*Δ*vam7*Δ*,* but not in *pep4*Δ*, tlg2*Δ*tlg1*Δ or *pep12*Δ (Fig. 5.5D upper panel and middle panel). Presence of free GFP in wild type strain and missing of free GFP in *pep4*Δ strain suggested a vacuole targeting of GFP-p33. And disruption of vesicle transport pathway by deletion of certain SNARE genes abolished the targeting of GFP-p33 to vacuole.

Over-expression of SAR1 dominant mutant blocks vacuole targeting of p33 and reduces TBSV replication. Most of membrane proteins secreted to endocytic pathway through Golgi are dependent upon anterograde transportation pathway (235, 238). SAR1 encode a GTPase which regulate anterograde transportation COP-II vesicle coat assembly and disassembly (272). Expression of GTP locked mutant SAR1-H77L could block cargo transportation to golgi (273, 274). Thus we tested its effects on p33 vacuole targeting as well as TBSV replication.

A C-terminal Flag-tagged SAR1-H77L was induced under controllable CUP1 promoter at the same time point as the GFP-tagged viral proteins. After 24 hours protein expression, total proteins from different treatments were subjected to western blot analysis using anti-GFP antibody (Fig. 5.6A). As previously shown (Fig. 5.5 C &D), free GFP were detected in wild type yeast but not in *pep4*Δ strain (Fig. 5.6A). In wild type yeast co-expressing wild type SAR1 gene, free GFP was also detected in a similar amount as in wild type yeast. However in yeast co-expressing a SAR1 dominant mutant SAR1-H77L, free GFP was present in reduced amount in comparison with wild type yeast (Fig. 5.6A).

To test effect of SAR1-H77L on TBSV replication, vectors expressing wild type SAR1 or SAR1-H77L, or an empty vector were transformed into yeasts together with TBSV p33, p92 and repRNA expressing plasmids. Viral components were induced together with SAR1 mutant for 24 hours. Total RNA and proteins were extracted from different treatments for RNA and protein blot analysis (Fig. 5.6B). Over-expression of wild type SAR1 did not affect TBSV repRNA accumulation, while over-expression of SAR1-H77L reduced TBSV repRNA accumulation to ~23%.

Expression of ARF1 dominant-active mutant ARF1-Q71L, but not dominant-negative mutant ARF1-T31N, blocks TBSV replication. Since p33 is partially localized to TGN, and disruption of TLG2, tSNARE of TGN, aborted PE enrichment on peroxisome and reduced TBSV replication (Fig. 5.4), retrograde transportation from TGN could be a potential pathway that TBSV might hijack, and thus benefit to PE enrichment on peroxisome. To test this hypothesis, we utilized dominant mutants of ARF1, dominant-negative mutant ARF1-T31N (275), or dominant-active mutant ARF1-Q71L (275, 276). Dominant negative mutant ARF1-T31N blocks the formation of COP-I vesicle, thus blocks COP-I-dependent retrograde transport. Dominant-active ARF1-Q71L stimulates formation of COP-I vesicles coats but blocks coatomer disassembly, thus also blocks retrograde transportation.

Empty vector, or vectors expressing controllable CUP1 promoter driven ARF1, ARF1-T31N and ARF1-Q71L ORFs were co-transformed with plasmids expressing TBSV viral proteins and repRNA. TBSV replication was induced in galactose containing media supplemented with copper to induce ARF1 and mutants expression. After 24 hours

induction of replicaiton, total RNA or proteins were extracted from samples and analyzed using RNA blot or western blot (Fig. 5.7A). RepRNA accumulation from samples over-expressing ARF1 or ARF1-T31N did not show significant difference comparing to yeast samples transformed with an empty vector. While over-expression of dominant active ARF1-Q71L reduced replication to ~34%. Viral protein accumulation in ARF1-Q71L (lower panels in Fig. 5.7A) did not show significant difference comparing to those expressing an empty vector, ARF1 or ARF1-T31N.

Alpha subunit of COP-I vesicle coatomer, Cop1p, inhibits TBSV replication. ARF1-Q71L encodes a GTP locked form of ARF1, which stimulates the assembly of COP-I vesicle coatomer. To test if formation of COP-I vesicle benefits or inhibits TBSV replication in yeast, we tested TBSV replication while alpha subunit of COP-I vesicle was down-regulated. In yeast, COP1 encodes alpha subunit of COP-I vesicle coatomer and is essential to yeast growth (277). Replacing the COP1 promoter on the genome with a tetracycline (tet)-regulatable promoter would allow control of the expression of COP1 and study its function (278, 279).

We first obtained yeast strain of Tet-COP1 from Tet-promoters Hughes Collection (yTHC) (278). When 10 μg/ml doxycycline was added to media, Tet-COP1 yeast growth was inhibited, suggesting genomic expression of COP1 was shut down. However expression of COP1 driven by a constitutive promoter from plasmid pRS315-COP1 could rescue the inhibitory effect, thus allowed Tet-COP1 growth in doxycycline containing media (Fig. 5.7B).

Vectors expressing TBSV replication proteins and repRNA were transformed to Tet-COP1 strain with or without pRS315-COP1. Yeasts were cultured to induce TBSV replication with or without doxycycline. In the growth media with doxycycline where COP1 expression was inhibited, TBSV repRNA accumulation increased ~3 fold, comparing to that in yeast without doxycycline treatment. However, over-expression of COP1 under a constitutive promoter from plasmid inhibited TBSV repRNA accumulation to ~30% in the growth condition either with or without doxycycline, suggesting that COP1 or formation of COP-I complex inhibited TBSV replication.

5.4 Discussion

Can PE synthesis pathway be co-opted by TBSV? In chapter 4, TBSV p33 was demonstrated to induce PE accumulation in peroxisomal membranes, the site of TBSV replication. To better understand the virus-driven lipid sorting process, we tested yeast mutants with deletion of genes involved in PE synthesis pathways for TBSV replication. From previous studies (268, 280, 281) we know that PE is essential for yeast growth, three PE synthesis pathways could not be deleted in the same yeast, but single or double deletion of the three pathways are possible. This suggests that PE from any of the three pathways could be transported to other cellular components where PE is needed. However, this endogenous PE transportation process has not yet revealed, except that a study using purified yeast post-Golgi vesicles in an cell-free environment showed that yeast post-golgi secretory vesicles contains ~80% of PE in the cytosolic leaflet, and P4 ATPases Drs2p and Dnf3p are required to maintain the assymetry (282).

We tested TBSV replication in yeast strains with single or double deletions of PE synthesis pathways genes (Fig. 5.1), and found none of these deletions caused TBSV replication to drop more than 50% comparing to that in the wild type yeast.

However, we noticed that in the presence of ethanolamine, in the yeast mutant *psd2*Δ*ept1*Δ*cpt1*Δ where the only PE source come from the PSD1 pathway, TBSV repRNA accumulation reduced to ~60% (Fig. 5.1C). These data suggesting that deletion of PE source from PSD2 and EPT1 would affect TBSV replication, although not totally required. Meanwhile, in yeast strain *psd1*Δ*ept1*Δ*cpt1*Δ, TBSV repRNA accumulation increased to 180%, suggesting that in this yeast strain PE could be more accessible for TBSV. PSD2 pathway is the only PE source in *psd1*Δ*ept1*Δ*cpt1*Δ, and thus TBSV may utilize PE from PSD2 pathway more easily.

We also tested growth condition without ethanolamine. In this growth condition, PSD1 or PSD2 pathway contribute to the major cellular PE sources, while double deletion mutant *psd1*Δ *psd2*Δ could not grow due to lack of ethanolamine which is PE precursor. TBSV repRNA accumulation increased to ~2-2.5 fold in the yeast strain *psd1*Δ *or psd1*Δ*ept1*Δ*cpt1*Δ, comparing to that of the wild type. In these strains, PSD2 pathway is the dominant/only PE synthesis pathway. PSD2 localized at TGN (259, 260), endosomes(260) and vacuole membrane (259). This finding is in line with the hypothesis that PE from post-Golgi compartments could be accessed by TBSV easier than from other pathways.

TGN tSNARE Tlg2 co-localizes with TBSV p33 and affects PE redistribution to peroxisome as well as TBSV replication. In addition to peroxisome localization of p33,

we also observe diffused pattern of GFP-p33 outside the peroxisome marker Pex13p-mRFP (Fig. 5.2A), especially when cells were harvested at 10-12 hours after the induction of viral protein expression in yeast. A TGN tSNARE Tlg2p was shown to localize with the diffused GFP-p33 (Fig. 5.2B). This finding added new level of sub-cellular dynamics of TBSV infection. Indeed in a study performed by another research group, similar pattern of TBSV p33 distribution outside of peroxisome was also detected in plant cells after 24 hours of plasmids bombardment (18). The observed reticular distribution of p33 was claimed to be peroxisomal-ER (pER) based on its co-localization with Chloramphenicol acetyltransferase tagged to 36 C-terminal residues of Peroxisomal ascorbate peroxidase (CAT-APX), which was believed to be sorted to peroxisome through a sub-domain of ER (pER). But they also found that the reticular p33 pattern did not co-localiz either with concanavalin A-stained ER or immunostained ER endogenous protein calreticulin (18). However, whether p33 interferes with the targeting of CAT-APX to peroxisome remains unknown. In other words, CAT-APX localization may changed during p33 expression, thus its co-localization with reticular p33 pattern may not suggest their presence in a sub-domain of ER.

We later demonstrated that PE was not only enriched in peroxisomal membranes by p33, but also enriched at TGN (Fig. 5.3B). Based on this finding, we hypothesize that enrichment of PE driven by p33 may be connected to cellular functions of TGN. Indeed, when TLG2 was deleted, PE did not co-localized with p33 (Fig. 5.4B). Although p33 localization to the peroxisome was not affected. Since tSNARE is essential for TGN's function, this finding supported previous hypothesis that cellular function of TGN is required for PE enrichment with p33.

Disruption of vesicle transport in endocytic pathway inhibited replication. We previously hypothesis PSD2 pathway of PE synthesis was more accessible for TBSV p33 to hijack, and we also showed that cellular function of TGN is important for viral hijacking of PE. Psd2 localized with TGN (259, 260), endosome (260) and Vacuolar membrane(259), and tSNARE proteins from these sub-cellular compartments also important for TBSV replication similar to that of *tlg2*Δ. It might be that disruption of vesicle transport in endocytic pathway would interfere transportation of PE from PSD2 source. It is also surprising to see minor amount of GFP-p33 is targeted to vacuole, whether p33 is directly involved in PE re-distribution to peroxisomal membranes remains to be tested.

Arf1 regulated retrograde transportation is not needed for, but could interfere with, TBSV replication. One question may raise due to complicated locations and functions of TBSV p33: how does the presence of p33 in endocytic pathway benefit assembly of TBSV replication complexes?

One possibility maybe that p33 was retro-transported from TGN to ER or peroxisome and PE was hijacked from the carrying vesicle. Although previous evidences suggested that asymmetrical distribution of PE on one side of membrane bilayers only happened on post golgi organelles and ER possess a symmetrical lipid distribution across the bilayer (282), we still tested the hypothesis.

By over-expression a dominant negative mutant of ARF1, ARF1-T31N, which inhibit COP-I dependent coatomer assembly, we showed that COP-I dependent

retrograde transportation is not required for TBSV replication. However over-expression of ARF1-Q71L, which stimulate COP-I coatomer assembly but not disassembly, inhibited TBSV replication to ~34%. The difference of these to mutants was probably due to stimulation of assembly of COP-I vesicles by ARF1-Q71L also led a consumption of phospholipids, including PE, from TGN, thus interfere with PE recruitment by TBSV.

Summary: In this chapter, efforts were made for finding the PE source for TBSV replication. However, deletion of single or double PE synthesis genes did not lead to significantly reduced TBSV replication in yeast. However, PSD2 mediated PE synthesis pathway was favored among three PE synthesis pathways by TBSV.

TBSV p33 was demonstrated to localize to both TGN and peroxisome. PE was also enriched at both TGN and peroxisome together with p33. Moreover, a TGN tSNARE Tlg2p was shown to have major function in TBSV replication, possibly due to its ability to regulate PE enrichment in replication complexes.

By using GFP tagged TBSV replication proteins, a vacuole targeting pathway of p33 and p92 was identified. This p33/p92 targeting requires vesicle transportation pathway on the TGN and endocytic compartments. And disruption of vesicle transport in the endocytic pathway also have negative effect on TBSV replication.

This p33/p92 secretion was shown to be dependent on COP-II mediated anterograde transportation from ER to Golgi, and was essential for TBSV replication in yeast. However, a COP-I dependent retrograde transportation seems not to contribute to TBSV replication, but interfere with replication.

Overall, we found evidences that p33 secretion from ER to vacuole through COP-II dependent early secretory pathway contributed to TBSV replication. An TGN tSNARE Tlg2p was also shown to regulate PE enrichment at TBSV site of replication.

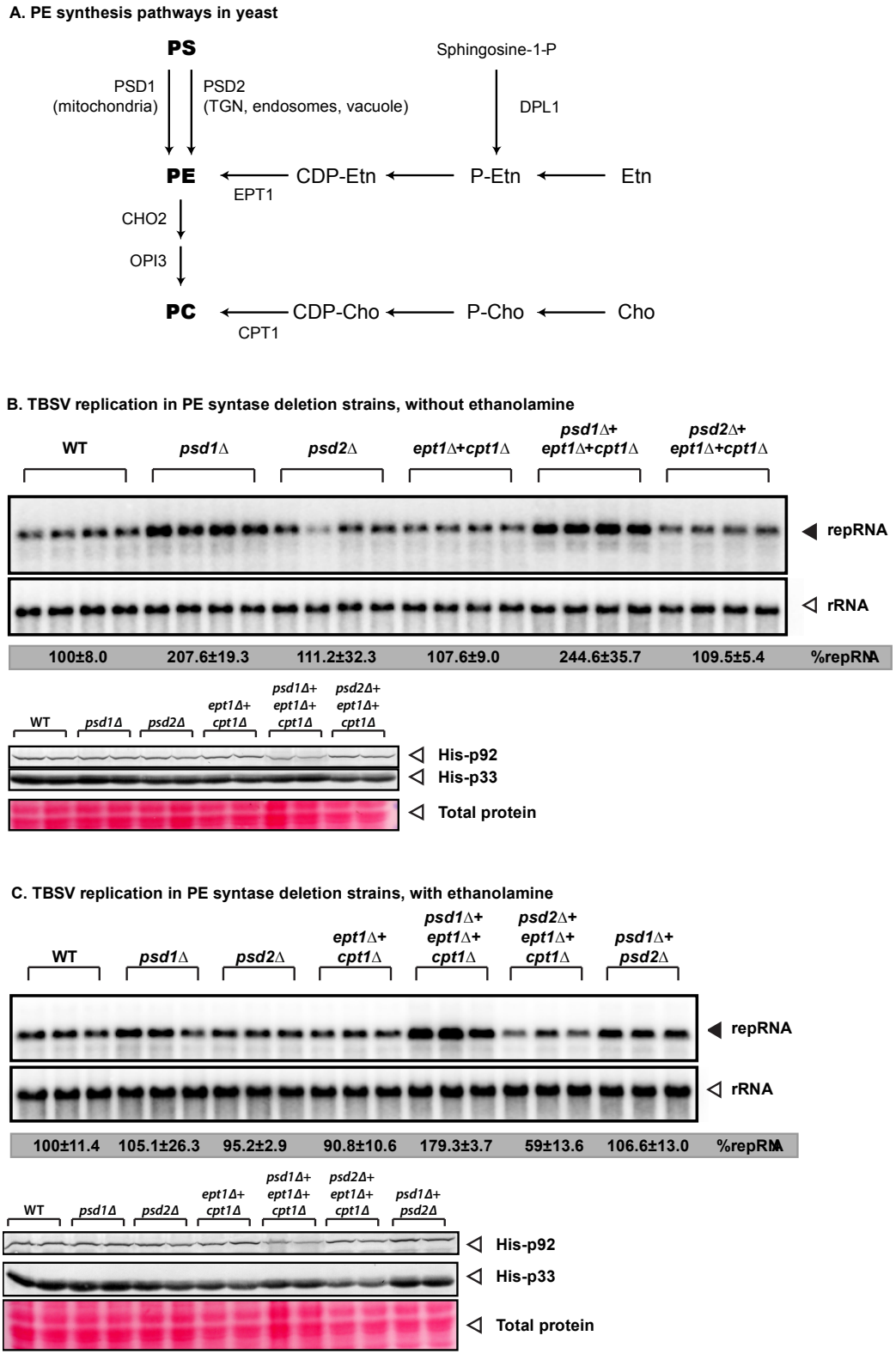
A. PE synthesis pathways in yeast
PS
Sphingosine-1-P
PSD1
(mitochondria)
PSD2
(TGN, endosomes, vacuole)
DPL1
PE
CDP-Etn
P-Etn
Etn
EPT1
CHO2
OPI3
PC
CDP-Cho
P-Cho
Cho
CPT1
B. TBSV replication in PE syntase deletion strains, without ethanolamine
WT
psd1Δ
psd2Δ
ept1Δ+cpt1Δ
psd1Δ+ ept1Δ+cpt1Δ
psd2Δ+ ept1Δ+cpt1Δ
repRNA
rRNA
100±8.0
207.6±19.3
111.2±32.3
107.6±9.0
244.6±35.7
109.5±5.4
%repRNA
WT
psd1Δ
psd2Δ
ept1Δ+ cpt1Δ
psd1Δ+ ept1Δ+ cpt1Δ
psd2Δ+ ept1Δ+ cpt1Δ
His-p92
His-p33
Total protein
C. TBSV replication in PE syntase deletion strains, with ethanolamine
WT
psd1Δ
psd2Δ
ept1Δ+ cpt1Δ
psd1Δ+ ept1Δ+ cpt1Δ
psd2Δ+ ept1Δ+ cpt1Δ
psd1Δ+ psd2Δ
repRNA
rRNA
100±11.4
105.1±26.3
95.2±2.9
90.8±10.6
179.3±3.7
59±13.6
106.6±13.0
%repRNA
WT
psd1Δ
psd2Δ
ept1Δ+ cpt1Δ
psd1Δ+ ept1Δ+ cpt1Δ
psd2Δ+ ept1Δ+ cpt1Δ
psd1Δ+ psd2Δ
His-p92
His-p33
Total protein

Fig. 5.1

Fig. 5.1 Reduced TBSV replication in PE synthesis pathways deletion yeast strains.

(A) Schematic of three PE synthesis pathways in yeast. (B) Replication of TBSV in yeast deletion strains grown in media without ethanolamine. Upper Panel: Northern blot of repRNA and 18S ribosomal RNA. Lower Panel: Western blot of total proteins extracted from different strains tested. TBSV p33 and p92 were tagged with HIS_6 tag on their N-terminals and detected with an anti-HIS antibody. Total proteins were stained with Ponceau S on PVDF membrane after transfer. (C) Replication of TBSV in yeast in deletion strains grown in media with ethanolamine. Note that *psd1*Δ*psd2*Δ strain was able to grow under this condition. See further details described in panel B. Each experiment was repeated.

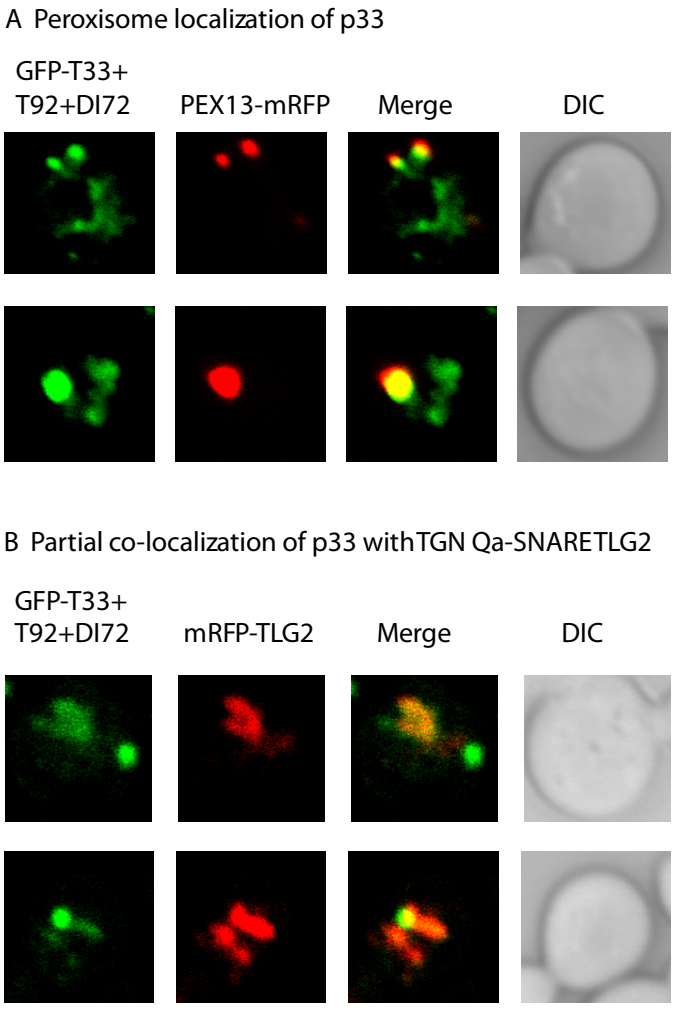
A Peroxisome localization of p33
GFP-T33+
T92+DI72
PEX13-mRFP
Merge
DIC
B Partial co-localization of p33 withTGN Qa-SNARETLG2
GFP-T33+
T92+DI72
mRFP-TLG2
Merge
DIC

Fig. 5.2

Fig. 5.2 p33 co-localization to peroxisomes and TGN.

(A) GFP-tagged p33 localized in peroxisomal membrane. Wild type yeast was transformed with vectors expressing GFP-tagged p33, p92 and DI-72, as well as pex13p-mRFP. Viral components were induced in yeast grown in SC media containing 2% galactose for 10 hours. Cells were collected and subjected to confocal laser microscopy analysis. Results showed partial co-localization of TBSV GFP-p33 with peroxisomal marker Pex13p-mRFP. DIC (differential interference contrast) images are shown on the right. (B) Confocal laser microscopy images showed that TBSV GFP-p33 also partially co-localized with TGN marker Tlg2p-mRFP.

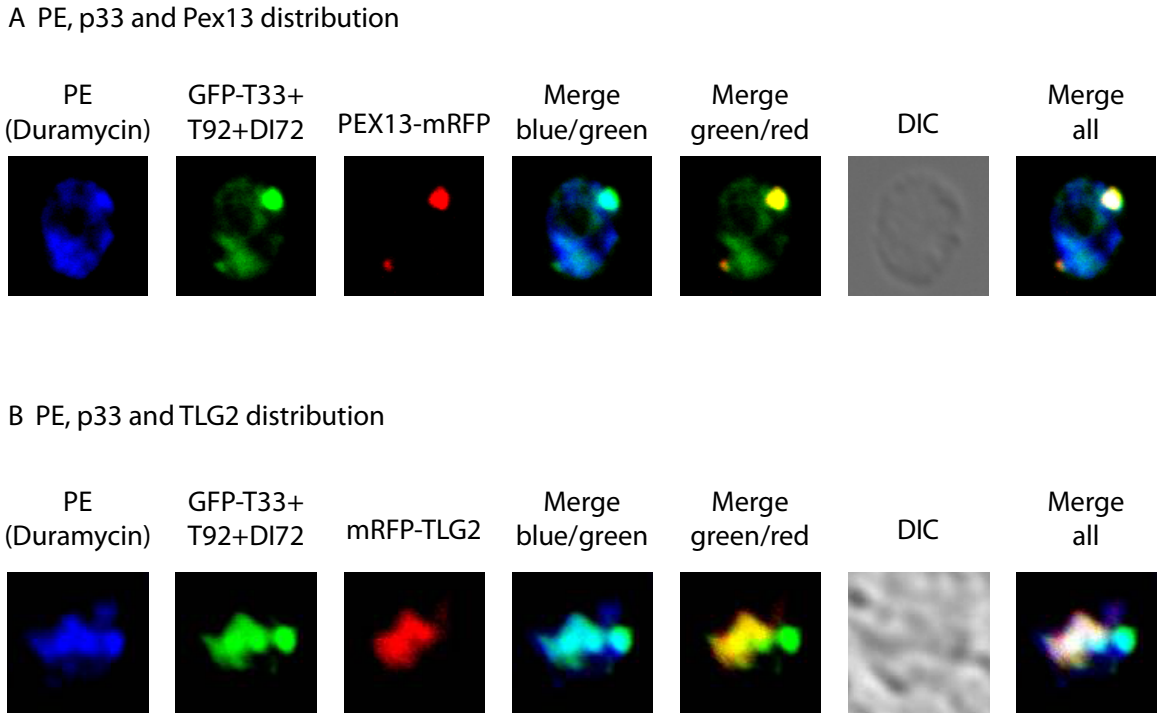
A PE, p33 and Pex13 distribution
PE (Duramycin)
GFP-T33+ T92+DI72
PEX13-mRFP
Merge blue/green
Merge green/red
DIC
Merge all
B PE, p33 and TLG2 distribution
PE (Duramycin)
GFP-T33+ T92+DI72
mRFP-TLG2
Merge blue/green
Merge green/red
DIC
Merge all

Fig. 5.3

Fig. 5.3 PE is enriched in both peroxisome and TGN where TBSV GFP-p33 is localized.

(A) Confocal laser microscope image showed that PE was enriched at sites of GFP-p33 accumulation and partially co-localized with peroxisomal marker Pex13p-mRFP as punctuate structures. PE was visualized using biotinylated duramycin and streptavidin conjugated with Alexa-405. (B) TGN localization of GFP-p33 where PE was also enriched showed diffused pattern, which is visually distinguishable from peroxisomal punctuate structures.

A TBSV replication in tlg2Δ yeast

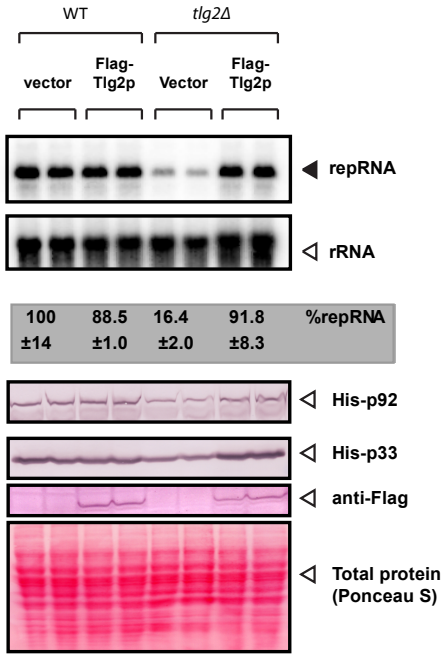

B PE, p33 and Pex13 distribution in tlg2Δ yeast

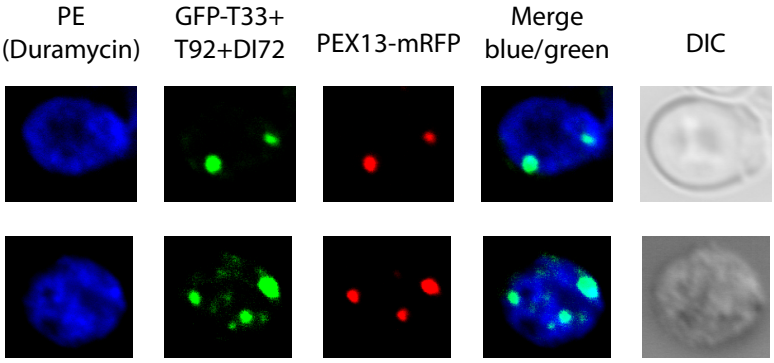

Fig. 5.4

Fig. 5.4 TGN tSNARE Tlg2 is required for efficient TBSV replication in yeast, affecting PE enrichment to sites of replication.

(A) Deletion of *TLG2* dramatically reduced TBSV replication, and expression of a N-terminal Flag-tagged Tlg2 from a vector complemented the effect caused by deletion of *TLG2* from genome. Upper panel: Northern blot repRNA and ribosomal 18S RNA. Lower panel: Western blot detecting viral proteins as well as Flag-Tlg2p by anti-HIS antibody or anti-FLAG antibody. Total protein was detected with Ponceau S on PVDF membrane after transfer. Experiments were repeated. (B) Confocal microscope images showed that unlike in wt yeast PE was not enriched at sites of replication in *tlg2*Δ yeast. See further description of yeast growth condition in Fig. 5.2, PE detection method in Fig. 5.3.

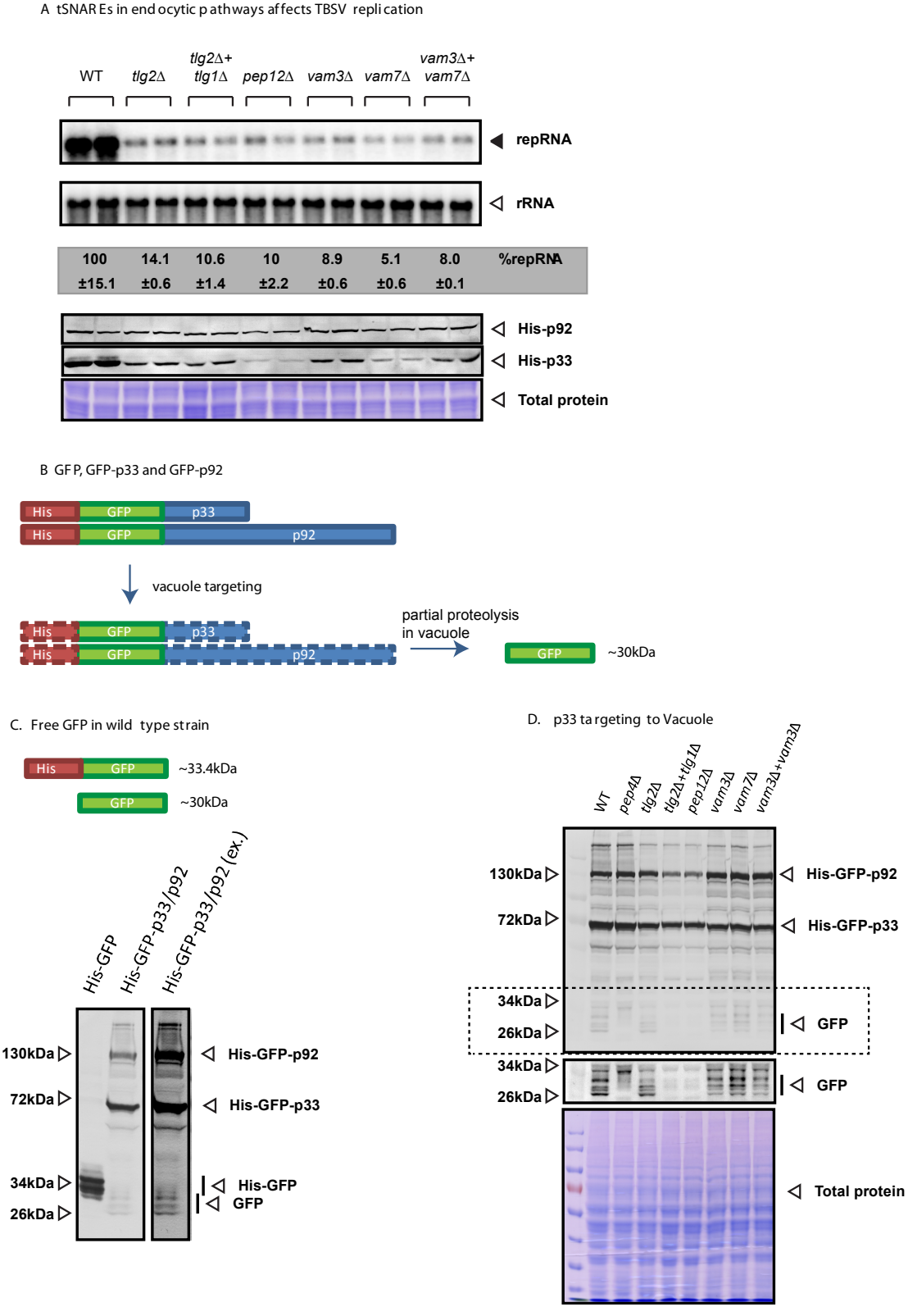
A tSNAREs in endocytic pathways affects TBSV replication
WT
tlg2Δ
tlg2Δ+ tlg1Δ
pep12Δ
vam3Δ
vam7Δ
vam3Δ+ vam7Δ
repRNA
rRNA
100 ±15.1
14.1 ±0.6
10.6 ±1.4
10 ±2.2
8.9 ±0.6
5.1 ±0.6
8.0 ±0.1
%repRNA
His-p92
His-p33
Total protein
B GFP, GFP-p33 and GFP-p92
His
GFP
p33
p92
vacuole targeting
partial proteolysis in vacuole
~30kDa
C. Free GFP in wild type strain
~33.4kDa
~30kDa
His-GFP
His-GFP-p33/p92
His-GFP-p33/p92 (ex.)
130kDa
72kDa
34kDa
26kDa
His-GFP-p92
His-GFP-p33
His-GFP
GFP
D. p33 targeting to Vacuole
WT
pep4Δ
tlg2Δ
tlg2Δ+tlg1Δ
pep12Δ
vam3Δ
vam7Δ
vam3Δ+vam3Δ
130kDa
72kDa
34kDa
26kDa
His-GFP-p92
His-GFP-p33
GFP
Total protein

Fig. 5.5

Fig. 5.5 Targeting of TBSV p33/p92 to vacuole through vesicle transport pathway.

(A) Deletion of tSNARE genes of TGN or endocytic pathway dramatically reduced TBSV replication. (B) Cartoon representation of partial proteolysis of GFP tagged viral proteins in vacuole. (C) Free GFP was detected in wild type yeast expressing GFP tagged p33/p92 using anti-GFP antibody. Arrows on the left showed sizes of protein markers. Arrows on the right showed expected bands of Free GFP or GFP tagged viral proteins. Right panel is a digitally over-exposed (ex.) copy of His-GFP-p33/p92 sample. (D) Free GFP was not detected in *pep4*Δ*, tlg2tlg1*Δ or *pep12*Δ yeast strains expressing GFP-tagged p33/p92. Upper panel: protein blot of total protein from different yeast strains expressing GFP-tagged p33/p92 using anti-GFP antibody. Middle panel: Small portion of digitally over-exposed image of boxed area from upper panel, showing the free GFP bands. Noting that Free GFP was not detected in *pep4*Δ*, tlg2tlg1*Δ or *pep12*Δ yeast strains. Lower panel: coomassie blue staining of total protein loaded.

A SAR1 dominant mutant blocks vacuole targeting of p33

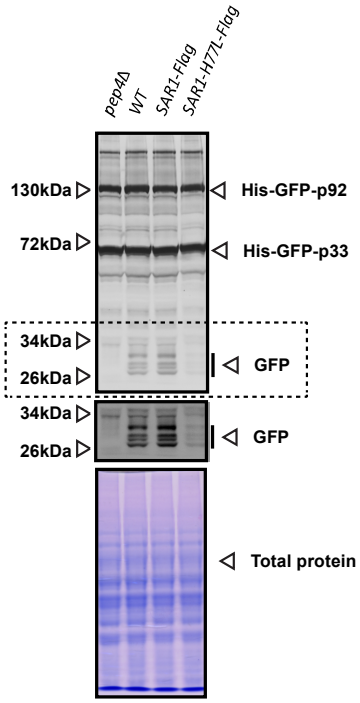

B SAR1 dominant mutant inhibits TBSV replication

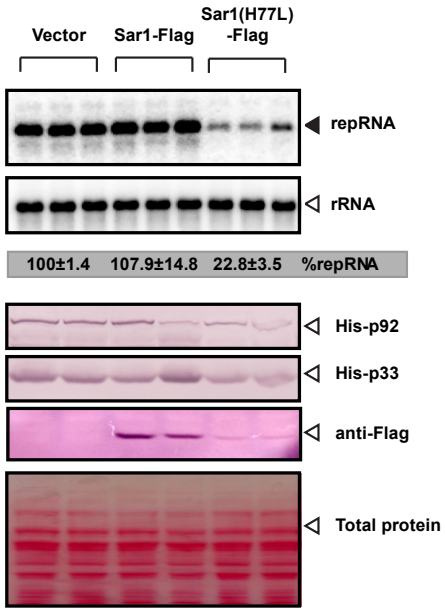

Fig. 5.6

Fig. 5.6 SAR1 dominant mutant SAR1-H77L inhibits vacuole targeting of GFP-p33/p92 as well as TBSV replication.

(A) SAR1-H77L inhibited GFP-p33/p92 targeting to vacuole, based on less amount of free GFP detected. See further details on Fig.5.5C and D. (B) Reduced TBSV replication in SAR1-H77L-Flag expressing yeast. Upper panel shows repRNA accumulation reduced upon expression of Sar1(H77L)-Flag. Lower panel shows protein expression level of TBSV p33, p92 and Sar1 or Sar1(H77L). Total protein was stained by ponceau S.

A. ARF1 dominant mutants

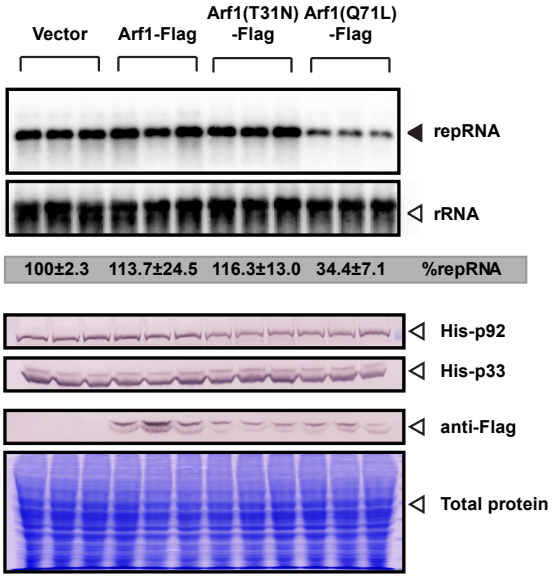

B. Tetracycline-controlled transcriptional inhibiton of COP1 from chromosome

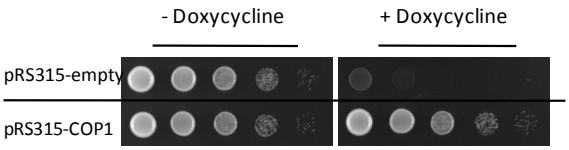

C. Downregulation of COP1 leads to eleveated TBSV repRNA accumulation

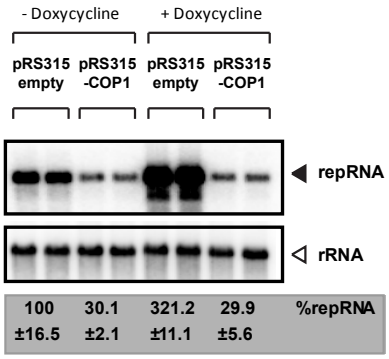

Fig. 5.7

Fig. 5.7 COP-I dependent retrograde transport from TGN to ER is not required for TBSV replication in yeast.

(A) ARF1 dominant active mutant ARF1-Q71L inhibit TBSV replication, but not dominant negative mutant ARF1-T31N. See further detail about RNA and protein blot from Fig. 5.6B. (B) Doxycycline inhibited a yeast strain whose COP1 was under a tetracycline (tet)-regulatable promoter, while plasmid (pRS315-COP1) expression of COP1 rescued yeast growth caused by doxycycline. (C) Over-expression of COP1 from pRS315-COP1 inhibited TBSV replication, while down-regulation of COP1 from genome under tetracycline (tet)-regulatable promoter by adding doxycycline into growth media stimulated TBSV repRNA accumulation to ~3 fold comparing to that of without adding doxycycline.

Chapter 6

CLASS III PHOSPHOINOSITIDE 3-KINASE VPS34 IS A KEY HOST FACTOR IN TOMBUSVIRUS REPLICATION

6.1 Introduction

During the past decades, PI3K or its product Phosphatidylinositol 3-phosphate (PI3P) emerged as an important host factor regulating diseases caused by various of pathogens (284), including influenza viruses (285), hepatitis C virus (286), human pathogenic bacteria(287, 288), plasmodium (284) and pathogenic fungi (284, 289).

Phosphatidylinositide 3-kinases (PI3Ks) are a group of proteins defined by their enzymatic activity to phosphorylate the 3 position hydroxyl group of the inositol ring of phosphatidylinositol (PtdIns), or 4 , 5 position phosphorylated PtdIns . There are three classes of PI3Ks based on their substrate specificity *in vitro* and protein size (290, 291). Class I PI3Ks, usually ~110 kDa in size, could phosphorylate Phosphatidylinositol (PI), Phosphatidylinositol 4-phosphate (PI4P) or Phosphatidylinositol (4,5)-bisphosphate ($PI(4,5)P_2$), but with substrate preference toward $PI(4,5)P_2$. Class II PI3Ks , about ~170 kDa, prefer PI over PI4P over $PI(4,5)P_2$ for substrate (290, 291).

Although two classes of PI3Ks play important role in human and animal cells, they are not found in yeast and in plants (292, 293). Class III PI3Ks, or Vps34 (Vacuole protein sorting 34), is the only class of PI3Ks present in yeast and plants. It has substrate activity solely toward PI. VPS34's function was firstly known in regulating vacuole

protein sorting, as indicated by its name. Deletion of VPS34 from plants, at least in Arabidopsis thaliana, is lethal for plant development and growth (293). However deletion of VPS34 in yeast is viable for yeast growth .

Besides genetic approaches, chemical inhibitors were developed to inhibit the activity of the lipid kinase domain of PI3Ks. There are many PI3Ks inhibitors been developed and used in PI3K functional studies. These inhibitors showed varied inhibitory sensitivity towards different forms/classes of PI3Ks. For example, the famous PI3K inhibitor Wortamanin have significantly less half maximal inhibitory concentration (IC_{50}) value with mammalian hVps34 than with yeast Vps34p (294). Specificity of different PI3K inhibitors restricted the study of different PI3Ks functions. However this issue is minor in yeast and plant in which Vps34p is the only PI3K.

Vps34p is involved in many cellular protein and membrane trafficking processes, including vacuole protein targeting, macroautophagy, endocytosis, Gpa1p signaling, et al (292). Different Vps34p complexes are responsible for different functions (292). There are two major distinct Vps34p complexes in yeast proposed by Kihara, A. et al. (295), both contain Vps34p, Vps15p and Vps30p. Complex I contains one additional protein Atg14, and is required for autophagy (296). Complex II contains protein Vps38p, regulating vacuole sorting of the lysosomal hydrolase CPY (carboxypeptidase Y). Complex I is localized to vacuolar membrane and perivacuolar pre-autophagosomal structure (PAS), while complex II is localized to TGN, late endosome and vacuolar membrane (295-298).

However, deletion of VPS30 does not affect vacuole targeting and processing of newly synthesized protease A or protease B (292, 295). In additon, GTP-binding alpha

subunit of the heterotrimeric G protein (Gpa1p) forms complex with Vps34p and Vps15p and controls pheromone signalling (299). Thus, based on these information, Jonathan M. Backer proposed two additional Vps34p complexes in yeast (292) (Fig. 6.3A).

Single-copy AtVPS34 is the only PI3K in *Arabidopsis thaliana*. Although heterozygous T-DNA insertion mutant of AtVPS34 exist, homozygous *vps34* mutation is not viable, since VPS34 is essential for plant growth, including pollen development (293). Blocking of the PI3P in plant cells by over-expression of a PI3P specific binding domain from human early endosome antigen 1 inhibited targeting of vacuolar protein sporamin (300). Treatment of tobacco cells with PI3K inhibitor Wortmannin also inhibited the vacuole targeting of COOH-terminal propeptide (CTPP) of the barley lectin precursor, but not the sporamin precursor (301). Plant Vps34 as well as Vps30, Atg3, Atg7 were shown to restrict spreading of hypersensitive reaction (HR) of tobacco mosaic virus (TMV) infected cells to adjacent cells in leaves (302).

In this Chapter, we show evidence supporting a novel and essential function of VPS34 for positive RNA virus replication in yeast and in plant. We will also discuss the molecular and cellular mechanism of VPS34 in TBSV replication.

6.2 Materials and Methods

***Yeast strains and expression plasmids*.** Yeast strains BY4741 (MAT a *his3Δ1 leu2Δ0 met15Δ0 ura3Δ0*) and *vps34*Δ, *vps30*Δ, *vps38*Δ or *atg14*Δ (single-gene deletion strain) were obtained from Open Biosystems (Huntsville, AL, USA).

For yeast plasmid expressing Vps34p, VPS34 gene fragment was amplified from yeast genomic DNA using primer pair #5014 (GGAAGATCTAAAATGTCACTGAACAACATAACATTCTGTG)/ #5015 (GCCCTGCAGGGTCCGCCAGTATTGTGCC), digested with BglII/PstI and inserted into BamHI/PstI digested pRS315-CFlag (Chapter 5), generating pRS315-Vps34-CFlag. PCR fragment of mRFP1 or rsGFP using primer pair #2691 (CGGAGATCTATGGCCTCCTCCGAGGAC)/ #2631 (GGACTCGAGTTAGGCGCCGGTGGAGTGG) or #4568 (GGCAGATCTGGTAAAGGAGAAGAACTTTTCACT)/ #3721 (GCCGAGATCTCGGATAACAATTTCACACAG) were digested with BglII/XhoI and inserted into BglII/SalI digested pRS315-Vps34-mRFP1, or pRS315-Vps34-GFP.

PI3K inhibitor AS604850. AS604850 was obtained from Selleck Chemicals, dissolved in DMSO in concentration of 5mM.

Split-Ubiquitin based Y2H assay. For pray constructs pPR3N-Vps34 or pPR3C-Vps34, VPS34 was amplified from genomic DNA using primer pair #5104/#5105, digested with BglII, and inserted into BamHI/SmaI digested pPR-N-RE or pPR-C-RE (99). Bait construct pGAD-BT3-N-His33 or pGAD-BT3-N-His92 (110) together with pray construct were co-transformed into yeast NMY51 [*MAT***a***his3*Δ *200 trp1-901 leu2-3, 112 ade2 LYS2*::(*lexAop*)$_4$-*HIS3 ura3*::(*lexAop*)$_8$-*lacZ ade2*::(*lexAop*)$_8$-*ADE2 GAL4*] (Dualsystems), and plated onto Trp−/Leu− synthetic minimal medium plates. Transformed colonies were picked, re-suspended in water, diluted 4 times with 10 fold

dilution each time, and spotted onto TLHA− (Trp−/Leu−/His−/Ade−) plates to test bait and pray interaction.

6.3 Results

VPS34 deletion affects PE enrichment in peroxisomal membrane and dramatically reduces TBSV replication in yeast. To test the role of VPS34 in TBSV replication, we utilized *vps34*Δ deletion yeast strain. Plasmids (9) (pESC-T33/DI72, pYES-T92) expressing viral replication components together with empty vector or pRS315-VPS34-CFlag were transformed into wild type or *vps34*Δ deletion yeast strain. Cells were grown in SC media containing 2% galactose to induce TBSV replication, and harvested at 1 day post induction. Total RNA and protein were extracted and subjected for RNA and protein blot analysis. In *vps34*Δ strain, we observed a reduction by 90% of repRNA accumulation compared to that from wild type. However, a plasmid expressing Vps34p-Flag complemented TBSV replication caused by deletion of VPS34. Viral protein p33 and p92 accumulation was reduced comparing to that in wild type yeast, while p92 also showed less accumulation level.

This reduction of p33/p92 protein level was also observed in TBSV replicating cells where TLG2 or other tSNAREs in endocytic pathways were deleted (In Chapter 5). Since TLG2 deletion could affect virus driven enrichment of PE in peroxisomal membrane during TBSV replication, we also tested the PE localization in *vps34*Δ strain (Fig. 6.1B). Surprisingly, PE was not enriched at the site of replication, however TBSV

p33/p92 still localized to peroxisome, as shown by co-localization of peroxisome marker Pex13p-GFP and mRFP-p33/p92.

PI3K inhibitor AS604850 inhibits (+)RNA virus replication in yeast and in plant. AS604850 is a specific PI3K inhibitor, with higher specificity toward Class I PI3K isoform γ (PI3Kγ /p110γ) comparing to isoform α/β (303, 304). We tested its effect on TBSV replication in yeast and in plants (Fig. 6.2A/B).

At the concentration of 4μM, AS604850 inhibited TBSV replication in yeast as the repRNA accumulation was reduced to ~13% comparing to that in wild type. Similarly to deletion of VPS34, we observed an reduction in p33 accumulation level (Fig. 6.2A, lower panel). In Nicotiana benthamiana protoplast transfected with TBSV full length genomic RNA, 0.5 μM AS604850 inhibited TBSV genomic replication by 80% comparing to that of adding the solvent only. At concentration of 2.5 or 5 μM, TBSV replication is close to detection limit (Fig. 6.2B).

CIRV replication proteins or CNV replication proteins could also replicate DI-72 repRNA in yeast mitochondria outer (9) or peroxisome membranes (10), respectively. Different concentrations of AS604850 were also added to growth media of yeast transformed with pESC-C36/DI72 and pYES-C95, or pESC-HisCNVp33-DI72 and pYES-CNVp92 (9). Interestingly, 4μM AS604850 could also effectively inhibit repRNA replication by CIRV or CNV replication proteins (Fig. 6.2C upper & middle panels).

AS604850 was also used to test its effect on Nodamura virus (NoV), a unrelated positive strand RNA virus replication using the mitochondrial outer membrane (109, 224,

305). At concentration of 4μM, AS604850 inhibited Nov replication, similar to the results obtained with TBSV, CIRV and CNV.

Deletion of genes encoding components of different Vps34p complexes reveals a role for vacuole targeting complexes in viral replication. We have tested single gene encoding deletions encoding protein components of different Vps34p complexes (Fig. 6.3A) for their effects on supporting tombusvirus replication.

Deletion of VPS15 dramatically reduced repRNA accumulation in yeast cells expressing TBSV p33, p92 and DI72 to ~5% of wild type yeast strain. While VPS30 and VPS38 deletion also reduced repRNA accumulation to ~48% and ~27% respectively. However, deletion of ATG14, which is responsible for autophagy or pheromone signaling did not affect TBSV replication (Fig. 6.3B Upper panel). TBSV p33 accumulation in *vps15*Δ and *vps38*Δ reduced significantly, similar to that in *vps34*Δ strain (Fig. 6.3B lower panel).

RepRNA DI-72 replication by CNV replication proteins was also tested (Fig. 6.4C). In VPS15 deletion strain, repRNA was reduced to ~42%, however replication was not significantly affected in *vps30*Δ, *atg14*Δ or *vps38*Δ strains. The above results suggested involvement of different Vps34p complexes controlling vacuole protein targeting are involved in TBSV or CNV replication in yeast.

Vps34p is co-localized with TBSV p33 in yeast. To observe the localization of Vps34p during TBSV replication, we utilized a plasmid-borne C-terminal mRFP1 tagged Vps34p and GFP-tagged p33. Plasmids pESC-GFP-T33/DI72, pYES-T92 (9) and pRS315-

Vps34-mRFP1 were transformed into *vps34*Δ yeast strain. Yeast cells were induced to support repRNA replication in growth media containing 2% galactose for 4, 6 or 24 hours and subjected to confocal microscope analysis (Fig. 6.4A). We observed Vps34p-mRFP1 showed punctuate structures in yeast, and some of Vps34p-mRFP1 containing punctuates co-localized with GFP-p33 after 4, 6 or 24 hours induction of viral replication. These co-localized Vps34p-p33 structures may represent Vps34p complexes responsible for TBSV replication (Fig. 6.3).

Pex13p tagged with mRFP on its C-terminal end was also used to test Vps34p localization during TBSV repRNA replication in yeast. Plasmids pESC-T33/DI72, pYES-T92, pRS315-pex13-mRFP and pRS314-Vps34-GFP were transformed to diploid Sc1 yeast strain. RepRNA replication was induced in growth media containing 2% galactose for 24hours. Yeast cells were collected and subjected to confocal laser microscope analysis. Vps34p-GFP forms many punctuate structures similar to the observation using Vps34p-mRFP1, and some of the Vps34p-GFP punctuate structures were co-localized with peroxisome marker Pex13p-mRFP (Fig. 6.4B). Thus these observations supported that some of the Vps34p localized to peroxisome in TBSV replicating yeast.

Vps34p does not interact with tombusvirus replication proteins in Split- Ubiquitin based yeast two hybrid assay. To test if Vps34p interacts with TBSV replication proteins, we utilized a split-ubiquitin based yeast two hybrid assay, designed for testing the interaction of a pray protein with a membrane bait protein (110).

Vps34p was tagged with N-terminal half of ubiquitin (NubG) on its N-terminal or C-terminal and expressed from a plasmid which was co-transformed into yeast strain NMY51 (110) together with a plasmid expressing C-terminal Cub (C-terminal half of ubiquitin)-tagged CNV p33 or p92. Transformed yeast cells were spotted on Trp-/Leu-/His-/Ade- (TLHA-) or Trp-/Leu- (TL-) media with 10X dilution sequentially for 5 times (Fig. 6.5 A&B right panels). Growing of the yeast cells from TLHA- media suggested interaction between bait and prey proteins. A known interacting protein Ssa1p (101) was used as positive control, while an empty plasmid was used as negative control.

Yeasts transformed with plasmids containing Cub-tagged p33 or p92 with NubG tagged Ssa1p grown in TLHA- media suggested an interaction between viral proteins and Ssa1p. However, yeast co-expressing N or C terminal NubG tagged Vps34p and viral proteins did not show growth, suggesting lack of interaction between viral proteins and Vps34p.

TBSV replication does not induce pexophagy. Pexophagy is selective macro-autophagy for peroxisome, which is controlled by VPS34 (306). The pexophagy event is usually monitored by vacuolar degradation of peroxisome matrix protein Pot1p (306), or visualization of vacuolar localization of peroxisomal matrix targeted BFP-SKL (307), or free GFP caused by vacuolar degradation GFP-tagged peroxisome membrane proteins, including Pex11p-GFP(283).

Since minor amount of free GFP was detected from yeast cells expressing GFP-p33/p92 (Chapter 5, Fig. 5.5C&D) , it could be possible that pexophagy was also involved besides previously identified COP-II dependent secretion and endocytic

pathway that transfers p33 from ER to TGN/endosome/vacuole (Chapter 5, Fig. 5.5 & 5.6). To test if pexophagy contributes to TBSV replication, we utilized GFP-tagged p33/p92 expressed in wild type or *vps34*Δ deletion yeast strain. GFP-p33/p92 accumulation was dramatically reduced in *vps34*Δ yeast strain (Fig. 6.6A), in which pexophagy did not occur due to deletion of VPS34. The reduced GFP-p33/p92 accumulation level in pexophagy-free *vps34*Δ yeast strain was contrary to the vacuolar degradation of pexophagic cargo proteins, suggesting pexophagy is not involved in targeting GPF-p33/p92 to vacuole.

To test if TBSV viral protein expression induces pexophagic degradation of peroxisomal matrix protein Pot1p/Fox3p, we detected Pot1p protein level by protein blot using anti-Pot1p antibody (kindly provided by Daniel J. Klionsky from University of Michigan) between samples with or without TBSV replication, in wild type or *vps34*Δ deletion strain (Fig. 6.6B). We found that Pot1p level was not significantly different between different samples described above. Total protein, mitochondria membrane protein Porin, ER membrane protein Sec61p and cytosolic protein PGK were used as control to show equal loading between samples. Thus, our data suggest that TBSV replication in yeast does not induce pexophagy, and the role of Vps34p function in TBSV replication is not related to pexophagy-like event. This finding supported the previous finding that ATG14 deletion did not affect TBSV replication in yeast (Fig. 6.3).

6.4 Discussion

VPS34 is involved in RNA viruses replication. Based on genetic study on model host yeast for TBSV replication, as well as utilizing a PI3K inhibitor AS604850 in yeast and plant cells, we identified VPS34/PI3K as a host factor important for TBSV replication (Fig. 6.1A, 6.2A&B). In plant protoplast cells transfected with TBSV full genomic RNA, TBSV replication was almost eliminated by adding 5 μM AS604850 into the incubation media (Fig. 6.2B). In yeast, either deletion of VPS34 or 4 μM AS604850 could reduce repRNA accumulation to ~11%. Interestingly, the accumulation of plasmid driven viral protein was also reduced dramatically. Such reduced level of repRNA as well as lower viral protein accumulation as also observed when tSNAREs from endocytic pathway or TGN were deleted. It could be interesting if PE distribution was affected during TBSV replication, since deletion of TGN tSNARE TLG2 abolished PE enrichment in peroxisome at the presence of TBSV replication. Interestingly, PE also did not accumulate in peroxisome in *vps34*Δ when mRFP tagged p33/p92 were expressed (Fig. 6.1B).

PI3K inhibitor AS604850 was also tested for its effect on DI-72 replication using CIRV or CNV replication proteins in yeast, and Nodamura virus genomic RNA1 replication in yeast. Results showed that at concentration of 4 μM, it inhibited viral replication in all these three cases (Fig. 6.2C). It is notable that PE was also enriched at site of CIRV, CNV or Nov replication (Chapter 4).

Identifying a vacuolar protein targeting function of VPS34 in TBSV replication. As TBSV driven PE enrichment in peroxisome was affected in *tlg2*Δ or *vps34*Δ deletion strains, we wonder if these two gene have common functions? Vps34p in yeast is known

to function in distinct complexes (Fig. 6.3A), containing additional proteins including Vps15p, Vps30p, Vps38p or Atg14p (292, 295). We used single gene deletion yeast strains of *vps15*Δ, *vps30*Δ, *vps38*Δ or *atg14*Δ to dissect different functions of VPS34 in tombusvirus replication. Deletion of VPS15 reduced TBSV repRNA and proteins accumulation to similar level comparing to VPS34 deletion, while deletion of VPS30 or VPS38 also reduced TBSV replication (Fig. 6.3B). In case where DI-72 was replicated by CNV p33 and p92 (Fig. 6.3C), repRNA accumulation was only reduced in VPS15 deletion strain, and did not change in VPS30, VPS38 or ATG14 deletions.

Based on Jonathan M. BACKER's model of four Vps34p complexes (292), I demonstrated that vacuole protein targeting function of VPS34 seems to be involved in TBSV replication. This results agreed with the finding that PE was not enriched in peroxisome in yeast deletion strain of TGN tSNARE TLG2, which is involved in vesicle/protein transportation.

Vps34p localized at site of TBSV replication, but does not interact with p33/p92. In vps34Δ yeast expressing Vps34p-mRFP1, GFP-p33/p92, of which fluorescence under confocal laser microscope, co-localized with some of the punctuate-like structures of Vps34p-mRFP1, suggesting a direct involvement of Vps34p in TBSV replication. This result was confirmed by co-localization of Vps34p-GFP and a peroxisome marker Pex13p-mRFP in a diploid yeast cell when TBSV replication (Fig. 6.4).

We asked if Vps34p directly interacts with TBSV replication proteins. In a split ubiquitin based yeast membrane protein two hybrid system, Vps34p does not show interaction with p33 or p92 (Fig. 6.5). However other components of the Vps34p

complexes were not tested for their interaction with TBSV p33/p92 yet. Besides direct interaction, an existing function of Vps34p on peroxisome may be co-opted by TBSV to aid its replication.

Pexophagy pathway is not co-opted for TBSV replication. A known function of VPS34 in peroxisome regulation involves pexophagy during nutrition stressed environment (306). We tested degradation pattern of TBSV viral proteins GFP-p33/p92 and peroxisomal matrix protein Pot1p accumulation in wild type as well as pexophagy-free *vps34*Δ yeast strains (306). Pot1p level was similar in samples with or without TBSV in both WT and *vps34*Δ yeast strains, suggesting TBSV replication does not induce detectable pexophagy. GFP-p33/p92 accumulation reduced, not increased, in pexophagy free yeast strain suggesting that pexophagy does not play a role in stability of TBSV protein. Pexophagy is a selective macro-autophagy event, which is controlled by VPS15, VPS30 and ATG14, but not VPS38 (306). Absence of involvement of pexophagy in TBSV replication agreed with previously identified non-autophagy function of VPS34 (Fig. 6.3).

Summary: In this chapter, we show evidence that VPS34 is involved in TBSV replication in yeast and in plant, and possibly in CIRV, CNV and NoV replication in yeast. I identified a role in the vacuole protein targeting of Vps34 in TBSV replication. Co-localization of Vps34p and TBSV p33/p92 suggests involvement of cellular functions of Vps34p in peroxisome that might be co-opted for TBSV replication. However this cellular function is not pexophagy, instead a non-autophagic function, possibly

vesicle/protein transport function of Vps34p, is involved in TBSV replication. Importantly I discovered that VPS34's function correlates to PE enrichment in peroxisome during TBSV replication.

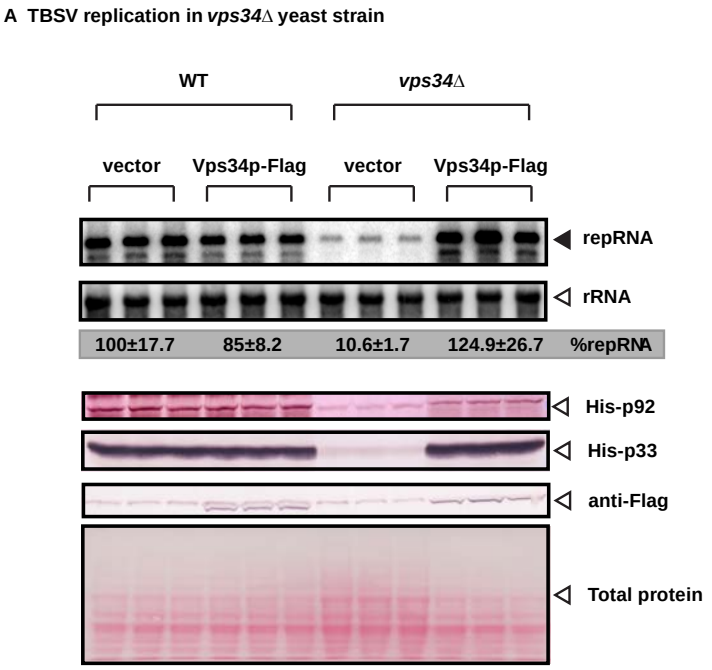
A TBSV replication in vps34Δ yeast strain
WT
vps34Δ
vector
Vps34p-Flag
vector
Vps34p-Flag
repRNA
rRNA
100±17.7
85±8.2
10.6±1.7
124.9±26.7
%repRNA
His-p92
His-p33
anti-Flag
Total protein

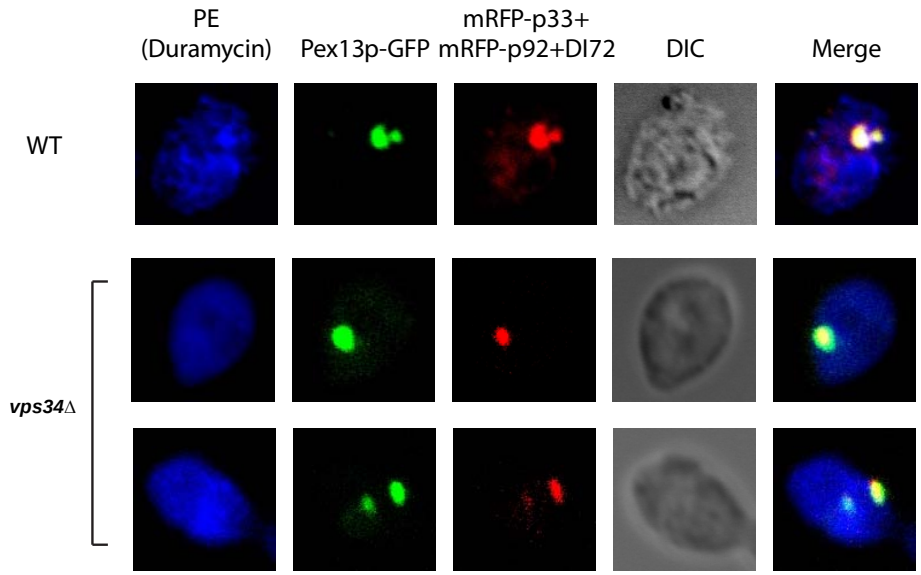
B PE localization in wild type and vps34Δ yeast strain during replication
PE
(Duramycin)
Pex13p-GFP
mRFP-p33+
mRFP-p92+DI72
DIC
Merge
WT
vps34Δ

Fig. 6.1

Fig. 6.1 VPS34 is required for efficient TBSV replication in yeast and is involved in PE enrichment at the site of replication.

(A) TBSV replication in WT or vps34Δ strain was induced by expression of TBSV His6-p33 and His6-p92 under the galactose-inducible GAL1 promoter and DI-72 (+)repRNA from the galactose-inducible GAL10 promoter at 23°C for 24 hours. Northern blot analysis of DI-72 accumulation or 18S rRNA accumulation was shown in upper panels. DI-72 accumulation data was normalized based on 18S rRNA. Each experiment was repeated three times. Lower panels: Western blot of TBSV p33, p92 or Flag-tagged Vps34p was performed using anti-HIS or anti-Flag antibodies. Total protein was shown as loading control. (B) Confocal microscope images showed that PE was not enriched at sites of replication in vps34Δ yeast. See further description of yeast growth condition in Fig. 5.2, PE detection method in Fig. 5.3.

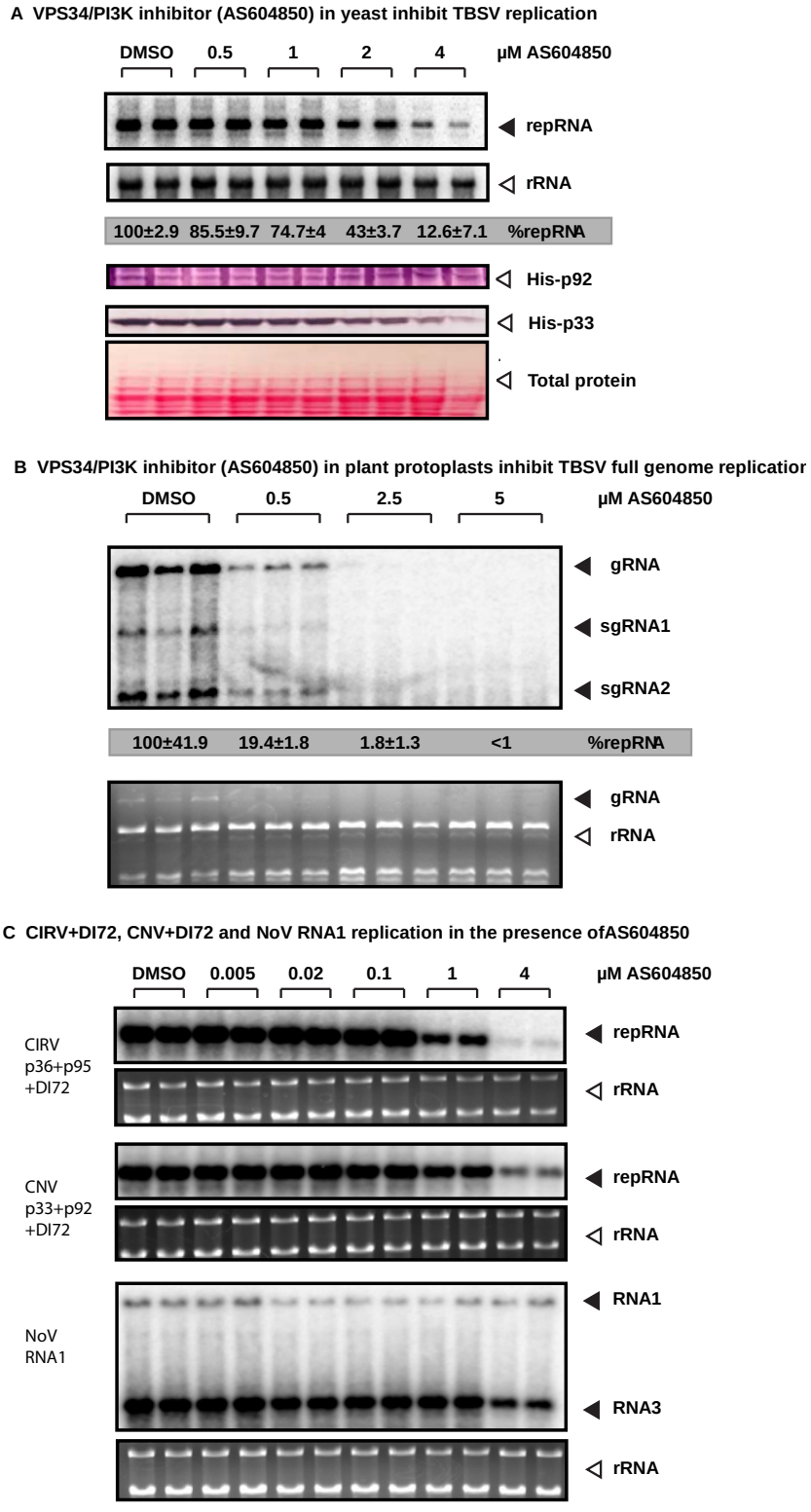
A VPS34/PI3K inhibitor (AS604850) in yeast inhibit TBSV replication
DMSO 0.5 1 2 4 μM AS604850
repRNA
rRNA
100±2.9 85.5±9.7 74.7±4 43±3.7 12.6±7.1 %repRNA
His-p92
His-p33
Total protein
B VPS34/PI3K inhibitor (AS604850) in plant protoplasts inhibit TBSV full genome replicatior
DMSO 0.5 2.5 5 μM AS604850
gRNA
sgRNA1
sgRNA2
100±41.9 19.4±1.8 1.8±1.3 <1 %repRNA
gRNA
rRNA
C CIRV+DI72, CNV+DI72 and NoV RNA1 replication in the presence ofAS604850
DMSO 0.005 0.02 0.1 1 4 μM AS604850
CIRV p36+p95 +DI72
repRNA
rRNA
CNV p33+p92 +DI72
repRNA
rRNA
NoV RNA1
RNA1
RNA3
rRNA

Fig. 6.2

Fig. 6.2 PI3K inhibitor AS604850 inhibits positive strand RNA viruses replication.

(A) AS604850 inhibited TBSV repliation in yeast at different concentrations. Notably at 4μM, AS604850 inhibited TBSV repRNA accumulation to ~13% comparing to that of adding solvent DMSO alone. See further detail of RNA and protein blot in Fig. 6.1A (B) Genome replication of TBSV in plant protoplasts was inhibited by AS604850, as shown by RNA blot analysis of genomic TBSV RNA as well two sub-genomic RNA generated during TBSV genomic RNA replication (Upper panel). Lower panel: ribosomal RNA stained by ethidium bromide was shown as a loading control.

A. Vps34p complexes in yeast (adapted from Biochem. J. (2008) 410, 1–17)

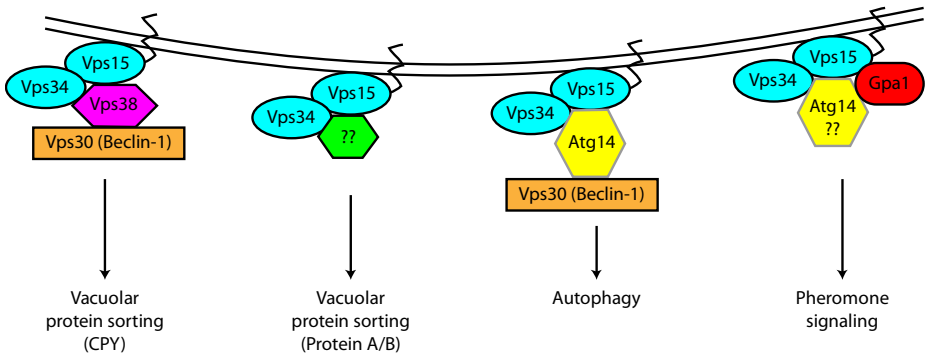

B TBSV DI-72 replication in yeast lacking components of the Vps34 complexs

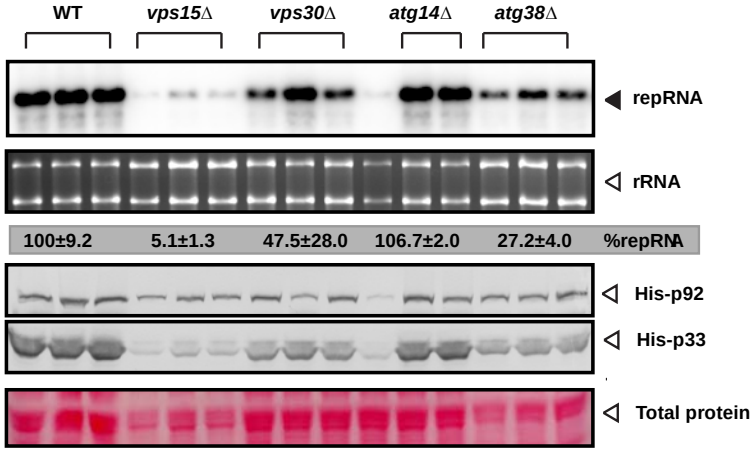

C CNV-driven DI-72 replication in yeast lacking components of the Vps34 complexs

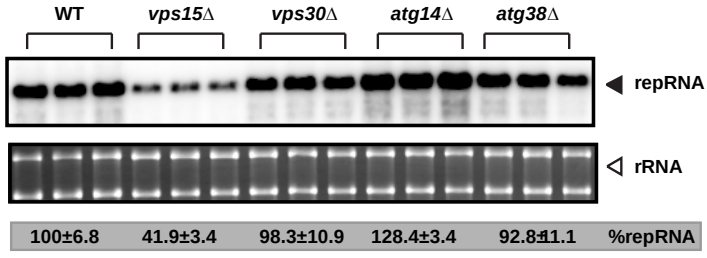

Fig. 6.3

Fig. 6.3 Dissecting the function of different Vps34p complexes in tombusvirus replication.

(A) A cartoon illustration of Vps34p complexes as proposed by Jonathan M. Backer (292).(B) TBSV repRNA replication in wild type, vps15Δ, vps30Δ, atg14Δ or vps38Δ. Upper panel: RNA blot of repRNA accumulation and 18S rRNA accumulation. Lower panel: Protein analysis of TBSV p33, p92 See further detail about growth condition and RNA or protein blot on Fig. 6.1A. (C) DI-72 replication by CNV His6-p33 and His6-p92 driven under the galactose-inducible GAL1 promoter.

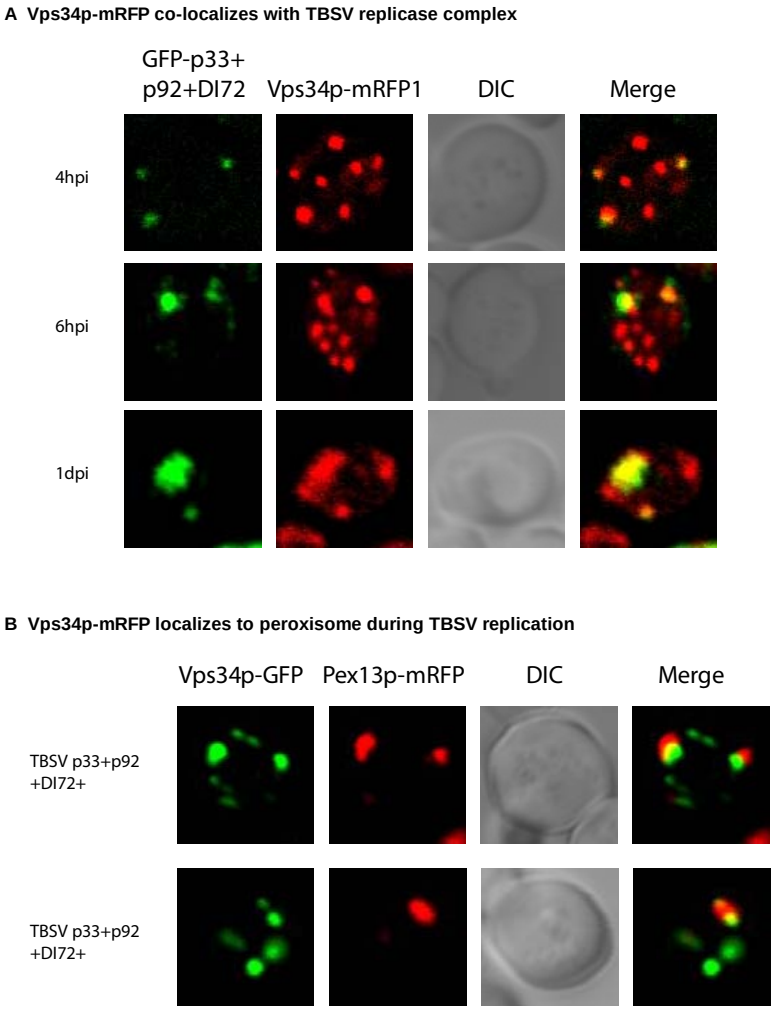
A Vps34p-mRFP co-localizes with TBSV replicase complex
GFP-p33+
p92+DI72
Vps34p-mRFP1
DIC
Merge
4hpi
6hpi
1dpi
B Vps34p-mRFP localizes to peroxisome during TBSV replication
Vps34p-GFP
Pex13p-mRFP
DIC
Merge
TBSV p33+p92
+DI72+
TBSV p33+p92
+DI72+

Fig. 6.4

Fig. 6.4 Confocal laser microscope analysis of Vps34p localization during TBSV replication in yeast.

(A): Vps34p-mRFP is localized to site of TBSV replication visualized by GFP-tagged p33 expression in *vps34*Δ yeast strain. (B) Vps34p-GFP is localized to peroxisome during TBSV replication in yeast.

A p33

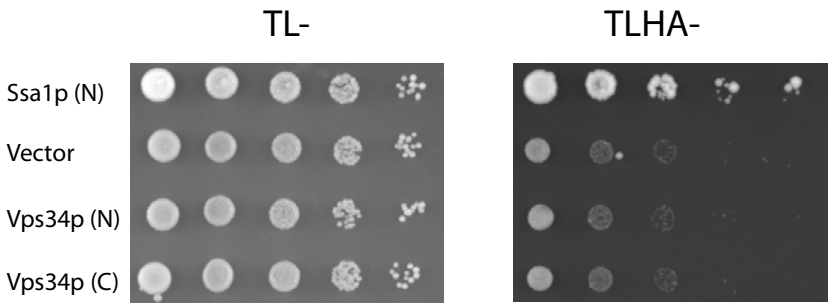

B p92

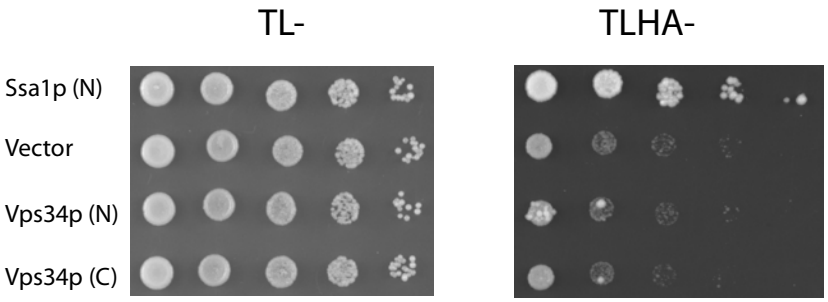

Fig. 6.5

Fig. 6.5 Split-ubiquitin based Y2H assay to test viral protein interaction with Vps34p.

(A) Bait protein TBSV p33 was used to test the interaction with Vps34p tagged with N-terminal half of ubiquitin (NubG) on its N-terminal or C-terminal. (B) Bait protein TBSV p92 was used to test the interaction with Vps34p.

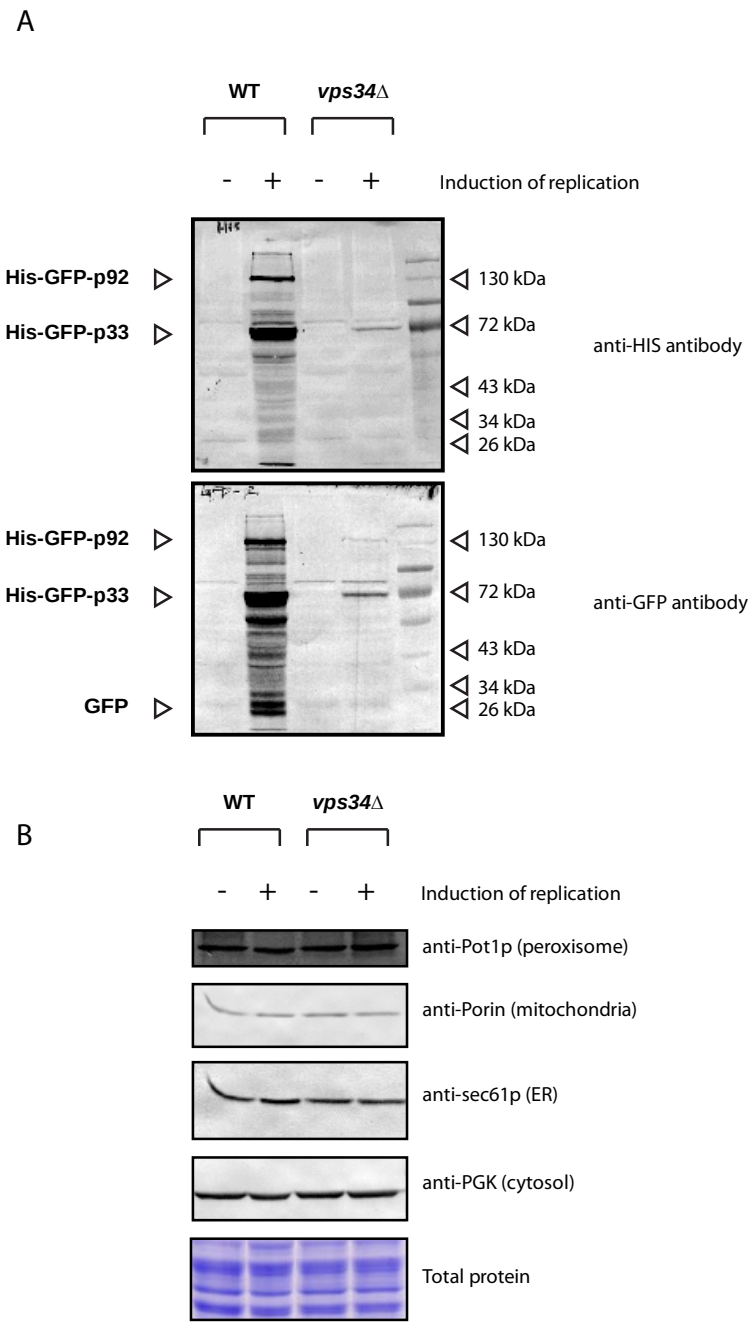
A
WT
vps34Δ
- + - +
Induction of replication
His-GFP-p92
His-GFP-p33
130 kDa
72 kDa
43 kDa
34 kDa
26 kDa
anti-HIS antibody
His-GFP-p92
His-GFP-p33
GFP
130 kDa
72 kDa
43 kDa
34 kDa
26 kDa
anti-GFP antibody
B
WT
vps34Δ
- + - +
Induction of replication
anti-Pot1p (peroxisome)
anti-Porin (mitochondria)
anti-sec61p (ER)
anti-PGK (cytosol)
Total protein

Fig. 6.6

Fig. 6.6 GFP-p33/p92 and a peroxisomal matrix protein Pot1p were analyzed for accumulation during TBSV repRNA replication in wild type and vps34Δ yeast strains.

(A) Western blot analysis of GFP-p33/p92 of yeast cells with or without induction repRNA replication Both anti-HIS and anti-GFP antibody were used. Note that: free GFP was detected when using anti-GFP antibody in wild type yeast with repRNA replication. (B) Western blot analysis of Pot1p, mitochondria porin, ER membrane protein Sec61p and cytosolic protein PGK of samples prepared as in Fig. 6.6A. No significant change of Pot1p accumulation was observed in wild type cells with viral protein expression.

Chapter 7

CONCLUSION AND PERSPECTIVE

7.1 Conclusion

(+)RNA virus replication can take place on alternative organellar membranes. In Chapter 2, we demonstrated that in a cell-free environment, peroxisome/ER-based tombusvirus TBSV could utilize mitochondrial membrane to assemble replicase complexes, supporting asymmetric replication of (+)repRNA. While mitochondria-based CIRV could use ER membrane for assembly of replicase complexes only inefficiently. The ability of using ER or mitochondria membranes depended on the p33/p36 region of TBSV/CIRV replicase protein. Despite the C-terminal RdRp region coming from TBSV p92 or CIRV p95, p33 prefers ER and p36 prefers mitochondria to assemble the replicase complexes. The difference might come from co-evolution of TBSV or CIRV with different cellular membrane environments, however, it was surprising that TBSV or CIRV have the potential to explore alternative sub-cellular membranes for viral replication. Thus these viruses are more flexible in exploiting various membranes as previously anticipated.

Cymbidium ringspot virus (CymRSV) is a tombusvirus closely related with TBSV, replicating on peroxisome membrane. Previous study using chimeric viruses made between CymRSV and CIRV also suggested swapping a small N-terminal region of CIRV p36/p95 with CymRSV p33/p92 could led to a recombinant CymRSV (majority of

genome from CymRSV which replicates on peroxisomal membrane) to replicate on mitochondrial outer membrane (114). While replacing the N-terminal region of CIRV p36/p95 with CymRSV p33/p92 could make a recombinant CIRV replicating on peroxisome (114). Although this study suggested that recombination event could change the sub-cellular replication site, it was still not answered if a non-modified tombusvirus could explore an alternative sub-cellular membrane for replication. Later studies on the N-terminal region of CymRSV (8) or CIRV (19) replication proteins proposed that this region contains perixosome or mitochondria targeting sequences as well as two trans-membrane domains.

Similar study of changing sub-cellular replication site by modifying replicase protein was shown with an animal virus, Flock house virus (FHV). By replacing mitochondria targeting domain in FHV RdRp Protein A with three different types of ER targeting sequences, the replication of FHV was re-targeted from mitochondrial outer membrane to ER membrane (308). Surprisingly the replication of FHV increased when FHV was replicating on ER membrane.

Are the sites of replication of (+)RNA viruses simply decided by the organelle targeting sequence in their replication proteins? Or are other motifs in (+)RNA virus replication proteins also important for choosing the replication sites? In my studies in Chapter 2, when TBSV or CIRV replicase proteins were simply mixed with purified organellar membranes without a cellular targeting event, the wild type viral replicase proteins could utilize different organelles for viral replication, suggesting that the native replicase proteins have the ability of using an alternative membrane. However, their preference in using the native organellar membranes also suggested that non-organelle

targeting motifs of the replicase proteins could be co-evolved within the native membrane environment and contribute to selectivity of (+)RNA virus replication sites. It is also possible that viruses use the alternative membranes when the original membranes are becoming saturated with viral proteins during late infection.

Studies of TBSV or CymRSV also showed that genetic modification of a host cell could also lead to change in viral replication site. Pex3p is a peroxisomal membrane protein which controls peroxisome biogenesis (309). Deletion of PEX3 abolishes peroxisome biogenesis and relocates replication site of TBSV or CymRSV from peroxisome to ER (15, 32) in yeast model host. Recent study also showed that in the absence of an important lipid biogenesis gene, PAH1 (phosphatidic acid phosphohydrolase), TBSV replication switched from peroxisome to ER (310).

These studies discussed above including my study in chapter 2 suggest an emerging picture that (+)RNA viruses have the ability of using alternative replication sites in host cell (Summarized in Fig. 7.1). Such event could be observed in cell-free environment (9), viral protein recombination/modification (114, 308) or genetically altered host cell (15, 32, 310).

TPR domain containing protein Sti1p inhibits CIRV replication. Previous work showed that some members of TPR-containing protein family act as cell-intrinsic negative regulators of tombusviruses replication (109, 150). Study on Sti1p which inhibited CIRV, not TBSV, replication provided a more detailed picture on how these TRP-containing proteins, often Heat shock protein 70 co-chaperones, affect tombusviruses replication. Specificity of Sti1p's inhibition of CIRV replication could provide more information on

CIRV replication protein targeting and replicase assembly process on mitochondria outer membrane, and emphasize importance of further analysis of more proteins from this TPR-containing proteins family.

PE is required for TBSV replication. Utilizing a novel artificial vesicle-based cell-free replication system, different phospholipids showed different effects in three steps of TBSV replication: 1) viral replication protein association with membranes, 2) viral RNA recruitment by viral replication proteins to membranes, 3) asymmetric viral RNA replication. PE was the only phospholipid capable of supporting all three processes. These findings suggested that sub-cellular membrane is not simply a bilayer platform that functions as a scaffold, different head groups of different lipids may directly interact with viral replication proteins to stimulate their RdRp activity, or may introduce membrane curvature (For example, negative membrane curvature introduced by PE) which is favored for viral RdRp activity.

Finding pathway for PE re-localization to the site of viral replication. Building up of PE enriched micro-environment by TBSV replication protein p33 was a surprising finding, suggesting that heavy modification of phospholipid transportation could be achieved by a single viral protein expression in a host cell. Finding the exact pathway of p33 induced PE enrichment to peroxisome could pioneeringly contribute to understanding of the cell biology of virus infected cell.

To hijack an PE synthesis pathway to build up PE enriched micro-environment, could require recruitment of PE synthesis enzyme/s to peroxisome, and also need PS or

CDP-ethanolamine, the precursors of PE synthesis in two different pathways, to be funneling to peroxisome. By deleting different PE synthesis genes, we concluded that no single PE synthesis pathway directly contribute to the virus-driven PE enrichment in peroxisomes. I have demonstrated that vesicle transport pathway is involved in PE enrichment in peroxisome driven by TBSV p33.

I provide multiple evidence supporting that TBSV p33/p92 are indeed targeted to post-Golgi compartment. Inhibition of p33/p92 secretion from ER to golgi inhibited TBSV replication suggesting post-Golgi p33 is essential for efficient viral replication. TGN localization of p33 as well as abolishment of PE enrichment in *tlg2*Δ yeast strain suggested that post-golgi p33 may directly induce PE enrichment in peroxisome through vesicle transport pathway.

7.2 Perspective

PE source for TBSV replication. PE is an important lipid for autophagy pathway. Lipidation of LC3 (Atg8p) requires covalently linking its molecule with PE, and serves as marker for autophagy event (247, 298). However membrane source of pre-autophagosomal structure (PAS) was extensively studied and still remains unclear (244, 246, 247, 249, 251). By studying the role of VPS34 and associated components in TBSV replication, we learned that autophagy is unlikely required for TBSV replication.

By utilizing yeast genetics as well as cell biology tools, we were able to narrow down certain pathway/s affecting PE enrichment in peroxisome. Current results

suggested vesicle transport pathway is involved in PE enrichment. Next question is WHY?

Aminophospholipid flippase could be involved in PE enrichment at peroxisome. Aminophospholipid flippases belong to P4 subfamily of P-type ATPases, which introduce phospholipid asymmetry on different sides of membrane bilayer (282). There are five P4 ATPase in yeast with overlapping functions, namely Drs2p, Dnf1p, Dnf2p, Dnf3p, and Neo1p (282). Dnf1p and Dnf2p are localized primarily at plasma membrane (311), Drs2p and Dnf3p are mostly localized at TGN (312), while Neo1p is mainly localized at endosomes (313). Nele Alder-Baerens and co-workers showed that phospholipid asymmetry exists on post-Golgi vesicles, including up to 80% of PE on the cytosolic leaflet of the total post-Golgi vesicles, while deletion of Drs2p and Dnf3p could abolish most of the PE asymmetry (282).

PE is the pro-fusion kind of phospholipid, which facilitates vesicle fusion into membrane bilayer (57, 314, 315). It could be that by hijacking post-Golgi vesicles generated from TGN or endosomes with enriched PE at cytosolic leaflets, TBSV might build up PE enriched micro-environment on peroxisomal membranes. This hypothesis fits to the current results that vesicle transport rather single PE synthesis pathway is required for PE enrichment in peroxisome. However since the asymmetric distribution could not change the overall PE content on post-golgi vesicles, this hypothesis could not directly explain why PE is enriched in peroxisome as observed under the confocal laser microscope, unless other cellular host factors also contribute to this hypothetic pathway.

Role of Vps34p during TBSV replication. Vps34p forms complexes with Vps15p, Vps30p and Vps38p at late golgi, late endosome and vacuole to regulate vesicle transport (295, 297, 298). A major organizer of endosomal and vaclular membrane/protein sorting is phosphoinositide phosphatidylinositol-3-phosphate (PI3P), a product of Vps34p, serving as a molecular signal (316). PI3P is predominantly localized at late endosome or in multivesicle bodies (MVB), and recruits many effectors containing PI3P binding domains, such as PX (Phox homology) and FYVE (Fab1, YOTB, Vac1, EEA1) domains (317). These effectors facilitates various membrane rearrangement events as the retromer-coated tubules budding (SNX1,2,6,27), the fusion of endosomes (EEA1) and the ESCRT-dependent intraluminal sorting of ubiquitinated cargos in multivesicular endosomes (Hrs) (316).

The accumulation of Vps34p at peroxisome was especially interesting, since one role of Vps34p on peroxisome is to induce pexophagy. However no macro-autophagy events was induced upon TBSV replication (Fig. 6.6). If PI3P on peroxisome membrane does not facilitate autophagy, it might instead recruits those effectors which have PI3P binding modules and introduce various endosome/ multivesicle bodies (MVB) -like events. One of the ESCRT-I component Vps23p was recruited to peroxisome upon TBSV replication (81). ESCRT factors, including Vps23p, Vps24p, Snf7p and Vps4p have been shown to help TBSV assemble replication complexes by introducing membrane invagination (81). CIRV could also recruit Vps23p to mitochondria upon infection (318). Very interestingly, these invaginated peroxisomes or mitochondria upon tombusvirus infections possessed MVB-like morphology, and were once called MVB by scientists (114). Vps23p has been shown to bind to p33 or p36, however the binding sites between

Vps23p and these viral replication proteins were quite different (81, 86, 318). N-terminal ubiquitin E2 domain of Vps23p was shown to bind to p33 depending on ubiquitination of two lysine sites N-terminals of p33 and a "late domain" between two trans-membrane domains (86). However, Vps23p C-terminal steadiness box domain showed ability to bind to N-terminal 16 amino-acid long sequence in CIRV p36 (318). Lack of conserving binding domain of vps23p to two related tombusviruses replication proteins may suggested a possibility that this binding maybe a result rather than a cause of vps23p recruitment.

ESCRT-I components are involved in ubiquitin-dependent sorting of proteins into the endosome/MVB (319), and Vps34p/PI3P controls ESCRT-I dependent intraluminal sorting into MVB (316). It is possible that Vps34p/PI3P controls the ESCRT-I recruitment to viral replication sites.

Since CIRV replication on mitochondria also led to PE enrichment (Chapter 4) and required Vps34p (Fig. 6.2), it is possible that PI3P serves as molecular signal on peroxisome or mitochondria to recruit ESCRT factors and other effectors which leads to PE enrichment and membrane invagination. It is quite interesting that PE possesses a physical property which favors negative curvature during formation of virus-induced spherules in peroxisomes or mitochondria, suggesting that membrane invagination introduced by ESCRT might be accompanied with PE enrichment.

PE was also shown to be enriched at site of Nodamura virus (NoV) replication (Chapter 4). At early stage of NoV infected muscle cells of suckling mouse, membrane invagination on mitochondria outer membrane (or vesiculation of mitochondria outter membrane) was observed (224), suggesting PE might play a common role for membrane

invagination. Interestingly, PI3P inhibitor also inhibited NoV replication (Fig. 6.2C), suggesting function of Vps34p during NoV replication could also be similar to its function in TBSV or CIRV replication.

In summary, we found that p33 was transported to TGN through COP-II dependent vesicle transport from ER, and peroxisome possibly via pex19p mediated proxisomal protein targeting (107). We hypothesize that TGN localized p33 as well as peroxisome localized Vps34p may induce vesicle transport from TGN and endocytic pathway to peroxisome, lead to a MVB-like peroxisome in TBSV replicating cells as well as PE enrichment in peroxisome (Summarized in Fig. 7.2).

Role of secretory pathway. Current studies (235, 236) on trans-membrane protein sorting through early secretory and endocytic pathways shed a light on our understanding of (+)RNA virus RdRp function. Most of the (+)RNA virus RdRp or their auxiliary proteins are membrane associated, and their function depends on their sub-cellular association with membrane (20).

Membrane proteins accounts for 20-30% of the total protein products produced from eukaryotic genome (320). Their sorting were believed to be contributed by motifs residing on cytosolic part of the protein (321), however trans-membrane domain of these proteins also received attentions for their functions in determining protein localization and transport (235, 236). TMDs were shown to function in ER retention, golgi or plasma membrane localization and sorting through endocytic pathways [reviewed in (235)]. The sorting function of TMDs together with cytosolic organellar targeting signals on viral

replication proteins could explain various sub-cellular locations of (+)RNA viruses replication sites.

Current progress showed that early secretory pathways are involved in (+)RNA virus replication (33, 72, 226-228, 232, 322). Despite that other viral factors may join and modify ER membranes as well as early secretory pathway, TMDs within viral replication proteins could be a driving force of (+)RNA viruses to find the replication site on cellular membranes during evolution.

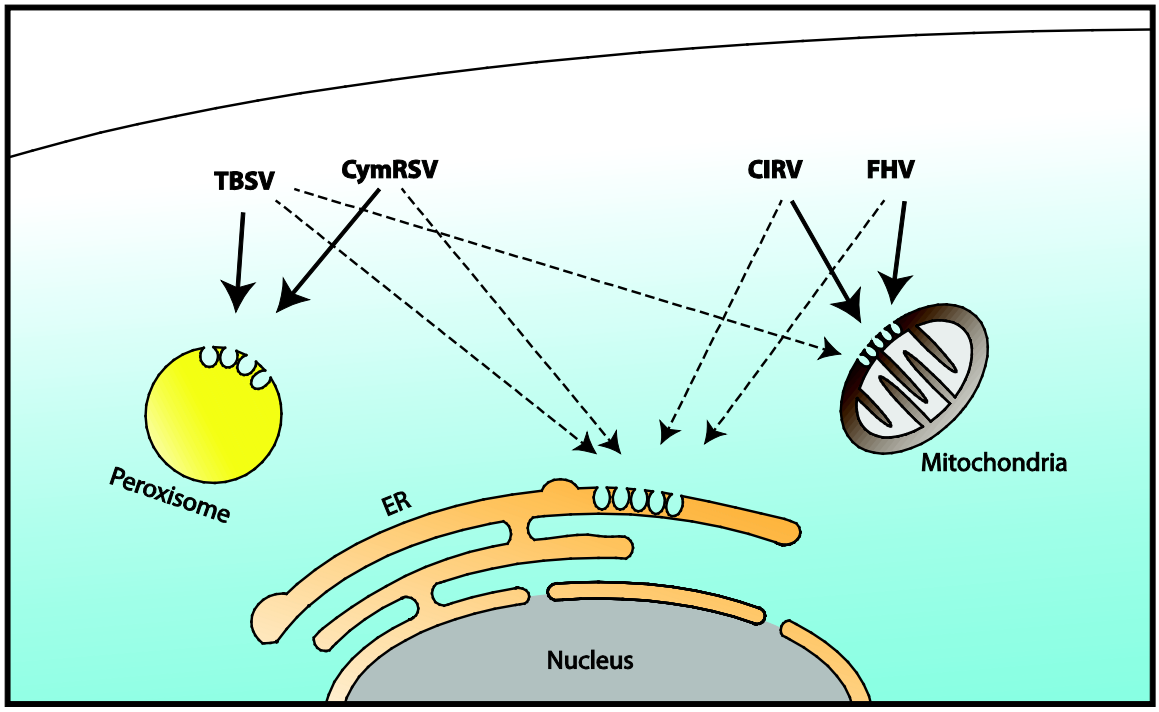

Fig. 7.1 Alternative replication sites found for different (+)RNA viruses.

Solid lines show original replication sites for TBSV, CymRSV, CIRV and FHV. Dotted lines show alternative replication sites of these (+)RNA viruses in different experimental systems.

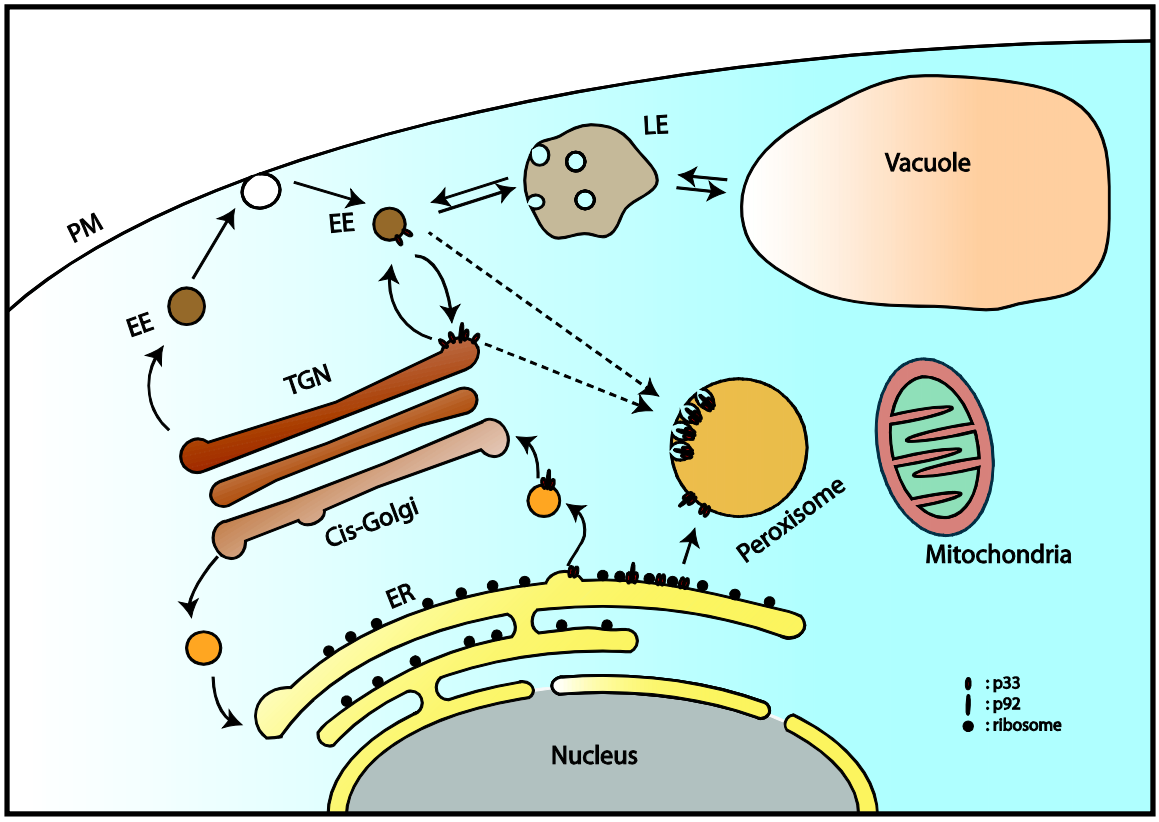

Fig. 7.2 Working Model for sub-cellular transport of TBSV replicase proteins.

Portion of TBSV p33 and p92 molecules translated on ER or in cytoplasm are transported directly to peroxisome, while part of p33/p92 are transported to TGN and beyond through COP-II dependent early secretory pathway. Dotted lines suggest a proposed role played by p33, in which p33 induces vesicle transportation from TGN or early endosome (EE) to peroxisome, and thus produce MVB-like structures as well as PE enriched micro-environment. See text for further detail and possible role of Vps34p in this model.

REFERENCES:

1. **White KA, Nagy PD.** 2004. Advances in the molecular biology of tombusviruses: gene expression, genome replication, and recombination. Prog Nucleic Acid Res Mol Biol **78:**187-226.
2. **Panaviene Z, Panavas T, Nagy PD.** 2005. Role of an internal and two 3'-terminal RNA elements in assembly of tombusvirus replicase. J Virol **79:**10608-10618.
3. **Pogany J, White KA, Nagy PD.** 2005. Specific binding of tombusvirus replication protein p33 to an internal replication element in the viral RNA is essential for replication. J Virol **79:**4859-4869.
4. **Pathak KB, Pogany J, Xu K, White KA, Nagy PD.** 2012. Defining the Roles of cis-Acting RNA Elements in Tombusvirus Replicase Assembly In Vitro. J Virol **86:**156-171.
5. **Panavas T, Nagy PD.** 2003. Yeast as a model host to study replication and recombination of defective interfering RNA of Tomato bushy stunt virus. Virology **314:**315-325.
6. **Oster SK, Wu B, White KA.** 1998. Uncoupled expression of p33 and p92 permits amplification of tomato bushy stunt virus RNAs. J Virol **72:**5845-5851.
7. **Stork J, Kovalev N, Sasvari Z, Nagy PD.** 2011. RNA chaperone activity of the tombusviral p33 replication protein facilitates initiation of RNA synthesis by the viral RdRp in vitro. Virology **409:**338-347.
8. **Navarro B, Rubino L, Russo M.** 2004. Expression of the Cymbidium ringspot virus 33-kilodalton protein in Saccharomyces cerevisiae and molecular dissection of the peroxisomal targeting signal. J Virol **78:**4744-4752.
9. **Xu K, Huang TS, Nagy PD.** 2012. Authentic in vitro replication of two tombusviruses in isolated mitochondrial and endoplasmic reticulum membranes. J Virol **86:**12779-12794.
10. **Panavas T, Hawkins CM, Panaviene Z, Nagy PD.** 2005. The role of the p33:p33/p92 interaction domain in RNA replication and intracellular localization of p33 and p92 proteins of Cucumber necrosis tombusvirus. Virology **338:**81-95.
11. **Rajendran KS, Nagy PD.** 2006. Kinetics and functional studies on interaction between the replicase proteins of Tomato Bushy Stunt Virus: requirement of p33:p92 interaction for replicase assembly. Virology **345:**270-279.
12. **Panavas T, Serviene E, Brasher J, Nagy PD.** 2005. Yeast genome-wide screen reveals dissimilar sets of host genes affecting replication of RNA viruses. Proc Natl Acad Sci U S A **102:**7326-7331.
13. **Nagy PD.** 2008. Yeast as a model host to explore plant virus-host interactions. Annu Rev Phytopathol **46:**217-242.
14. **Rubino L, Burgyan J, Russo M.** 1995. Molecular cloning and complete nucleotide sequence of carnation Italian ringspot tombusvirus genomic and defective interfering RNAs. Archives of virology **140:**2027-2039.
15. **Rubino L, Navarro B, Russo M.** 2007. Cymbidium ringspot virus defective interfering RNA replication in yeast cells occurs on endoplasmic reticulum-derived membranes in the absence of peroxisomes. J Gen Virol **88:**1634-1642.

16. **White KA, Morris TJ.** 1994. Nonhomologous RNA recombination in tombusviruses: generation and evolution of defective interfering RNAs by stepwise deletions. J Virol **68:**14-24.
17. **White KA, Morris TJ.** 1994. Recombination between defective tombusvirus RNAs generates functional hybrid genomes. Proc Natl Acad Sci U S A **91:**3642-3646.
18. **McCartney AW, Greenwood JS, Fabian MR, White KA, Mullen RT.** 2005. Localization of the tomato bushy stunt virus replication protein p33 reveals a peroxisome-to-endoplasmic reticulum sorting pathway. Plant Cell **17:**3513-3531.
19. **Hwang YT, McCartney AW, Gidda SK, Mullen RT.** 2008. Localization of the Carnation Italian ringspot virus replication protein p36 to the mitochondrial outer membrane is mediated by an internal targeting signal and the TOM complex. BMC Cell Biol **9:**54.
20. **den Boon JA, Ahlquist P.** 2010. Organelle-like membrane compartmentalization of positive-strand RNA virus replication factories. Annual review of microbiology **64:**241-256.
21. **Aylward RB, Mansour E, El Said AO, Haridi A, Abu El Kheir A, Hassan A.** 1997. The eradication of poliomyelitis in Egypt: critical factors affecting progress to date. The Journal of infectious diseases **175 Suppl 1:**S56-61.
22. **Xia X, Luo J, Bai J, Yu R.** 2008. Epidemiology of hepatitis C virus infection among injection drug users in China: systematic review and meta-analysis. Public health **122:**990-1003.
23. **Cornberg M, Razavi HA, Alberti A, Bernasconi E, Buti M, Cooper C, Dalgard O, Dillion JF, Flisiak R, Forns X, Frankova S, Goldis A, Goulis I, Halota W, Hunyady B, Lagging M, Largen A, Makara M, Manolakopoulos S, Marcellin P, Marinho RT, Pol S, Poynard T, Puoti M, Sagalova O, Sibbel S, Simon K, Wallace C, Young K, Yurdaydin C, Zuckerman E, Negro F, Zeuzem S.** 2011. A systematic review of hepatitis C virus epidemiology in Europe, Canada and Israel. Liver international : official journal of the International Association for the Study of the Liver **31 Suppl 2:**30-60.
24. **Sievert W, Altraif I, Razavi HA, Abdo A, Ahmed EA, Alomair A, Amarapurkar D, Chen CH, Dou X, El Khayat H, Elshazly M, Esmat G, Guan R, Han KH, Koike K, Largen A, McCaughan G, Mogawer S, Monis A, Nawaz A, Piratvisuth T, Sanai FM, Sharara AI, Sibbel S, Sood A, Suh DJ, Wallace C, Young K, Negro F.** 2011. A systematic review of hepatitis C virus epidemiology in Asia, Australia and Egypt. Liver international : official journal of the International Association for the Study of the Liver **31 Suppl 2:**61-80.
25. **Mohamoud YA, Mumtaz GR, Riome S, Miller D, Abu-Raddad LJ.** 2013. The epidemiology of hepatitis C virus in Egypt: a systematic review and data synthesis. BMC infectious diseases **13:**288.
26. **Anez G, Rios M.** 2013. Dengue in the United States of America: a worsening scenario? BioMed research international **2013:**678645.
27. 2002. The West Nile Virus epidemic. Child health alert **20:**1.
28. **Hayes EB, Gubler DJ.** 2006. West Nile virus: epidemiology and clinical features of an emerging epidemic in the United States. Annual review of medicine **57:**181-194.

29. **de Vlas SJ, Cao WC, Richardus JH.** 2009. Documenting the SARS epidemic in mainland China. Tropical medicine & international health : TM & IH **14 Suppl 1:**1-3.
30. **Feng D, de Vlas SJ, Fang LQ, Han XN, Zhao WJ, Sheng S, Yang H, Jia ZW, Richardus JH, Cao WC.** 2009. The SARS epidemic in mainland China: bringing together all epidemiological data. Tropical medicine & international health : TM & IH **14 Suppl 1:**4-13.
31. **Lee WM, Ahlquist P.** 2003. Membrane synthesis, specific lipid requirements, and localized lipid composition changes associated with a positive-strand RNA virus RNA replication protein. J Virol **77:**12819-12828.
32. **Jonczyk M, Pathak KB, Sharma M, Nagy PD.** 2007. Exploiting alternative subcellular location for replication: tombusvirus replication switches to the endoplasmic reticulum in the absence of peroxisomes. Virology **362:**320-330.
33. **Hsu NY, Ilnytska O, Belov G, Santiana M, Chen YH, Takvorian PM, Pau C, van der Schaar H, Kaushik-Basu N, Balla T, Cameron CE, Ehrenfeld E, van Kuppeveld FJ, Altan-Bonnet N.** 2010. Viral reorganization of the secretory pathway generates distinct organelles for RNA replication. Cell **141:**799-811.
34. **Welsch S, Miller S, Romero-Brey I, Merz A, Bleck CK, Walther P, Fuller SD, Antony C, Krijnse-Locker J, Bartenschlager R.** 2009. Composition and three-dimensional architecture of the dengue virus replication and assembly sites. Cell Host Microbe **5:**365-375.
35. **Knoops K, Kikkert M, Worm SH, Zevenhoven-Dobbe JC, van der Meer Y, Koster AJ, Mommaas AM, Snijder EJ.** 2008. SARS-coronavirus replication is supported by a reticulovesicular network of modified endoplasmic reticulum. PLoS biology **6:**e226.
36. **Venter PA, Krishna NK, Schneemann A.** 2005. Capsid protein synthesis from replicating RNA directs specific packaging of the genome of a multipartite, positive-strand RNA virus. J Virol **79:**6239-6248.
37. **Wang RY, Nagy PD.** 2008. Tomato bushy stunt virus Co-Opts the RNA-Binding Function of a Host Metabolic Enzyme for Viral Genomic RNA Synthesis. Cell Host Microbe **3:**178-187.
38. **Chen J, Ahlquist P.** 2000. Brome mosaic virus polymerase-like protein 2a is directed to the endoplasmic reticulum by helicase-like viral protein 1a. J Virol **74:**4310-4318.
39. **Fernandez-Garcia MD, Mazzon M, Jacobs M, Amara A.** 2009. Pathogenesis of flavivirus infections: using and abusing the host cell. Cell Host Microbe **5:**318-328.
40. **Fischl W, Bartenschlager R.** 2011. Exploitation of cellular pathways by Dengue virus. Curr Opin Microbiol **14:**470-475.
41. **Knoops K, Barcena M, Limpens RW, Koster AJ, Mommaas AM, Snijder EJ.** 2012. Ultrastructural characterization of arterivirus replication structures: reshaping the endoplasmic reticulum to accommodate viral RNA synthesis. J Virol **86:**2474-2487.
42. **Froshauer S, Kartenbeck J, Helenius A.** 1988. Alphavirus RNA replicase is located on the cytoplasmic surface of endosomes and lysosomes. J Cell Biol **107:**2075-2086.

43. **Van Der Heijden MW, Carette JE, Reinhoud PJ, Haegi A, Bol JF.** 2001. Alfalfa mosaic virus replicase proteins P1 and P2 interact and colocalize at the vacuolar membrane. J Virol **75:**1879-1887.
44. **Ibrahim A, Hutchens HM, Berg RH, Loesch-Fries LS.** 2012. Alfalfa mosaic virus replicase proteins, P1 and P2, localize to the tonoplast in the presence of virus RNA. Virology **433:**449-461.
45. **Hagiwara Y, Komoda K, Yamanaka T, Tamai A, Meshi T, Funada R, Tsuchiya T, Naito S, Ishikawa M.** 2003. Subcellular localization of host and viral proteins associated with tobamovirus RNA replication. EMBO J **22:**344-353.
46. **Miller DJ, Schwartz MD, Ahlquist P.** 2001. Flock house virus RNA replicates on outer mitochondrial membranes in Drosophila cells. J Virol **75:**11664-11676.
47. **Russo M, Martelli GP.** 1982. Ultrastructure of turnip crinkle- and saguaro cactus virus-infected tissues. Virology **118:**109-116.
48. **Weber-Lotfi F, Dietrich A, Russo M, Rubino L.** 2002. Mitochondrial targeting and membrane anchoring of a viral replicase in plant and yeast cells. J Virol **76:**10485-10496.
49. **Pogany J, Nagy PD.** 2008. Authentic replication and recombination of Tomato bushy stunt virus RNA in a cell-free extract from yeast. J Virol **82:**5967-5980.
50. **Daum G.** 1985. Lipids of mitochondria. Biochimica et biophysica acta **822:**1-42.
51. **van Meer G, Voelker DR, Feigenson GW.** 2008. Membrane lipids: where they are and how they behave. Nat Rev Mol Cell Biol **9:**112-124.
52. **de Kroon AI, Dolis D, Mayer A, Lill R, de Kruijff B.** 1997. Phospholipid composition of highly purified mitochondrial outer membranes of rat liver and Neurospora crassa. Is cardiolipin present in the mitochondrial outer membrane? Biochimica et biophysica acta **1325:**108-116.
53. **Zinser E, Sperka-Gottlieb CD, Fasch EV, Kohlwein SD, Paltauf F, Daum G.** 1991. Phospholipid synthesis and lipid composition of subcellular membranes in the unicellular eukaryote Saccharomyces cerevisiae. Journal of bacteriology **173:**2026-2034.
54. **Vance JE, Steenbergen R.** 2005. Metabolism and functions of phosphatidylserine. Progress in lipid research **44:**207-234.
55. **Teissier E, Pecheur EI.** 2007. Lipids as modulators of membrane fusion mediated by viral fusion proteins. European biophysics journal : EBJ **36:**887-899.
56. **Marsh D.** 2007. Lateral pressure profile, spontaneous curvature frustration, and the incorporation and conformation of proteins in membranes. Biophysical journal **93:**3884-3899.
57. **Schoggins JW, Randall G.** 2013. Lipids in innate antiviral defense. Cell Host Microbe **14:**379-385.
58. **Yeung T, Grinstein S.** 2007. Lipid signaling and the modulation of surface charge during phagocytosis. Immunological reviews **219:**17-36.
59. **Robbe K, Otto-Bruc A, Chardin P, Antonny B.** 2003. Dissociation of GDP dissociation inhibitor and membrane translocation are required for efficient activation of Rac by the Dbl homology-pleckstrin homology region of Tiam. The Journal of biological chemistry **278:**4756-4762.

60. **Igarashi K, Kaneda M, Yamaji A, Saido TC, Kikkawa U, Ono Y, Inoue K, Umeda M.** 1995. A novel phosphatidylserine-binding peptide motif defined by an anti-idiotypic monoclonal antibody. Localization of phosphatidylserine-specific binding sites on protein kinase C and phosphatidylserine decarboxylase. The Journal of biological chemistry **270:**29075-29078.
61. **Yu JW, Lemmon MA.** 2001. All phox homology (PX) domains from Saccharomyces cerevisiae specifically recognize phosphatidylinositol 3-phosphate. The Journal of biological chemistry **276:**44179-44184.
62. **Nchoutmboube JA, Viktorova EG, Scott AJ, Ford LA, Pei Z, Watkins PA, Ernst RK, Belov GA.** 2013. Increased long chain acyl-Coa synthetase activity and fatty acid import is linked to membrane synthesis for development of picornavirus replication organelles. PLoS Pathog **9:**e1003401.
63. **Wilsky S, Sobotta K, Wiesener N, Pilas J, Althof N, Munder T, Wutzler P, Henke A.** 2012. Inhibition of fatty acid synthase by amentoflavone reduces coxsackievirus B3 replication. Archives of virology **157:**259-269.
64. **Heaton NS, Perera R, Berger KL, Khadka S, Lacount DJ, Kuhn RJ, Randall G.** 2010. Dengue virus nonstructural protein 3 redistributes fatty acid synthase to sites of viral replication and increases cellular fatty acid synthesis. Proc Natl Acad Sci U S A **107:**17345-17350.
65. **Martin-Acebes MA, Blazquez AB, Jimenez de Oya N, Escribano-Romero E, Saiz JC.** 2011. West Nile virus replication requires fatty acid synthesis but is independent on phosphatidylinositol-4-phosphate lipids. PloS one **6:**e24970.
66. **Diamond DL, Syder AJ, Jacobs JM, Sorensen CM, Walters KA, Proll SC, McDermott JE, Gritsenko MA, Zhang Q, Zhao R, Metz TO, Camp DG, 2nd, Waters KM, Smith RD, Rice CM, Katze MG.** 2010. Temporal proteome and lipidome profiles reveal hepatitis C virus-associated reprogramming of hepatocellular metabolism and bioenergetics. PLoS pathogens **6:**e1000719.
67. **Perera R, Riley C, Isaac G, Hopf-Jannasch AS, Moore RJ, Weitz KW, Pasa-Tolic L, Metz TO, Adamec J, Kuhn RJ.** 2012. Dengue virus infection perturbs lipid homeostasis in infected mosquito cells. PLoS pathogens **8:**e1002584.
68. **Thibaut HJ, van der Schaar HM, Lanke KH, Verbeken E, Andrews M, Leyssen P, Neyts J, van Kuppeveld FJ.** 2013. Fitness and virulence of a coxsackievirus mutant that can circumnavigate the need for PI4KIIIbeta. Journal of virology.
69. **van der Schaar HM, van der Linden L, Lanke KH, Strating JR, Purstinger G, de Vries E, de Haan CA, Neyts J, van Kuppeveld FJ.** 2012. Coxsackievirus mutants that can bypass host factor PI4KIIIbeta and the need for high levels of PI4P lipids for replication. Cell research **22:**1576-1592.
70. **Berger KL, Kelly SM, Jordan TX, Tartell MA, Randall G.** 2011. Hepatitis C virus stimulates the phosphatidylinositol 4-kinase III alpha-dependent phosphatidylinositol 4-phosphate production that is essential for its replication. J Virol **85:**8870-8883.
71. **Mackenzie JM, Khromykh AA, Parton RG.** 2007. Cholesterol manipulation by West Nile virus perturbs the cellular immune response. Cell Host Microbe **2:**229-239.

72. **Ilnytska O, Santiana M, Hsu NY, Du WL, Chen YH, Viktorova EG, Belov G, Brinker A, Storch J, Moore C, Dixon JL, Altan-Bonnet N.** 2013. Enteroviruses harness the cellular endocytic machinery to remodel the host cell cholesterol landscape for effective viral replication. Cell Host Microbe **14:**281-293.
73. **Nagy PD, Pogany J.** 2008. Multiple roles of viral replication proteins in plant RNA virus replication. Methods Mol Biol **451:**55-68.
74. **Nagy PD, Wang RY, Pogany J, Hafren A, Makinen K.** 2011. Emerging picture of host chaperone and cyclophilin roles in RNA virus replication. Virology **411:**374-382.
75. **Li Z, Nagy PD.** 2011. Diverse roles of host RNA binding proteins in RNA virus replication. RNA Biol **8:**305-315.
76. **den Boon JA, Diaz A, Ahlquist P.** 2010. Cytoplasmic viral replication complexes. Cell Host Microbe **8:**77-85.
77. **Salonen A, Ahola T, Kaariainen L.** 2005. Viral RNA replication in association with cellular membranes. Curr Top Microbiol Immunol **285:**139-173.
78. **Miller S, Krijnse-Locker J.** 2008. Modification of intracellular membrane structures for virus replication. Nat Rev Microbiol **6:**363-374.
79. **Nagy PD, Pogany J.** 2012. The dependence of viral RNA replication on co-opted host factors. Nature Reviews Microbiology **10:**137-149.
80. **Bartenschlager R, Cosset FL, Lohmann V.** 2010. Hepatitis C virus replication cycle. Journal of Hepatology **53:**583-585.
81. **Barajas D, Jiang Y, Nagy PD.** 2009. A unique role for the host ESCRT proteins in replication of Tomato bushy stunt virus. PLoS Pathog **5:**e1000705.
82. **Reiss S, Rebhan I, Backes P, Romero-Brey I, Erfle H, Matula P, Kaderali L, Poenisch M, Blankenburg H, Hiet MS, Longerich T, Diehl S, Ramirez F, Balla T, Rohr K, Kaul A, Buhler S, Pepperkok R, Lengauer T, Albrecht M, Eils R, Schirmacher P, Lohmann V, Bartenschlager R.** 2011. Recruitment and activation of a lipid kinase by hepatitis C virus NS5A is essential for integrity of the membranous replication compartment. Cell Host Microbe **9:**32-45.
83. **Sasvari Z, Nagy PD.** 2010. Making of viral replication organelles by remodeling interior membranes. Viruses **2:**2436-2442.
84. **Diaz A, Wang X, Ahlquist P.** 2010. Membrane-shaping host reticulon proteins play crucial roles in viral RNA replication compartment formation and function. Proc Natl Acad Sci U S A.
85. **Neuvonen M, Kazlauskas A, Martikainen M, Hinkkanen A, Ahola T, Saksela K.** 2011. SH3 domain-mediated recruitment of host cell amphiphysins by alphavirus nsP3 promotes viral RNA replication. PLoS Pathog **7:**e1002383.
86. **Barajas D, Nagy PD.** 2010. Ubiquitination of tombusvirus p33 replication protein plays a role in virus replication and binding to the host Vps23p ESCRT protein. Virology **397:**358-368.
87. **Castorena KM, Stapleford KA, Miller DJ.** 2010. Complementary transcriptomic, lipidomic, and targeted functional genetic analyses in cultured Drosophila cells highlight the role of glycerophospholipid metabolism in Flock House virus RNA replication. BMC Genomics **11:**183.

88. **Kapadia SB, Chisari FV.** 2005. Hepatitis C virus RNA replication is regulated by host geranylgeranylation and fatty acids. Proc Natl Acad Sci U S A **102:**2561-2566.
89. **Sharma M, Sasvari Z, Nagy PD.** 2011. Inhibition of phospholipid biosynthesis decreases the activity of the tombusvirus replicase and alters the subcellular localization of replication proteins. Virology **415:**141-152.
90. **Sharma M, Sasvari Z, Nagy PD.** 2010. Inhibition of sterol biosynthesis reduces tombusvirus replication in yeast and plants. J Virol **84:**2270-2281.
91. **Nagy PD, Pogany J.** 2006. Yeast as a model host to dissect functions of viral and host factors in tombusvirus replication. Virology **344:**211-220.
92. **Panaviene Z, Panavas T, Serva S, Nagy PD.** 2004. Purification of the cucumber necrosis virus replicase from yeast cells: role of coexpressed viral RNA in stimulation of replicase activity. J Virol **78:**8254-8263.
93. **Serviene E, Shapka N, Cheng CP, Panavas T, Phuangrat B, Baker J, Nagy PD.** 2005. Genome-wide screen identifies host genes affecting viral RNA recombination. Proc Natl Acad Sci U S A **102:**10545-10550.
94. **Serviene E, Jiang Y, Cheng CP, Baker J, Nagy PD.** 2006. Screening of the yeast yTHC collection identifies essential host factors affecting tombusvirus RNA recombination. J Virol **80:**1231-1241.
95. **Jiang Y, Serviene E, Gal J, Panavas T, Nagy PD.** 2006. Identification of essential host factors affecting tombusvirus RNA replication based on the yeast Tet promoters Hughes Collection. J Virol **80:**7394-7404.
96. **Shah Nawaz-Ul-Rehman M, Martinez-Ochoa N, Pascal H, Sasvari Z, Herbst C, Xu K, Baker J, Sharma M, Herbst A, Nagy PD.** 2012. Proteome-wide overexpression of host proteins for identification of factors affecting tombusvirus RNA replication: an inhibitory role of protein kinase C. J Virol **86:**9384-9395.
97. **Li Z, Pogany J, Panavas T, Xu K, Esposito AM, Kinzy TG, Nagy PD.** 2009. Translation elongation factor 1A is a component of the tombusvirus replicase complex and affects the stability of the p33 replication co-factor. Virology **385:**245-260.
98. **Serva S, Nagy PD.** 2006. Proteomics analysis of the tombusvirus replicase: Hsp70 molecular chaperone is associated with the replicase and enhances viral RNA replication. J Virol **80:**2162-2169.
99. **Li Z, Barajas D, Panavas T, Herbst DA, Nagy PD.** 2008. Cdc34p ubiquitin-conjugating enzyme is a component of the tombusvirus replicase complex and ubiquitinates p33 replication protein. J Virol **82:**6911-6926.
100. **Wang RY, Stork J, Pogany J, Nagy PD.** 2009. A temperature sensitive mutant of heat shock protein 70 reveals an essential role during the early steps of tombusvirus replication. Virology **394:**28-38.
101. **Wang RY, Stork J, Nagy PD.** 2009. A key role for heat shock protein 70 in the localization and insertion of tombusvirus replication proteins to intracellular membranes. J Virol **83:**3276-3287.
102. **Pogany J, Stork J, Li Z, Nagy PD.** 2008. In vitro assembly of the Tomato bushy stunt virus replicase requires the host Heat shock protein 70. Proc Natl Acad Sci U S A **105:**19956-19961.

103. **Li Z, Pogany J, Tupman S, Esposito AM, Kinzy TG, Nagy PD.** 2010. Translation elongation factor 1A facilitates the assembly of the tombusvirus replicase and stimulates minus-strand synthesis. PLoS Pathog **6:**e1001175.
104. **Sasvari Z, Izotova L, Kinzy TG, Nagy PD.** 2011. Synergistic Roles of Eukaryotic Translation Elongation Factors 1Bgamma and 1A in Stimulation of Tombusvirus Minus-Strand Synthesis. PLoS Pathog **7:**e1002438.
105. **Huang TS, Nagy PD.** 2011. Direct inhibition of tombusvirus plus-strand RNA synthesis by a dominant negative mutant of a host metabolic enzyme, glyceraldehyde-3-phosphate dehydrogenase, in yeast and plants. J Virol **85:**9090-9102.
106. **Kovalev N, Pogany J, Nagy PD.** 2012. A Co-Opted DEAD-Box RNA Helicase Enhances Tombusvirus Plus-Strand Synthesis. PLoS Pathog **8:**e1002537.
107. **Pathak KB, Sasvari Z, Nagy PD.** 2008. The host Pex19p plays a role in peroxisomal localization of tombusvirus replication proteins. Virology **379:**294-305.
108. **Qin J, Barajas D, Nagy PD.** 2012. An inhibitory function of WW domain-containing host proteins in RNA virus replication. Virology **426:**106-119.
109. **Lin JY, Mendu V, Pogany J, Qin J, Nagy PD.** 2012. The TPR Domain in the Host Cyp40-like Cyclophilin Binds to the Viral Replication Protein and Inhibits the Assembly of the Tombusviral Replicase. PLoS Pathog **8:**e1002491.
110. **Mendu V, Chiu M, Barajas D, Li Z, Nagy PD.** 2010. Cpr1 cyclophilin and Ess1 parvulin prolyl isomerases interact with the tombusvirus replication protein and inhibit viral replication in yeast model host. Virology **406:**342-351.
111. **Barajas D, Li Z, Nagy PD.** 2009. The Nedd4-Type Rsp5p Ubiquitin Ligase Inhibits Tombusvirus Replication by Regulating Degradation of the p92 Replication Protein and Decreasing the Activity of the Tombusvirus Replicase. J Virol **83:**11751-11764.
112. **Jiang Y, Li Z, Nagy PD.** 2010. Nucleolin/Nsr1p binds to the 3' noncoding region of the tombusvirus RNA and inhibits replication. Virology **396:**10-20.
113. **Navarro B, Russo M, Pantaleo V, Rubino L.** 2006. Cytological analysis of Saccharomyces cerevisiae cells supporting cymbidium ringspot virus defective interfering RNA replication. J Gen Virol **87:**705-714.
114. **Burgyan J, Rubino L, Russo M.** 1996. The 5'-terminal region of a tombusvirus genome determines the origin of multivesicular bodies. J Gen Virol **77 (Pt 8):**1967-1974.
115. **Chakrabarty R, Banerjee R, Chung SM, Farman M, Citovsky V, Hogenhout SA, Tzfira T, Goodin M.** 2007. PSITE vectors for stable integration or transient expression of autofluorescent protein fusions in plants: probing Nicotiana benthamiana-virus interactions. Mol Plant Microbe Interact **20:**740-750.
116. **Waters MG, Blobel G.** 1986. Secretory protein translocation in a yeast cell-free system can occur posttranslationally and requires ATP hydrolysis. J Cell Biol **102:**1543-1550.
117. **Meisinger C, Sommer T, Pfanner N.** 2000. Purification of Saccharomcyes cerevisiae mitochondria devoid of microsomal and cytosolic contaminations. Anal Biochem **287:**339-342.

118. **Rieder SE, Emr SD.** 2001. Isolation of subcellular fractions from the yeast Saccharomyces cerevisiae. Curr Protoc Cell Biol **Chapter 3:**Unit 3 8.
119. **Rajendran KS, Nagy PD.** 2004. Interaction between the replicase proteins of Tomato bushy stunt virus in vitro and in vivo. Virology **326:**250-261.
120. **Durr M, Escobar-Henriques M, Merz S, Geimer S, Langer T, Westermann B.** 2006. Nonredundant roles of mitochondria-associated F-box proteins Mfb1 and Mdm30 in maintenance of mitochondrial morphology in yeast. Mol Biol Cell **17:**3745-3755.
121. **Nowikovsky K, Froschauer EM, Zsurka G, Samaj J, Reipert S, Kolisek M, Wiesenberger G, Schweyen RJ.** 2004. The LETM1/YOL027 gene family encodes a factor of the mitochondrial K+ homeostasis with a potential role in the Wolf-Hirschhorn syndrome. J Biol Chem **279:**30307-30315.
122. **Quesada I, Verdugo P.** 2005. InsP3 signaling induces pulse-modulated Ca2+ signals in the nucleus of airway epithelial ciliated cells. Biophys J **88:**3946-3953.
123. **Rajendran KS, Nagy PD.** 2003. Characterization of the RNA-binding domains in the replicase proteins of tomato bushy stunt virus. J Virol **77:**9244-9258.
124. **Russo M, Burgyan J, Martelli GP.** 1994. Molecular biology of tombusviridae. Adv Virus Res **44:**381-428.
125. **Hofmann L, Saunier R, Cossard R, Esposito M, Rinaldi T, Delahodde A.** 2009. A nonproteolytic proteasome activity controls organelle fission in yeast. J Cell Sci **122:**3673-3683.
126. **Nagy PD.** 2011. The roles of host factors in tombusvirus RNA recombination. Adv Virus Res **81:**63-84.
127. **Jaag HM, Lu Q, Schmitt ME, Nagy PD.** 2011. Role of RNase MRP in viral RNA degradation and RNA recombination. J Virol **85:**243-253.
128. **Jaag HM, Pogany J, Nagy PD.** 2010. A host Ca2+/Mn2+ ion pump is a factor in the emergence of viral RNA recombinants. Cell Host Microbe **7:**74-81.
129. **Jaag HM, Nagy PD.** 2010. The combined effect of environmental and host factors on the emergence of viral RNA recombinants. PLoS Pathog **6:**e1001156.
130. **Cheng CP, Nagy PD.** 2003. Mechanism of RNA recombination in carmo- and tombusviruses: evidence for template switching by the RNA-dependent RNA polymerase in vitro. J Virol **77:**12033-12047.
131. **Koenig R, Lesemann DE, Pfeilstetter E.** 2009. New isolates of carnation Italian ringspot virus differ from the original one by having replication-associated proteins with a typical tombusvirus-like N-terminus and by inducing peroxisome- rather than mitochondrion-derived multivesicular bodies. Archives of virology **154:**1695-1698.
132. **Laliberte JF, Sanfacon H.** 2010. Cellular remodeling during plant virus infection. Annu Rev Phytopathol **48:**69-91.
133. **Diamond MS, Gale M, Jr.** 2012. Cell-intrinsic innate immune control of West Nile virus infection. Trends Immunol **33:**522-530.
134. **Aoshi T, Koyama S, Kobiyama K, Akira S, Ishii KJ.** 2011. Innate and adaptive immune responses to viral infection and vaccination. Curr Opin Virol **1:**226-232.
135. **Jensen S, Thomsen AR.** 2012. Sensing of RNA viruses: a review of innate immune receptors involved in recognizing RNA virus invasion. J Virol **86:**2900-2910.

136. **Ding SW.** 2010. RNA-based antiviral immunity. Nat Rev Immunol **10:**632-644.
137. **Diamond MS, Farzan M.** 2013. The broad-spectrum antiviral functions of IFIT and IFITM proteins. Nat Rev Immunol **13:**46-57.
138. **Yasunaga A, Hanna SL, Li J, Cho H, Rose PP, Spiridigliozzi A, Gold B, Diamond MS, Cherry S.** 2014. Genome-Wide RNAi Screen Identifies Broadly-Acting Host Factors That Inhibit Arbovirus Infection. PLoS Pathog **10:**e1003914.
139. **Xu J, Cherry S.** 2014. Viruses and antiviral immunity in Drosophila. Dev Comp Immunol **42:**67-84.
140. **Cherry S, Doukas T, Armknecht S, Whelan S, Wang H, Sarnow P, Perrimon N.** 2005. Genome-wide RNAi screen reveals a specific sensitivity of IRES-containing RNA viruses to host translation inhibition. Genes Dev **19:**445-452.
141. **Kushner DB, Lindenbach BD, Grdzelishvili VZ, Noueiry AO, Paul SM, Ahlquist P.** 2003. Systematic, genome-wide identification of host genes affecting replication of a positive-strand RNA virus. Proc Natl Acad Sci U S A **100:**15764-15769.
142. **Krishnan MN, Ng A, Sukumaran B, Gilfoy FD, Uchil PD, Sultana H, Brass AL, Adametz R, Tsui M, Qian F, Montgomery RR, Lev S, Mason PW, Koski RA, Elledge SJ, Xavier RJ, Agaisse H, Fikrig E.** 2008. RNA interference screen for human genes associated with West Nile virus infection. Nature.
143. **Li Q, Brass AL, Ng A, Hu Z, Xavier RJ, Liang TJ, Elledge SJ.** 2009. A genome-wide genetic screen for host factors required for hepatitis C virus propagation. Proc Natl Acad Sci U S A **106:**16410-16415.
144. **Randall G, Panis M, Cooper JD, Tellinghuisen TL, Sukhodolets KE, Pfeffer S, Landthaler M, Landgraf P, Kan S, Lindenbach BD, Chien M, Weir DB, Russo JJ, Ju J, Brownstein MJ, Sheridan R, Sander C, Zavolan M, Tuschl T, Rice CM.** 2007. Cellular cofactors affecting hepatitis C virus infection and replication. Proc Natl Acad Sci U S A **104:**12884-12889.
145. **Sessions OM, Barrows NJ, Souza-Neto JA, Robinson TJ, Hershey CL, Rodgers MA, Ramirez JL, Dimopoulos G, Yang PL, Pearson JL, Garcia-Blanco MA.** 2009. Discovery of insect and human dengue virus host factors. Nature **458:**1047-1050.
146. **Tai AW, Benita Y, Peng LF, Kim SS, Sakamoto N, Xavier RJ, Chung RT.** 2009. A functional genomic screen identifies cellular cofactors of hepatitis C virus replication. Cell Host Microbe **5:**298-307.
147. **Nawaz-Ul-Rehman MS, Reddisiva Prasanth K, Baker J, Nagy PD.** 2012. Yeast screens for host factors in positive-strand RNA virus replication based on a library of temperature-sensitive mutants. Methods.
148. **Nagy PD, Pogany J.** 2010. Global genomics and proteomics approaches to identify host factors as targets to induce resistance against Tomato bushy stunt virus. Adv Virus Res **76:**123-177.
149. **Xu K, Nagy PD.** 2010. Dissecting Virus-Plant Interactions Through Proteomics Approaches. Current Proteomics **7:**316-327.
150. **Lin JY, Nagy PD.** 2013. Identification of Novel Host Factors via Conserved Domain Search: Cns1 Cochaperone Is a Novel Restriction Factor of Tombusvirus Replication in Yeast. J Virol **87:**12600-12610.

151. **Kovalev N, Nagy PD.** 2013. Cyclophilin a binds to the viral RNA and replication proteins, resulting in inhibition of tombusviral replicase assembly. J Virol **87:**13330-13342.
152. **Nagy PD, Barajas D, Pogany J.** 2012. Host factors with regulatory roles in tombusvirus replication. Curr Opin Virol.
153. **Huang TS, Nagy PD.** 2011. Direct inhibition of tombusvirus plus-strand RNA synthesis by a dominant-negative mutant of a host metabolic enzyme, GAPDH, in yeast and plants. J Virol.
154. **Kovalev N, Barajas D, Nagy PD.** 2012. Similar roles for yeast Dbp2 and Arabidopsis RH20 DEAD-box RNA helicases to Ded1 helicase in tombusvirus plus-strand synthesis. Virology **432:**470-484.
155. **D'Andrea LD, Regan L.** 2003. TPR proteins: the versatile helix. Trends Biochem Sci **28:**655-662.
156. **Allan RK, Ratajczak T.** 2011. Versatile TPR domains accommodate different modes of target protein recognition and function. Cell Stress Chaperones **16:**353-367.
157. **Haslbeck V, Eckl JM, Kaiser CJ, Papsdorf K, Hessling M, Richter K.** 2013. Chaperone-interacting TPR proteins in Caenorhabditis elegans. J Mol Biol **425:**2922-2939.
158. **Xiol J, Cora E, Koglgruber R, Chuma S, Subramanian S, Hosokawa M, Reuter M, Yang Z, Berninger P, Palencia A, Benes V, Penninger J, Sachidanandam R, Pillai RS.** 2012. A role for Fkbp6 and the chaperone machinery in piRNA amplification and transposon silencing. Mol Cell **47:**970-979.
159. **Stawowczyk M, Van Scoy S, Kumar KP, Reich NC.** 2011. The interferon stimulated gene 54 promotes apoptosis. J Biol Chem **286:**7257-7266.
160. **Cerveny L, Straskova A, Dankova V, Hartlova A, Ceckova M, Staud F, Stulik J.** 2013. Tetratricopeptide repeat motifs in the world of bacterial pathogens: role in virulence mechanisms. Infect Immun **81:**629-635.
161. **Assimon VA, Gillies AT, Rauch JN, Gestwicki JE.** 2013. Hsp70 protein complexes as drug targets. Curr Pharm Des **19:**404-417.
162. **Nordling E, Abraham-Nordling M.** 2012. Colonic amyloidosis, computational analysis of the major amyloidogenic species, Serum Amyloid A. Comput Biol Chem **39:**29-34.
163. **Adams CJ, Pike AC, Maniam S, Sharpe TD, Coutts AS, Knapp S, La Thangue NB, Bullock AN.** 2012. The p53 cofactor Strap exhibits an unexpected TPR motif and oligonucleotide-binding (OB)-fold structure. Proc Natl Acad Sci U S A **109:**3778-3783.
164. **Banasavadi-Siddegowda YK, Mai J, Fan Y, Bhattacharya S, Giovannucci DR, Sanchez ER, Fischer G, Wang X.** 2011. FKBP38 peptidylprolyl isomerase promotes the folding of cystic fibrosis transmembrane conductance regulator in the endoplasmic reticulum. J Biol Chem **286:**43071-43080.
165. **Kubota H, Yamamoto S, Itoh E, Abe Y, Nakamura A, Izumi Y, Okada H, Iida M, Nanjo H, Itoh H, Yamamoto Y.** 2010. Increased expression of co-chaperone HOP with HSP90 and HSC70 and complex formation in human colonic carcinoma. Cell Stress Chaperones **15:**1003-1011.

166. **Bourai M, Lucas-Hourani M, Gad HH, Drosten C, Jacob Y, Tafforeau L, Cassonnet P, Jones LM, Judith D, Couderc T, Lecuit M, Andre P, Kummerer BM, Lotteau V, Despres P, Tangy F, Vidalain PO.** 2012. Mapping of Chikungunya virus interactions with host proteins identified nsP2 as a highly connected viral component. J Virol **86:**3121-3134.
167. **Fensterl V, Wetzel JL, Ramachandran S, Ogino T, Stohlman SA, Bergmann CC, Diamond MS, Virgin HW, Sen GC.** 2012. Interferon-induced Ifit2/ISG54 protects mice from lethal VSV neuropathogenesis. PLoS Pathog **8:**e1002712.
168. **Miettinen JJ, Matikainen S, Nyman TA.** 2012. Global secretome characterization of herpes simplex virus 1-infected human primary macrophages. J Virol **86:**12770-12778.
169. **Danquah JO, Botchway S, Jeshtadi A, King LA.** 2012. Direct interaction of baculovirus capsid proteins VP39 and EXON0 with kinesin-1 in insect cells determined by fluorescence resonance energy transfer-fluorescence lifetime imaging microscopy. J Virol **86:**844-853.
170. **Jeshtadi A, Burgos P, Stubbs CD, Parker AW, King LA, Skinner MA, Botchway SW.** 2010. Interaction of poxvirus intracellular mature virion proteins with the TPR domain of kinesin light chain in live infected cells revealed by two-photon-induced fluorescence resonance energy transfer fluorescence lifetime imaging microscopy. J Virol **84:**12886-12894.
171. **Daffis S, Szretter KJ, Schriewer J, Li J, Youn S, Errett J, Lin TY, Schneller S, Zust R, Dong H, Thiel V, Sen GC, Fensterl V, Klimstra WB, Pierson TC, Buller RM, Gale M, Jr., Shi PY, Diamond MS.** 2010. 2'-O methylation of the viral mRNA cap evades host restriction by IFIT family members. Nature **468:**452-456.
172. **Iki T, Yoshikawa M, Meshi T, Ishikawa M.** 2012. Cyclophilin 40 facilitates HSP90-mediated RISC assembly in plants. EMBO J **31:**267-278.
173. **Liu XY, Chen W, Wei B, Shan YF, Wang C.** 2011. IFN-induced TPR protein IFIT3 potentiates antiviral signaling by bridging MAVS and TBK1. J Immunol **187:**2559-2568.
174. **Pichlmair A, Lassnig C, Eberle CA, Gorna MW, Baumann CL, Burkard TR, Burckstummer T, Stefanovic A, Krieger S, Bennett KL, Rulicke T, Weber F, Colinge J, Muller M, Superti-Furga G.** 2011. IFIT1 is an antiviral protein that recognizes 5'-triphosphate RNA. Nat Immunol **12:**624-630.
175. **Flom G, Behal RH, Rosen L, Cole DG, Johnson JL.** 2007. Definition of the minimal fragments of Sti1 required for dimerization, interaction with Hsp70 and Hsp90 and in vivo functions. Biochem J **404:**159-167.
176. **Wegele H, Haslbeck M, Reinstein J, Buchner J.** 2003. Sti1 is a novel activator of the Ssa proteins. J Biol Chem **278:**25970-25976.
177. **Schmid AB, Lagleder S, Grawert MA, Rohl A, Hagn F, Wandinger SK, Cox MB, Demmer O, Richter K, Groll M, Kessler H, Buchner J.** 2012. The architecture of functional modules in the Hsp90 co-chaperone Sti1/Hop. EMBO J **31:**1506-1517.
178. **Odunuga OO, Hornby JA, Bies C, Zimmermann R, Pugh DJ, Blatch GL.** 2003. Tetratricopeptide repeat motif-mediated Hsc70-mSTI1 interaction.

Molecular characterization of the critical contacts for successful binding and specificity. J Biol Chem **278:**6896-6904.

179. **Reidy M, Masison DC.** 2010. Sti1 regulation of Hsp70 and Hsp90 is critical for curing of Saccharomyces cerevisiae [PSI+] prions by Hsp104. Molecular and cellular biology **30:**3542-3552.
180. **Song Y, Masison DC.** 2005. Independent regulation of Hsp70 and Hsp90 chaperones by Hsp70/Hsp90-organizing protein Sti1 (Hop1). J Biol Chem **280:**34178-34185.
181. **Krishna P, Gloor G.** 2001. The Hsp90 family of proteins in Arabidopsis thaliana. Cell Stress Chaperones **6:**238-246.
182. **Pogany J, Panavas, T., Serviene, E., Nawaz-Ul-Rehman, MS., and Nagy, PD.** 2010. A high-throughput approach for studying virus replication in yeast. Current Protocols in Microbiology **19:**16J.11.11-16J.11.15.
183. **Jaag HM, Nagy PD.** 2009. Silencing of Nicotiana benthamiana Xrn4p exoribonuclease promotes tombusvirus RNA accumulation and recombination. Virology **386:**344-352.
184. **Iyer K, Burkle L, Auerbach D, Thaminy S, Dinkel M, Engels K, Stagljar I.** 2005. Utilizing the split-ubiquitin membrane yeast two-hybrid system to identify protein-protein interactions of integral membrane proteins. Sci STKE **2005:**pl3.
185. **Kittanakom S, Chuk M, Wong V, Snyder J, Edmonds D, Lydakis A, Zhang Z, Auerbach D, Stagljar I.** 2009. Analysis of membrane protein complexes using the split-ubiquitin membrane yeast two-hybrid (MYTH) system. Methods Mol Biol **548:**247-271.
186. **Flom G, Weekes J, Williams JJ, Johnson JL.** 2006. Effect of mutation of the tetratricopeptide repeat and asparatate-proline 2 domains of Sti1 on Hsp90 signaling and interaction in Saccharomyces cerevisiae. Genetics **172:**41-51.
187. **Pathak KB, Pogany J, Nagy PD.** 2011. Non-template functions of the viral RNA in plant RNA virus replication. Curr Opin Virol **1:**332-338.
188. **Zhang Z, Quick MK, Kanelakis KC, Gijzen M, Krishna P.** 2003. Characterization of a plant homolog of hop, a cochaperone of hsp90. Plant Physiol **131:**525-535.
189. **Dufresne PJ, Thivierge K, Cotton S, Beauchemin C, Ide C, Ubalijoro E, Laliberte JF, Fortin MG.** 2008. Heat shock 70 protein interaction with Turnip mosaic virus RNA-dependent RNA polymerase within virus-induced membrane vesicles. Virology **374:**217-227.
190. **Kampmueller KM, Miller DJ.** 2005. The cellular chaperone heat shock protein 90 facilitates Flock House virus RNA replication in Drosophila cells. J Virol **79:**6827-6837.
191. **Mayer MP.** 2005. Recruitment of Hsp70 chaperones: a crucial part of viral survival strategies. Rev Physiol Biochem Pharmacol **153:**1-46.
192. **Okamoto T, Nishimura Y, Ichimura T, Suzuki K, Miyamura T, Suzuki T, Moriishi K, Matsuura Y.** 2006. Hepatitis C virus RNA replication is regulated by FKBP8 and Hsp90. Embo J **25:**5015-5025.
193. **Tomita Y, Mizuno T, Diez J, Naito S, Ahlquist P, Ishikawa M.** 2003. Mutation of host DnaJ homolog inhibits brome mosaic virus negative-strand RNA synthesis. J Virol **77:**2990-2997.

194. **Weeks SA, Miller DJ.** 2008. The heat shock protein 70 cochaperone YDJ1 is required for efficient membrane-specific flock house virus RNA replication complex assembly and function in Saccharomyces cerevisiae. J Virol **82:**2004-2012.
195. **Weeks SA, Shield WP, Sahi C, Craig EA, Rospert S, Miller DJ.** 2010. A targeted analysis of cellular chaperones reveals contrasting roles for heat shock protein 70 in flock house virus RNA replication. J Virol **84:**330-339.
196. **Taipale M, Jarosz DF, Lindquist S.** 2010. HSP90 at the hub of protein homeostasis: emerging mechanistic insights. Nat Rev Mol Cell Biol **11:**515-528.
197. **Mayer MP.** 2010. Gymnastics of molecular chaperones. Mol Cell **39:**321-331.
198. **Kampinga HH, Craig EA.** 2010. The HSP70 chaperone machinery: J proteins as drivers of functional specificity. Nat Rev Mol Cell Biol **11:**579-592.
199. **Fellerer C, Schweiger R, Schongruber K, Soll J, Schwenkert S.** 2011. Cytosolic HSP90 cochaperones HOP and FKBP interact with freshly synthesized chloroplast preproteins of Arabidopsis. Mol Plant **4:**1133-1145.
200. **Bhangoo MK, Tzankov S, Fan AC, Dejgaard K, Thomas DY, Young JC.** 2007. Multiple 40-kDa heat-shock protein chaperones function in Tom70-dependent mitochondrial import. Mol Biol Cell **18:**3414-3428.
201. **Young JC, Hoogenraad NJ, Hartl FU.** 2003. Molecular chaperones Hsp90 and Hsp70 deliver preproteins to the mitochondrial import receptor Tom70. Cell **112:**41-50.
202. **Monkewich S, Lin HX, Fabian MR, Xu W, Na H, Ray D, Chernysheva OA, Nagy PD, White KA.** 2005. The p92 polymerase coding region contains an internal RNA element required at an early step in Tombusvirus genome replication. J Virol **79:**4848-4858.
203. **Pogany J, Nagy PD.** 2012. p33-Independent Activation of a Truncated p92 RNA-Dependent RNA Polymerase of Tomato Bushy Stunt Virus in Yeast Cell-Free Extract. J Virol **86:**12025-12038.
204. **Panaviene Z, Baker JM, Nagy PD.** 2003. The overlapping RNA-binding domains of p33 and p92 replicase proteins are essential for tombusvirus replication. Virology **308:**191-205.
205. **Pathak KB, Jiang Z, Ochanine V, Sharma M, Pogany J, Nagy PD.** 2013. Characterization of dominant-negative and temperature-sensitive mutants of tombusvirus replication proteins affecting replicase assembly. Virology **437:**48-61.
206. **Lee CT, Graf C, Mayer FJ, Richter SM, Mayer MP.** 2012. Dynamics of the regulation of Hsp90 by the co-chaperone Sti1. EMBO J **31:**1518-1528.
207. **Wegele H, Wandinger SK, Schmid AB, Reinstein J, Buchner J.** 2006. Substrate transfer from the chaperone Hsp70 to Hsp90. J Mol Biol **356:**802-811.
208. **Mine A, Okuno T.** 2012. Composition of plant virus RNA replicase complexes. Curr Opin Virol **2:**669-675.
209. **Chen L, Hamada S, Fujiwara M, Zhu T, Thao NP, Wong HL, Krishna P, Ueda T, Kaku H, Shibuya N, Kawasaki T, Shimamoto K.** 2010. The Hop/Sti1-Hsp90 chaperone complex facilitates the maturation and transport of a PAMP receptor in rice innate immunity. Cell Host Microbe **7:**185-196.

210. **Jones G, Song Y, Chung S, Masison DC.** 2004. Propagation of Saccharomyces cerevisiae [PSI+] prion is impaired by factors that regulate Hsp70 substrate binding. Molecular and cellular biology **24:**3928-3937.
211. **Honore B, Leffers H, Madsen P, Rasmussen HH, Vandekerckhove J, Celis JE.** 1992. Molecular cloning and expression of a transformation-sensitive human protein containing the TPR motif and sharing identity to the stress-inducible yeast protein STI1. J Biol Chem **267:**8485-8491.
212. **Stapleford KA, Rapaport D, Miller DJ.** 2009. Mitochondrion-enriched anionic phospholipids facilitate flock house virus RNA polymerase membrane association. Journal of virology **83:**4498-4507.
213. **Li W, Wang R, Li M, Li L, Wang C, Welti R, Wang X.** 2008. Differential degradation of extraplastidic and plastidic lipids during freezing and post-freezing recovery in Arabidopsis thaliana. The Journal of biological chemistry **283:**461-468.
214. **Makino A, Baba T, Fujimoto K, Iwamoto K, Yano Y, Terada N, Ohno S, Sato SB, Ohta A, Umeda M, Matsuzaki K, Kobayashi T.** 2003. Cinnamycin (Ro 09-0198) promotes cell binding and toxicity by inducing transbilayer lipid movement. The Journal of biological chemistry **278:**3204-3209.
215. **Aoki Y, Uenaka T, Aoki J, Umeda M, Inoue K.** 1994. A novel peptide probe for studying the transbilayer movement of phosphatidylethanolamine. Journal of biochemistry **116:**291-297.
216. **Grant AM, Hanson PK, Malone L, Nichols JW.** 2001. NBD-labeled phosphatidylcholine and phosphatidylethanolamine are internalized by transbilayer transport across the yeast plasma membrane. Traffic **2:**37-50.
217. **Zhao M.** 2011. Lantibiotics as probes for phosphatidylethanolamine. Amino acids **41:**1071-1079.
218. **Kodaki T, Yamashita S.** 1989. Characterization of the methyltransferases in the yeast phosphatidylethanolamine methylation pathway by selective gene disruption. European journal of biochemistry / FEBS **185:**243-251.
219. **Wriessnegger T, Gubitz G, Leitner E, Ingolic E, Cregg J, de la Cruz BJ, Daum G.** 2007. Lipid composition of peroxisomes from the yeast Pichia pastoris grown on different carbon sources. Biochimica et biophysica acta **1771:**455-461.
220. **Wriessnegger T, Leitner E, Belegratis MR, Ingolic E, Daum G.** 2009. Lipid analysis of mitochondrial membranes from the yeast Pichia pastoris. Biochimica et biophysica acta **1791:**166-172.
221. **Donaldson RP, Beevers H.** 1977. Lipid composition of organelles from germinating castor bean endosperm. Plant Physiol **59:**259-263.
222. **Kovalev N, Pogany J, Nagy PD.** 2014. A template role of double-stranded RNA in tombusvirus replication. J Virol.
223. **Rochon D, Singh B, Reade R, Theilmann J, Ghoshal K, Alam SB, Maghodia A.** 2014. The p33 auxiliary replicase protein of Cucumber necrosis virus targets peroxisomes and infection induces de novo peroxisome formation from the endoplasmic reticulum. Virology **452-453:**133-142.
224. **Garzon S, Strykowski H, Charpentier G.** 1990. Implication of mitochondria in the replication of Nodamura virus in larvae of the Lepidoptera, Galleria mellonella (L.) and in suckling mice. Archives of virology **113:**165-176.

225. **Perttila J, Spuul P, Ahola T.** 2013. Early secretory pathway localization and lack of processing for hepatitis E virus replication protein pORF1. J Gen Virol **94:**807-816.
226. **Midgley R, Moffat K, Berryman S, Hawes P, Simpson J, Fullen D, Stephens DJ, Burman A, Jackson T.** 2013. A role for endoplasmic reticulum exit sites in foot-and-mouth disease virus infection. J Gen Virol **94:**2636-2646.
227. **Patarroyo C, Laliberte JF, Zheng H.** 2012. Hijack it, change it: how do plant viruses utilize the host secretory pathway for efficient viral replication and spread? Frontiers in plant science **3:**308.
228. **Hyodo K, Mine A, Taniguchi T, Kaido M, Mise K, Taniguchi H, Okuno T.** 2013. ADP ribosylation factor 1 plays an essential role in the replication of a plant RNA virus. J Virol **87:**163-176.
229. **Schlegel A, Giddings TH, Jr., Ladinsky MS, Kirkegaard K.** 1996. Cellular origin and ultrastructure of membranes induced during poliovirus infection. J Virol **70:**6576-6588.
230. **Egger D, Teterina N, Ehrenfeld E, Bienz K.** 2000. Formation of the poliovirus replication complex requires coupled viral translation, vesicle production, and viral RNA synthesis. J Virol **74:**6570-6580.
231. **Belov GA, Habbersett C, Franco D, Ehrenfeld E.** 2007. Activation of cellular Arf GTPases by poliovirus protein 3CD correlates with virus replication. J Virol **81:**9259-9267.
232. **Belov GA, Altan-Bonnet N, Kovtunovych G, Jackson CL, Lippincott-Schwartz J, Ehrenfeld E.** 2007. Hijacking components of the cellular secretory pathway for replication of poliovirus RNA. J Virol **81:**558-567.
233. **Dorobantu CM, van der Schaar HM, Ford LA, Strating JR, Ulferts R, Fang Y, Belov G, van Kuppeveld FJ.** 2014. Recruitment of PI4KIIIbeta to Coxsackievirus B3 Replication Organelles Is Independent of ACBD3, GBF1, and Arf1. J Virol **88:**2725-2736.
234. **Turner KA, Sit TL, Callaway AS, Allen NS, Lommel SA.** 2004. Red clover necrotic mosaic virus replication proteins accumulate at the endoplasmic reticulum. Virology **320:**276-290.
235. **Cosson P, Perrin J, Bonifacino JS.** 2013. Anchors aweigh: protein localization and transport mediated by transmembrane domains. Trends in cell biology **23:**511-517.
236. **Sharpe HJ, Stevens TJ, Munro S.** 2010. A comprehensive comparison of transmembrane domains reveals organelle-specific properties. Cell **142:**158-169.
237. **Nishikawa S, Nakano A.** 1993. Identification of a gene required for membrane protein retention in the early secretory pathway. Proc Natl Acad Sci U S A **90:**8179-8183.
238. **Letourneur F, Cosson P.** 1998. Targeting to the endoplasmic reticulum in yeast cells by determinants present in transmembrane domains. J Biol Chem **273:**33273-33278.
239. **Sato K, Sato M, Nakano A.** 2001. Rer1p, a retrieval receptor for endoplasmic reticulum membrane proteins, is dynamically localized to the Golgi apparatus by coatomer. J Cell Biol **152:**935-944.

240. **Herzig Y, Sharpe HJ, Elbaz Y, Munro S, Schuldiner M.** 2012. A systematic approach to pair secretory cargo receptors with their cargo suggests a mechanism for cargo selection by Erv14. PLoS biology **10:**e1001329.
241. **Ronchi P, Colombo S, Francolini M, Borgese N.** 2008. Transmembrane domain-dependent partitioning of membrane proteins within the endoplasmic reticulum. J Cell Biol **181:**105-118.
242. **Hayashi-Nishino M, Fujita N, Noda T, Yamaguchi A, Yoshimori T, Yamamoto A.** 2009. A subdomain of the endoplasmic reticulum forms a cradle for autophagosome formation. Nature cell biology **11:**1433-1437.
243. **Hailey DW, Rambold AS, Satpute-Krishnan P, Mitra K, Sougrat R, Kim PK, Lippincott-Schwartz J.** 2010. Mitochondria supply membranes for autophagosome biogenesis during starvation. Cell **141:**656-667.
244. **Hamasaki M, Furuta N, Matsuda A, Nezu A, Yamamoto A, Fujita N, Oomori H, Noda T, Haraguchi T, Hiraoka Y, Amano A, Yoshimori T.** 2013. Autophagosomes form at ER-mitochondria contact sites. Nature **495:**389-393.
245. **Moreau K, Ravikumar B, Renna M, Puri C, Rubinsztein DC.** 2011. Autophagosome precursor maturation requires homotypic fusion. Cell **146:**303-317.
246. **Ravikumar B, Moreau K, Jahreiss L, Puri C, Rubinsztein DC.** 2010. Plasma membrane contributes to the formation of pre-autophagosomal structures. Nature cell biology **12:**747-757.
247. **Geng J, Nair U, Yasumura-Yorimitsu K, Klionsky DJ.** 2010. Post-Golgi Sec proteins are required for autophagy in Saccharomyces cerevisiae. Mol Biol Cell **21:**2257-2269.
248. **Yen WL, Shintani T, Nair U, Cao Y, Richardson BC, Li Z, Hughson FM, Baba M, Klionsky DJ.** 2010. The conserved oligomeric Golgi complex is involved in double-membrane vesicle formation during autophagy. J Cell Biol **188:**101-114.
249. **Ohashi Y, Munro S.** 2010. Membrane delivery to the yeast autophagosome from the Golgi-endosomal system. Mol Biol Cell **21:**3998-4008.
250. **van der Vaart A, Griffith J, Reggiori F.** 2010. Exit from the Golgi is required for the expansion of the autophagosomal phagophore in yeast Saccharomyces cerevisiae. Mol Biol Cell **21:**2270-2284.
251. **Guo Y, Chang C, Huang R, Liu B, Bao L, Liu W.** 2012. AP1 is essential for generation of autophagosomes from the trans-Golgi network. J Cell Sci **125:**1706-1715.
252. **Longatti A, Lamb CA, Razi M, Yoshimura S, Barr FA, Tooze SA.** 2012. TBC1D14 regulates autophagosome formation via Rab11- and ULK1-positive recycling endosomes. J Cell Biol **197:**659-675.
253. **Zoppino FC, Militello RD, Slavin I, Alvarez C, Colombo MI.** 2010. Autophagosome formation depends on the small GTPase Rab1 and functional ER exit sites. Traffic **11:**1246-1261.
254. **Hamasaki M, Noda T, Ohsumi Y.** 2003. The early secretory pathway contributes to autophagy in yeast. Cell structure and function **28:**49-54.

255. **Ge L, Melville D, Zhang M, Schekman R.** 2013. The ER-Golgi intermediate compartment is a key membrane source for the LC3 lipidation step of autophagosome biogenesis. eLife **2:**e00947.
256. **Clancey CJ, Chang SC, Dowhan W.** 1993. Cloning of a gene (PSD1) encoding phosphatidylserine decarboxylase from Saccharomyces cerevisiae by complementation of an Escherichia coli mutant. J Biol Chem **268:**24580-24590.
257. **Trotter PJ, Pedretti J, Yates R, Voelker DR.** 1995. Phosphatidylserine decarboxylase 2 of Saccharomyces cerevisiae. Cloning and mapping of the gene, heterologous expression, and creation of the null allele. J Biol Chem **270:**6071-6080.
258. **Trotter PJ, Pedretti J, Voelker DR.** 1993. Phosphatidylserine decarboxylase from Saccharomyces cerevisiae. Isolation of mutants, cloning of the gene, and creation of a null allele. J Biol Chem **268:**21416-21424.
259. **Trotter PJ, Voelker DR.** 1995. Identification of a non-mitochondrial phosphatidylserine decarboxylase activity (PSD2) in the yeast Saccharomyces cerevisiae. J Biol Chem **270:**6062-6070.
260. **Gulshan K, Shahi P, Moye-Rowley WS.** 2010. Compartment-specific synthesis of phosphatidylethanolamine is required for normal heavy metal resistance. Mol Biol Cell **21:**443-455.
261. **Nerlich A, von Orlow M, Rontein D, Hanson AD, Dormann P.** 2007. Deficiency in phosphatidylserine decarboxylase activity in the psd1 psd2 psd3 triple mutant of Arabidopsis affects phosphatidylethanolamine accumulation in mitochondria. Plant Physiol **144:**904-914.
262. **McMaster CR, Bell RM.** 1994. Phosphatidylcholine biosynthesis via the CDP-choline pathway in Saccharomyces cerevisiae. Multiple mechanisms of regulation. J Biol Chem **269:**14776-14783.
263. **Yang W, Moroney JV, Moore TS.** 2004. Membrane lipid biosynthesis in Chlamydomonas reinhardtii: ethanolaminephosphotransferase is capable of synthesizing both phosphatidylcholine and phosphatidylethanolamine. Archives of biochemistry and biophysics **430:**198-209.
264. **Sutoh K, Sanuki N, Sakaki T, Imai R.** 2010. Specific induction of TaAAPT1, an ER- and Golgi-localized ECPT-type aminoalcoholphosphotransferase, results in preferential accumulation of the phosphatidylethanolamine membrane phospholipid during cold acclimation in wheat. Plant molecular biology **72:**519-531.
265. **Qi Q, Huang YF, Cutler AJ, Abrams SR, Taylor DC.** 2003. Molecular and biochemical characterization of an aminoalcoholphosphotransferase (AAPT1) from Brassica napus: effects of low temperature and abscisic acid treatments on AAPT expression in Arabidopsis plants and effects of over-expression of BnAAPT1 in transgenic Arabidopsis. Planta **217:**547-558.
266. **Choi YH, Lee JK, Lee CH, Cho SH.** 2000. cDNA cloning and expression of an aminoalcoholphosphotransferase isoform in Chinese cabbage. Plant & cell physiology **41:**1080-1084.
267. **Henneberry AL, Wright MM, McMaster CR.** 2002. The major sites of cellular phospholipid synthesis and molecular determinants of Fatty Acid and lipid head group specificity. Mol Biol Cell **13:**3148-3161.

268. **Birner R, Burgermeister M, Schneiter R, Daum G.** 2001. Roles of phosphatidylethanolamine and of its several biosynthetic pathways in Saccharomyces cerevisiae. Mol Biol Cell **12:**997-1007.
269. **Janke C, Magiera MM, Rathfelder N, Taxis C, Reber S, Maekawa H, Moreno-Borchart A, Doenges G, Schwob E, Schiebel E, Knop M.** 2004. A versatile toolbox for PCR-based tagging of yeast genes: new fluorescent proteins, more markers and promoter substitution cassettes. Yeast **21:**947-962.
270. **Holthuis JC, Nichols BJ, Dhruvakumar S, Pelham HR.** 1998. Two syntaxin homologues in the TGN/endosomal system of yeast. EMBO J **17:**113-126.
271. **Parr CL, Keates RA, Bryksa BC, Ogawa M, Yada RY.** 2007. The structure and function of Saccharomyces cerevisiae proteinase A. Yeast **24:**467-480.
272. **Hughes H, Stephens DJ.** 2008. Assembly, organization, and function of the COPII coat. Histochemistry and cell biology **129:**129-151.
273. **Bacia K, Futai E, Prinz S, Meister A, Daum S, Glatte D, Briggs JA, Schekman R.** 2011. Multibudded tubules formed by COPII on artificial liposomes. Scientific reports **1:**17.
274. **Saito Y, Kimura K, Oka T, Nakano A.** 1998. Activities of mutant Sar1 proteins in guanine nucleotide binding, GTP hydrolysis, and cell-free transport from the endoplasmic reticulum to the Golgi apparatus. Journal of biochemistry **124:**816-823.
275. **Eugster A, Frigerio G, Dale M, Duden R.** 2000. COP I domains required for coatomer integrity, and novel interactions with ARF and ARF-GAP. EMBO J **19:**3905-3917.
276. **Yahara N, Sato K, Nakano A.** 2006. The Arf1p GTPase-activating protein Glo3p executes its regulatory function through a conserved repeat motif at its C-terminus. J Cell Sci **119:**2604-2612.
277. **Gerich B, Orci L, Tschochner H, Lottspeich F, Ravazzola M, Amherdt M, Wieland F, Harter C.** 1995. Non-clathrin-coat protein alpha is a conserved subunit of coatomer and in Saccharomyces cerevisiae is essential for growth. Proc Natl Acad Sci U S A **92:**3229-3233.
278. **Mnaimneh S, Davierwala AP, Haynes J, Moffat J, Peng WT, Zhang W, Yang X, Pootoolal J, Chua G, Lopez A, Trochesset M, Morse D, Krogan NJ, Hiley SL, Li Z, Morris Q, Grigull J, Mitsakakis N, Roberts CJ, Greenblatt JF, Boone C, Kaiser CA, Andrews BJ, Hughes TR.** 2004. Exploration of essential gene functions via titratable promoter alleles. Cell **118:**31-44.
279. **Gari E, Piedrafita L, Aldea M, Herrero E.** 1997. A set of vectors with a tetracycline-regulatable promoter system for modulated gene expression in Saccharomyces cerevisiae. Yeast **13:**837-848.
280. **Opekarova M, Robl I, Tanner W.** 2002. Phosphatidyl ethanolamine is essential for targeting the arginine transporter Can1p to the plasma membrane of yeast. Biochimica et biophysica acta **1564:**9-13.
281. **Robl I, Grassl R, Tanner W, Opekarova M.** 2001. Construction of phosphatidylethanolamine-less strain of Saccharomyces cerevisiae. Effect on amino acid transport. Yeast **18:**251-260.

282. **Alder-Baerens N, Lisman Q, Luong L, Pomorski T, Holthuis JC.** 2006. Loss of P4 ATPases Drs2p and Dnf3p disrupts aminophospholipid transport and asymmetry in yeast post-Golgi secretory vesicles. Mol Biol Cell **17:**1632-1642.
283. **Motley AM, Nuttall JM, Hettema EH.** 2012. Pex3-anchored Atg36 tags peroxisomes for degradation in Saccharomyces cerevisiae. EMBO J **31:**2852-2868.
284. **Jiang RH, Stahelin RV, Bhattacharjee S, Haldar K.** 2013. Eukaryotic virulence determinants utilize phosphoinositides at the ER and host cell surface. Trends in microbiology **21:**145-156.
285. **Ehrhardt C, Ludwig S.** 2009. A new player in a deadly game: influenza viruses and the PI3K/Akt signalling pathway. Cellular microbiology **11:**863-871.
286. **Su WC, Chao TC, Huang YL, Weng SC, Jeng KS, Lai MM.** 2011. Rab5 and class III phosphoinositide 3-kinase Vps34 are involved in hepatitis C virus NS4B-induced autophagy. J Virol **85:**10561-10571.
287. **Mallo GV, Espina M, Smith AC, Terebiznik MR, Aleman A, Finlay BB, Rameh LE, Grinstein S, Brumell JH.** 2008. SopB promotes phosphatidylinositol 3-phosphate formation on Salmonella vacuoles by recruiting Rab5 and Vps34. J Cell Biol **182:**741-752.
288. **Huang J, Birmingham CL, Shahnazari S, Shiu J, Zheng YT, Smith AC, Campellone KG, Heo WD, Gruenheid S, Meyer T, Welch MD, Ktistakis NT, Kim PK, Klionsky DJ, Brumell JH.** 2011. Antibacterial autophagy occurs at PI(3)P-enriched domains of the endoplasmic reticulum and requires Rab1 GTPase. Autophagy **7:**17-26.
289. **Kale SD, Gu B, Capelluto DG, Dou D, Feldman E, Rumore A, Arredondo FD, Hanlon R, Fudal I, Rouxel T, Lawrence CB, Shan W, Tyler BM.** 2010. External lipid PI3P mediates entry of eukaryotic pathogen effectors into plant and animal host cells. Cell **142:**284-295.
290. **Leevers SJ, Vanhaesebroeck B, Waterfield MD.** 1999. Signalling through phosphoinositide 3-kinases: the lipids take centre stage. Current opinion in cell biology **11:**219-225.
291. **Vanhaesebroeck B, Leevers SJ, Ahmadi K, Timms J, Katso R, Driscoll PC, Woscholski R, Parker PJ, Waterfield MD.** 2001. Synthesis and function of 3-phosphorylated inositol lipids. Annual review of biochemistry **70:**535-602.
292. **Backer JM.** 2008. The regulation and function of Class III PI3Ks: novel roles for Vps34. Biochem J **410:**1-17.
293. **Lee Y, Kim ES, Choi Y, Hwang I, Staiger CJ, Chung YY, Lee Y.** 2008. The Arabidopsis phosphatidylinositol 3-kinase is important for pollen development. Plant Physiol **147:**1886-1897.
294. **Stack JH, Emr SD.** 1994. Vps34p required for yeast vacuolar protein sorting is a multiple specificity kinase that exhibits both protein kinase and phosphatidylinositol-specific PI 3-kinase activities. J Biol Chem **269:**31552-31562.
295. **Kihara A, Noda T, Ishihara N, Ohsumi Y.** 2001. Two distinct Vps34 phosphatidylinositol 3-kinase complexes function in autophagy and carboxypeptidase Y sorting in Saccharomyces cerevisiae. J Cell Biol **152:**519-530.

296. **Kametaka S, Okano T, Ohsumi M, Ohsumi Y.** 1998. Apg14p and Apg6/Vps30p form a protein complex essential for autophagy in the yeast, Saccharomyces cerevisiae. J Biol Chem **273:**22284-22291.
297. **Obara K, Sekito T, Ohsumi Y.** 2006. Assortment of phosphatidylinositol 3-kinase complexes--Atg14p directs association of complex I to the pre-autophagosomal structure in Saccharomyces cerevisiae. Mol Biol Cell **17:**1527-1539.
298. **Klionsky DJ.** 2005. The molecular machinery of autophagy: unanswered questions. J Cell Sci **118:**7-18.
299. **Slessareva JE, Routt SM, Temple B, Bankaitis VA, Dohlman HG.** 2006. Activation of the phosphatidylinositol 3-kinase Vps34 by a G protein alpha subunit at the endosome. Cell **126:**191-203.
300. **Kim DH, Eu YJ, Yoo CM, Kim YW, Pih KT, Jin JB, Kim SJ, Stenmark H, Hwang I.** 2001. Trafficking of phosphatidylinositol 3-phosphate from the trans-Golgi network to the lumen of the central vacuole in plant cells. Plant Cell **13:**287-301.
301. **Matsuoka K, Bassham DC, Raikhel NV, Nakamura K.** 1995. Different sensitivity to wortmannin of two vacuolar sorting signals indicates the presence of distinct sorting machineries in tobacco cells. J Cell Biol **130:**1307-1318.
302. **Liu Y, Schiff M, Czymmek K, Talloczy Z, Levine B, Dinesh-Kumar SP.** 2005. Autophagy regulates programmed cell death during the plant innate immune response. Cell **121:**567-577.
303. **Hohenester S, Gates A, Wimmer R, Beuers U, Anwer MS, Rust C, Webster CR.** 2010. Phosphatidylinositol-3-kinase p110gamma contributes to bile salt-induced apoptosis in primary rat hepatocytes and human hepatoma cells. J Hepatol **53:**918-926.
304. **Hasan AM, Mourtada-Maarabouni M, Hameed MS, Williams GT, Dent G.** 2010. Phosphoinositide 3-kinase gamma mediates chemotactic responses of human eosinophils to platelet-activating factor. International immunopharmacology **10:**1017-1021.
305. **Price BD, Eckerle LD, Ball LA, Johnson KL.** 2005. Nodamura virus RNA replication in Saccharomyces cerevisiae: heterologous gene expression allows replication-dependent colony formation. J Virol **79:**495-502.
306. **Grunau S, Lay D, Mindthoff S, Platta HW, Girzalsky W, Just WW, Erdmann R.** 2011. The phosphoinositide 3-kinase Vps34p is required for pexophagy in Saccharomyces cerevisiae. Biochem J **434:**161-170.
307. **Farre JC, Burkenroad A, Burnett SF, Subramani S.** 2013. Phosphorylation of mitophagy and pexophagy receptors coordinates their interaction with Atg8 and Atg11. EMBO reports **14:**441-449.
308. **Miller DJ, Schwartz MD, Dye BT, Ahlquist P.** 2003. Engineered retargeting of viral RNA replication complexes to an alternative intracellular membrane. J Virol **77:**12193-12202.
309. **Kragt A, Voorn-Brouwer T, van den Berg M, Distel B.** 2005. Endoplasmic reticulum-directed Pex3p routes to peroxisomes and restores peroxisome formation in a Saccharomyces cerevisiae pex3Delta strain. J Biol Chem **280:**34350-34357.

310. **Chuang C, Barajas D, Qin J, Nagy PD.** 2014. Inactivation of the host lipin gene accelerates RNA virus replication through viral exploitation of the expanded endoplasmic reticulum membrane. PLoS Pathog **10:**e1003944.
311. **Pomorski T, Lombardi R, Riezman H, Devaux PF, van Meer G, Holthuis JC.** 2003. Drs2p-related P-type ATPases Dnf1p and Dnf2p are required for phospholipid translocation across the yeast plasma membrane and serve a role in endocytosis. Mol Biol Cell **14:**1240-1254.
312. **Hua Z, Fatheddin P, Graham TR.** 2002. An essential subfamily of Drs2p-related P-type ATPases is required for protein trafficking between Golgi complex and endosomal/vacuolar system. Mol Biol Cell **13:**3162-3177.
313. **Wicky S, Schwarz H, Singer-Kruger B.** 2004. Molecular interactions of yeast Neo1p, an essential member of the Drs2 family of aminophospholipid translocases, and its role in membrane trafficking within the endomembrane system. Molecular and cellular biology **24:**7402-7418.
314. **Marrink SJ, Mark AE.** 2003. The mechanism of vesicle fusion as revealed by molecular dynamics simulations. Journal of the American Chemical Society **125:**11144-11145.
315. **Domanska MK, Kiessling V, Tamm LK.** 2010. Docking and fast fusion of synaptobrevin vesicles depends on the lipid compositions of the vesicle and the acceptor SNARE complex-containing target membrane. Biophys J **99:**2936-2946.
316. **Morel E, Chamoun Z, Lasiecka ZM, Chan RB, Williamson RL, Vetanovetz C, Dall'Armi C, Simoes S, Point Du Jour KS, McCabe BD, Small SA, Di Paolo G.** 2013. Phosphatidylinositol-3-phosphate regulates sorting and processing of amyloid precursor protein through the endosomal system. Nature communications **4:**2250.
317. **Raiborg C, Schink KO, Stenmark H.** 2013. Class III phosphatidylinositol 3-kinase and its catalytic product PtdIns3P in regulation of endocytic membrane traffic. The FEBS journal **280:**2730-2742.
318. **Richardson LG, Clendening EA, Sheen H, Gidda SK, White KA, Mullen RT.** 2014. A unique N-terminal Sequence in the Carnation Italian Ringspot Virus p36 Replicase-Associated Protein Interacts with the Host-Cell ESCRT-I Component Vps23. J Virol.
319. **Katzmann DJ, Babst M, Emr SD.** 2001. Ubiquitin-dependent sorting into the multivesicular body pathway requires the function of a conserved endosomal protein sorting complex, ESCRT-I. Cell **106:**145-155.
320. **Wallin E, von Heijne G.** 1998. Genome-wide analysis of integral membrane proteins from eubacterial, archaean, and eukaryotic organisms. Protein science : a publication of the Protein Society **7:**1029-1038.
321. **Traub LM.** 2009. Tickets to ride: selecting cargo for clathrin-regulated internalization. Nat Rev Mol Cell Biol **10:**583-596.
322. **Wei T, Wang A.** 2008. Biogenesis of cytoplasmic membranous vesicles for plant potyvirus replication occurs at endoplasmic reticulum exit sites in a COPI- and COPII-dependent manner. J Virol **82:**12252-12264.

VITA

Xu, Kai

Education:

2001-2005, Bachelor degree in Biological Sciences, China Agricultural University, Beijing, China

Award and scholarships:

1. Travel award from 2010 American Society for Virology Annual Meeting

2. Travel award from International Union of Microbiological Societies 2011 Congress

3. Travel award from 2012 American Society for Virology Annual Meeting

4. Excellent graduate with Bachelor degree from China Agricultural University 2005

Publications:

1. **Xu K**, Lin JY, Nagy PD. The Hop-like stress induced protein 1 co-chaperone is a novel cell-intrinsic restriction factor for mitochondrial tombusvirus replication. *Journal of Virology*. 2014 published ahead of print 11 June 2014

2.**Xu K**, Huang TS, Nagy PD. Authentic in vitro replication of two tombusviruses in isolated mitochondrial and endoplasmic reticulum membranes. *Journal of Virology*. 2012 Dec;86(23):12779-94.

3.Shah Nawaz-ul-Rehman M, Martinez-Ochoa N, Pascal H, Sasvari Z, Herbst C, **Xu K**, Baker J, Sharma M, Herbst A, Nagy PD. Proteome-wide overexpression of host proteins for identification of factors affecting tombusvirus RNA replication: an inhibitory role of protein kinase C. *Journal of Virology*. 2012 Sep;86(17):9384-95.

4.Pathak KB, Pogany J, **Xu K**, White KA, Nagy PD. Defining the roles of cis-acting RNA elements in tombusvirusreplicase assembly in vitro. *Journal of Virology*. 2012 Jan;86(1):156-71.

5.**Xu K**, Nagy PD. Dissecting Virus-Plant Interactions Through Proteomics Approaches. *Current proteomics* 2010 Dec; 7(4): 316-27

6.**Xu K**, Yoshida R.Statistical Analysis on Detecting Recombination Sites in DNA-β Satellites Associated with Old World Geminiviruses. *Frontiers in Psychiatry*. 2010 Oct 25;1:138.

7.Li Z, Pogany J, Panavas T, **Xu K**, Esposito AM, Kinzy TG, Nagy PD. Translation elongation factor 1A is a component of the tombusvirusreplicase complex and affects the stability of the p33 replication co-factor. *Virology*. 2009 Mar 1;385(1):245-60.

8. Niu S, Wang B, Guo X, Yu J, Wang X, **Xu K**, Zhai Y, Wang J, Liu Z.Identification of two RNA silencing suppressors from banana bunchy top virus. *Archives in Virology*. 2009;154(11):1775-83.

Meeting Presentations:

1.**Xu K**, Nagy PD. Role of glycerophospholipid biosynthesis in tombusvirus replication.2012 American Society for Virology Annual Meeting, oral presentation

2.**Xu K**, Nagy PD. Tombusvirusesreplicase proteins play important roles targeting and activation of replicase complex.International Union of Microbiological Societies 2011 Congress, Poster presentation

3.**Xu K**, Nagy PD. In vitro assembly of tombusvirusreplicase complex on purified yeast organelles.2010 American Society for Virology Annual Meeting, oral presentation

Society membership

American Society for Virology

Association of Plant Pathology Scholars, University of Kentucky

Delta Epsilon Iota Academic Honor Society